4-1-2010

Investigations Into the Application of Single-Beam Acoustic Backscatter for Describing Shallow Water Marine Habitats

Greg Foster
Nova Southeastern University

NOVA SOUTHEASTERN UNIVERSITY OCEANOGRAPHIC CENTER

INVESTIGATIONS INTO THE APPLICATION OF SINGLE-BEAM ACOUSTIC BACKSCATTER FOR DESCRIBING SHALLOW WATER MARINE HABITATS

by

Greg Foster

Submitted to the Faculty of

Nova Southeastern University Oceanographic Center

in partial fulfillment of the requirements for the degree

of Doctor of Philosophy in Oceanography

April 2010

Doctor of Philosophy

INVESTIGATIONS INTO THE APPLICATION OF SINGLE-BEAM ACOUSTIC BACKSCATTER FOR DESCRIBING SHALLOW WATER MARINE HABITATS

Greg Foster

Bernhard M. Riegl, Ph.D., Nova Southeastern University

Richard E. Dodge, Ph.D., Nova Southeastern University

Samuel J. Purkis, Ph.D., Nova Southeastern University

John Brock, Ph.D., Department of the Interior

Table of Contents

Table of Figures

Table of Tables

Table of Appendices

Statement of Contributions to Jointly Authored Works Contained in the Thesis

The full reference to manuscripts either published or under-review are provided after the table.

Chapter / Site / Document	Contributor	Task Performed
Chapter 1	G. Foster	Field survey design, execution, post-processing, analysis, manuscript
Palm Beach County, FL	K. Foster	Field survey execution
Foster, Walker, and Riegl (2009)	B. Walker	LIDAR GIS (topographic complexity and benthic habitat map)
		Manuscript review
	B. Riegl	Manuscript review
Chapter 2		
Palau, Micronesia	G. Foster	Field survey design, execution, post-processing, analysis, manuscript
Foster, Ticzon, Riegl, & Mumby (2010)	V. Ticzon	Micro-habitat definitions, training sample collection
(under review)		Manuscript review
	B. Riegl	Manuscript review
	P. Mumby	Manuscript review
	NOAA	Benthic Habitat Map of the Republic of Palau
Chapter 3	G. Foster	Field survey design, execution, post-processing, analysis, report
Indian River Lagoon, FL	K. Foster	Field survey execution
Chapter 4	G. Foster	Field survey design, execution, post-processing, analysis, report
Indian River Lagoon, FL	K. Foster	Field survey execution
	L. Morris	Post-survey accuracy assessment
	J. Steward	Post-survey accuracy assessment
	L. Hall	Post-survey accuracy assessment
Chapter 5	G. Foster	Field survey design, execution, post-processing, analysis, report
Sanibel Island, FL	K. Foster	Field survey execution
	R. Grizzle	Co-design of bottom classification scheme
Chapter 6	G. Foster	Field survey design, execution, post-processing, analysis, manuscript
Broward County, FL	K. Foster	Field survey execution
(in prep)	B. Walker	Acropora patch delineation
	L. Larson	Acropora patch ground-truthing
	D. Gilliam	Acropora monitoring program manager

Foster, G., Walker, B.K., & Riegl, B.M. (2009) Interpretation of single-beam acoustic backscatter using LIDAR-derived topographic complexity and benthic habitat classifications in a coral reef environment. *Journal of Coastal Research*, SI 53, 16-26.

Foster, G., Ticzon, V.S., Riegl, B.M., & Mumby, P.J. (in review) Detecting end-member structural and biological attributes of a coral reef using an acoustic ground discrimination system. *ICES Journal of Marine Science*.

A Brief History of AGDS

The majority of single-beam acoustic ground discrimination (AGDS) studies have been conducted in relatively homogeneous sedimentary environments such as bays, lochs, and coastal shelves. Of the 28 or so AGDS studies published in refereed journals over the past 15 years, 22 have been conducted in primarily clastic environments. Of the 22 clasic studies, 16 were exclusively soft-bottom sediments (Table 1). In a typical study, the AGDS is trained by comparing acoustic signatures to measured granulometric properties, e.g. particle size distribution of silt, sand, gravel, rocks, and boulders. The capability of single-beam AGDS to infer grain size has been well-established, particularly for first echo shape classification algorithms of the Quester Tangent Corporation (QTC) IMPACT post-processing software. IMPACT defines 166 highly-correlated parameters (echo shape, power spectrum, wavelet analysis) for each echo envelope, reduces the data to three principle components, and then clusters to an optimum number of classes based on the Bayesian Information Criterion (QTC 2002). Freitas et al. made a particularly compelling case for acoustic classification of monotonous soft bottom sediments from a mid-shelf survey (Freitas et al., 2003b) followed by extensive *a posteriori* validation (Freitas et al., 2006). Similar successes have been reported for the multi-echo RoxAnn and EchoPLUS AGDS, which are similar in function to the BioSonics system utilized throughout this dissertation. This branch of AGDS compute the integrated echo intensity for the trailing edge of the first echo (E1) and the complete second echo (E2). The latter is created by a portion of the first echo reflecting off the water-air interface and interacting with the bottom a second time prior to returning to the transducer. For the case of flat soft bottom sediments, E1 and E2 are related to bottom roughness and hardness, respectively (interpreting the significance of E1 and E2 grows more difficult as topographic complexity increases). In the original multi-echo classification scheme (Orlowski, 1984; Burns et al., 1989; and Chivers et al.. 1990), boxes are drawn around ground-validated E1:E2 data-pairs that are presumed to represent benthic habitat classes. Compared to the body of QTC studies, the experiences reported with RoxAnn are less uniformly

positive. On the one hand, Foster-Smith and Sotheran (2004) reported high accuracies (86.2-96.4%) for an external accuracy assessment that compared RoxAnn classifications to four bottom classes derived from visual classification of side-scan topographic surfaces. On the other hand, Brown et al. (2005) reported external accuracies in the range of 20-30% for six classes of mud, sand, gravel, rock, and boulders.

Only a small number of AGDS studies have attempted to expand the utility of classification schemes beyond predictions of grain size within monotonous soft bottom environments, and these are largely cautionary tales. Hamilton et al. (1999) reported on a joint QTC and RoxAnn survey within a back-reef lagoon; classifications were restricted to combinations of mud, sand, and gravel and the acoustic interpretation of coral reefs was reported as problematic, e.g. a widely oscillating E2. Kloser et al. (2001) reported on a RoxAnn coastal shelf survey that included deep fossil reefs, but reported that RoxAnn E1 and E2 values were severely depth-contaminated and could not reliably discriminate the soft/smooth, soft/rough, hard/smooth, and hard/rough classes obtained from a Simrad EX500 echosounder. Moyer et al. (2005) reported on a QTC survey of the coral reefs of Broward County, FL; the accuracy of a sand, rubble, reef classification scheme was 61%, but dropped to 39% for multiple hardbottom classes (sand, rubble, reef types 1-3). Riegl and Purkis (2005) reported on a dual-frequency QTC survey of nearshore coral reefs in the Arabian Gulf; four general acoustic classes were discriminated at an accuracy of 56% by combining the 50 kHz (hard versus soft) and 200 kHz (smooth versus rough) signals. White et al. (2003) reported on a RoxAnn survey of a diverse coral reef in the Philippines; despite collecting a large training dataset (161 samples), classification beyond a relatively simple mud, sand, and "everything else" scheme (Po=86%, Tau=63%) was not found to be warranted. So while both QTC and RoxAnn AGDS have been largely proven in sedimentary systems, neither has been shown to be successful in discriminating between classes of hardbottom.

Table 1. (top) Summary of single-beam AGDS seabed classification studies appearing in peer-reviewed journals, arranged by the nature of the bottom surface, from purely soft sediment bottoms to purely clastic bottoms (e.g. includes rocks/boulders) to reef or reef-like environments. (bottom) Summary of dissertation chapters.

Author	Year	QTC		RoxAnn		EchoPLUS		Beam	Depth (m)		Bedform	# of Classes		Description of Acoustic Classes
		low	high	low	high	low	high	Width	min	max		Total	HB	
Purely Soft Bottom Sediments														
Bax et al.	1999				120			10	40	60	Coastal Shelf	3	0	Soft, hard, rough
Collier and Brown	2005				200			10	-	-	Loch	n/a	0	Related E1 and E2 to side-scan backscatter (combinations of mud, sand, gravel).
Ellingsen et al.	2002	50						13.5	5	72	Fjord	6	0	Combinations of fine/medium silt, sand, pebbles, shell debris
Foster-Smith et al.	2004		200		200			18	-	-	Ocean Channel	4	0	Grain size plus epi- and infaunal communities
Freitas et al.	2003a	50						44	5	40	Coastal Shelf	3	0	Very fine, fine, and coarse sand
Freitas et al.	2003b	50x2						44 / 19	30	90	Mid-Shelf	3	0	Fine sand with low silt, silty very fine sand, and mud
Hetzinger et al.	2006		200					-	-	-	Gulf	4	0	Fine-med sand, med-coarse sand, coarse aand very-coarse sand granule
Humborstead et al.	2004			38				7	94 ± 7		Coastal Shelf	n/a	0	Compared RoxAnn to side-scan imagery and towed-video.
Hutin et al.	2005	38/50						7 / 42	20	70	Scallop bed	1	0	Scallop bed
Magorrian et al.	1995			50				-	-	-	Loch		0	Mud/silt, mussels/scallops
Morrison et al.	2001		200					7	5	20	Bay	7	0	Visually-apparent transition between soft bottom sediment zones.
Pinn and Robertson	2001			?				-	-	-	Firth	n/a	0	Burrow density versus E1 and E2
Riegl et al.	2005	50					200	24 / 6	1	5	Lagoon	3	0	Bare sediment, seagrass, drift macroalgae
von Szalay and McConnaughey	2002	38x2						7 / 13	22	226	Straits	6	0	Combination of mud, sand, pebbles, and cobbles
Wienberg and Bartholoma	2005		200					7.4	6	20	Estuary	3	0	Fine-medium sand (low shell), medium sand (moderate shell), med-coarse sand.
Wilding et al.	2003			200				10	10	25	Loch	n/a	0	Related stone cover to E1 and E2
Purely Clastic Environments														
Anderson et al.	2002	38						10	10	220	Bay	4	0	Mud, gravel, rock, macroalgae on rock
Brown et al.	2005				200			10	15	60	Firth	6	0	Combinations of mud, sand, gravel, rock, boulders
Foster-Smith and Sotheran	2003			38	200			-	-	-	Loch	12	0	Up to 12 biotopes
Freitas et al.	2005	50						19	5	25	River Channel	4	1	Fine sand, medium sand, coarse sand, hardbottom.
Greenstreet et al.	1997			38				-	~15	80	Firth	7	0	Combinations of mud, fine sand, coarse sand, gravel, boulder/rock
Pinn and Robertson	2003			38				-	30	180	Minch	4	0	Combinations of mud, sand, stone, boulders, and bedrock
Reef or Reef-Like Environments														
Hamilton et al.	1999	38		50				- / 50	10<	55	Backreef Lagoon	5/10	0	Combinations of mud, silt,and gravel; 10 QTC classes vs 5 RoxAnn
Kloser et al.	2001		120					11.2	30	230	Coastal Shelf	4	2	Soft/smooth, soft/rough, hard/smooth, hard/rough
Moyer et al.	2005	50						24	3	35	Coral Reef	3	1	Sand, rubble, reef
Reigl et al.	2007	50				50		42	5	40	Bay (reef-like)	4	2	Rocky ridges, rock and hardround, sand-sorted, sand-unsorted
Riegl and Purkis	2005	50	200					42 / 12	1	10	Coral Reef	4	1	50 kHz (sand vs hardground) and 200 kHz (corals and sand ripples vs flat areas)
White et al.	2003			200				18	2.6	70	Coral Reef	3	0	Mud, sand with algae, and a mixed class of sand, algae, gorgs, rubble, and coral.
Dissertation						BioSonics								
Chapter 1	2006					38	420		11	35	Coral Reef	5	4	Sand, sand over HB, ridge + S&G, patch reef, colonized pavement + linear reef. Detected gorogonian abundance (420) and discriminated sand veneer over HB (38 kHz)
Chapter 2	2008					38	420		1	5	Lagoon	3	0	Bare substrate, short SAV (10cm<), and drift macroalgae
Chapter 3	2008					38			1	5	Lagoon	n/a	n/a	Vertical extent of surficial muck deposits using the 38 kHz sub-bottom profile
Chapter 4	2006						420		1	18	Coral Reef	6	3	Sand, patchy seagrass, rubble, flat hardbottom, rugose hardbottom, branching coral
Chapter 5	2009					38	420		2	12	Coastal Shelf	5	1	Mud/sand, mud/sand/shell, packed shell in mud/sand, shell hash & live HB, seagrass
Chapter 6	2009					38	420		3	9	Coral Reef	4	3	Sand, pavement, gorgonians (on pavement), *Acropora cervicornis* (on pavement)

Research Aims and Objectives

A recurring theme of the aforementioned forays into higher-complexity and higher-resolution AGDS mapping, regarding the nature and certainty of the relationship between acoustic and environmental variables, is that far more questions are raised than answered. That is the state of affairs from which this dissertation attempts to depart; therefore, while each chapter is a new or rare application of AGDS, the main emphasis of this dissertation is on the solidity of methodological foundation itself. For each application, the goal was to provide such a preponderance of evidence so as to leave as little doubt as possible surrounding the efficacy of the classification process. Pursuant to this goal, a parallel can be drawn between the supervised classifications found in this dissertation (groupings of bottom types inferred from acoustic parameters) to more traditional ecological studies (groupings of individuals forced by environmental parameters). In this sense, the generalized hypothesis is that individuals (individual training samples) form groups (bottom classes) that can be predicted from linear combinations of environmental variables (acoustic parameters). The discriminant analysis classification scheme used throughout this dissertation allows for significance testing of the independent variables and of the descriptive discriminant analysis model.

This dissertation opens with an exhaustive demonstration of the capability of a single-beam AGDS to discriminate between 4 coral reef hardbottom habitats, and goes on to discriminate 6 bottom classes of a Palauan coral reef, 3 of which were hardbottom habitats (Table 1, chapters 1 and 4). The methodology employed in Chapter 1 is illustrative of the emphasis on certainty. Previous studies have utilized backdrops of side-scan (Collier and Brown, 2005; Foster-Smith et al., 2004) or LIDAR (Moyer et al., 2005) to assess acoustic classification schemes, by comparing the classifications of acoustic points to the side-scan or LIDAR polygons in which they fall. Such a procedure was also utilized in Chapter 1, but only after directly assessing how the individual acoustic parameters E1 and E2 interpreted LIDAR-derived topographic complexity and habitat

class. Indeed, it was this series of comparisons that made it possible to disentangle the influences of substrate and biotic habitat components on the acoustic interpretation of complex coral reef habitats.

For the example of supervised classification (chapters 2, 4, and 5), the training datasets were; (1) very large, ranging from 62 samples for 5 classes to 131 samples for 3 classes (each sample being a discrete hydroacoustic file ranging from 30 to 120 seconds in duration), (2) ground-validated using a drop-camera trailing behind the transducer, (3) checked for temporal (as much as one year) and spatial (as much as 120 km) consistency, (4) carefully groomed prior to classification, and (5) tested for critical assumptions of normality and dispersion. Furthermore, the number of pre-defined bottom classes was compared to the number of clusters predicted by a stopping rule, and the assignment of individual samples to the pre-defined categories was reviewed prior to final classification. On the back end, the fate of individual training samples was tracked to illustrate that the acoustic interpretation was consistent between samples, which were often collected over large expanses of space and time. Finally, the supervised classification workflow (albeit a work-in-progress) was essentially the same for all applications and used the same output of the same commercially-available post-processing software. Given the number of diverse applications that were processed using the same basic methodology and examined in such detail, it is proposed that as a whole the following chapters advance the position of single-beam AGDS as a powerful tool for investigating shallow-water benthos.

Introduction to Single-Beam AGDS

The same BioSonics DT-X echo-sounder was used for all chapters; the descriptions that follow are specific to that unit, but are generally applicable to the similar RoxAnn and ECHO*plus* multi-echo AGDS. The data acquisition cycle begins when the transmitter within the DT-X echo-sounder generates an electrical signal and transmits it to a transducer oriented perpendicular to the seabed. The transducer converts the electrical signal into an acoustic pulse of a specified duration and directs the signal into the water. The echo returning to the transducer is converted back to an electrical signal, filtered and then sampled at a rate of 41,667 kHz and stored as a digitized waveform. To compute the acoustic energy and shape parameters, the digitized waveform is converted to an echo envelope (echo intensity (dB) versus depth, which equates to time via the speed of sound in water). BioSonics Visual Bottom Typer (VBT) seabed classification software computes the values of the acoustic energy parameters as the time integral of echo intensity within a given bottom sampling window (dashed lines in below figures). The starting and ending positions of the bottom sampling windows can be adjusted in VBT. Because of the chaotic nature of echo returns, some degree of smoothing is necessary to achieving signal stability. Throughout this dissertation, pings were generated at a frequency of 5 Hz (i.e. 5 pings per second). Each hydroacoustic 'record' was a statck of five pings (so that 'records' were collected at a frequency of 1 Hz).

Defining Echo Intensity: Acoustic intensity is the sound power per unit area (W/m^2). The acoustic intensity level (L_I) is a base 10 logarithmic measure of the acoustic intensity in comparison to a reference level of 10^{-12} W/m^2, using the following equation

$$L_I = 10 \log_{10} (I_1 / I_0) \quad (1)$$

Throughout this document, echo intensity refers to the acoustic intensity level (LI). The units are dimensionless decibels and the values are by convention negative (i.e. I_1 is always less than I_0).

NOTE: The majority of post-processing was conducted with VBT. The operation of Visual Analyzer and EcoSAV post-processing software are discussed in Chapters 3 and 6, respectively.

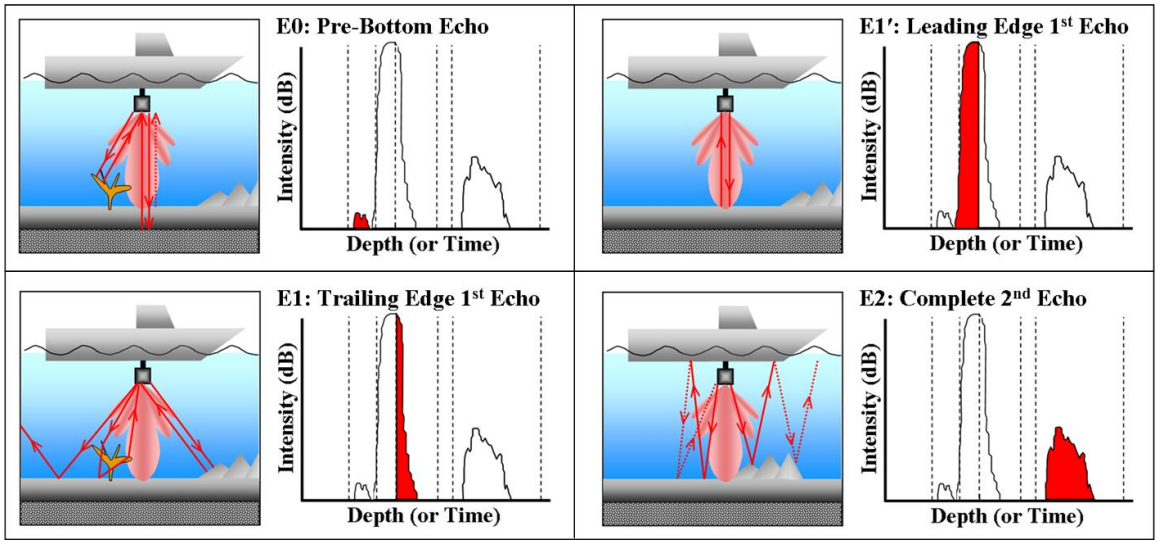

Depiction of the four acoustic energy parameters (E0, E1', E1, E2) computed from echo envelopes.

As do the other more popular multi-echo single-beam AGDS (RoxAnn, ECHO*plus*), the BioSonics Visual Bottom Typer seabed classification software outputs the acoustic energy parameters E1, E2, and depth. In addition, the BioSonics software also outputs E0, E1′, and a fractal dimension. These are all discussed below.

E0 (~pre-bottom backscatter) - The energy reflected back to the transducer prior to the main beam making contact with the true bottom. It can result either from low bulk-density sediments overlying a harder "true" seabed or by the presence of epibiota.

E1′ (~bottom hardness signature) - The leading edge of the first echo, composed primarily of coherent (aka specular, normal incidence, near-nadir) reflection from the bottom. Coherent backscatter is generally considered to be that portion of the beam making contact with the bottom within 20^{o} off nadir. Because it is primarily comprised of specular reflection, it is particularly sensitive to vessel pitch and roll.

E1 (~bottom roughness signature) - The trailing edge of the first echo, comprised primarily of incoherent backscatter reflected from a combination of seabed roughness (geomorphology) and epibenthic biota.

E2 (~bottom hardness signature) - The complete second echo, resulting from a double specular reflection from the seabed and a single reflection off the survey vessel or air-water interface. For flat surfaces E2 contains the bottom hardness signature. Rough surfaces cause extremely diminished values of E2, as scattering greatly decreases the probability of the multi-path echo returning to the transducer.

Fractal Dimension (~shape irregularities of first echo) – Computed as the Hausdorff dimension of the first echo, simplified by gridding the echo envelope into 'box' dimensions. The assumption is that the layers of the seabed have a fractal shape, and that this shape is transferred to the shape of the echo envelope (Tegowski and Lubniewski, 2000).

The most basic approach to acoustic habitat classification, developed by Orlowski (1984) and refined by Burns et al. (1989) and Chivers, Emerson, and Burns (1990), is to plot E1:E2 data-pairs onto a Cartesian XY plane and manually draw boxes around clusters of data that are presumed to represent benthic habitat classes. This classification scheme simplistically arranges bottom types on the basis on smooth/rough (low/high E1) and hard/soft (high/low E2), provided the bottom surfaces are flat.

Chapter Synopsis and Key Findings

Chapter 1: Interpretation of Single-Beam Acoustic Backscatter Using LIDAR-Derived Topographic Complexity and Benthic Habitat Classifications in a Coral Reef Environment

The work contained in this chapter was a keystone for all subsequent chapters, in that it firmly established the BioSonics single-beam acoustic ground discrimination system (AGDS) as a viable tool for interpreting shallow-water benthic habitats. This was accomplished by pairing 7000+ acoustic records, acquired within a 2.3 km^2 plot offshore Palm Beach County, with spatially-coincident values of LIDAR-derived topographic complexity and habitat classifications. Having such a wealth of comparisons not only lifted the fog of uncertainty that so often accompanies acoustic remote-sensing, but also pointed the way to new post-processing methodologies used throughout the following chapters.

Chapter 1 Key Findings

- The raw E1 and E2 values obtained from post-processing in BioSonics Visual Bottom Typer (VBT) seabed classification software were both found to be significantly depth contaminated;
    - VBT compensates for depth-related spherical spreading and absorption losses with time-varied gain compensation, but does not normalize echo duration to a reference depth. Both can potentially affect values of E1′ and E1 (E2 is a special case – see below).
    - Not normalizing echo duration to a reference depth affects division of the first echo into E1′ and E1 (magnitude is dependent on the range of depth). Echoes tend to become wider and flatter with increasing depth. The start of the E1′ is identified by the maximum rate of rise of echo intensity (where the echo first contacts the bottom). But the end of E1′ (and the start of E1) is specified in units of time. By not compensating for the depth-related aspect ratio of the echo envelope, the relative proportions of E1′ and E1 can be affected (e.g. as depth increases, proportionally more of the echo would fall into the E1 bottom sampling window).

- However, not normalizing to a reference depth would not affect E2 (complete second echo envelope), provided the bottom sampling gate was sufficiently wide to accommodate the deepest and widest echoes (which it was).
- Therefore, the VBT time-varied gain compensation algorithm apparently did not adequately address depth-related spherical spreading and absorption losses to maintain a depth-invariant E2 for a given bottom type (presumably, the other parameters were similarly affected).

- It was possible to empirically "fix" the depth-contamination using depth-normalization curves developed from data acquired over sand and deep-sand habitats.
  - Sand habitats spanned the entire depth range of survey and are homogeneous and smooth, so depth could be assumed to be the primary variable affecting the values of E1 and E2.
  - This apparently worked, as similar habitats of different depths occupied the same E1vsE2 space at both acoustic frequencies (e.g. sand, deep sand, and sand over hardbottom).
- The depth-normalized 38 and 418 kHz E1 and E2 acoustic energy parameters rationally interpreted the seven arbitrarily-selected levels of LIDAR-derived topographic complexity in strict order. E1 was positively correlated with topographic complexity (roughness = more backscatter), E2 negatively (rougher = lower probability of multi-path echo returning to transducer).
- The 38 and 418 kHz E1 and E2 acoustic energy parameters generally arranged the eight benthic habitats in order of their LIDAR-derived topographic complexity, with a few telling exceptions;
  - The linear reef and colonized pavement habitats both had high E1 and low E2, even though the LIDAR-derived topographic complexities differed markedly (linear reef high, colonized pavement low).
  - However both habitats had high gorgonian abundance, suggesting E1 and E2 were informed by a combination of topographic complexity and gorgonian abundance.
- E1vsE2 scatterplots at both acoustic frequencies, after heavy percentile filtering (retaining 20-80th percentiles of E1 and E2) revealed clusters of benthic habitat classes, suggesting it may be possible to discriminate between habitats provided more information is available (i.e. the multivariate classification scheme utilized in Chapters 2, 4, 5, and 6).

- The stability of the 38 and 418 kHz signals did not deteriorate over rocky reefal substrate or high inclinations.
- The 38 kHz signal differentiated nearshore sand deposits from a thin veneer of sand over hardbottom.
- The 418 kHz signal best detected the canopy of erect colonies of gorgonians.

Chapter 2: Mapping the Distribution and Abundance of Seasonal Drift Macroalgae in the Indian River Lagoon

In Chapter 1 it was found that an E1:E2 scatterplot at a single-frequency carried insufficient information to unambiguously discriminate between bottom classes. In this chapter the basic framework for a dual-frequency, multivariate, multi-pass discriminant analysis (DA) methodology was established for the purpose of acoustically mapping the distribution and abundance of seasonal drift macroalgae in the Indian River Lagoon, FL. The full output of BioSonics Visual Bottom Typer (VBT) seabed classification software (E1′, E1, E2, fractal dimension) at two frequencies (38 and 418 kHz) were combined into a single dataset and utilized for discriminating drift macroalgae from a background of bare substrate and short SAV (10cm<). A training dataset was constructed from 131 ground-validated hydroacoustic samples collected during the 2007 pilot program and the 2008 lagoon-wide survey. The training dataset was refined into pure end-member categories of BARE (bare substrate), SHORT SAV (submerged aquatic vegetation, typically *Caluerpa prolifera*, 10cm<), and drift macroalgae (DMA) by multiple passes through DA, retaining only those records that classified correctly and exceeded a minimum probability of group membership.

Chapter 2 Key Findings

- The small acoustic footprint of the narrow-beam transducers made it possible to refine heterogeneous training samples into pure end-member categories of bare pavement, short SAV, and drift macroalgae, which in turn allowed for simple and direct computation of vegetative abundance.

- Concurrent towed video and hydroacoustic samples were essential for training the supervised classification, due to the small-scale patchiness of vegetative cover

- The dual-frequency multi-pass DA reliably detected DMA; for the 12 accuracy assessment samples with the highest ground-truthed DMA cover (average = 91%), 71% of the pings were acoustically classified as DMA.
- *C. prolifera* was detected less reliably than drift macroalgae, concomitant with its smaller gross morphology and canopy height. But the multi-pass DA classification scheme allowed for removal of these misses from the training dataset, which was necessary for distinguishing between the true *C. prolifera* acoustic signature and that of bare substrate.
- The acoustic interpretation of bare substrate, short SAV, and DMA was temporally consistent over a one year period, and spatially consistent over the 120 km span of the survey, as demonstrated by the equitable distribution of records among the 131 training samples that passed through the multi-pass DA.
- The discriminatory power of the multivariate, multi-pass discriminant analysis classification scheme was much greater than single-frequency E1:E2 scatterplots.
- The 418 kHz parameters supplied most of the discriminatory power. Adding the 38 kHz parameters only marginally improved the internal classification of the training dataset (not surprising, as the shorter wavelength of the 418 kHz signal would more likely to interact with SAV.

Recurring Themes

- The non-linear behavior of the acoustic parameters in very shallow depths was successfully treated post-survey using empirically-derived depth-normalization curves.

Chapter 3: Mapping the Spatial Distribution and Vertical Extent of Muck in the Indian River Lagoon

The same acoustic dataset acquired for the acoustic-estimation of drift macroalgae biomass in the Indian River Lagoon was used to estimate the spatial distribution and vertical extent of surficial muck deposits within the lagoon. While quantifying the thickness of sedimentary layers is a

common application of single-beam sub-bottom profilers, this chapter nonetheless demonstrates the richness of information contained within the vertical-incidence waveforms of an acoustic ground discrimination system.

Chapter 3 Key Findings

- The vertical extent of surficial muck deposits can be accurately quantified by a simple measurement of 38 kHz sub-bottom echo energy profile, without the need for coring or estimation of acoustic impedance.
- A clear north-south gradient of muck within the navigation channels was detected, suggesting the headwaters of Indian River are a significant source of muck.
- The acoustically-predicted distribution of muck deposits suggested a strong tendency for muck to accumulate in deep sinks within the lagoon.

Recurring Themes

- A multiple linear regression demonstrated that the acoustic bottom thickness was independent of bottom depth and year of acquisition, indicating the spatial and temporal consistency of the acoustically-derived muck layer thickness.

Chapter 4: Detecting end-member structural and biological attributes of a coral reef using an acoustic ground discrimination system

The multivariate, multi-pass classification scheme developed for mapping submerged aquatic vegetation in the Indian River Lagoon was used to produce a thematic benthic habitat map of coral reef habitat in Palau, Micronesia. The methodology was proven at a site for which high quality satellite imagery already existed, as an example of the potential for single-beam systems to thematically map coral reefs in deep or turbid settings where optical methods are unsatisfactory. A benthic habitat map created from satellite imagery and concurrent spatially co-located video transects were used to judge the fit of the acoustic classification.

Chapter 4 Key Findings

- The acoustic classifications of sand, seagrass, rubble, flat hardbottom, rugose hardbottom, and branching coral were found to (i) conform to visually-apparent contours of satellite imagery, (ii) agree with the structural and biological delineations of the NOAA benthic habitat map, and (iii) yield values of benthic cover that agreed closely with independent, contemporaneous video transects.
- Making increasingly finer distinctions between bottom classes, such as those found on a tropical coral reef, required exceedingly greater care in arranging and grooming of the training dataset. The successful results reported here followed numerous failed attempts as this lesson was learned.
- It was shown quantitatively that the frequently heterogeneous samples were correctly resolved into their structural and biological elements.
- The Variance Ratio Criterion, an independent prediction of optimum clusters, obtained from a PCA + K-means of the training dataset, validated the number of predefined groups. A comparison matrix of DA groups (k=7) versus PCA + K-means clusters (k=8) showed that 6 of the 8 K-means clusters were dominated by a single DA group.

Recurring Themes

- The empirical depth-normalization developed in Chapter 1 and used in Chapter 2 was found to eliminate depth contamination, because; (i) depth was not a major predictor variable, (ii) depth was not strongly correlated with other predictor variables, and (iii) the depth range of habitat classes was greater for the predictive DA of survey data than it was for the descriptive DA of training data, i.e. depth as an independent variable did not place an artificial constraint on classification.
- The small acoustic footprint afforded by a narrow beam-width and shallow depth proved critical for refining the training dataset into micro-scale, pure end-member elements that could be reliably discriminated by the acoustic parameters.
- The ability to resolve micro-scale features circumvented the dilemma typically imposed on coral reef AGDS studies utilizing wide-beam transducers, which is to either train the AGDS on homogeneous benthos and leave the heterogeneous benthos un-classified, or attempt to capture the many ‘mixed’ classes and overwhelm the discriminatory capability of the AGDS.

- The proportions of records rejected in the multi-pass DA were equitably demonstrated among the 65 training samples, showing the acoustic variables were interpreting spatially and temporally consistent characteristics of the predefined groups.
- Following the 3rd-Pass DA, the training dataset was found to generally meet the critical assumptions of discriminant analysis, including; (i) skewness and kurtosis, (ii) homogeneous dispersion of variances and covariances, and (iii) a low degree of multicollinearity.

Chapter 5: Using hydroacoustics to create a benthic map of the potential for drift macroalgae attachment

The multivariate multi-pass discriminant analysis method was used to classify a dual-frequency survey into categories of visually-apparent surficial roughness, as a proxy for the probability the substrate could serve as an attachment site for drift macroalgae. Methods for arranging and grooming of the training dataset prior to classification were formalized.

Chapter 5 Key Findings

- The acoustically-derived map of bottom roughness revealed two previously unknown areas of high bottom roughness with spatial extents large enough to support a nuisance drift macroalgae bloom.
- It was possible to define habitat class on the basis of visually-apparent surficial roughness, but the class assignment of individual samples must be independently checked prior to final classification of the training dataset, i.e. sometimes samples "sound" differently than they "look".

Recurring Themes

- The empirical depth-normalization developed in Chapter 1 and used in Chapters 2 and 4 was found to eliminate depth contamination, because; (i) depth was not strongly correlated with other predictor variables, and (ii) the depth range of habitat classes was greater for the predictive DA of survey data than it was for the descriptive DA of training data, i.e. depth as an independent variable did not place an artificial constraint on classification.
- Temporal consistency and spatial consistency was clearly evident by;

  - The similarity of the October 2008 and May 2009 data used to construct the empirical depth-normalization models, collected from several locations around the island and ground-validated as uncolonized, unconsolidated sand.
  - The equitable distribution of records among the 50 training samples that passed through the multi-pass DA; the training samples were collected in 2008 and 2009, from several locations around the island.
- As found in Chapter 2, the 418 kHz parameters supplied most of the discriminatory power. Adding the 38 kHz parameters only marginally improved the internal classification of the training dataset.
- Following the 3rd-Pass DA, the training dataset was found to generally meet the critical assumptions of discriminant analysis, including; (i) skewness and kurtosis, (ii) homogeneous dispersion of variances and covariances, and (iii) a low degree of multicollinearity.
- The Variance Ratio Criterion, an independent prediction of optimum clusters, obtained from a PCA + K-means of the training dataset, validated the number of predefined groups. A comparison matrix of DA groups (k=5) versus PCA + K-means clusters (k=5) showed that 4 of the 5 K-means clusters were dominated by a single DA group.

Chapter 6: Mapping *Acropora cervicornis* and gorgonian abundance using an acoustic ground discrimination system

This Chapter was composed of two main components. The first was a set of controlled field experiments conducted with the survey vessel triple-anchored over bare pavement, gorgonians, and *Acropora cervicornis* (a formerly abundant branching coral, that along with *A. palmata* dominated reef crests throughout the Caribbean and Western Atlantic prior to basin-wide mass mortalities beginning in the 1970's). Anchoring over target eliminated the uncertainty of what had been ensonified, providing an unequivocal demonstration of how epibiota are encoded in the digitized echo waveform. Furthermore, the depths of the anchoring sites were all 4.8 m, eliminating the potential intrusion of depth-contamination into the interpretation of the acoustic parameters. The second component was a survey of two previously delineated and ground-

truthed patches of *A. cervicornis*. Using the anchored datasets as a guide, the BioSonics EcoSAV plant-detection software was tuned to detect general epibiotic cover, and new methods were developed to allocate the undifferentiated cover into either gorgonians or *A. cervicornis*. The same multi-pass discriminant analysis (DA) methodology developed in Chapters 2, 4 and 5 was also used to classify survey data.

Chapter 6 Key Findings

- Anchored over 100% *A. cervicornis* cover, the EcoSAV predictions of cover were 82.0% at 38 kHz and 72.5% at 418 kHz.
- Anchored over high gorgonian cover, the EcoSAV predictions of cover were 38.4% at 38 kHz and 69.7% at 418 kHz.
- This frequency-dependent differential detection of *A. cervicornis* and gorgonians was exploited to allocate the undifferentiated 418 kHz EcoSAV cover to either *A. cervicornis* or gorgonian.
- The boundaries of *A. cervicornis* patches predicted by the EcoSAV and DA methods were consistent and agreed closely with the on-the-ground delineations.
- The EcoSAV-predicted canopy height agreed closely with field measurements; 0.69 versus 0.58 m (Acropora) and 1.09 versus 0.91 m (gorgonians), respectively.
- Echo envelopes acquired while anchored over bare pavement, *A. cervicornis*, and gorgonians showed consistent and predictable patterns of shape. In the presence of epibiota the first echo was shifted to the right, i.e. the first part of the echo (E1′) diminished as proportionally more energy returned in the trailing edge, evident as multiple protracted peaks and a characteristic saw-toothed shoulder. The second echo also evidenced the longer path length imparted by scattering within the canopy, evident as a sizable delay in its appearance (theoretically twice the depth as the first echo).
- The combination of high slope and rough surfaces (e.g. boulders, broken pavement) along the ledges at both sites caused a high degree of false-positive detection of epibiota.

Recurring Themes

- Following the 2nd-Pass DA, the training dataset was found to generally meet the critical assumptions of discriminant analysis, including; (i) skewness and kurtosis, (ii) homogeneous dispersion of variances and covariances, and (iii) a low degree of multicollinearity.

Chapter 1: Interpretation of Single-Beam Acoustic Backscatter Using LIDAR-Derived Topographic Complexity and Benthic Habitat Classifications in a Coral Reef Environment

FORWARD

The preponderance of published single-beam acoustic ground discrimination (AGDS) studies have been conducted in relatively homogenous sedimentary habitats, in which the AGDS is trained against grain size (i.e. varying combinations of clay, silt, sand, pebble, rock, and boulder) and various associated metrics (e.g. surficial roughness, porosity, bulk density). The most common acoustic classification schemes in these studies are some variant of hard/soft and rough/smooth. Only a handful of studies have attempted to map coral reef habitats (HALLEY and BRUCE, 2007; HAMILTON et al., 1999, MOYER et al. 2005, RIEGL and PURKIS, 2005; WHITE et al., 2003). These are largely cautionary tales of the difficulties of expanding the interpretation of acoustic backscatter beyond the hard/soft rough/smooth scheme; only MOYER et al. 2005 and RIEGL and PURKIS, 2005, and WHITE et al., 2003 attempted to map individual hardbottom classes. These studies only hint at the capability of single-beam AGDS to discriminate between carbonate structures, as confidence for these finer distinctions diminished greatly compared to the soft/hard classifications. While a map of unconsolidated sediment and hardbottom is of value when waters are either too deep or turbid for optical classification, clearly there would be a benefit to resolving levels of topographic complexity. The work contained in this chapter was a keystone for all subsequent chapters, as it unambiguously established the capability of single-beam AGDS to rationally interpret the topographic complexity of the coral reef habitats offshore Palm Beach County, FL. Moreover, it also showed how acoustics could complement image-based maps by (i) distinguishing deep sand deposits from a thin sand veneer, and (ii) quantifying epibiotic abundance (in this case, gorgonians).

The main obstacles to calibrating an AGDS in a heterogeneous environment are the constraints of time and expense, which limits both the number and quality of ground-validated reference points (for accuracy assessment in an unsupervised classification, or split between accuracy assessment and training in a supervised classification). In this study a previous LIDAR survey provided a invaluable backdrop for calibration; each hydroacoustic record was paired with a spatially-coincident value of (1) a LIDAR-derived proxy for topographic complexity (Reef Volume) and benthic habitat classification and (2) benthic habitat classifications derived from visual interpretation of the LIDAR surface, video ground-truthing, and characterization of the epibenthic community. After filtering and merging 38 and 418 kHz acoustic datasets, this resulted in a staggering 7000+ ground-validated acoustic records within a 2.3 km^2 survey area. The hydroacoustic variables examined in this study were the acoustic energy parameters E1 (integrated energy of the trailing edge of 1^{st} echo envelope) and E2 (complete 2^{nd} echo). A brief description of the computation of acoustic energy parameters is provided at the end of this section.

A pivotal result of this study was the finding that E1 and E2 were no less stable over the rocky and steep reefal terrain than over the flat hardbottom habitats, as had been observed or suggested in several QTC studies (HAMILTON et al., 1999, VON SZALAY and MCCONNAUGHEY, 2002; GLEASON et al., 2006). This meant the observed trends of E1 and E2 with the LIDAR metrics could be interpreted as meaningful responses, and not simply artifacts of signal degradation. Comparing the acoustic response to both LIDAR Reef Volume and benthic habitat was a linchpin for unraveling the acoustic interpretation of higher-complexity coral reef habitats. The E1 of both the 38 and 418 kHz frequencies was found to be significantly and positively correlated with Reef Volume (i.e. topographic complexity), in agreement with the prevailing rationale for seabed classification. E2 was found to be significantly and negatively correlated with Reef Volume. At first glance this seemed at odds with the prevailing rationale that E2 contains the bottom hardness

signature, i.e. in this study, soft sand with a low Reef Volume had a higher E2 than hard reef with a high Reef Volume. But after examining the acoustic interpretation of benthic habitats, it became clear that E1 and E2 were both under the primary control of seabed roughness, and that seabed roughness was a combination of topographic complexity and gorgonian abundance.

This was revealed by comparing the acoustic interpretations of Reef Volume and benthic habitat. Whereas the ordering of the seven levels of Reef Volume by E1 and E2 was thoroughly consistent, the ordering of benthic habitats was generally consistent, but with exceptions. Most notably, the colonized pavement habitat had a moderate value of Reef Volume but was acoustically ranked alongside the more topographically complex linear reef habitat. What these habitats had in common were relatively high abundances of erect gorgonians, evidenced by ground-truthing samples and quantified by processing with BioSonics EcoSAV software (this technique was later refined and expanded to differential detection of gorgonians and Acropora cervicornis, based on this initial observation of lower acoustic interaction with the gorgonian canopy at 38 kHz compared to 418 kHz). The contribution of gorgonians to acoustic roughness on the reefal habitats provided the explanation for the observed coupling between E1 and E2. On the other hand, the flat and un-colonized sedimentary habitats of this study (sand, deep sand and sand over hardbottom) were found to conform to the general rationale for seabed classification. The sand habitats had lower values of E1 (flat) and E2 (soft) compared to the rougher and harder sand over hardbottom habitats. It also warrants mentioning that the sand over hardbottom habitat was delineated using the 38 kHz acoustic survey as a guide (the boundary was apparent in the LIDAR imagery but had previously been dismissed as an artifact of image stitching).

This chapter also saw the development of data cleansing techniques that would become essential elements of all subsequent chapters. Without doubt the most significant of these was treatment of depth contamination. Unlike the RoxAnn or ECHO*plus* systems, the current version of

BioSonics VBT does not normalize echo length to a reference depth (though at the time of this writing a pre-release version with depth-normalization has become available). Depth normalization entails adjusting the width of the E1′ and E1 bottom sampling windows to maintain a consistent first echo division, as the echo predictably stretches and flattens with increasing depth. The lack of depth-normalization turned out to be a boon for subsequent multivariate classification, for the E2 and fractal dimension (FD) outputs were also found to be depth-contaminated. While the depth-contamination of FD remains a bit of a mystery, it is clear that E2 should not require normalization to a reference depth, provided the bottom sampling gate is adequately wide to capture the entire second echo across the range of depths. The presumed source of E2 depth contamination was imperfect compensation for spherical spreading and absorption losses by the time-varied gain (TVG) algorithm used by VBT. In all subsequent chapters, the values of E1′, E1, E2, and FD were found to be depth-contaminated at both 38 and 418 kHz. In this chapter, the availability of classified LIDAR imagery lent itself to the first development of method for empirical depth-normalization. Acoustic survey records were selected over the featureless sand and deep sand habitats, where depth could be assumed to be the primary factor affecting the echo returns. This sub-set of data was then curve-fit for each acoustic parameter and used to normalize the acoustic parameters to the median survey depth. The take home message is that while a built-in VBT depth-normalization algorithm would have been useful, it wouldn't have had any effect on E2 or FD, nor would it have addressed the issue of imperfect TVG compensation (which RoxAnn and ECHO*plus* lack altogether).

Another critical discovery made in this chapter resulted was gleaned from scatterplots of depth-normalized, log-transformed, and 1/99 percentile-filtered E1 and E2 values, with the individual records color-coded by benthic habitat class. The 38 and 418 kHz E1vsE2 scatterplots both appeared more like shotgun scatter than clusters. But taking a heart-cut of the data, i.e. the 20-80 percentile computed individually for E1 and E2 by habitat class, revealed that the acoustics did

indeed create clear groupings (although considerable overlap remained between some). This simplistic single-frequency bivariate refinement was later expanded to the multiple-frequency multivariate technique of refining training datasets by multiple passes through discriminant analysis algorithms, used throughout the remaining chapters.

ABSTRACT

Producing thematic coral reef benthic habitat maps from single-beam acoustic backscatter has been hindered by uncertainties in interpreting the acoustic energy parameters E1 (~roughness) and E2 (~hardness), typically limiting such maps to sediment classification schemes. In this study acoustic interpretation was guided by high-resolution LIDAR (Light Detection And Ranging) bathymetry. Each acoustic record, acquired from a BioSonics DT-X echosounder and multiplexed 38 and 418 kHz transducers, was paired with a spatially-coincident value of a LIDAR-derived proxy for topographic complexity (Reef-Volume) and its membership to one of eight LIDAR-delineated benthic habitat classes. The discriminatory capabilities of the 38 and 418 kHz signals were generally similar. Individually, the E1 and E2 parameters of both frequencies differentiated between levels of LIDAR Reef-Volume and most benthic habitat classes, but could not unambiguously delineate benthic habitats. Plotted in E1:E2 Cartesian space, both frequencies formed two main groupings: uncolonized sand habitats and colonized reefal habitats. E1 and E2 were significantly correlated at both frequencies; positively over the sand habitats and negatively over the reefal habitats, where the scattering influence of epibenthic biota strengthened the E1:E2 interdependence. However, sufficient independence existed between E1 and E2 to clearly delineate habitats using the multi-echo E1/E2 Bottom Ratio method. The point-by-point calibration provided by the LIDAR data was essential for resolving the uncertainties surrounding the factors informing the acoustic parameters in a large, survey-scale dataset. The findings of this study indicate that properly interpreted single-beam acoustic data can be used to thematically categorize coral reef benthic habitats.

1.1 INTRODUCTION

Considerable effort has been spent on defining the operational and ecological parameters within which single-beam Acoustic Ground Discrimination Systems (AGDS) can be used for benthic classification. Their popularity is largely due to their relatively low cost, ease of deployment, rapid assessment potential, and comparative insensitivity to water column effects. Hamilton (2001) and Penrose et al. (2005) provide comprehensive reviews of commercially available AGDS, their underlying physics and principles of operation, and case studies. The common approach to acoustic seabed classification has been to use sediment classification as a surrogate for benthic habitat, using either the first-echo shape analysis approach of QTC View, or a multi-echo approach as with RoxAnn, ECHO*plus*, or BioSonics echosounders. There is an obvious need for thematic mapping of shallow-water coral reef habitats, and while progress has been made with single-beam AGDS, technical challenges to thematic classification remain (Halley and Bruce, 2007; Hamilton et al., 1999, Moyer et al. 2005, Riegl and Purkis, 2005; Walker, Riegl, and Dodge, 2008; White et al., 2003).

A major impediment to using the multi-echo approach for classifying topographically complex coral reef habitats is interpretation of the E1 (trailing edge of 1st echo) and E2 (complete 2nd echo) acoustic energy parameters. "E1 and E2 are often referred to as 'roughness' and 'hardness', implying measures of mechanical hardness and geometrical or physical roughness, but they are simply acoustic indices with some unknown relation to seabed conditions (Hamilton et al., 1999)." Several physical attributes associated with coral reef environments add to the list of uncertainties, e.g. patchiness, rocky outcrops, steep slopes. Other associated difficulties include an acoustic footprint that varies with depth and variable spatial and temporal presence of epibenthic biota. Physical properties of the seabed can rarely be satisfactorily related to values of

E1 and E2, due to constraints of time and expense with regards to conventional ground-truthing methods such as video drop cameras or scuba divers.

This paper presents the results of using a spatially co-located LIDAR survey as the backdrop for a point-by-point interpretation of acoustic data acquired from a single-beam multiple-frequency AGDS survey encompassing 2.3 km^2 of sand, hardbottom, and reefal habitats in the waters offshore Palm Beach County, FL. The linkage between topographic complexity and benthic habitat was validated by comparison of a LIDAR-derived proxy for topographic complexity, Reef-Volume, and the eight LIDAR-delineated benthic habitats within the study area. The relationships between the acoustic parameters and the physical properties of the seabed were examined by comparison of E1 and E2 values to the LIDAR Reef-Volume metric, and then to the eight benthic habitat classes. The discriminatory capabilities of the 38 and 418 kHz acoustic energy parameters were compared using the E1/E2 Bottom Ratio method to categorize the E1:E2 pairs into benthic habitat classes, and quantified using error matrices.

1.2. Methods

1.2.1 LIDAR Survey

In November 2002, a laser bathymetric survey was conducted by Tenix LADS Corporation of Australia, using the Laser Airborne Depth Sounder (LADS) system with a sounding rate of 900 Hz (3.24 million soundings per hour), a positioning accuracy of 95% at 5 m circular error probable (CEP), a horizontal sounding density of 4m x 4m, a swath width of 240 meters, area coverage of 64 Km^2/hr, and a depth range of up to 35m, depending on water clarity. This survey encompassed north Broward County, all of Palm Beach County, and southern Martin County, approximately 75 km in shoreline length, from the shore eastward to depths of ~40m. The entire survey area covered approximately 254 square kilometers of marine habitat.

1.2.2 Acoustic Survey

The acoustic survey of the study area was conducted on June 27-28, 2006 and extended from the nearshore sand flats (depth = 11 m) to the seaward slope of the outer reef terrace (depth = 35 m) offshore Palm Beach County, FL, encompassing an area of 2.3 km^2 (Figure 1.1).

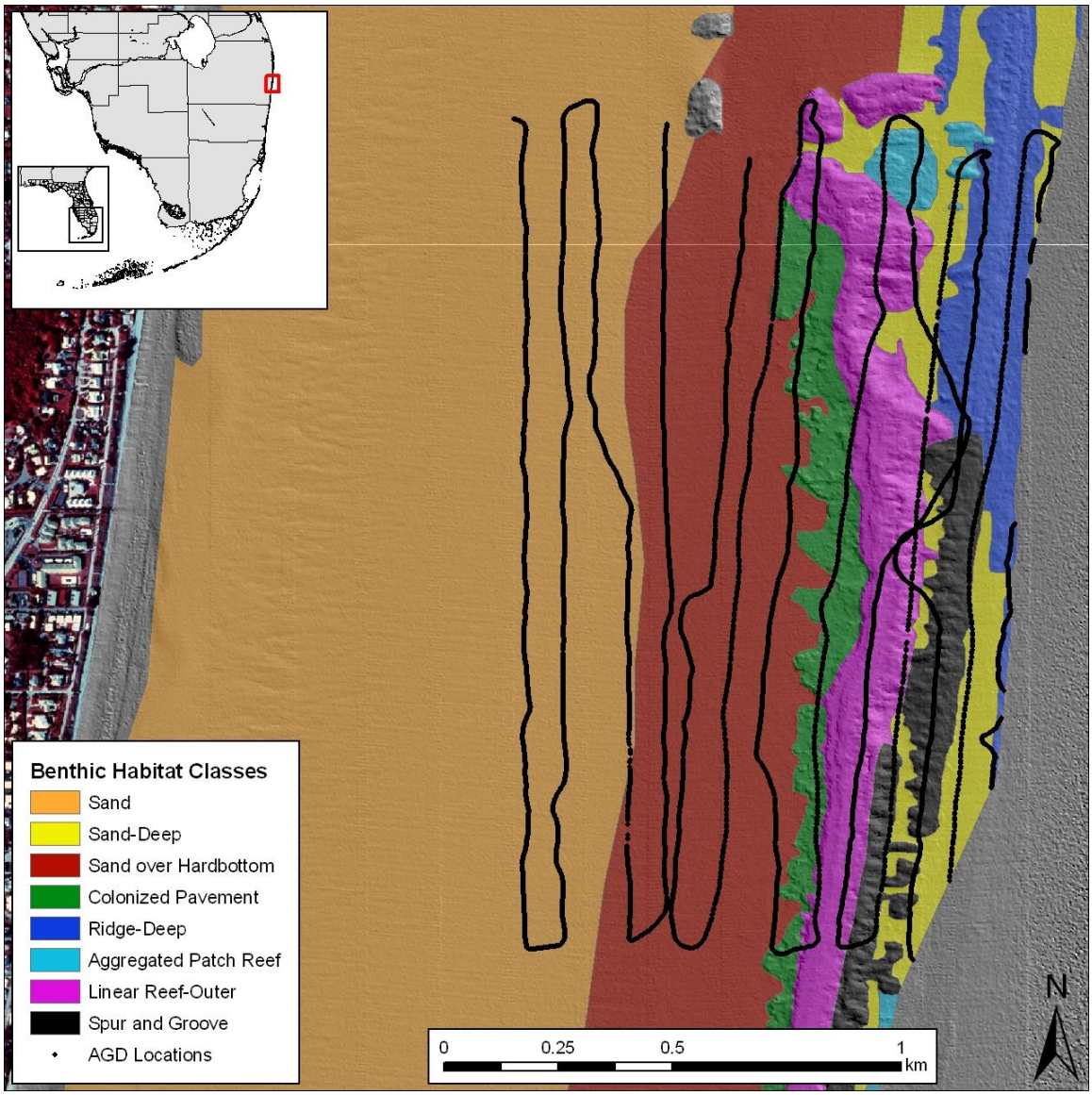

Figure 1.1 Acoustic survey track-lines (75m spacing) overlaying LIDAR bathymetry. Color shading denotes LIDAR-delineated benthic habitat classes.

The study site was part of a larger benthic habitat survey that covered all of Palm Beach County from depths of 3 - 35 m. Survey lines were spaced 75 m apart and ran parallel to the linear reef tract. Acoustic data was acquired with a BioSonics DT-X echosounder and two multiplexed, single-beam digital transducers operating at frequencies and full beamwidths of 38 kHz/10^{o} and 418 kHz/6.4^{o}, which produced footprint widths of approximately 11% and 17% of water depth, respectively. The pulse rate and duration of both transducers was 5 pings per second and 0.4 ms. The survey was conducted from a 7.5 m v-hull boat equipped with a rigid swing-arm onto which the two transducers were mounted front (38 kHz) to back (418 kHz), with the GPS antennae mounted directly above, for optimal integration of acoustical and positional data strings. Global positioning data were collected with a Trimble Ag132 dGPS system that provided an integrated NMEA GGA string to the navigational and BioSonics Visual Acquisition software. The GPS signal was differentially corrected against coast guard beacons and WAAS signal to achieve positioning accuracies less than 0.9 m horizontal dilution of precision. To avoid turbulence-induced signal contamination, evident as a rolling oscillation on the real-time BioSonics Visual Acquisition display, vessel speed was adjusted to maintain net speed (vessel+current) at approximately 4.5 knots.

1.2.3 Benthic Habitat Mapping

Benthic habitats were identified and outlined by visual interpretation of the LIDAR image in ArcGIS 9.3 at a scale of 1:6000 using a one acre minimum mapping unit. The LIDAR data were gridded by triangulation with linear interpolation, sun-shaded at a 45° angle and azimuth, and mosaicked with aerial photography of the land. This final image was used as the foundation for benthic habitat mapping along with video groundtruthing of the substrate and characterization of the epibenthic community. Accuracy assessment via confusion matrix approach yielded a total map accuracy of 89.2%. Further details of the mapping methodology can be found in Walker,

Riegl, and Dodge (2008). Brief descriptions of the benthic habitats present within the acoustic survey extent, derived from Kendall et al. (2001), include;

Sand: Coarse, unconsolidated sediment typically found in areas exposed to currents or wave energy.

Deep Sand: Sand habitat beyond the 25 m contour, with variable rubble content.

Sand over Hardbottom: A thin veneer of **s**and habitat covering uncolonized hardbottom, apparent as an undulating, stepped, or otherwise uneven surface underneath the sand.

Colonized Pavement: Flat, low-relief, solid carbonate rock with coverage of macroalgae, hard coral, gorgonians, and other sessile invertebrates that are dense enough to partially obscure the underlying carbonate rock

Ridge: Linear, shore-parallel, low-relief features that appear to be submerged cemented beach dunes. Characterized as hardground with variable and shifting sand cover and benthic communities, similar in community structure to Colonized Pavement but less abundant overall.

Aggregated Patch Reef: Clustered patch reefs that individually are too small or are too close together to map separately, interspersed in sand.

Linear Reef: Linear coral formations oriented parallel to shore; essentially forms the reef crest of the outer reef tract of Broward and Palm Beach Counties.

Spur and Groove: Alternating sand and coral formations oriented perpendicular to shore, occurring in the fore reef or bank/shelf escarpment of the outer reef tract.

1.2.4 Data Processing

The 38 and 418 kHz survey data were processed using BioSonics Visual Bottom Typer (VBT) seabed classification software (v1.10.6.3) to obtain values of the integrated energies (dB) of the E1 (2^{nd} half of 1^{st} echo) and E2 (complete 2^{nd} echo) echo envelopes. Critical values of user-defined parameters used for both frequencies include; bottom sampling windows of 25 (E1′), 75 (E1), and 150 samples (E2), time-varied gain = 20 logR, minimum data processing filter threshold (dB) = -75, pings per report = 5, and energy filter = 50%. The energy filter was useful for maintaining echo stability over the reefal terrains of this study, as observed by Hamilton et al. (1999), who suggested using the average of the one-third highest values in a ping set under the assumption that higher energy returns are least affected by roughness effects.

The raw energy values of E1 and E2 were passed through 2.5 and 97.5 percentile filters, calculated individually for each of the four acoustic parameters. Because the current version of VBT does not normalize echoes to a reference depth (Dommisse et al., 2005), the percentile-filtered E1 and E2 values were empirically normalized to the average survey depth using third-order polynomials fit to each of the four acoustic energy parameters (Figure 1.2). The depth-correction models were constructed from data collected from and adjacent to the study area, and constrained to the relatively featureless sand and deep sand habitats, where depth could be assumed to be the primary factor affecting the echo returns.

A GIS-measured Reef-Volume value from the LIDAR dataset was calculated for each acoustic record. A 7.62 m diameter circular polygon was created around each acoustic data point location (Figure 1.3). Then the volume of reef below the 3-dimensional LIDAR surface to the maximum

depth within each polygon was calculated in ArcView 3.3 using the "Surface Tools (v.1.6)" extension (Jenness, 2006). These data were then classified according to their benthic habitat

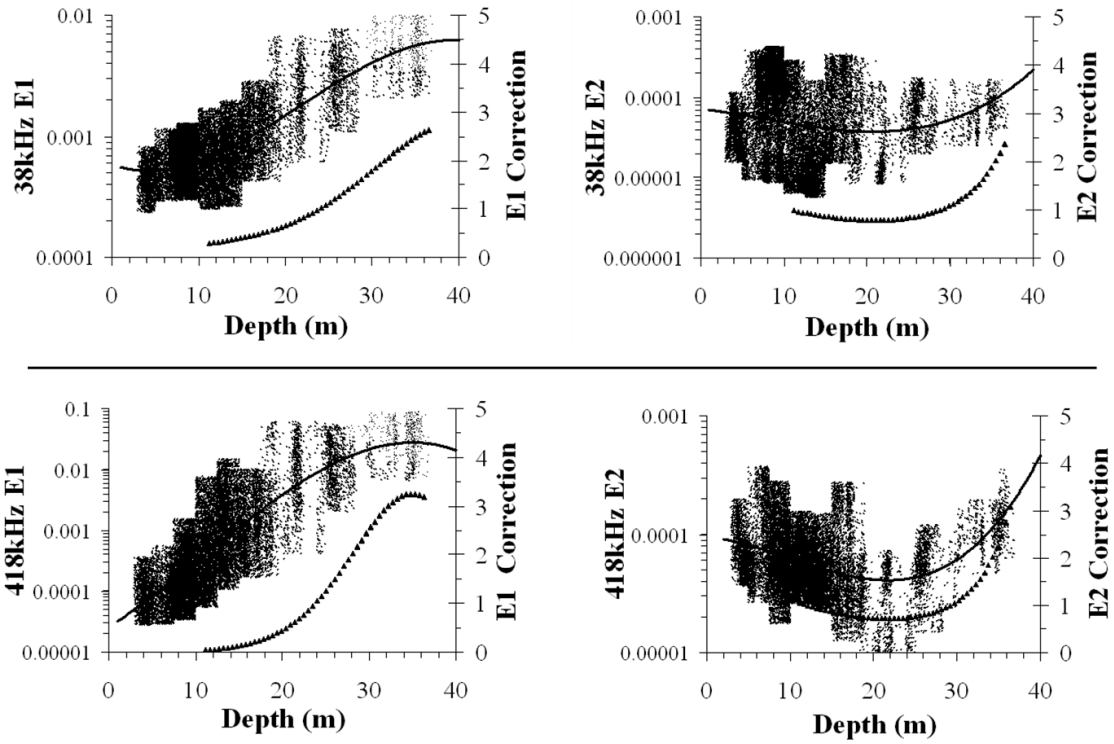

Figure 1.2 Normalization of acoustic energy parameters to average survey depth, using data collected over sand and deep sand habitats within and adjacent to the survey area. (Solid Line) Third-order polynomial fit to data. (▲) Correction factors derived from polynomial.

association. Each of the four merged acoustic datasets was sorted by benthic habitat class and outlying (+/- 3 σ) values of Reef-Volume and log-transformed values of E1 and E2 were removed from each dataset.

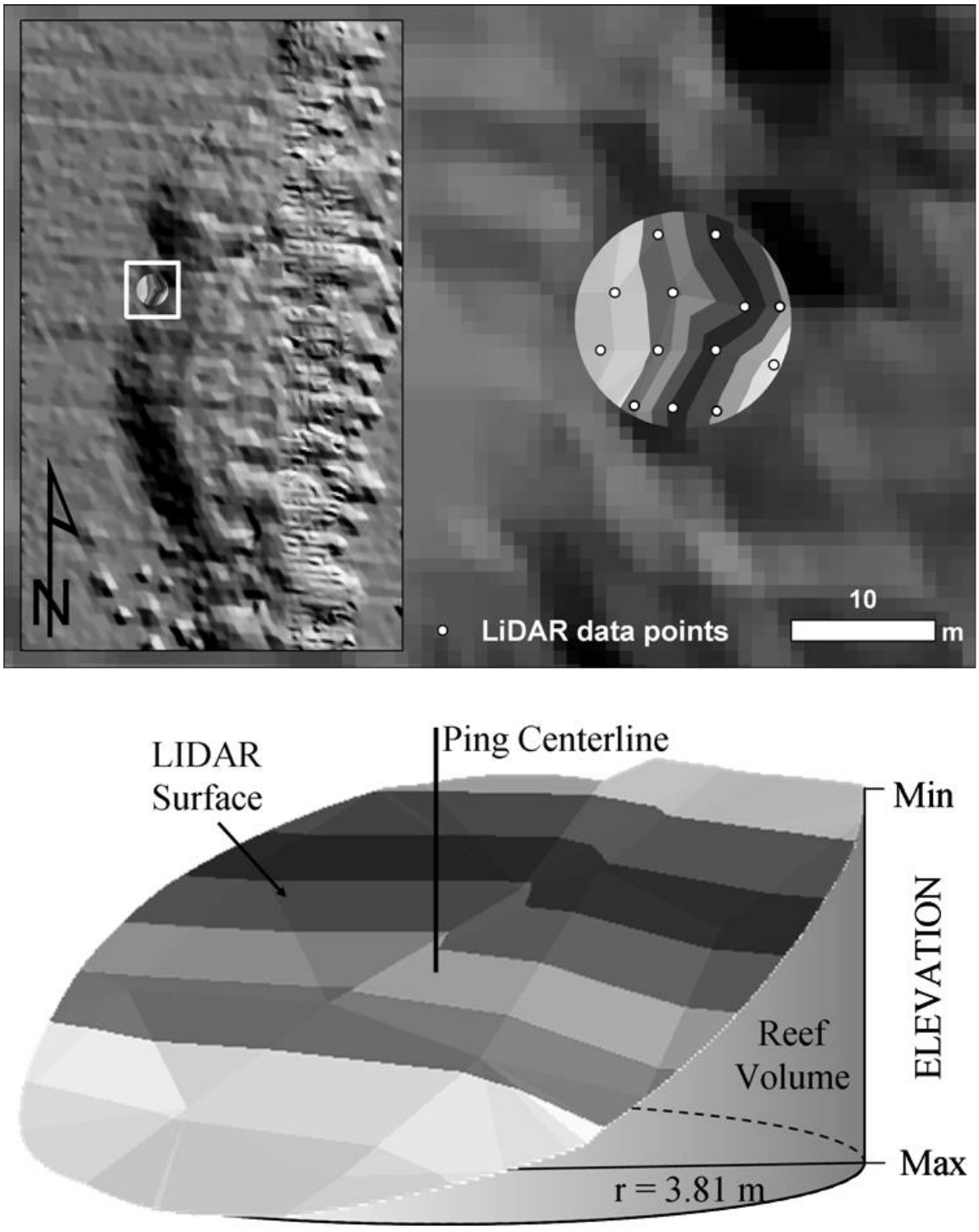

Figure 1.3 Example of Reef-Volume calculation. (Above) A single 7.62m diameter search buffer overlying LIDAR bathymetry. (Close-Up) Typical twelve LIDAR data points defining 3D LIDAR surface used for GIS-measurement of Reef-Volume (m^3). (Below) Illustration of Reef-Volume, defined as the volume beneath a LIDAR surface bound by a 7.62m diameter cylinder with height equal to ΔElevation. Reef-Volume in this example is 133 m^3 (90'th Percentile of study area).

1.2.5 E1/E2 Bottom Ratio Method

Acoustic habitat classification was performed using the E1:E2 Bottom Ratio Method developed by Orlowski (1984) and refined by Burns et al. (1989) and Chivers, Emerson, and Burns (1990). Depth-corrected, log-transformed, outlier-filtered (+/- 3 σ) acoustic data was further refined by passing though 20 and 80 percentile filters. The E1:E2 data-pairs were plotted onto a Cartesian XY plane and user-defined boxes were drawn around clusters of data representing benthic habitat classes. Predictive error matrices were produced from comparisons of acoustic versus LIDAR habitat classifications for records falling within the user-defined boxes.

1.2.6 EcoSAV Canopy Height

The 418 kHz acoustic data was also processed with BioSonics EcoSAV (v1.0) software, which predicts areal cover and canopy height of submerged aquatic vegetation (SAV) based on a series of pattern-recognition algorithms that detect plant features between the near-field and the trailing edge of the first echo (Guan et al., 1999; Sabol and Melton, 1996). The EcoSAV program was tuned by adjusting user-defined settings to account for a number of equipment and environmental variables, including transducer frequency and pulse duration, seabed sedimentary characteristics, and the acoustic strength and physical dimensions of the acoustic target, which in this study was erect gorgonian colonies. The most critical settings were the plant height detection threshold and the bottom detection threshold, which were set to 16 and 26 depth increments, respectively.

1.2.7 Ground-Truthing

Ground-truthing was conducted immediately following completion of the acoustic survey by deploying a weighted video camera overboard and recording 10-20 seconds of geo-referenced video with the vessel at idle speed. A total of 38 ground-truthing samples were taken within the acoustic survey perimeter along east-west corridors (334 such samples were taken for the total extent of the survey). The areal cover and canopy height of erect gorgonian colonies was

estimated from review of the video files.

1.2.8 Statistical Analysis

Post-hoc Tukey's honest significant difference (Tukey HSD) testing with a modification to control for sample size (Kramer, 1956) was used to test the discriminatory capability of (1) Reef-Volume to resolve benthic habitat class, (2) acoustic energy parameters to resolve values of Reef-Volume, and (3) acoustic energy parameters to resolve benthic habitat class. The Kolmogorov-Smirnov statistic was used to test assumptions of normality. The stability of E1 and E2 values over varying topographies was evaluated by coefficients of variation ($\sigma/\mu \cdot 100$) calculated for each of the four acoustic parameters at the seven arbitrarily-selected levels of Reef-Volume. The interdependence of the E1 and E2 parameters was quantified by the correlation coefficient (r), using the 20-80 percentile-filtered acoustic data. Discriminant analyses (Production Facility v11.0.0, SPSS Inc, Chicago, Illinois, USA) were used to assess the relative discriminatory powers of the four acoustic energy parameters to resolve levels of Reef-Volume and benthic habitat class, also using the 20-80 percentile acoustic data.

1.3. RESULTS

1.3.1 Reef-Volume vs. Benthic Habitat Class

The rankings and cumulative frequencies of LIDAR-derived Reef-Volume conformed to the visually apparent topographic complexity of the eight LIDAR-delineated benthic habitat classes (Figure 1.4). The featureless sand, deep sand, and sand over hardbottom habitats grouped on the low end of Reef-Volume measurements and the topographically complex linear reef and spur and groove habitats grouped on the high end. The colonized pavement (flat, low relief carbonate rock), aggregated patch reef (low to medium relief patch reefs interspersed in sand), and ridge

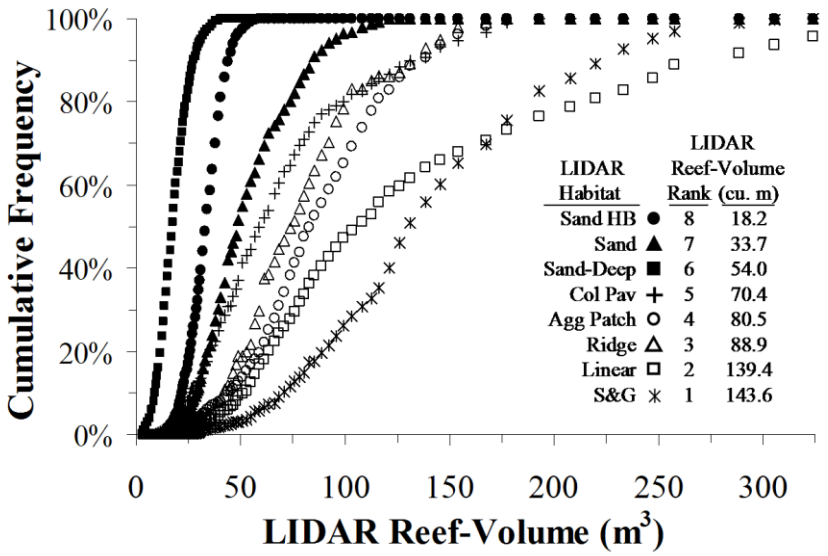

Figure 1.4 Cumulative frequencies and averages of LIDAR-derived Reef-Volume for the eight LIDAR-delineated benthic habitat classes. Reef-Volume defined as the volume beneath a LIDAR surface bound by a 7.62m diameter cylinder with height equal to ΔElevation.

habitats (hardground with variable sand cover) fell midway along the continuum of Reef-Volume measurements, consistent with their intermediate or variable topographic complexity. Tukey HSD testing ($\alpha = 0.05$), with modification to control for sample size, showed the means of Reef-Volume to differ significantly between 89.3% of the $k \cdot (k-1)/2=21$ habitat comparisons (Table 1.1). This is not to say that LIDAR Reef-Volume is a suitable stand-alone parameter for benthic habitat classification, as there is considerable overlap between many of the habitat categories. For example, the cumulative frequencies of the colonized pavement, aggregated patch reef, and ridge habitats were co-mingled, as were the linear reef and spur and groove habitats. Dropping a vertical from where the former three habitats approach 100% cumulative frequency down to the latter two habitats reveals approximately 70% overlap between the five habitats (Figure 1.4).

1.3.2 E1 and E2 vs. Reef Volume

Regardless of Reef-Volume's unsuitability for stand-alone categorization, the finding of a high percentage of significant differences provided a basis for assessing the discriminatory capabilities

Table 1.1. Summary of Tukey HSD testing of LIDAR Reef-Volume for the eight LIDAR-delineated benthic habitat classes (±3σ outliers removed). Significant differences (α = 0.05) between means denoted by '≠'.

LIDAR ReefVolume - Tukey HSD						Means Different = 89.3%		
n	2090	2351	716	405	109	849	996	591
Habitat Class	Sand HB	Sand	Sand - Deep	Col Pav	Agg Patch	Ridge	Linear Reef	S&G
Sand HB		≠	≠	≠	≠	≠	≠	≠
Sand			≠	≠	≠	≠	≠	≠
Sand - Deep				≠	≠	≠	≠	≠
Col Pav					-	≠	≠	≠
Agg Patch						-	≠	≠
Ridge							≠	≠
Linear Reef								-
S&G								

of the acoustic energy parameters. The acoustic interpretation of topographic complexity was first examined by comparing E1 and E2 values to seven arbitrary levels of Reef-Volume. This intermediate step provided a bridge between Reef-Volume, a straight-forward quantitative interpretation of the LIDAR surface, and the more esoteric parameters E1 and E2. The acoustic interpretation of benthic habitat class was then assessed by comparing E1 and E2 to the eight LIDAR-delineated benthic habitats.

1.3.2.1 Reef-Volume: 38 kHz vs. 418 kHz

The interpretation of LIDAR Reef-Volume by the acoustic energy parameters was thoroughly consistent between the two frequencies, as judged by the cumulative frequencies and rankings of E1 and E2 values for the seven arbitrarily-selected ranges of Reef-Volume (Figure 1.5). Both 38 and 418 kHz E1's were positively correlated with Reef-Volume and both E2's were negatively correlated. That two frequencies at the extremes typically used for single-beam AGDS (Penrose

et al., 2005) should yield such similar results is not entirely surprising. Brekhovskikh and Lysanov (1982) reported that seabed roughness begins to play a dominant role over sediment class at frequencies greater than a few kHz, and it has been speculated that surficial sediments appear to dominate backscatter at frequencies in the range of 10-100 kHz (Applied Physics Laboratory, 1989).

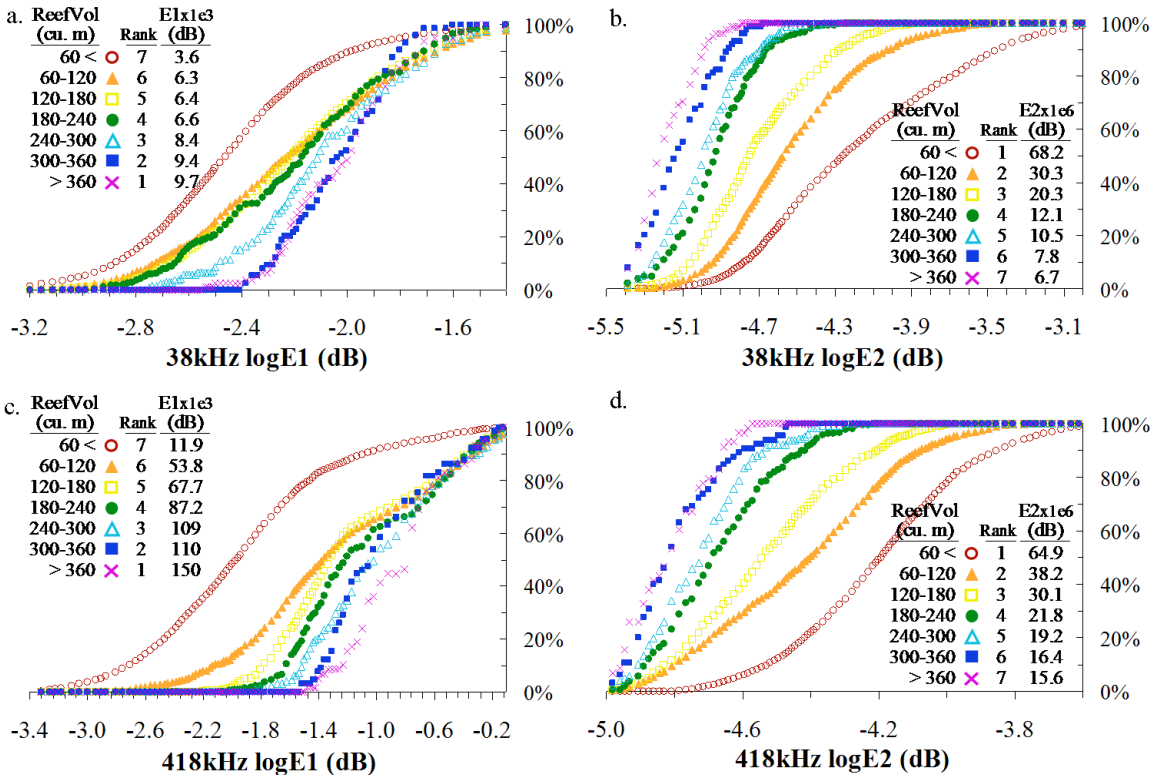

Figure 1.5 Acoustic interpretation of LIDAR Reef Volume. Cumulative frequencies of the depth-corrected and log-transformed acoustic energy parameters (a,c) E1 (2nd half of 1st echo) and (b,d) E2 (complete 2nd echo) for the seven arbitrarily-selected ranges of LIDAR Reef-Volume. Ranks are in order of increasing average values of acoustic energy parameters.

1.3.2.2 Reef-Volume: 38 kHz E1 vs. 418 kHz E1

The positive correlation of E1 with increasing Reef-Volume, i.e. topographic complexity, agrees with the general empirical rationale for seabed classification that a rougher seabed surface creates more scattering of the transmitted echo contacting the seabed at an oblique angle of incidence, increasing the proportion of signal returning to the transducer in the second half of the first echo,

i.e. E1 (Burczynski, 1999). The 418 kHz E1 provided greater discrimination than the 38 kHz E1, evidenced by larger gaps between individual trends of cumulative frequency and a larger range of E1 values (Figure 1.5a-c), and by the greater value of standardized canonical discriminant function coefficient (Table 1.2a). The four acoustic parameters showed no signs of instability over increasingly topographically complex terrain as judged by coefficients of variation calculated for each of the seven levels of Reef-Volume (Table 1.3).

Table 1.2 Standardized canonical discriminant function coefficients of the first discriminant function for (a) the seven arbitrarily-selected levels of LIDAR Reef-volume, and (b) the five consolidated benthic habitat classes used for the E1/E2 Bottom Ratio seabed classification method. Predictor variables were depth-corrected and log-transformed values of E1 and E2.

	Standardized Canonical Discriminant Function Coefficents							
	a. LIDAR Reef-Volume (7 Groups) 1st Discriminant Function				b. LIDAR Habitat Class (5 Groups) 1st Discriminant Function			
(kHz)	log E1	log E2	Variance	Canonical Correlation	log E1	log E2	Variance	Canonical Correlation
38	-0.471	**0.855**	98.4%	0.538	-0.580	**0.836**	76.7%	0.912
418	-0.570	**0.704**	97.8%	0.608	**0.820**	-0.629	94.2%	0.952

Table 1.3 Coefficients of Variation of the seven arbitrarily-selected levels of LIDAR-derived Reef-Volume, calculated individually for each of the four depth-corrected and log-transformed acoustic energy parameters.

Coefficient of Variation ($\sigma/\mu \cdot 100$) of Log-Transformed E Values								
		LIDAR Reef-Volume Levels (m^3)						
(kHz)	Echo	60<	60-120	120-180	180-240	240-300	300-360	>360
38	E1	-14.7	-18.1	-16.6	-16.0	-14.9	-9.2	-10.9
38	E2	-12.1	-7.8	-6.4	-4.5	-4.2	-3.7	-2.9
418	E1	-32.7	-51.9	-44.0	-45.4	-45.5	-37.5	-40.0
418	E2	-6.1	-6.2	-5.0	-3.6	-3.1	-2.8	-2.4

1.3.2.3 Reef-Volume: 38 kHz E2 vs. 418 kHz E2

The E2 parameter of both frequencies steadily decreased with increasing values of LIDAR Reef-Volume (and hence seabed hardness), in the exact reverse order of E1 (Figure 1.5). This could at first be seen as a contradiction to the general empirical rationale for seabed classification, which would have the multi-path E2 increasing, not decreasing, with increasing seabed hardness. But specular reflection is related to seabed hardness only for a flat surface (Burczynski, 1999). The 38 kHz E2 provided greater discrimination than the 418 kHz E2, evidenced by larger gaps between trends of cumulative frequency and a larger range of E2 values (Figure 1.5b-d), and by the greater value of the standardized canonical discriminant function coefficient (Table 1.2a).

1.3.2.4 Reef-Volume: Acoustic Discrimination

Tukey HSD testing ($\alpha = 0.05$) showed significant differences between the means of all four acoustic parameters for most of the seven arbitrarily-assigned ranges of LIDAR Reef-Volume. The E2 parameters of both frequencies provided greater discrimination; significant differences were found in 85.7 and 81.0% of the $k \cdot (k-1)/2=21$ comparisons for the 38 and 418 kHz E2 parameters, respectively, compared to 66.7 and 61.9% for the 38 and 418 kHz E1 parameters (Table 1.4). The greater discrimination of E2 at both 38 and 418 kHz was also evidenced by the greater values of standardized canonical discriminant function coefficients (Table 1.2a). The greater acuity of the E2 parameter is presumably a result of both E1 and E2 being controlled by seabed roughness, affecting the multi-path E2 more than the single-path E1.

Having established statistically significant relationships between; (1) the LIDAR-delineated benthic habitat classes and the LIDAR-derived Reef-Volume, and (2) Reef-Volume and the acoustic parameters E1 and E2, the final step was to evaluate the relationships between the acoustic parameters and the benthic habitat classes.

Table 1.4 Summary of Tukey HSD testing of depth-corrected and log-transformed acoustic energy parameters E1 and E2 for the seven arbitrarily-selected ranges of LIDAR Reef-Volume (m^3). ±3σ outliers removed for normality. Significant differences (α = 0.05) between means denoted by '≠'. 38 kHz E1 and E2 results in upper- and lower-left corners, 418 kHz E1 and E2 results in upper- and lower-right corners, respectively.

Tukey HSD - Differences Between Means: 38E1=66.7%, 38E2=85.7%, 418E1=61.9%, 418E2=81.0%													
log38kHz n	5350		1496		661		239		139		74		81	
log418kHz n	4877		1380		591		215		127		65		58	
Reef Volume	60 <		60 - 120		120 - 180		180 - 240		240 - 300		300 - 360		> 360	
60 <	38E1	418E1	≠	≠	≠	≠	≠	≠	≠	≠	≠	≠	≠	≠
	38E2	418E2	≠	≠	≠	≠	≠	≠	≠	≠	≠	≠	≠	≠
60 - 120					-	≠	-	≠	≠	≠	≠	≠	≠	≠
					≠	≠	≠	≠	≠	≠	≠	≠	≠	≠
120 - 180							-	-	≠	≠	≠	-	≠	≠
							≠	≠	≠	≠	≠	≠	≠	≠
180 - 240									-	-	≠	-	≠	-
									-	-	≠	≠	≠	≠
240 - 300											-	-	-	-
											-	-	≠	-
300 - 360													-	-
													-	-
> 360														

1.3.3 Habitat Class: 38 kHz vs. 418 kHz

The interpretation of the eight benthic habitat classes by the four acoustic energy parameters was very similar between the two frequencies, as judged by the cumulative frequencies and rankings of the averages of acoustic energy parameters (Figure 1.6). The 38 and 418 kHz E1 rankings were the same for four of the eight habitat classes and differed by only one place for the other four habitat classes (Figure 1.6a,c, Table 1.5). The 38 and 418 kHz E2 rankings were the same for six of the eight habitat classes and differed by only one place for the other two habitat classes (Figure 1.6b,d, Table 1.5).

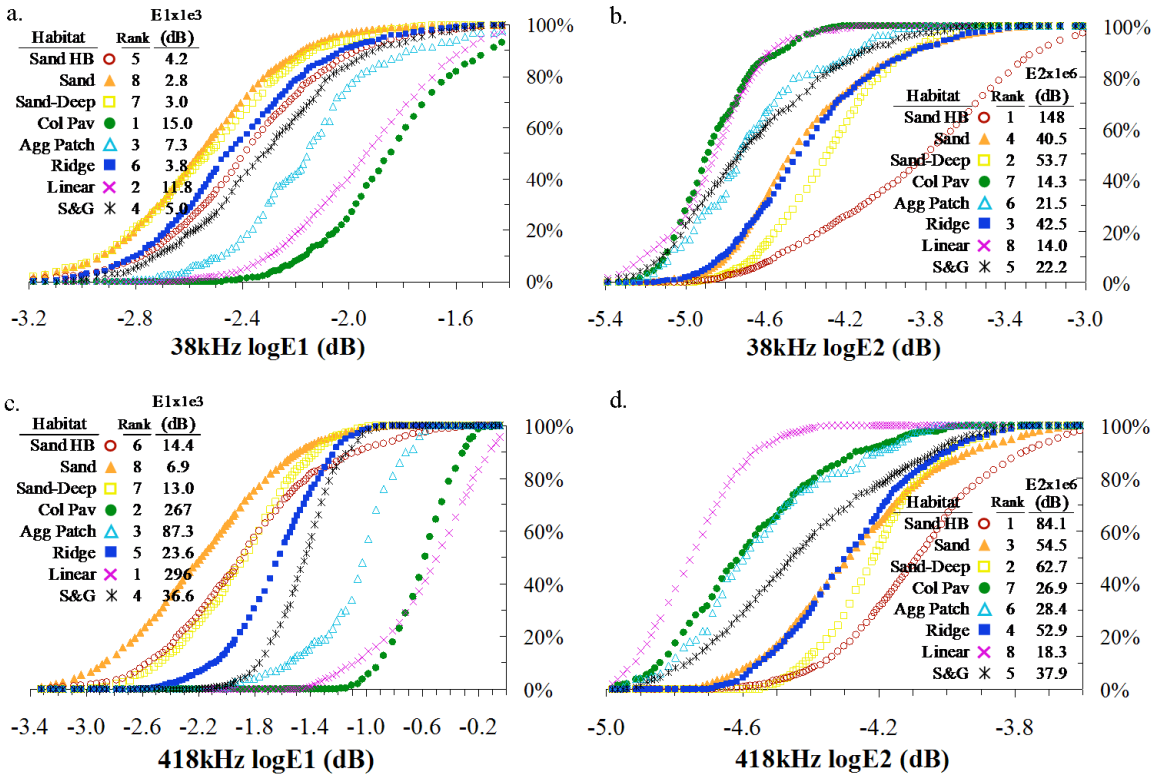

Figure 1.6 Cumulative frequencies of the depth-corrected and log-transformed acoustic energy parameters E1 (2nd half of 1st echo) and E2 (complete 2nd echo) for the eight LIDAR-delineated benthic habitat classes. Ranks are in order of increasing average values of acoustic energy parameters.

Table 1.5 Summary of the ranking orders of the eight LIDAR-delineated benthic habitat classes by the 38 and 418 kHz E1 and E2 (depth-corrected and log-transformed), and by the LIDAR-derived proxy for topographic complexity, Reef-Volume.

38kHz E1	Order Ascend	Sand	Sand-Deep	Ridge	Sand HB	Spur & Groove	Aggreg. Patch	Linear Reef	Colon. Pave.
38kHz E2	Order Descend	Sand HB	Sand-Deep	Ridge	Sand	Spur & Groove	Aggreg. Patch	Colon. Pave.	Linear Reef
418kHz E1	Order Ascend	Sand	Sand-Deep	Sand HB	Ridge	Spur & Groove	Aggreg. Patch	Colon. Pave.	Linear Reef
418kHz E2	Order Descend	Sand HB	Sand-Deep	Sand	Ridge	Spur & Groove	Aggreg. Patch	Colon. Pave.	Linear Reef
Reef Volume	Order Ascend	Sand HB	Sand	Sand-Deep	Colon. Pave.	Aggreg. Patch	Ridge	Linear Reef	Spur & Groove

1.3.3.1 Habitat Class: 38 kHz E1 vs. 418 kHz E1

The E1 parameters of both frequencies were positively correlated with the visually interpreted ordering of topographic complexity of the eight benthic habitat classes, consistent with the positive correlation between E1 and Reef-Volume found in the previous section. The sand, deep sand, and sand over hardbottom habitats grouped on the low-end of E1 values for both 38 and 418 kHz frequencies, consistent with the visually apparent flatness of those substrates and the low values of Reef-Volume. The spur and groove and aggregated patch reef habitats grouped in the mid-range of both E1 values, and the colonized pavement and linear reef habitats grouped on the high-end of both E1 values. The aggregated patch reef and linear reef rankings were consistent with the visually apparent topographic complexity and Reef-Volume rankings, but the colonized pavement had higher than expected E1 values and the spur and groove habitat had lower than expected E1 values. The 418 kHz E1 provided greater discrimination than the 38 kHz E1, evidenced by larger gaps between individual trends of cumulative frequency and a larger range of E1 values (Figure 1.6a,c), and by the greater value of standardized canonical discriminant function coefficient (Table 1.2b).

1.3.3.2 Habitat Class: 38 kHz E2 vs. 418 kHz E2

The E2 rankings of both frequencies were generally in reverse order to the E1 rankings, particularly at 418 kHz, where only the ordering of the sand and sand over hardbottom categories differed (Table 1.5). The reverse-ordering by E1 and E2 rankings was also observed for the seven ranges of LIDAR Reef-Volume, indicating both E1 and E2 are primarily informed by seabed roughness. Increased roughness created more incoherent backscatter, which increased the value of E1 and decreased the value of E2, as the incoherent backscatter was less likely to complete the multi-path circuit. The 38 kHz E2 provided greater discrimination than the 418 kHz E2 as judged by the greater value of standardized canonical discriminant function coefficient (Table 1.2b), which was heavily weighted by the sand over hardbottom class at 38 kHz.

Otherwise, the gaps between individual trends of cumulative frequency and the range of E2 values (Figure 1.6b,d) were not clearly different at the two frequencies.

The sole exception to E1:E2 reverse-ordering was the sand over hardbottom category, for which the 38 kHz E1 was expectedly low and the 38 kHz E2 unusually high, clearly standing out from the other habitats (Figure 1.6a-b). The sand over hardbottom habitat is characterized as flat, solid carbonate rock covered by a layer of coarse carbonate sediment typically a few centimeters thick. That exceptionally high E2 values were recorded at 38 kHz but not at 418 kHz suggests the lower frequency penetrated the thin surficial carbonate sediments to a greater extent and allowed the underlying carbonate rock to act as a subsurface reflector. Greenstreet et al. (1997) speculated that a 38 kHz echo could penetrate as far as 1 m into the seabed depending on sediment density and water content. That supports the observed differences between the 38 and 418 kHz signals, as does the finding of greater sediment penetration at 40 kHz than at 208 kHz reported by Schlagintweit (1993).

1.3.3.3 Epibenthic Biota: Detection and Influence

For the acoustic parameters to rationally order the benthic habitats differently than Reef-Volume, some factor other than topographic complexity must be informing the acoustic parameters. This factor is believed to be the presence of erect colonies of gorgonians, which are locally abundant and variable within and between the reefal and hardbottom habitats of Palm Beach County, FL. To test this idea the 418 kHz acoustic data was processed with BioSonics EcoSAV software, which predicts areal cover and canopy height of submerged aquatic vegetation based on a series of pattern-recognition algorithms that detect plant features between the near-field and the trailing edge of the first echo (Guan et al., 1999; Sabol and Melton, 1996). To obtain meaningful information related to gorgonian abundance, the user-defined parameters were adjusted to force the EcoSAV algorithms to predict near-complete areal coverage, and the resultant plant canopy

height estimates (adjusted to achieve zero height for sand habitat) were used as a proxy for gorgonian abundance (Table 1.6). The colonized pavement habitat, which had higher values of E1 than would be expected from the visually apparent topographic complexity and LIDAR Reef-Volume, was found to have the highest average of EcoSAV-predicted canopy height. The ridge habitat, which ranked third by Reef-Volume but only sixth and fifth by the 38 and 418 kHz E1 values, ranked fifth by predicted canopy height. The spur and groove habitat, which had the highest average Reef-Volume but ranked fifth by both the 38 and 418 kHz E1 values, ranked sixth by predicted canopy height. All suggest that signal scattering within the canopy of erect gorgonian colonies was significantly informing the values of the E1 parameter. Groundtruthing within the survey area generally supported the EcoSAV predictions, though more intensive sampling is necessary for full validation.

Table 1.6 Average predicted Canopy Heights of the eight LIDAR-delineated benthic habitat classes obtained from processing the 418 kHz signal with BioSonics EcoSAV software. Average Canopy Height is a surrogate measure of abundance of erect colonies of gorgonians.

EcoSAV Predicted Canopy Height (m)							
Sand	Sand HB	Sand Deep	Ridge	Agg Patch	Spur& Groove	Linear Reef	Col Pav
0.00	0.00	0.06	0.11	0.26	0.29	0.34	0.36

Assuming the larger than expected E1 values of the colonized pavement and linear reef habitats was due to the presence of gorgonian colonies, it can be inferred that E1 was more informed by scattering from the gorgonian canopy at 418 kHz than at 38 kHz. The composite E1 value of the colonized pavement and linear reef habitats (two highest EcoSAV-predicted gorgonian abundances) was 470% greater than the composite E1 of the aggregated patch reef / ridge / spur and groove habitats at 418 kHz, versus 150% at 38 kHz. The greater sensitivity of the 418 kHz signal to the presence of gorgonians is presumed to relate to its shorter wavelength (approximately 0.37 cm versus 4.04 cm at 38 kHz), which is well below the typical branch

thicknesses of the *Pseudoplexaura* spp. and *Pseudopterogoria* spp. that dominate the denser patches of large erect gorgonian colonies on the deep reefs of Palm Beach County. Kloser (2001) also reported that echo energies related to a combination of seabed hardness and roughness attributes, including epibenthic biota, and that the acoustic relationships were frequency dependent.

1.3.3.4 Habitat Class: Acoustic Discrimination

Tukey HSD testing ($\alpha = 0.05$) confirmed significant differences between the means of all four acoustic parameters for most of the benthic habitat comparisons. Significant differences were found in 96.4, 89.3, 92.9, and 92.9% of the $k \cdot (k-1)/2=28$ comparisons for 38 kHz E1, 38 kHz E2, 418 kHz E1 and 418 kHz E2, respectively (Table 1.7), comparing favorably to the number of significant differences (89.3%) found in the same analysis using LIDAR Reef-Volume (Table 1.1). While finding such a high percentage of significant differences is useful for validating the potential discriminatory power of the acoustic parameters, in practice the significant but small differences in means of individual E1 and E2 parameters would be difficult to exploit in a classification scheme, as there is considerable overlap between classes (Figure 1.6a-d).

1.3.5 E1/E2 Bottom Ratio Method

The discriminatory potential of the 38 and 418 kHz acoustic energy parameters were further evaluated using the E1/E2 Bottom Ratio method developed by Orlowski (1984), refined by Burns et al. (1989) and Chivers, Emerson, and Burns (1990), and first commercialized by SonaVision, Ltd for their Rox-Ann product line, from which it came to be known as the RoxAnn Squares method. To reduce overlap between habitat classes and facilitate the arbitrary boundaries of E1:E2 boxes, only the 20-80 percentiles of E1 and E2 values were plotted (Figure 1.7). The original eight LIDAR-delineated benthic habitat classes were consolidated to five by combining sand + deep sand and colonized pavement + linear reef (38 and 418 kHz), aggregated patch reef +

spur and groove Reef (38 kHz) and ridge + spur and groove (418 kHz). The overall predictive accuracies using the same 20-80 percentile training data were similar for the two frequencies, 79.8% at 38 kHz and 82.3% at 418 kHz (Table 1.8). Submitting the complete dataset, sans 20-80 percentile filtering, to the same five E1:E2 boxes reduced overall accuracies to 51.6% at 38 kHz and 58.0% at 418 kHz. These reductions in accuracy reflected the fact that some reefal habitats were a mixture of substrate types, e.g. the aggregated patch reef habitat was a mosaic of patch reefs interspersed in sand.

Table 1.7 Summary of Tukey HSD testing of E1 (2nd half of 1st echo) and E2 (complete 2nd echo) for the eight LIDAR-delineated benthic habitat classes. ±3σ outliers removed for normality. Significant differences (α = 0.05) between means denoted by '≠'. 38 kHz E1 and E2 results in upper- and lower-left corners, 418 kHz E1 and E2 results in upper- and lower-right corners, respectively.

Tukey HSD - Differences Between Means: 38logE1=96.4%, 38logE2=89.3%, 418logE1=92.9%, 418logE2=92.9%															
log38kHz	n	2049	2296	695	388	107	828	942	578						
log418kHz	n	1833	2167	628	386	100	742	811	522						
Habitat Class		Sand HB	Sand	Sand - Deep	Col Pav	Agg Patch	Ridge	Linear Reef	Spur & Groove						
Sand HB	38E1 418E1		≠ ≠	≠ -	≠ ≠	≠ ≠	≠ ≠	≠ ≠	≠ ≠						
	38E2 418E2		≠ ≠	≠ ≠	≠ ≠	≠ ≠	≠ ≠	≠ ≠	≠ ≠						
Sand				- ≠	≠ ≠	≠ ≠	≠ ≠	≠ ≠	≠ ≠						
				≠ ≠	≠ ≠	≠ ≠	- -	≠ ≠	≠ ≠						
Sand - Deep					≠ ≠	≠ ≠	≠ ≠	≠ ≠	≠ ≠						
					≠ ≠	≠ ≠	≠ ≠	≠ ≠	≠ ≠						
Col Pav						≠ ≠	≠ ≠	≠ -	≠ ≠						
						≠ -	≠ ≠	- ≠	≠ ≠						
Agg Patch							≠ ≠	≠ ≠	≠ ≠						
							≠ ≠	≠ ≠	- ≠						
Ridge								≠ ≠	≠ ≠						
								≠ ≠	≠ ≠						
Linear Reef									≠ ≠						
									≠ ≠						
Spur & Groove															

Table 1.8 Error matrix for E1/E2 Bottom Method seabed classification of depth-corrected and log-transformed E1:E2 pairs into the LIDAR-delineated benthic habitat classes, consolidated to five classes for the 20-80 percentile sub-set of (a) 38 kHz data and (b) 418 kHz data.

a.

38 kHz	LIDAR-Delineated Benthic Habitat Class						
E1:E2 Acoustic Class	Sand & Sand-Deep	Sand Over Hard Bottom	Ridge	Agg. Patch + Spur& Groove	Col. Pav. & Linear	Total Rows	User Accuracy
Sand & Sand-Deep	990	104	217	50	0	1361	72.7%
Sand Over HardBottom	0	573	0	0	0	573	100.0%
Ridge	64	45	95	40	1	245	38.8%
Agg. Patch + Spur&Groove	0	7	0	145	9	161	90.1%
Col. Pav. & Linear Reef	0	0	0	39	471	510	92.4%
Total Columns	1054	729	312	274	481	2850	
Producer Accuracy	93.9%	78.6%	30.4%	52.9%	97.9%		79.8%

b.

418 kHz	LIDAR-Delineated Benthic Habitat Class						
E1:E2 Acoustic Class	Sand & Sand-Deep	Sand Over Hard Bottom	Ridge + Spur& Groove	Aggregate Patch Reef	Col. Pav. & Linear	Total Rows	User Accuracy
Sand & Sand-Deep	941	212	77	0	0	1230	76.5%
Sand Over HardBottom	36	376	0	0	0	412	91.3%
Ridge	47	76	377	10	0	510	73.9%
Aggregate Patch Reef	0	0	0	47	5	52	90.4%
Col. Pav. & Linear Reef	0	0	0	7	439	446	98.4%
Total Columns	1024	664	454	64	444	2650	
Producer Accuracy	91.9%	56.6%	83.0%	73.4%	98.9%		82.3%

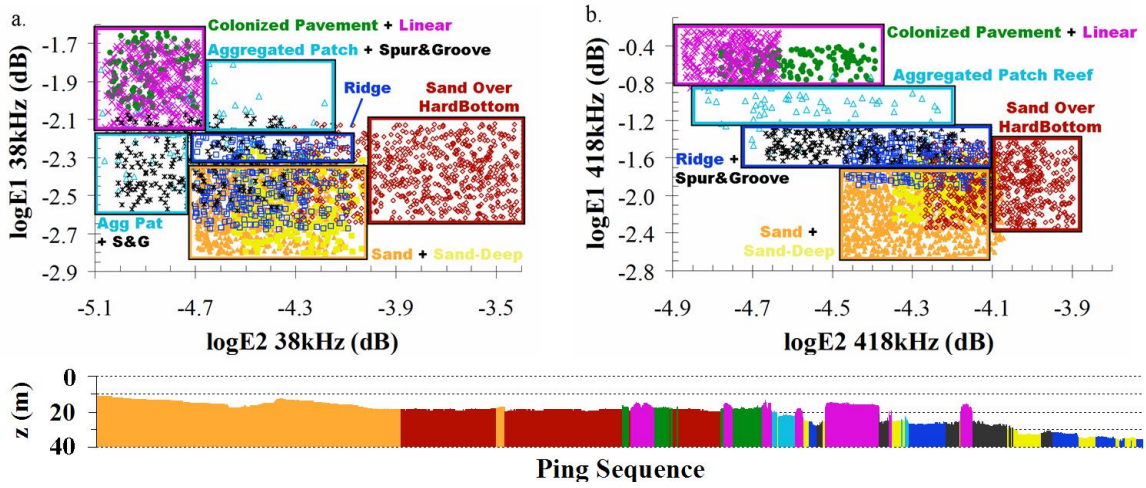

Figure 1.7 Values of E1 and E2, reduced to a 20-80 percentile sub-set, plotted in the XY Cartesian space of the E1/E2 Bottom Ratio classification method for the (a) 38 kHz signal and (b) 418 kHz signal. Boxes denote E1:E2 boundaries used for accuracy assessment of training dataset, with corresponding labels denoting LIDAR-delinated benthic habitat class membership within each. (Below) Depth profile of the eight LIDAR-delineated benthic habitat classes in order of acquisition and belonging to the 20-80 percentile sub-set.

1.4. DISCUSSION

The findings of this study indicate that single-beam acoustic data acquired with a BioSonics DT-X echosounder can be used to classify coral reef benthic habitats at either 38 or 418 kHz, using the multi-echo E1/E2 Bottom Ratio Method (Chivers, Emerson, and Burns, 1990; Orlowski, 1984), also known as the RoxAnn Squares Method (Burns et al., 1989). A precondition to this statement is that E1 and E2 values must be corrected for depth, as the current version of BioSonics VBT seabed classification software does not normalize echoes to a reference depth (Dommisse et al., 2005). That proviso was addressed in this study by empirically normalizing E1 and E2 values to the average survey depth using third-order polynomials fit to each of the four acoustic energy parameters (Figure 1.2). Another critical prerequisite for categorization of the five reefal habitats present in the study area was the finding of stable and meaningful values of the E1 and E2 parameters over the rocky, rough reefal terrain, as discussed in the following two sections.

1.4.1 Acoustic Discrimination: LIDAR Reef-Volume

The rankings of the 38 and 418 kHz E1 parameters ordered the seven arbitrarily-selected levels of Reef-Volume in strict ascending order while the E2 parameters ordered Reef-Volume in strict descending order, indicating a clear and rational acoustic interpretation of topographic complexity (Figure 1.5). However, Tukey HSD analyses revealed only one significant difference between the 240-300, 300-360, and >360 m^3 ranges of Reef-Volume (Table 1.4), indicating that the discriminatory capability of all four acoustic parameters diminished at the upper end of topographic complexity. Because values of Reef-Volume greater than 240 m^3 were strictly limited to the linear and spur and groove reefs, it can be further stated that acoustic discrimination diminished over the roughest areas of the most topographically complex reefal habitats. While these upper ranges of Reef-Volume represented only 18% of the 1587 records taken over the

linear and spur and groove reefs, it is nonetheless important to investigate the possible causes for diminished acoustic acuity before making general conclusions regarding the efficacy of acoustic classification.

One possible explanation for diminishing acuity could be instability of the E1 or E2 values over increasingly rough surfaces, as suggested by Lurton and Pouliquen (1992) and McKinney and Anderson (1964). However, none of the four acoustic energy parameters exhibited instability with increasing seabed roughness as judged by coefficients of variation (Table 1.3). Another possible explanation, based on general observations from video ground-truthing of the most rugose sections of reef habitat, is that at the upper ranges of Reef-Volume the horizontal scale of seabed variability dropped below what was detectable by the acoustic footprint (Rukavina 1997). The mean depth of records with Reef-Volumes exceeding 240 m^3 was 20.3 m, at which the diameter of the 38 and 418 kHz footprints would be 3.6 and 2.3 m, respectively. The repeating units of relict coral spires and surrounding valleys, typical of the roughest areas of the linear and spur and groove reefs, did indeed appear in the ground-truthing videos to occur at a sub-footprint scale, though controlled experimentation would be required for confirmation.

Alternatively (or additionally), the highest values of Reef-Volume could have coincided with areas characterized by inclinations large enough to interfere with echo acquisition. Voulgaris and Collins (1990) quote Jagodzinski (1960) as follows: "the second echo cannot be received unless the inclination of the bottom is smaller than the half beamwidth of the receiving oscillator. As a result the second echo may in some cases not be recorded, especially in the case of rocky bottoms…". Von Szalay and McConnaughey (2002) reported that bottom inclinations exceeding 5-8^o resulted in a total breakdown of QTC View classifications for two QTC View systems utilizing 38 kHz transducers with beamwidths of 7°x7° and 9°x13°, due to increased echo duration and side-lobe interactions affecting the shape of the first echo return. Gleason et al.

(2006) also observed highest QTC acoustic variability at the greatest substratum inclination. A small minority (approx. 10%) of records with Reef-Volumes in excess of 240 m^3 did fall near reef/sand breaks, where the sudden change in elevation could be great enough to interfere with signal acquisition. Most of the remaining 90% of points fell on the crest and slope of the linear and spur and groove reefs. Inclination measurements taken on the linear and spur and groove reefs in adjoining Broward County, FL ranged from 2.7-2.9^o on the crest and 3.2-7.6^o on the slope. These inclinations are either approaching or greater than the half-beamwidths of the 38 and 418 kHz transducers used in this study, yet the E2 value was not absent, or erratic (Hamilton, Mulhearn, and Poeckert, 1999), but simply smaller over the reefal habits compared to the sand habitats. The smaller values of E2 collected over the areas of high inclination could be due in part to the second echo return interacting less with the main beam and more with the side lobes (personal comm. Janusz Burczynksi).

If sub-footprint seabed roughness or high seabed inclinations were the only factors suppressing the values of E2 recorded over rough terrain, one would expect the flattest, hardest, and least colonized regions of the reefal habitats to occasionally produce values of E2 greater than those recorded over the softer sand or sand over hardbottom habitats. However, at 418 kHz the percentage of E2 records exceeding the 90th percentile of the composite sand classes (sand, deep sand, sand over hardbottom) was only 0.25% for the composite of colonized pavement, aggregated patch, and linear reef habitats and 4% for the composite of the ridge plus spur and groove habitats. This suggests the cause of consistently diminished values of E2 recorded over reefal habitats was instead the result of seabed roughness being the primary factor controlling both E1 and E2. The potential for the harder substrata of the reefal habitats to produce large values of E2 was overshadowed by the greater proportion of incoherent backscatter produced by the combined contribution of seabed roughness and epibenthic biota. The incoherent backscatter from the hard but rough reefal substrata increased the value of E1, in accordance with the general

empirical rationale for seabed classification, and likewise decreased the value of E2, as the incoherent backscatter would be less likely to complete the multi-path circuit. Similar results were reported by Riegl et al. (2007), and both suggest the values of E1 and E2 recorded over the rocky, rough habitats are indeed meaningful, although the effects of sub-footprint seabed roughness and high seabed inclination are likely contributing to the diminishing acoustic acuity at the highest levels of seabed roughness.

1.4.2 Acoustic Discrimination: E1/E2

The orientation of the sand, deep sand, and sand over hardbottom benthic habitat classes within E1:E2 space was generally the same as those of Greenstreet et al. (1997), Magorrian, Service, and Clarke (1995), and Chivers, Emerson, and Burns (1990), with the rougher and harder sand over hardbottom class positioned to the upper right (higher E1 and E2) of the smoother and softer sand classes. The remaining five reefal habitats, rather than continuing up and to the right as did the gravel and rock classes of Chivers, Emerson, and Burns (1990), are instead up and to the left of the sand habitats (higher E1, lower E2), supporting the idea that a positive correlation between seabed hardness and E2 is valid only for a flat surface (Burczynski, 1999).

While the effects of seabed inclination cannot be disregarded without controlled experiments, the relative orientations of individual reefal habitats in E1:E2 space offer the same alternative explanation for the low E2 values recorded over the rocky, rough substrata; that over reefal habitats, E1 and E2 are both primarily informed by the combined substrate plus epibenthic biota scattering components. For example, the relatively flat colonized pavement habitat grouped with the linear reef habitat in the upper-left corner of E1:E2 Cartesian space (Figure 1.7). These two habitats differ markedly in inclination and rugosity but have in common a high EcoSAV-predicted gorgonian abundance. Furthermore, the two habitats are less intermingled at 418 kHz than at 38 kHz, presumably due to the shorter wavelength of the 418 kHz signal being more

sensitive to between-habitat differences in gorgonian abundance. A second example is how the rugose spur and groove habitat grouped with the relatively flat ridge habitat, to the left and just above the sand habitats. These two reefal habitats also differ markedly in inclination but have in common a low EcoSAV-predicted gorgonian abundance. The grouping in E1:E2 space of habitats with disparate substrata but similar gorgonian abundance is in agreement with the findings of Kloser (2001), who reported that echo energies relate to a combination of seabed hardness and roughness attributes, including epibenthic biota.

To summarize, examination of the relationship of acoustic parameters to LIDAR Reef-Volume and to the orientation of habitat classes in E1:E2 space both suggest that meaningful acoustic discrimination of the rocky, rough reefal habitats is possible, although the underlying physical relationships remain to be uncovered through controlled experimentation.

1.4.3 Additional Insights: E1 and E2 Correlation

Distinctions between the discriminatory powers of the two frequencies can be inferred from the degree to which the E1 and E2 parameters were correlated. The correlation between E1 and E2 was examined for both frequencies at two different regions in E1:E2 Cartesian space, using the same 20-80 percentile sub-sets of acoustic data used in the E1/E2 Bottom Ratio analyses. Group 1 included the sand, deep sand, and sand over hardbottom classes. The orientation of these habitats conformed to the upward trend along the E1:E2 diagonal reported by Chivers, Emerson, and Burns (1990); Greenstreet et al. (1997); Magorrian, Service, and Clarke (1995); and Wilding, Sayer, and Provost (2003) for RoxAnn data. Group 2 included the remaining five reefal benthic habitat classes, which exhibited a general downward trend along the E1:E2 diagonal. The correlation coefficient (r) of the log-transformed E1 and E2 values was significant ($P < 0.0005$) for both groups and both frequencies. Wilding, Sayer, and Provost (2003) also reported significant correlations between E1 and E2 for RoxAnn data collected in Loch Linnhe, Scotland.

The E1:E2 correlation coefficient was slightly but significantly greater at 38 kHz than at 418 kHz for Group 1, 0.44 versus 0.34 ($P < 0.0005$). The finding of significant, positive correlations between E1 and E2 for Group 1 is consistent with the rationale of harder ground having a greater capability of exhibiting roughness (Burns et al., 1989; Wilding, Sayer, and Provost, 2003. The E1:E2 correlation coefficient was significantly greater at 418 kHz than at 38 kHz for Group 2, -0.79 versus -0.59, respectively ($P < 0.0005$). The finding of significant, negative correlations between E1 and E2 for Group 2 is consistent with previous observations in this study that both E1 and E2 are informed by seabed roughness. The finding of a greater correlation between E1 and E2 at 418 kHz for Group 2 is also consistent with previous observations of the 418 kHz being more sensitive to the presence of epibenthic biota.

Hearns et al. (1993) indicated a need for RoxAnn polygons instead of squares due to the diagonal orientation of correlated E1:E2 data. Although E1 and E2 were found to be significantly correlated on the whole, the arrangement of E1:E2 data within the individual habitat boxes was orthogonal at both 38 and 418 kHz (Figure 1.7), indicating the use of square boxes was appropriate. Furthermore, whereas individual values of E1 and E2 were able to differentiate but not unambiguously delineate benthic habitat classes, due to considerable overlap between most classes (Figure 1.6), there existed sufficient independence between the two acoustic parameters, at both frequencies, to successfully delineate benthic habitats using the E1/E2 Bottom Ratio seabed classification method.

1.4.4 Selection of Acoustic Frequency

The acoustic interpretation of Reef-Volume was effectively the same at either 38 or 418 kHz. The E1 parameters of both frequencies ordered the seven arbitrarily-selected levels of Reef-Volume in strictly ascending order and the E2 parameters of both frequencies ordered Reef-Volume in strictly descending order, similar to what was observed by Hamilton, Mulhearn,

Poeckert (1999) and Voulgaris and Collins (1990) for RoxAnn E1 and E2 values. The acoustic interpretation of benthic habitat classes was also similar for the two frequencies, though not to the same extent as found for Reef-Volume, presumably due to habitat-specific scattering from the variably abundant patches of erect gorgonian colonies. Discriminant analyses, trends of cumulative frequencies, and the range of acoustic energy values all agreed that E1 provided greater discrimination of both Reef-Volume and benthic habitat class than E2 at 418 kHz, while E2 provided greater discrimination than E1 at 38 kHz. This follows from the higher frequency being more sensitive to scattering and the lower frequency being more sensitive to sediment factors, consistent with the relationship between frequency and habitat-discrimination revealed by the E1/E2 Bottom Ratio classification.

While the overall predictive accuracies of the 38 and 418 kHz signals were very similar, the question of which frequency performed best depended on seabed type, as suggested by Schlagintweit (1993). The 38 kHz signal provided superior discrimination between the nearshore sand habitat and the adjacent sand over hardbottom habitat, indicating that the lower frequency penetrated the thin surficial carbonate sediments to a greater extent and allowed the underlying carbonate rock to act as a subsurface reflector, effectively amplifying the E2 parameter (Greenstreet et al., 1997; Schlagintweit, 1993). The 38 kHz signal was less adept than the 418 kHz signal at discriminating between the intermediate-complexity reefal habitats and the sand habits. For example, approximately 70% of the 38 kHz E1:E2 pairs collected over the ridge habitat fell within the sand E1:E2 box, compared to just 29.6% at 418 kHz (Figure 1.7). Some acoustic confusion between habitats, regardless of frequency, was inevitable owing to the one acre minimum mapping unit used to delineate habitat classes, which resulted in some reefal habitats being constituted of a mixture of substrate classes. The greater acoustic confusion between the ridge and sand habitats at 38 kHz was likely due to the longer wavelength of the 38 kHz signal (4.04 cm versus 0.37 cm at 418 kHz) interacting less with the canopy of erect

gorgonian colonies variably present in the ridge habitat but absent in the nearshore sand habitat. Similarly, the 418 kHz signal better separated the colonized pavement and linear reef habitats from the other reefal habitats, due to a greater proportion of signal scattering contributing to E1 at 418 kHz than at 38 kHz, but provided poor discrimination of the sand over hardbottom habitat from the sand and deep sand habitats. These observations support the opinion of Kloser (2001), that echo energies relate to a combination of seabed hardness and roughness attributes, including epibenthic biota, and that the acoustic relationships are frequency dependent.

1.5. CONCLUSIONS

Our study used spatially-coincident LIDAR bathymetry to quantitatively describe the acoustic interpretation of physical seabed characteristics over the extent of the survey area, instead of the common practice of using drop-video or scuba divers to collect validation data that may not adequately represent acoustic diversity. Inputs to the multi-echo classification method, E1 (2^{nd} half of 1^{st} echo) and E2 (complete 2^{nd} echo), were critically evaluated for discriminatory capability. The individual acoustic energy parameters E1 and E2, like the LIDAR-derived Reef-Volume metric, differentiated between but did not unambiguously delineate LIDAR-delineated benthic habitat class. Multiple lines of evidence indicated that in the presence of abundant signal-scattering epibenthic biota, e.g. erect colonies of gorgonians, both acoustic parameters were informed primarily by seabed roughness. Increasing seabed roughness created more incoherent backscatter, increasing the value of E1 and decreasing the value of E2, as incoherent backscatter was less likely to complete the multi-path circuit. In the absence of abundant signal-scattering epibenthic biota, E1 and E2 were positively correlated. Although E1 and E2 were significantly correlated at both frequencies, there existed sufficient independence between the two acoustic parameters to successfully delineate benthic habitats using the E1/E2 Bottom Ratio seabed classification method. By all measures, the 38 and 418 kHz signals performed similarly in terms

of detecting topographic complexity, substrate hardness, and the presence of epibenthic biota. The 418 kHz signal was found optimal for discriminating the rougher seabeds from a joint contribution of topographic complexity and the presence of epibenthic biota, owing largely to the shorter wavelength of the high-frequency signal. The 38 kHz signal was optimal for resolving the flat and comparatively featureless sand and sand over hardbottom habitats, owing to greater penetration of the lower-frequency signal. The comprehensive high-resolution LIDAR ground-truthing dataset was essential for these beginning steps towards uncovering the complicated relationships that exist between the acoustic energy parameters and the varied physical attributes of a coral reef environment.

ACKNOWLEDGEMENTS

We thank the various funding agencies that supported this work. This study was funded by DEP Agreement G0057 and NOAA Award NA160Z2440 to the Florida Marine Research Institute and National Coral Reef Institute. Special thanks to J. Bursczinsky and B. Moore at BioSonics Inc. for discussions and support, and to Kristi Foster for all her contributions to the acoustic survey.

Chapter 2: Mapping the Distribution and Abundance of Seasonal Drift Macroalgae in the Indian River Lagoon

FORWARD

Scientists at the St. Johns Water Management District have routinely conducted field surveys to estimate the distribution and abundance of seasonal drift macroalgae (DMA) blooms as a proxy for the location and degree of nutrient loading. While direct observations by snorkelers are unquestionably accurate, the costs associated with covering a system as large as the Indian River Lagoon limits the density of observations to widely-spaced spot checks. This was a tailor-made application for remote-sensing to provide abundant and affordable information to resource managers. Typically, an optical remote sensing method would have been utilized in this scenario, had the waters of Indian River Lagoon been clear enough. But most of the Indian River Lagoon is too turbid, and even if the DMA could have been imaged the varying species composition and seasonal cycle of pigmentation (from light green at the onset of the bloom to dark red at the end of the bloom) would have seriously complicated attempts at optical classification.

This is where acoustic remote sensing rose to the fore, with its relative insensitivity to water column effects and potential for differentiating drift macroalgae from other macrophytes by gross morphology (provided the numerous technical challenges presented by the environmental and biological variables could be overcome). At the time of writing, only two peer-reviewed studies of detecting submerged aquatic vegetation (SAV) using single-beam acoustic ground discrimination systems (AGDS) have been published, both using QTC systems (Riegl et al., 2005, Preston et al., 2006). The major hurdles to producing the desired acoustic mapping product were the shallow water depths, demonstrating temporal consistency, and the small and similar acoustic targets. The nature of these obstacles and their solutions are discussed below.

The depth of the Indian and Banana Rivers, excluding navigation channels, rarely exceeded 3 m. It is widely recognized that for a variety of reasons AGDS do not function well at depths shallower than 5 m. These reasons include the potential for insufficient sampling resulting from the very brief echoes (i.e. too few points to adequately define the wave envelope), clipping of waveforms due to insufficient dynamic range (i.e. to accommodate the high intensity returns), and collisions between the first and second echo returns (i.e. the second echo appears before the first echo fully dissipates). The problem of short echoes was not a major concern in this study, since acoustic energy parameters don't require many points to define the echo envelope. This is more of a concern for the QTC approach, which infers bottom features from fine details of wave envelope shape. Clipping was never observed, and a minimum depth filter of 1.3 m eliminated the problem of colliding echoes.

However, the time-varied gain compensation, which compensates for geometrical spreading and absorption losses, completely fell apart below 5 meters, resulting in extreme non-linear behaviors of the acoustic energy parameters with respect to depth. But the empirical depth-normalization procedure developed in Chapter 1 offered a workable solution to an otherwise intractable obstacle. Similar to Palm Beach County study, a depth-normalization dataset was constructed using 66 training samples ground-validated as bare (SAV<10%), so the only factor affecting the values of the acoustic parameters could be assumed to be related to depth. The general taboo of surveying in very shallow water was obvious from the 418 kHz depth normalization curves, typified by local minima and steep slopes which left un-treated would have overwhelmed the bottom signature with depth contamination.

Another technical hurdle was a need for temporal consistency, as this was proposed as a regular component of SJRWMD monitoring activities, i.e. the acoustically-derived estimates of drift macroalgae biomass estimates needed to be consistent from year to year. Temporal consistency

is not an attribute commonly associated with AGDS, but from a hardware standpoint the BioSonics transducers are unique in that the analog to digital conversion is performed within the transducer, removing the possibility for boat engine or electrical system noise to infiltrate the cable connecting the transducer to the data acquisition circuit board. The temporal consistency of the digital BioSonics system was clearly evident in a head-to-head comparison of 41 bare (SAV<10%) training samples collected during the April-May 2007 pilot program to 27 bare training samples collected during the lagoon-wide survey in April-May 2008. This also demonstrated spatial consistency, given that these samples were collected across the 120 km survey extent.

The final technical hurdle was the very small canopy heights of the targeted macrophytes; the DMA and SHORT SAV (typically *C. prolifera*) rarely exceeded 30 and 10 cm, respectively. Moreover, the DMA was frequently found overlying beds of *Syringodium filiforme* or *Caluerpa prolifera*. Attempting such a fine cut using a simplistic single-frequency E1vsE2 scatterplot (i.e. the RoxAnn Squares method) would not have yielded satisfactory discrimination (as graphically demonstrated later in this chapter). What was clearly needed was a multivariate technique that could utilize the full output of Visual Bottom Typer (i.e. 38 and 418 kHz E1′, E1, E2, and FD). Only one such instance of combining dual-frequencies into a single classification scheme has appeared in a refereed journal. Foster-Smith and Sotheran (2003) developed acoustic signatures for bottom classes within IDRISI using the E1, E2, acoustic variability, and depth obtained from two RoxAnn systems operated at 38 and 200 kHz; accuracy was found to improve from approximately 70% using either single 200 kHz, dual 200 kHz or dual 38 kHz to 88% using combined dual 38 and 200 kHz signals.

Of the various multivariate classification, clustering, and partitioning techniques, discriminant analysis (DA) was selected for a number of reasons. First and foremost, DA was designed to

maximize discrimination between pre-defined groups. Contrast this to principle components analysis, which is designed to minimize the potential for a Type II error. Similar to regression, DA produces a set of functions that can be used to classify new data (useful for very large survey datasets), as well as a large suite of interpretative statistics. DA also computes a probability of group membership, based on the user-selected distance (e.g. Mahalanobis) of the records from the group centroid.

DA was also well-suited to solve the problems associated with 'mixed' training samples. The 100+ training samples of this chapter were collected in the most efficient manner, with the vessel drifting in idle and the video camera trailing just beyond the sonar beam. At a typical drift velocity of 0.75 knots, the vessel traversed approximately 23 m over the course of a 60 second collection period. At this scale the bottom was frequently patchy, neither fully bare nor fully covered. Anchoring over 'pure' targets could have eliminated this problem, but would have been too laborious and time-consuming to collect so many replicate samples. Creating categories with multiple levels of cover would at first seem a potential workaround, until the issue of scale is fully considered. The acoustic footprints of the narrow-beam BioSonics transducers were only 0.22 m (418 kHz) and 0.35 m (38 kHz) at the average survey depth of 2.2 m. Such a small footprint meant that individual pings were generally pure, i.e. rafts of drift macroalgae were usually much larger than than acoustic footprint. So for a 60-second training sample acquired over 67% SAV, it was far more likely that 40 pings would ensonify 100% SAV and 20 would ensonify 0% SAV than it would be that 60 pings would ensonify 67% SAV. In other words, few of the individual waveforms constituting a 67% SAV training sample would actually encode information about a bottom with 67% cover. Most waveforms would have ensonified either bare bottom or near-complete cover. Attempting to cluster such a collection of hit/miss hydroacoustic records into categories of varying cover would clearly be ill-advised. The alternative and novel approach taken in this study was to instead refine the heterogeneous training samples into their

pure-end member components, i.e. BARE, SHORT SAV, or DMA. This was achieved by multiple-passes through discriminant analyses (DA), retaining only those records that classified correctly and exceeded a minimum probability of group membership. This refinement process also removed records from the SHORT SAV and DMA datasets for which the acoustic signal failed to detect the vegetative canopy. The set of Fisher's linear discriminant functions obtained from the final DA of the training dataset was then used to classify the survey data into one of three end-member categories; BARE, SHORT SAV, or DMA. This facilitated the ultimate goal of estimating the biomass of drift macroalgae, as the percent cover was easily computed as the percentage of "hits" within a group of ten records.

About EcoSAV - Prior to developing the multi-pass methodology, attempts were made to identify DMA using BioSonics EcoSAV software. EcoSAV was designed to predict the areal cover and canopy height of submerged aquatic vegetation (SAV), based on a series of heuristic pattern-recognition algorithms that look for "evidence" of plant features between the near-field and the trailing edge of the first echo. However, the DMA (and particularly the *C. prolifera*) presented too small a target for reliable detection. While it was possible to fine-tune EcoSAV to detect SAV in general, the plant feature encoded in the echo envelope was far too close to the noise threshold. This would require laborious re-tuning for the major categories of bottom sediment, as signal penetration into softer (bare) sediments created an echo envelope that EcoSAV mis-interpreted as SAV.

ABSTRACT

A large-scale acoustic survey was conducted in Apr-May 2008, with the objective of quantifying the abundance and distribution of seasonal drift macroalgae (DMA) in the Indian River Lagoon. Indian River was surveyed from the Sebastian Inlet to its northernmost extent in the Titusville area. Banana River was surveyed from its convergence with the Indian River northward to the Federal Manatee Zone near Cape Canaveral. The survey vessel was navigated along pre-planned lines running east-west and spaced 200 m apart. The river edges were surveyed to a minimum depth of approximately 1.3 m. Hydroacoustic data were collected with a BioSonics DT-X echosounder and two multi-plexed digital transducers operating at 38 and 418 kHz. The 38 and 418 kHz hydroacoustic data were processed with BioSonics Visual Bottom Typer (VBT) seabed classification software to obtain values of E1' (time integral of the squared amplitude of the 1st part of the 1st echo waveform), E1 (2nd part of 1st echo), E2 (complete 2nd echo), and FD (fractal dimension characterizing the shape of the 1st echo). Following quality analysis, a training dataset was compiled from 131 hydroacoustic + video samples collected across the extent of the study area. The 38 and 418 kHz E1', E1, E2, and FD datasets were merged and submitted to a series of three discriminant analyses (DA) to refine the training samples into three pure end-member categories; bare substrate, short SAV (typically *Caluerpa prolifera*, ~10cm or less), and DMA. The Fisher's linear discriminant functions from the third and final descriptive DA were used to classify each of the 480,000+ hydroacoustic survey records as either bare, short SAV, or DMA. The classified survey records were then used to calculate the biomass of DMA as the product of average DMA cover for a block of ten records times the wet weight of DMA. The DMA biomass was found to be 69,859 metric tons (wet weight) within the 293.1 km^2 study area. The acoustically-predicted mean percent cover of DMA was (i) significantly greater within the navigation channels (18.3%) than outside (12.2%), and (ii) significantly greater in the Indian River (12.9%) than in the Banana River (9.3%). The overall predictive accuracy of total SAV (i.e. short SAV plus DMA) was 78.9% (n=246) at three levels of cover (0-33, 33-66, and 66-

100%). The Tau coefficient, a measure of the improvement of the classification scheme over random assignment, was 0.683 ± 0.076 (95% CI), i.e. the rate of misclassifications was 68.3% less than would be expected from random assignment of hydroacoustic records to total SAV cover. The incorporation of multi-plexed digital transducers in conjunction with new post-processing techniques realized the goal of establishing an accurate, efficient, and temporally consistent method for acoustically mapping DMA biomass.

2.1 INTRODUCTION

Drainage of the St. Johns River marshlands for agricultural development began in the late 19th century and rapidly accelerated in the 1940's and 1950's. By the early 1970's nearly two-thirds of the historical marshlands had been drained. During this time a number of canals were also built to divert water from the Upper St. Johns Basin into the Indian River Lagoon. These and other hydrological alterations have subjected the estuarine Indian River Lagoon to pulses of freshwater and nutrient-rich agricultural runoff. Extensive commercial and residential development over past decades has added to the list of anthropogenic disturbances to water quality. Reduced water transparency, variable salinities, and elevated nutrient levels have contributed to a shift from seagrass to macroalgae. For example, the areal coverage of seagrass in the area of the Sebastian Inlet has declined by approximately 38% between the years 1951-1984 (Goodwin & Goodwin, 1976). In an effort to restore and preserve the lagoon, the IRL Program was created in 1996 under the leadership of the St. Johns River Water Management District. The immediate goals were to improve water and sediment quality and monitor seagrass beds, with an ultimate goal of reclaiming historical seagrass ranges. A component of this initiative involved a better understanding of seasonal drift macroalgae blooms, which (1) can exceed the biomass of seagrass in some areas of the lagoon (Virnstein & Carbonara, 1985), (2) exclude seagrass by shading (den Hartog, 1994), and (3) potentially act as a nutrient sink (Davis et al., 1983). Beginning in 2002 NCRI scientists began work on methods for the acoustic remote sensing of drift macroalgae using QTC and Echo*plus* echosounders (Riegl et al., 2005). In 2005, the author conducted the first lagoon-wide survey using a QTC echosounder. While these early attempts showed promise, predictive accuracies hovered near 50%. The results presented in this chapter begin in 2007, utilizing a BioSonics DT-X digital echosounder. It is with this system that the goal of an accurate and repeatable lagoon-wide survey of drift macroalgae biomass was first met.

2.2. METHODS

2.2.1 Survey Area

The acoustic survey was completed between the dates of April 1 - May 21, 2008, during the historic peak of drift macroalgae biomass. Indian River was surveyed from its origin in the Titusville area (28.7664^{o}N) southward to Wabasso, just below the Sebastian Inlet (27.8743^{o}N) (Appendix 2.A1). Banana River was surveyed from the Federal Manatee Zone near Cape Canaveral (28.4329^{o}N) southward to its convergence with Indian River in the Melbourne area (28.1571^{o}N). The survey vessel was navigated along pre-planned lines, running east-west and spaced 200 m apart. The depth of the water column ranged from 1.3 to 4.5 m and averaged 2.2 m.

2.2.2 Sonar Equipment

The survey was conducted from a 7.5 m v-hull boat with a 0.5 m draft (Figure 2.1). Hydroacoustic data was acquired with a BioSonics DT-X echosounder and two multiplexed, single-beam digital transducers with full beamwidths of 10^{o} (38 kHz) and 6.4^{o} (418 kHz), operated at 5-Hz sampling frequency and 0.4 ms pulse duration. The two transducers were located on a swing-arm mounted to the gunwale. The GPS antenna was mounted directly above for optimal integration of acoustical and positional data strings. Global positioning data were collected with a Trimble Ag132 dGPS, differentially corrected against the WAAS signal to achieve positioning accuracies less than 0.9 m horizontal dilution of precision. The dGPS signal was interfaced with navigational software to provide real-time monitoring of vessel position with respect to the aerial images and pre-planned survey lines. To avoid turbulence-induced signal contamination, evident as a rolling oscillation on the real-time Visual Acquisition display, vessel speed was adjusted to maintain a net speed (vessel+drift) of approximately 4.5 knots.

Figure 2.1 Survey equipment. (left) Swing-arm in horizontal (traveling) position with 420 and 38 kHz transducers and Trimble antenna. (middle) Inside v-berth of survey vessel with BioSonics DT-X echosounder, Trimble receiver, and acquisition PC. (right) Monitor displaying gps-navigation over pre-planned lines and real-time echo returns.

2.2.3 Data Processing

The 38 and 418 kHz hydroacoustic data were processed with BioSonics Visual Bottom Typer (VBT) seabed classification software (v1.10.6.3) to obtain values of E1' (time integral of the squared amplitude of the 1st part of the 1st echo waveform), E1 (2nd part of 1st echo), E2 (complete 2nd echo), and FD (fractal dimension characterizing the shape of the 1st echo). VBT allows the user to define the width of each Bottom Sampling Window in units of "samples", i.e. the 41,667 Hz clock-speed of the DT-X internal processor. This critical setting is better understood by converting to units of meters via the speed of sound in water, shown for representative echo envelopes acquired over bare substrate and over drift macroalgae (Figure 2.2). The split between E1' and E1 was set such that E1 would capture the trailing edge of the first echo. This emphasized sensitivity to the presence of SAV, as scattering from the vegetative canopy increases the proportion of signal returning to the transducer in the trailing edge of the first echo.

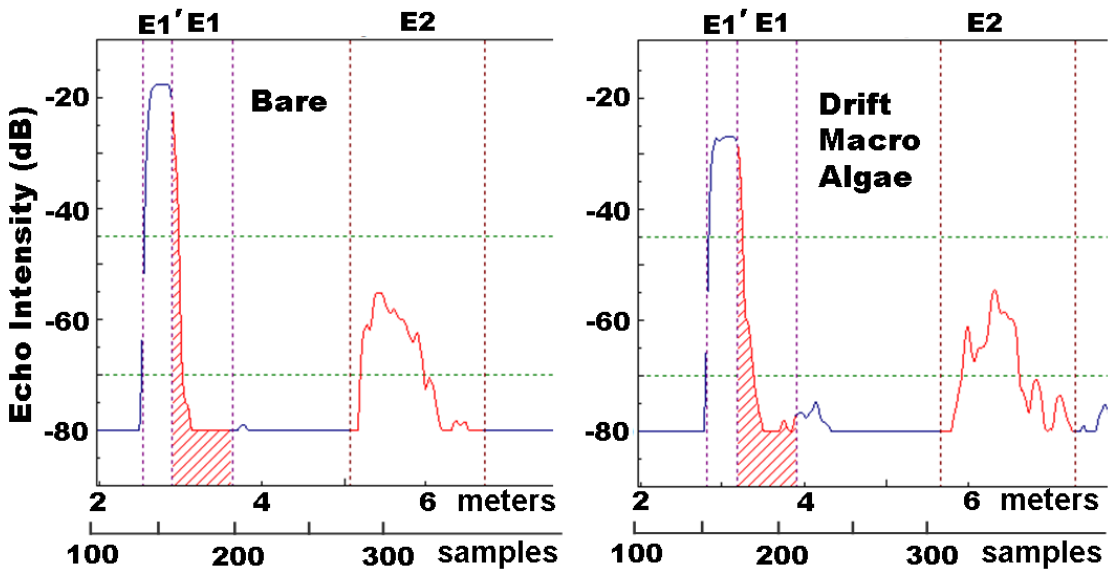

Figure 2.2 Representative waveforms acquired over bare substrate and drift macroalgae. The width of the E1′, E1, and E2 Bottom Sampling Windows are shown in units of samples (bottom scale) and in units of meters (top scale).

2.2.4 Quality Assurance

Log-transformed values of E1', E1, E2 and un-transformed values of FD were passed through a series of filters to identify and remove "irregular" hydroacoustic returns. The first filter checked the differential depth between successive pings against a specified maximum value. This filter removed waveforms that contacted the seabed at angles exceeding normal-incidence, typically caused by excessive vessel roll. The next filter removed records with depth-picks less than 1.3 m, at which point the first and second echo returns began to collide. The next filter removed records with depth-picks exceeding the 99.5 percentile recorded within a particular survey tile, usually the result of grossly misshapen waveforms. The remaining two filters protected against potentially excessive outliers by removing records for which any of the eight acoustic parameters fell beyond the 1 and 99 percentiles. Only those records for which all eight acoustic parameters passed all filters were passed onto the next stage of processing. Of the 600,000+ pings recorded

during the survey, approximately 20% were removed by the series of filters and the subsequent merging of the 38 and 418 kHz datasets.

2.2.5 Normalizing to Reference Depth

Depth normalization entails adjusting the width of the E1′ and E1 bottom sampling windows to maintain a consistent first echo division, as the echo predictably stretches and flattens with increasing depth. Because the current version of VBT does not normalize echo length to a reference depth, the log-transformed and filtered values of E1', E1, and E2 were empirically normalized to median survey depth to produce depth-invariant values of acoustic energy. Depth-normalization models were constructed using the "BARE" sub-set of the supervised catalog, for which it could be assumed that depth (via geometric spreading and absorption) was the primary factor affecting the shape of echo returns (and not varying abundance of SAV). Third-order polynomials were fit to plots of log(E) versus depth for each of the six acoustic energy parameters (Figure 2.3). Correction factors were applied to each hydroacoustic record, calculated as the ratio of model-predicted acoustic energy at actual depth divided by the model-predicted acoustic energy at the median depth. That depth-contamination of E2 implicates the TVG compensation for geometrical spreading and absorption losses, as E2 should not require normalization to a reference depth, given that the bottom sampling gate was adequately wide to capture the entire second echo across the range of depths.

2.2.6 Catalog Collection and Processing

A total of 195 training samples were collected within the study area, spanning the spectrum of vegetative cover. Each catalog sample consisted of a 30-90 second hydroacoustic file and a geo-referenced video file, acquired as the vessel drifted in idle. 109 catalog samples were collected

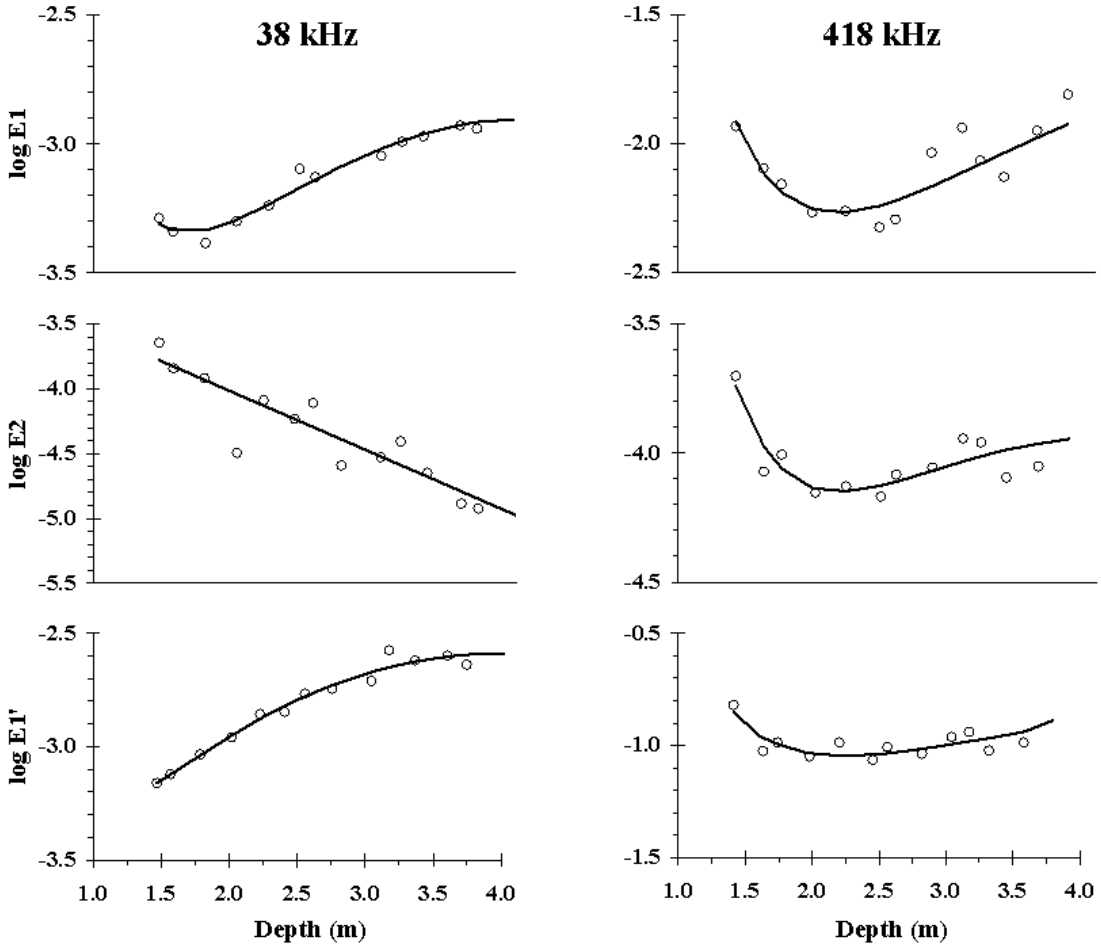

Figure 2.3 Empirical depth normalization. Depth trends of log-transformed echo returns (open circles) and fitted curves (solid lines) used for empirical depth-normalization of acoustic energy parameters. Data was limited to the "bare" sub-set of the supervised catalog, for which it could be assumed that depth, via geometric spreading, was the only factor affecting the echo return.

during the 2007 BioSonics trial and the remaining 86 were collected during the 2008 lagoon-wide survey. The catalog data was subjected to the same VBT post-processing, depth-normalization, and quality assurance as described previously for the survey data. 166 of the 195 catalog samples passed quality assurance, totaling 9,672 records. Most of the catalog samples that did not pass quality assurance were collected from depths of 1.0-1.3 m and were thus rejected by the minimum depth filter. Each video was reviewed post-survey and assigned a percent coverage of (1) bare substrate, (2) short SAV (~10cm<), and (3) drift macroalgae and tall SAV. Short SAV was typically *Caluerpa prolifera* but also included *Halophila spp*. and miscellaneous taxa of

macroalgae generally less than 10 cm tall. Tall SAV was predominantly *Syringodium filiforme* and occasionally *Thalassia testudinium*. In nearly every sample where tall SAV was observed, drift macroalgae was either interspersed between or overlying the tall SAV. Because of this, and the relatively low frequency of tall SAV compared to drift macroalgae, it was not attempted to acoustically distinguish tall SAV from drift macroalgae.

2.2.7 Selecting a Classification Scheme

Two factors dominated the selection of discriminant analysis (DA) as the appropriate classification scheme. First, the large number of acoustic survey records (500,000+) dictated a supervised classification scheme that would allow for post-hoc classification of survey records. Second, the need to distinguish between short SAV and drift macroalgae dictated a categorical classification scheme. Discriminant analysis was identified as the simplest and most established method meeting both these criteria, and was particularly desirable since it was designed to maximize between-group differences.

2.2.8 Creating the Classification Scheme

Ideally, the hydroacoustic records submitted to a DA classification scheme should be pure end-member classes, i.e. completely bare or contiguous SAV of a particular class. The catalog should also include as many locations as possible so that all ranges of depth and sediment class are adequately represented. Otherwise, extraneous geophysical factors could unknowingly inform the classification process. Because of the logistical difficulties of acquiring pure end-member hydroacoustic samples, e.g. finding and double-anchoring over a small patch of contiguous SAV, a novel method was developed for extracting pure end-member records from samples acquired over heterogeneous benthos.

The 166 catalog samples passing quality assurance were categorized based on the type and amount of SAV cover apparent in the accompanying videos. Samples with less than 10% total SAV cover were designated as BARE. Samples with greater than 33% cover of drift macroalgae and tall SAV were designated as DMA. Samples with greater than 50% cover of short SAV were designated as SHORT. 131 of the 166 catalog samples fell into one of these three categories, totally 7,523 records (Figure 2.4). 68 catalog samples were assigned to the BARE class; these samples had a weighted-average of 96% bare substrate. 29 catalog samples were assigned to the SHORT class; these samples had a weighted-average of 85% short SAV. 34 catalog samples were assigned to the DMA class; these samples had a weighted-average of 77% drift macroalgae and tall SAV.

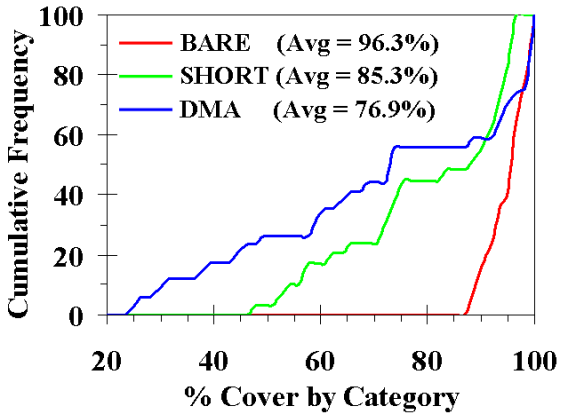

Figure 2.4 Overall 'purity' of training datasets, shown as cumulative frequencies of percent cover. BARE (68 individual 30-60 second samples), SHORT (29 samples), and DMA (34 samples). For example, 25% of the DMA training samples were >50% DMA cover. Values in parenthesis are the mean percent cover of the training samples constituting that category, e.g. the 68 BARE samples averaged 96.3% bare substrate.

Next, the 7,523 hydroacoustic records were passed through a series of three discriminant analyses, using the 38 and 418 kHz E1', E1, E2, and FD as predictor variables. Only those records that (1) correctly classed by the discriminant analysis and (2) exceeded a minimum

probability of group membership were passed onto the next DA (Figure 2.5). This had the effect of refining the training dataset into the desired end-member classes. For example, the small target offered by *C. prolifera* resulted in frequent false negatives, i.e. misses, within the SHORT training dataset. It was important to remove these misses, so as to distinguish them from truly bare pings. Conversely, hydroacoustic records acquired over bare sediment would need to be removed from a catalog sample characterized as 50% drift macroalgae and classified as DMA. Given the patchiness of vegetative cover, the close-coupling of acoustic + video ground-truthing was essential for this precise indexing of acoustic parameters to vegetative cover. Retaining only those samples with a relatively high level of targeted cover was found to be essential for successful classification, given the influence of well-defined group centroids on the critical 1st-Pass DA.

2.2.9 Classifying Hydroacoustic Records

Discriminant analysis generates a set of Fisher's linear discriminant functions, which are based on the linear combinations of predictor variables (38 and 418 kHz E1', E1, E2, FD) that provide the best discrimination between the groups represented in the catalog, i.e. bare, short SAV, and drift macroalgae (Figure 2.5). The Fisher's linear discriminant functions from the third-pass DA were used to classify survey records by multiplying each Fisher's coefficient by the value of the corresponding acoustic variable, summing the products, and adding the constant to get a score for each of the three categories (BARE, DMA, and SHORT). Each of the 500,000+ records was classified as the category with the largest score. The final layer of classification was to compute the percent cover of BARE, DMA, and SHORT assignments for a group of ten sequential acoustic records, yielding a total of 49,592 geo-located records.

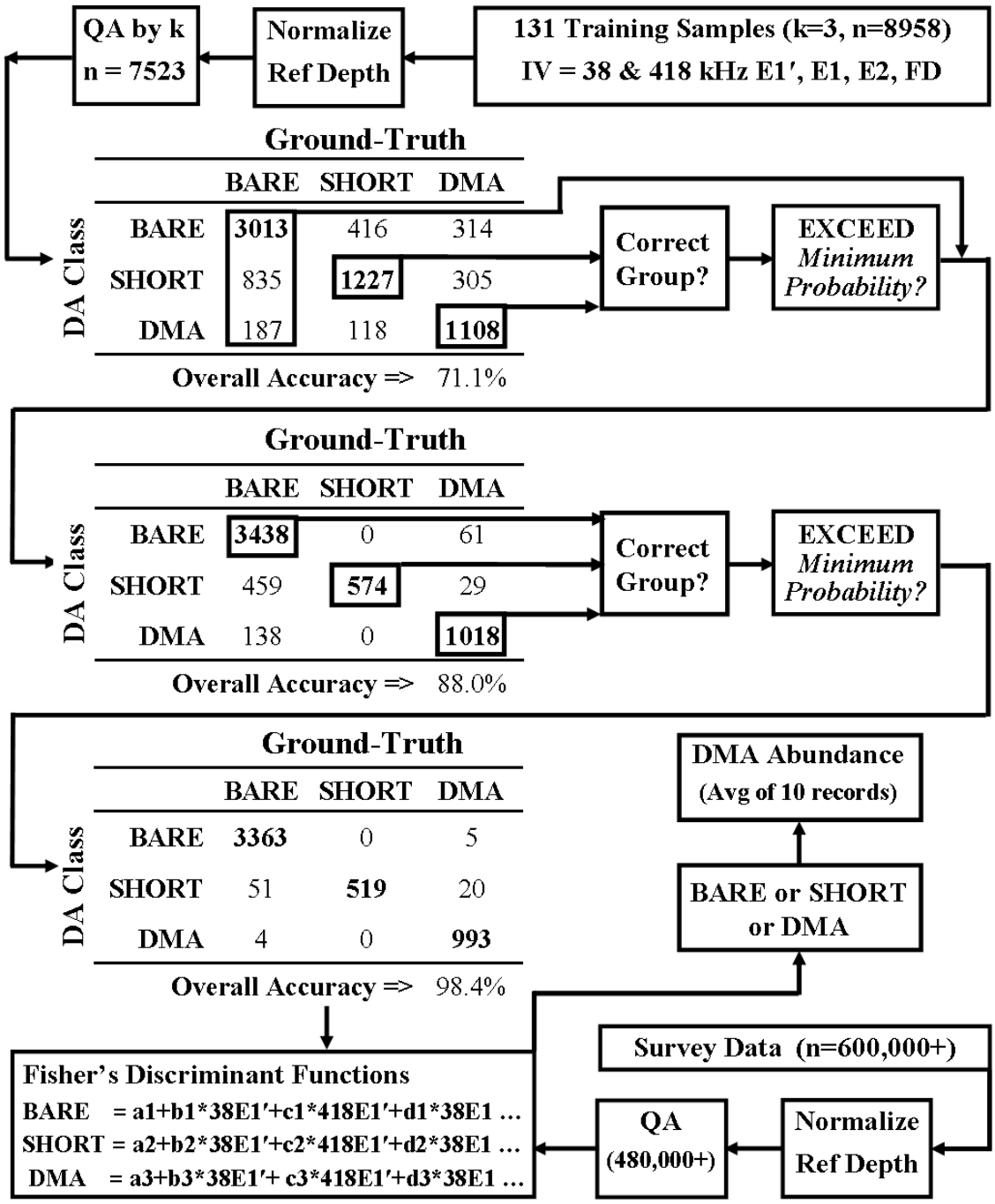

Figure 2.5 Multiple Discriminant analysis scheme for extracting pure end-member acoustic records from a catalog of 30-90 second hydroacoustic samples. Only those catalog records (1) classifying correctly and (2) exceeding a minimum probability for group membership pass onto the next Discriminant Analysis. The Fisher's Linear Discriminant Functions obtained from the 3rd Pass Discriminant Analysis were used to classify survey data into one of three end-member classes (bare, drift macroalgae, or short SAV).

2.2.10 Partitioning by SJRWMD Segments and Proximity to Navigation Channel

The 49,592 geo-located acoustic records were joined with a SJRWMD shapefile of Indian River Lagoon segments (IRL_Segments.shp) in ArcMap v 9.0. These records were further sub-divided by clipping to a SJRWMD shapefile of navigation channels (ICW.shp). The segment-average percent cover of SHORT and DMA were calculated as the simple average of acoustic records falling within a particular segment, either within or outside of navigation channels. The area surveyed within each segment was obtained by clipping the segment shapefile to the actual survey extent.

2.2.11 SAV Coverage Maps

Ordinary point kriging, a geostatistical method based on the spatial autocorrelation inherent in landscape patterns, was used to produce spatially continuous maps of SHORT and DMA percent cover. Each kriged contour feature was subsequently clipped to the perimeter of the area traversed within each survey tile, i.e. the boundaries of the contour maps do not extend beyond the area of acoustic sampling.

2.2.12 Accuracy Assessment

A total of 265 external accuracy assessment samples were collected in-line with the survey by intermittently slowing to idle speed, deploying a weighted video camera overboard, and continuing to record hydroacoustic data while simultaneously collecting video for a period of 30-60 seconds. The Trimble dGPS latitude and longitude and UTC time were burned onto the recorded video for post-survey synchronization with hydroacoustic data. The accuracy assessment videos were reviewed post-survey and assigned a visually-estimated percent coverage

of (1) bare substrate, (2) short SAV, and (3) drift macroalgae and tall SAV. The ground-truth data was subjected to the same VBT post-processing, depth-normalization, and quality assurance as described previously for the survey data. Of the 265 samples collected, 246 remained for accuracy assessment following QA, totaling 8,285 hydroacoustic records. Each of the 8,285 records was classified as either BARE, SHORT, or DMA using the same Fisher's linear discriminant functions used to classify the survey data. The acoustically-predicted cover of SHORT and DMA was then calculated for each of the 246 accuracy assessment samples, as the simple average of the 30-60 classified records per sample.

The accuracy assessment was performed directly on the hydroacoustic records, not on the kriged contour plots of percent cover, because (i) biomass was calculated directly from individual hydroacoustic records, and (ii) the heterogeneous nature of the benthos would introduce uncertainty if the area sampled was not within the acoustic footprint. A confusion matrix was constructed as a square array of numbers arranged in rows (discriminant analysis classification) and columns (ground-truth). An accuracy assessment could not easily be conducted on the individual percent cover of drift macroalgae and short SAV, since many ground-truthing samples were a mixture of both. The accuracy assessment was instead conducted on total SAV (short SAV plus drift macroalgae) grouped into three abundance categories; 0-33, 33-66, and 66-100% cover. The overall accuracy (Po) was calculated as the sum of the major diagonal, i.e. correct classifications, divided by the total number of ground-truth samples. Each diagonal element was divided by the column total to yield a producer's accuracy and by the row total to yield a user's accuracy. The producer's and user's accuracies provide different perspectives on classification accuracy. The producer's accuracy (omission/exclusion error) indicates how well the mapper classified a particular category, i.e. the percentage of times that substrate known to be sparsely covered was correctly interpreted sparse cover. The user's accuracy (commission/inclusion error)

indicates how often map categories were classified correctly, i.e. the percentage of times that a sample classified as sparse cover was actually sparse and not abundant or contiguous.

The Tau coefficient is a measure of the improvement of classification accuracy over a random assignment of map units to map categories. The form of Tau based on equal *a priori* probability of group membership (T_e) was used for this study. In this case, the probability of random agreement simplifies to the reciprocal of the number of categories ($1/r$), and T_e is simply an adjustment of P_o by the number of map categories. As the number of categories increases, the probability of random agreement diminishes, and T_e approaches P_o. Values of T_e were calculated as follows:

Tau coefficient for equal probability of group membership = $T_e = (P_o - 1/r) / (1 - 1/r)$

2.3. RESULTS

2.3.1 Verifying Temporal and Spatial Consistency

Supervised classification requires temporal and spatial consistency of predictor variables over the course of acquiring catalog and survey data. Otherwise, classification accuracy would diminish as the relationship between acoustic parameters and SAV abundance shifted, due either to instrument drift (temporal inconsistency) or intrusion of extraneous geophysical factors into the acoustic signature (spatial inconsistency). Temporal and spatial consistency was assessed using the 131 individual hydroacoustic samples constituting the training dataset. Training samples were ideal for this purpose as they were collected over long periods of time, from all over the

lagoon, and were ground-truthed and screened for minimum percent cover (i.e. the purity of each categories defining feature; bare substrate, short SAV, and DMA.

Training samples were collected within the Indian and Banana Rivers, from Mims in the north to Wabasso in the south (approx. 120 km distant); 79 were collected in 2007 and 52 in 2008 (Table 2.1). Spatial and temporal consistency of the relationship between the acoustic parameters and the interpretation of the bare, short SAV, and DMA bottom classes was evidenced by the equitable proportions of training records that passed through the multi-pass DA supervised classification (Table 2.1).

Table 2.1 Demonstration of temporal and spatial consistency by the equitable rejection of records among the 131 training samples by the multi-pass DA supervised classification, arranged by acoustic class and year acquired. Ordering individual training samples by the percentage of records that correctly classified in the 3rd-Pass DA (e.g. 31 of the 41 BARE samples acquired in 2007 had more than 80% of the records pass through the 3rd-Pass DA, i.e. retained for the final training catalog).

% Passing thru 3rd Pass DA	Training Dataset Acoustic Class					
	BARE		SHORT		DMA	
	2007	2008	2007	2008	2007	2008
80-100	31	15	1	0	4	5
60-80	7	7	0	0	1	5
40-60	1	4	9	0	1	2
20-40	1	0	6	1	4	7
10-20	0	0	3	1	0	0
5-10	0	0	3	0	2	1
0-5	1	1	3	2	1	1
Sub-Total	41	27	25	4	13	21
Total	68		29		34	
Ind Rvr	42		10		34	
Ban Rvr	26		19		0	

For example, of the 41 BARE samples collected in 2007 and submitted to the 1st-Pass DA (averaging 60 records per sample), 38 samples (92.7%) had 60-100% of their records pass through the 3rd-Pass DA. The 27 BARE samples collected in 2008 had similar proportions; 22 samples (81.5%) had 60-100% of their records pass through the 3rd-Pass DA. The DMA samples showed similar equitable proportions between 2007 and 2008. Of the 13 BARE samples

collected in 2007, 5 samples (38.5%) had 60-100% of their records pass through the 3rd-Pass DA. Of the 21 BARE samples collected in 2008, 10 samples (47.6%) had 60-100% of their records pass through the 3rd-Pass DA. Recalling that the weighted average percent cover of the 34 DMA training samples was 77% (Figure 2.4), the lower overall percentage of DMA records passing reflected the fact that the acoustics frequently failed to discriminate the DMA canopy from bare substrate. The SHORT group (typically *C. prolifera*) had even smaller proportions of records passing through the 3rd-Pass DA, concomitant with its shorter canopy height (Table 2.1). But as with the BARE and DMA classes, the proportions showed temporal consistency between the 2007 and 2008 samples.

That such far-flung points collected a year apart classified so similarly is very strong evidence for temporal and spatial consistency of the multivariate acoustic interpretation of the visually-defined classifications. More fundamentally, temporal consistency was also evident in the independent variables themselves. This can be seen in the E1vsE2, E1vsE1′, and E1vsFD scatterplots of the training dataset, at both frequencies, compiled from the 131 individual hydroacoustic samples (Figure 2.6). The center-points (average class value) and boundaries (1 standard deviation) are essentially identical for the 2007 vs 2008 comparisons for all three classes.

2.3.2 Assessing the Supervised Catalog

The effect of successive discriminant analyses (DA) can be seen as an increasing separation of data clouds in the scatterplots of canonical variable scores (Figure 2.7a), the result of refining the training samples. As discussed in the previous section, this refinement was not limited to removing pings from the SHORT or DMA datasets acquired over bare substrate. It also removed pings that failed to detect the vegetative canopy. The greater discriminatory power of the multivariate DA algorithm is apparent in the comparison of the discriminant function scatterplot

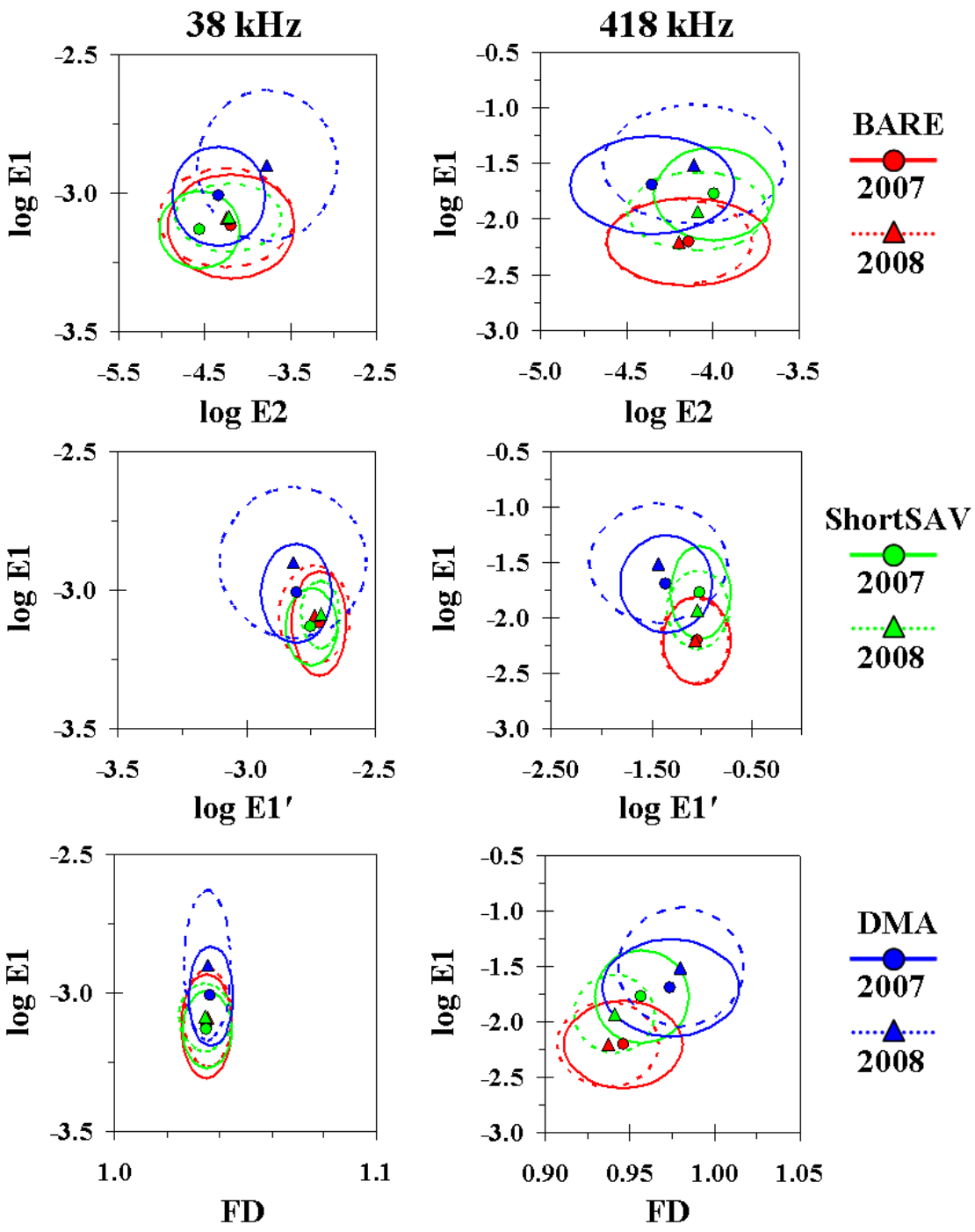

Figure 2.6 Scatterplots of 131 samples constituting the training dataset (68 BARE, 29 ShortSAV, 34 DMA) submitted to the 1st-Pass discriminant analysis. Computed separately for 2007 and 2008 samples to demonstrate temporal consistency. Centerpoints denote cluster averages, ellipses are dispersion (1 standard deviation) about x and y, calculated individually for samples acquired in 2007 and 2008.

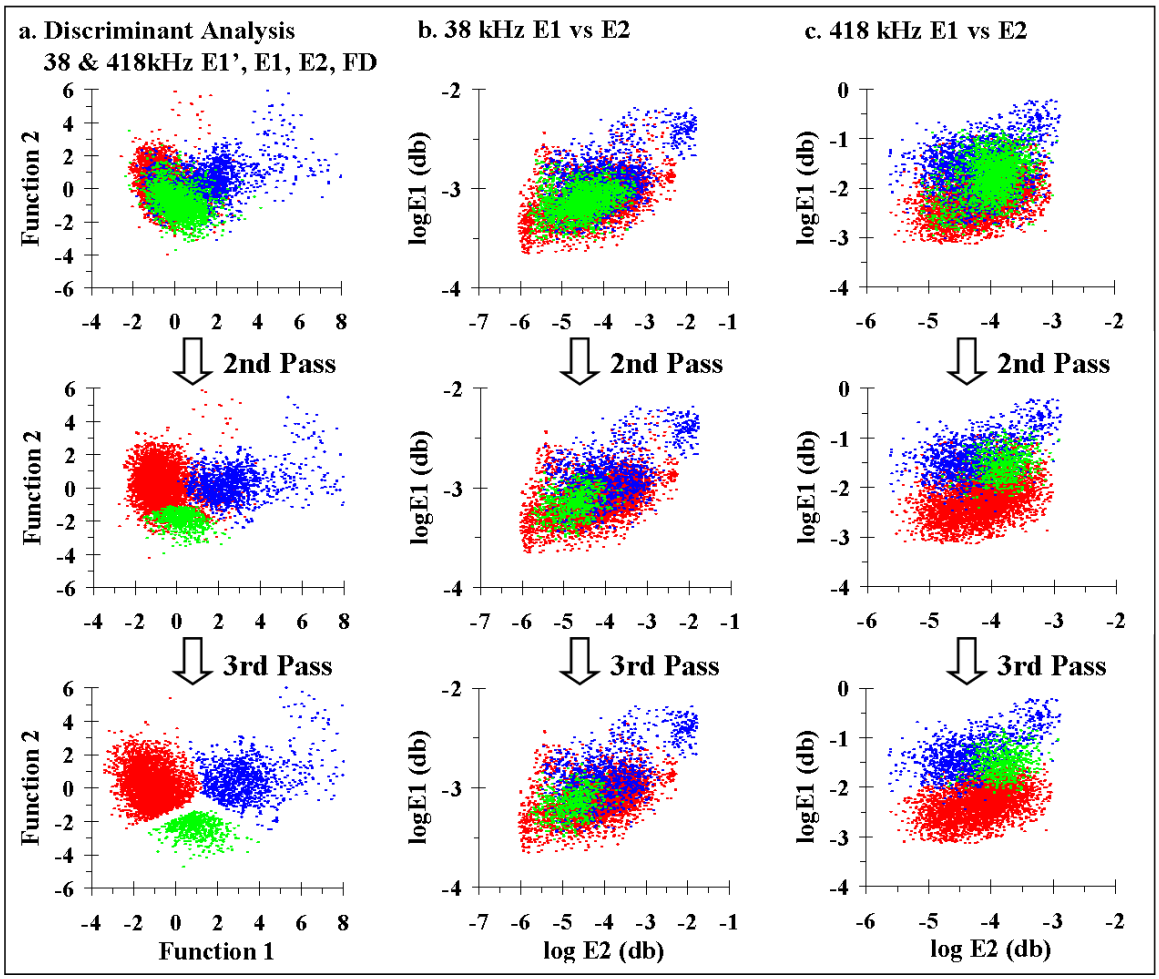

Figure 2.7 Clustering and refinement of training dataset. Discrimination of Bare (red), Drift MA (blue), and Short SAV (green) catalog records after multiple passes through (a) Discriminant analyses using 38 and 418 kHz E1', E1, E2, and FD as predictor variables. The advantage of utilizing eight acoustic variables is evident when the same data is presented as (b) the 38 kHz E1:E2 Bottom Ratio or (c) the 418 kHz E1:E2 Bottom Ratio.

to the individual 38 and 418 kHz E1vsE2 scatterplots, populated by the same DA datasets (Figure 2.7a vs Figures 2.7b-c). The E1vsE2 bottom ratio method is commonly employed for seabed classification (Orlowski, 1984; Burns et al., 1989; Chivers et. al., 1990), but as expected the reduced information resulting from using just two predictor variables at a single frequency provided much less discriminatory power than using a combined dataset of the full VBT output at two frequencies (Figure 2.7a). The DA was primarily informed by the 418 kHz variables, as can be seen in the confusion matrices of dual-frequency versus single-frequency classification of the

training data submitted to the 1st-Pass DA (Table 2.2). This is not surprising, as the 418 kHz signal would be expected to be more prone to scattering off the vegetative canopy.

Table 2.2 Confusion matrices for 1st-Pass discriminant analysis of training dataset utilizing (a) 38 and 418 kHz E1′, E1, E2, and FD, (b) 418 kHz only, and (c) 38 kHz only.

a. 38 & 418 kHz

		Ground-Truth		
		BARE	SHORT	DMA
DA Class	BARE	**3013**	416	314
	SHORT	835	**1227**	305
	DMA	187	118	**1108**
	Producer's	74.7%	69.7%	64.2%
	Overall Accuracy (P_o)			71.1%
	Tau (Te) = 0.663 ± 0.012			

b. 418 kHz

		Ground-Truth		
		BARE	SHORT	DMA
DA Class	BARE	**2960**	490	280
	SHORT	860	**1031**	343
	DMA	215	240	**1104**
		73.4%	58.5%	63.9%
	Overall Accuracy =>			67.7%
	Tau (Te) = 0.623 ± 0.012			

c. 38 kHz

		Ground-Truth		
		BARE	SHORT	DMA
DA Class	BARE	**2012**	643	533
	SHORT	1340	**978**	375
	DMA	683	140	**819**
		49.9%	55.5%	47.4%
	Overall Accuracy =>			50.6%
	Tau (Te) = 0.424 ± 0.013			

The DA catalog was checked for internal consistency by classifying the 166 catalog samples that passed quality assurance with the Fisher's linear discriminant functions from the third-pass discriminant analysis (Table 2.3). The acoustically-predicted cover of DMA and SHORT was calculated for each of the 166 catalog samples, as the simple average of the 30-90 classified hydroacoustic records belonging to each sample. Figure 2.8 displays the acoustically-predicted percent DMA and SHORT cover versus the visually-estimated cover of the 166 catalog samples. To better illustrate the overall trends, the average predicted values were also calculated for ground-truthed values in the range of 0-5, 5-10, 10-20, 20-40, 40-60, 60-80, and 80-100% cover (red triangles).

2.3.2.1 DMA Catalog

The DMA model generally performed well across the full range of drift macroalgae cover, as seen in both the scatterplot of predicted versus ground-truthed cover and in the model residuals

(predicted minus ground-truthed percent cover). The DMA model only slightly under-predicted cover (by approx. 10-20%) as ground-truthed cover exceeded 50%.

Table 2.3 Values of Fisher's Linear Discriminant Functions used to classify hydroacoustic records.

Variable	BARE	SHORT	DMA
E1 38kHz	-58.7	-60.9	-57.8
E2 38kHz	29.5	25.8	29.6
E1' 38kHz	-131.6	-129.3	-128.6
FD 38kHz	46314.8	46294.8	46362.3
E1 418kHz	-75.5	-64.1	-60.8
E2 418kHz	-44.0	-40.6	-47.3
E1' 418kHz	29.5	26.2	20.9
FD 418kHz	1397.7	1365.9	1418.5
Constant	-24595.2	-24529.6	-24651.5

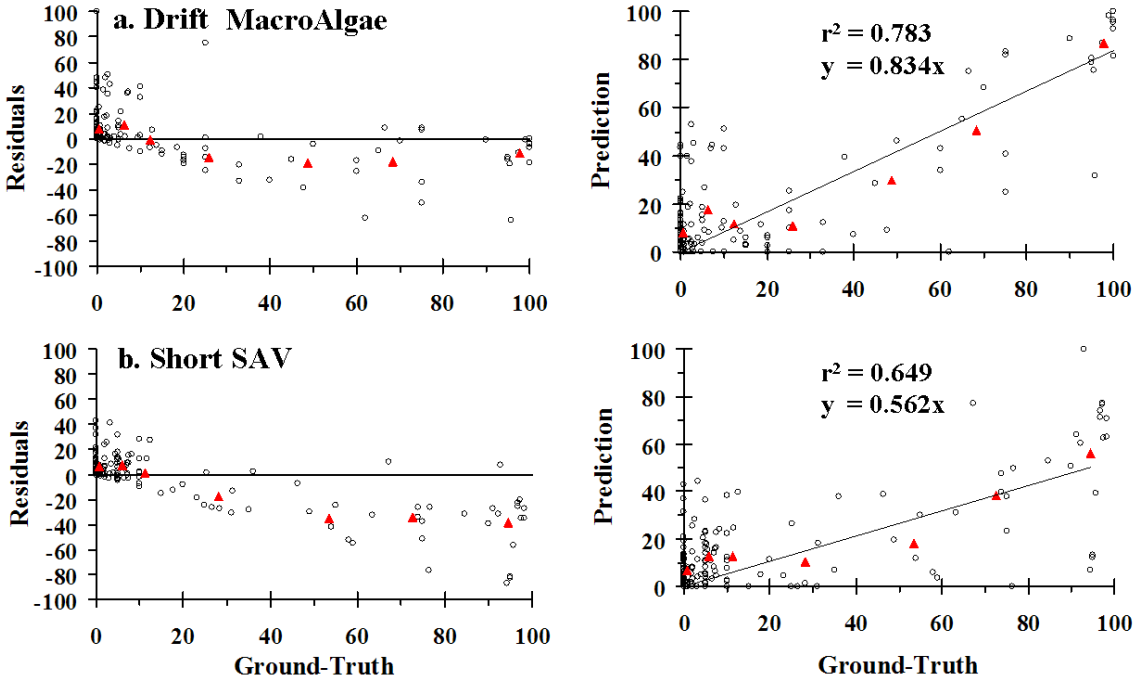

Figure 2.8 Internal accuracy assessment of predictive cover models. Comparison of acoustically-predicted values (right) and model residuals (left) of (a) drift macroalgae and (b) short SAV for the 166 catalog training samples. Displayed as individual catalog samples (open circle) and as the average of catalog samples falling within bins of ground-truthed cover (solid triangle). Linear regression was performed on individual samples.

2.3.2.2 SHORT SAV Catalog

The under-prediction of the SHORT model was more pronounced, averaging approximately 35% as ground-validated cover exceeded 50%. As previously discussed, the acoustics frequently failed to detect the SHORT SAV canopy, resulting in obvious overlap of the SHORT and BARE dataclouds in the training dataset submitted to the 1st-Pass DA (Figure 2.7). This necessitated passing all the BARE records through the 1st-Pass DA, regardless of whether the records classified as BARE, to prevent over-prediction of the SHORT group (Figure 2.5). By the end of the 3rd-Pass DA, the previous region of overlap had been allocated to the BARE category (and hence the under-estimation of short SAV at the upper range of coverage). But this underestimation was not critical to the final outcome, because (1) the primary objective was to quantify the biomass of drift macroalgae, and (2) based on ground-truthing samples, roughly two-thirds of the short SAV biomass came from areas of less than 50% cover.

2.3.3 Classifying Survey Data

The Fisher's linear discriminant functions (Table 2.3) resulting from the third-pass DA were used to classify each of the 500,000+ survey records as either BARE, DMA, or SHORT. This was done by multiplying each coefficient by the value of the corresponding acoustic parameter, summing the products, and adding the constant to get a score for each of the three categories. Survey records were assigned to the category with the largest discriminant function score. The final layer of classification was created by tallying the assignments for a range of ten consecutive records and computing the proportion of BARE, DMA, and SHORT assignments for each group of ten records.

2.3.4 SAV Coverage Maps

Ordinary point kriging, a geostatistical method based on the spatial autocorrelation inherent in landscape patterns, was used to produce spatially continuous maps of SHORT and DMA percent cover. Each kriged contour feature was subsequently clipped to the perimeter of the area traversed within each survey tile, i.e. the boundaries of the contour maps do not extend beyond the area of acoustic sampling (Appendix 2.A2-2.A9).

2.3.5 Accuracy Assessment

A confusion matrix could not be easily be produced for the individual categories of drift macroalgae and short SAV, since many ground-truthing samples were a mixture of both. Instead, the percent cover of drift macroalgae and short SAV were summed and grouped into three abundance categories; 0-33, 33-66, and 66-100% cover. The important distinction is that the confusion matrix was based on the classified hydroacoustic records, not on the kriged contour plots of percent cover. Performing accuracy assessment directly on the classified hydroacoustic records was deemed most appropriate, since biomass was calculated directly from individual hydroacoustic records. The overall predictive accuracy for the 246 external accuracy assessment samples was 78.9% for the three coverage categories of total SAV cover. The Tau coefficient for equal probability of group membership (T_e) was 0.683 ± 0.076 (α=0.05), i.e. the rate of misclassifications was 68.3% less than would be expected from random assignment of hydroacoustic records to SAV cover. (Table 2.4).

To assess the accuracy of the individual predictions of drift macroalgae and short SAV, the relationship between acoustically-predicted percent cover and the visually-estimated percent cover was also examined by simple linear regression. Figure 2.9 displays the acoustically-predicted percent cover drift macroalgae and short SAV versus the visually-estimated cover for

Table 2.4 Confusion matrix of 246 external accuracy assessment samples comparing acoustically-predicted versus visually-estimated for three abundance ranges of Total SAV (short SAV plus drift macroalgae).

		Ground-Truthed				
	Total SAV	**0 to 33**	**33 to 66**	**66 to 100**	**i+**	**Users**
Predicted	**0 to 33**	**157**	9	3	169	92.9%
	33 to 66	27	**19**	10	56	33.9%
	66 to 100	3	0	**18**	21	85.7%
	+i	187	28	31	194	**<= Diag**
	Producers	84.0%	67.9%	58.1%	**n =>**	246
					Overall Accuracy (P_o)	78.9%
					Tau (T_e) = 0.683 ± 0.076	

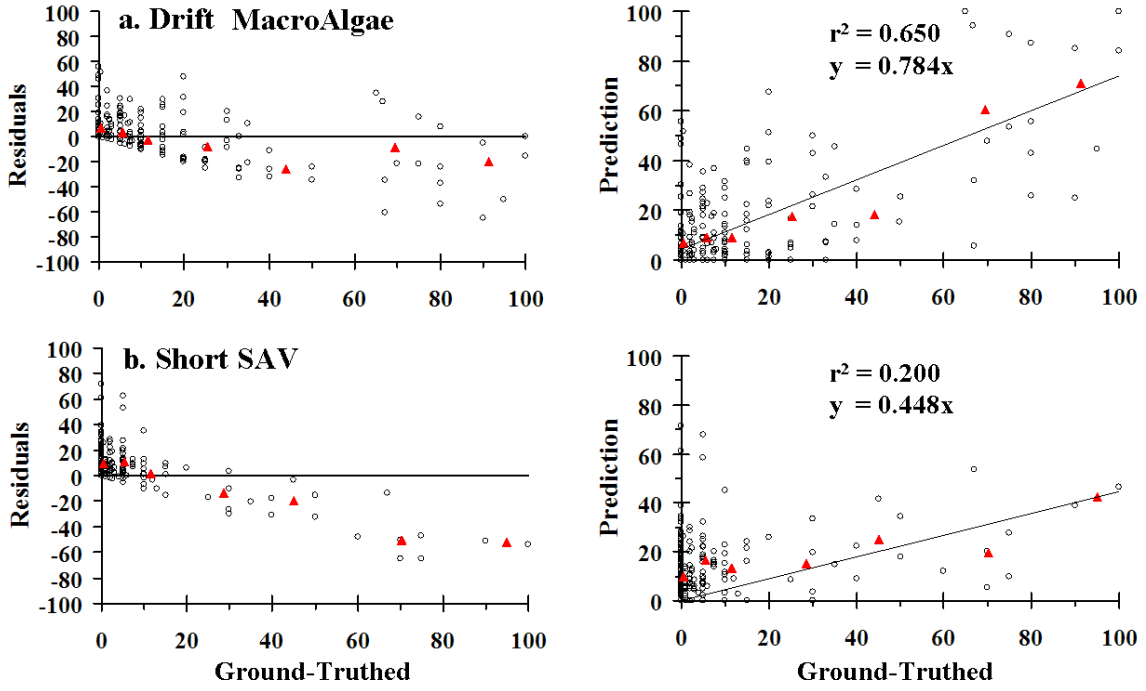

Figure 2.9 External accuracy assessment of predictive cover models. Acoustically-predicted values (right) and model residuals (left) of (a) drift macroalgae and (b) short SAV for the 246 external accuracy assessment samples. Displayed as individual ground-truth samples (open circle) and as the average of samples falling within bins of ground-truthed cover (solid triangle). Linear regression was performed on individual samples.

each of the 246 external accuracy assessment samples. To better illustrate the overall trends, the average predicted values were also calculated for ground-validated values in the range of 0-5, 5-10, 10-20, 20-40, 40-60, 60-80, and 80-100% cover.

2.3.5.1 DMA Accuracy

As seen previously in the internal accuracy assessment of training data, the DMA classification performed well across the full range of coverage as judged by both the scatterplot of predicted versus ground-truthed cover and the model residuals (predicted minus ground-truthed percent cover). DMA cover was slightly under-predicted as ground-validated cover increased beyond 20%. For the 12 accuracy assessment samples with the highest ground-truthed DMA cover (average = 91%), 71% of the pings were acoustically classified as DMA.

2.3.5.2 Short SAV Accuracy

As seen previously in the internal accuracy assessment of training data, SHORT cover was under-predicted at the upper ranges. This underestimation was not critical to the final outcome, because (1) the primary objective was to quantify the biomass of drift macroalgae, and (2) based on ground-truthing samples, roughly two-thirds of the short SAV biomass came from areas of less than 50% cover.

2.3.6 Drift Macroalgae Biomass

The average percent cover of short SAV and drift macroalgae was calculated individually for the SJRWMD segments shown in Appendix 2.A1, using the ten-record averages of classified hydroacoustic records (Table 2.5). The lagoon-wide percent cover of DMA and SHORT was found to be 11.2 and 24.1% respectively.

Table 2.5 Drift macroalgae biomass and proportions (0-1) of short SAV (~10cm<) and drift macroalgae cover, partitioned by SJRWMD segments and by proximity to navigation channels.

Survey Area		Inside Navigation Channel						Outside Navigation Channel						DMA wet wt metric tons
			Mean	Acoustic Cover			Survey		Mean	Acoustic Cover			Survey	
Name	Segment	n	Depth (m)	Short SAV	Drift MA	Total	Area (km^2)	n	Depth (m)	Short SAV	Drift MA	Total	Area (km^2)	
Mims	IR2	16	2.82	0.33	0.53	0.85	0.36	4254	1.78	0.31	0.09	0.40	33.60	6208
TitusvillA North	IR3	25	3.30	0.26	0.29	0.56	0.28	1155	1.81	0.33	0.05	0.37	7.31	736
TitusvillB North	IR4	66	3.72	0.08	0.21	0.29	0.36	859	2.10	0.17	0.10	0.27	5.12	1049
Titusville South	IR5	86	3.07	0.18	0.16	0.34	0.98	5542	2.25	0.25	0.10	0.35	46.33	9152
Port St. John	IR5	229	2.95	0.14	0.24	0.38	1.40	6177	2.14	0.19	0.13	0.32	31.97	8643
Cocoa	IR7	104	3.61	0.05	0.17	0.22	0.37	1591	2.61	0.18	0.16	0.34	5.85	1960
Rocklege	IR8	123	3.21	0.12	0.13	0.26	0.80	1988	2.82	0.18	0.10	0.28	10.03	2267
Pineda North	IR9	126	3.91	0.01	0.18	0.18	0.76	1968	2.99	0.14	0.19	0.33	9.56	4000
Pineda South	IR10	123	3.82	0.01	0.25	0.26	0.69	3482	3.12	0.12	0.19	0.31	16.98	6749
Eau Gallie	IR11	76	3.83	0.01	0.16	0.16	0.31	2466	2.79	0.14	0.13	0.27	11.80	3143
Crane Creek Seg	IR12A	48	3.47	0.04	0.10	0.14	0.30	1216	2.54	0.16	0.15	0.31	6.55	2082
Turkey Creek	IR12B	48	3.24	0.06	0.09	0.15	0.38	1717	2.59	0.13	0.15	0.27	8.90	2739
Malabar	IR13A	55	3.03	0.07	0.09	0.15	0.40	2401	2.34	0.16	0.12	0.27	11.76	2812
Grant	IR13B	85	2.84	0.20	0.16	0.36	0.57	723	2.05	0.24	0.15	0.39	4.91	1601
Sebastian Br C	IR14BRE	87	2.63	0.13	0.12	0.25	0.65	1596	1.83	0.15	0.13	0.28	9.51	2663
Sebastian IR C	IR14IND	70	2.46	0.31	0.07	0.38	0.55	1982	1.86	0.24	0.16	0.40	11.68	3933
Wabasso North	IR15	46	3.25	0.13	0.10	0.23	0.23	220	1.90	0.28	0.13	0.42	1.47	459
Cape Canaveral S	BR2	67	2.93	0.09	0.46	0.54	0.43	993	2.22	0.14	0.11	0.25	4.25	1067
Port Canaveral	BR3	18	3.25	0.04	0.17	0.21	0.12	2216	2.15	0.19	0.03	0.22	11.90	743
Cocoa Beach	BR4							481	2.01	0.35	0.14	0.50	3.68	1052
S. Cocoa Beach	BR5							4678	2.31	0.39	0.10	0.50	26.54	5556
Satellite Beach	BR7							389	2.11	0.24	0.18	0.43	3.38	1242
Total =>							10.0						283.1	69859
Weighted Lagoon Average =>			3.19	0.12	0.19	0.32			2.28	0.23	0.12	0.35		

The biomass of drift macroalgae within each SJRWMD segment was calculated as the product of the average percent cover of drift macroalgae, segment area, and the wet weight of drift macroalgae (2000 metric tons per km^2) measured in the 2004 pilot study. At the time of the survey (April 1 - May 21, 2008) the drift macroalgae biomass was found to be 69,859 metric tons w.w. within the 293.1 km^2 study area.

An independent samples t test was performed to assess whether a difference in mean drift macroalgae cover existed between (1) records from within the navigation channels versus outside of navigation channels, or (2) records from the Indian River versus the Banana River (excluding navigation channels). The Levene test showed a significant difference between the variances of both comparisons, so the unequal variances version of the t test was used. The mean percentage

of drift macroalgae was greater within the navigation channels (M=18.3%, n=1477) than outside (M=12.2%, n=48139), and the difference was found to be statistically significant ($p<0.001$, two-tailed). The 95% CI around the difference between these sample means ranged from 4.92 to 7.21%. The mean percentage of drift macroalgae was slightly greater in the Indian River (M=12.9%, n=39374) than in the Banana River (M=9.3%, n=8765), and the difference was found to be statistically significant ($p<0.001$, two-tailed). The 95% CI around the difference between these sample means ranged from 3.25 to 3.98%.

Chapter 3: Mapping the Spatial Distribution and Vertical Extent of Muck in the Indian River Lagoon

FORWARD

This was an ancillary study that utilized the same collection of digitized waveforms that were principally acquired for the drift macroalgae project. While clearly a diversion from the central theme of thematic benthic habitat classification, this dual-usage of raw data demonstrated the diversity of information contained with vertical-incident waveforms. It was also the first known report of a single-beam AGDS used to gather quantitative sub-bottom profiling data. Although imaging and quantifying sediment layers are common uses of single-beam sub-bottom profilers, the simplistic approach developed in this chapter does not require coring or tabled estimates of acoustic impedance to convert from a time domain to layer thickness. Morevoer, it is unlikely that a sub-bottom could detect a surficial muck layer, given the extremely high water content of this muck and the greater power output of sub-bottom profilers. In this and the preceding chapter, different aspects of the same echo envelopes are variably mined for information about the presence of vegetative cover (inferred from acoustic energy and shape parameters) and the vertical extent of muck deposits (inferred from the vertical profile of sub-bottom echo return intensity). These two branches of information fed into two entirely distinct investigations; the map of drift macroalgae biomass was used as a proxy for the location, magnitude, and timing of nutrient loadings, while the locations of muck deposits informed resource managers about the dynamics of muck transport and where to target efforts at muck removal. In a largely closed system such as Indian River Lagoon, accumulations of anoxic, nutrient-laden, and easily re-suspended muck pose threats to the health of seagrass beds and local diversity in general.

The decision to use Visual Analyzer was based on observations made during the 2007 drift macroalgae pilot study. While simultaneously watching real-time drop-camera video and the 38

kHz oscilloscope display, a relationship between the bottom type and sub-surface signal penetration became apparent. Over hard compacted sandy bottoms, a large portion of the 38 kHz signal reflected near the sediment-water interface. A small proportion of signal penetrated a short distance below the surface before echo intensity rapidly returned to the noise baseline. Over softer bottoms with higher silt content, proportionally more of the 38 kHz signal penetrated a greater distance below the sediment-water interface, but returned to baseline noise levels well before the start of the second echo. Over muck, the 38 kHz signal penetrated unimpeded all the way to the second echo. These observations are consistent with the principles of seismology, which state that the amount of energy reflected from an interface is proportional to the difference between the acoustic impedances (Z) of the two mediums, where Z is the product of the wet bulk density (ρ) and compressional wave velocity. This is expressed as the Reflection Coefficient (R),

$$R = P_r/P_i = (Z_2 - Z_1) / (Z_2 - Z_1) = (\rho_2 c_2 - \rho_1 c_1) / (\rho_2 c_2 - \rho_1 c_1) \quad (2)$$

which is defined as the fraction of the incident wave energy (P_i) that is reflected (P_r) at the boundary. The proportion of reflected energy approaches zero as the bulk densities of the two mediums approach equality. That is why so little energy is reflected at the water-muck interface; the muck was a free-flowing fluid with a very high water content.

The BioSonics fish-finding Visual Analyzer software offered a suitable platform for translating these observations into quantitative estimates of the vertical extent of muck, with only a few modifications to processing and relatively simple back-end algorithms. Visual Analyzer is designed to integrate echo energy between the near-field of the transducer and the water-sediment interface, in user-defined vertical and horizontal increments. Integrating echo energy below the water-sediment interface simply required over-riding the bottom-picking algorithms, so that Visual Analyzer would integrate echo energy across the entire span of acquired depth (the user defines the depth range over which to acquire hydroacoustic data). A series of back-end algorithms were developed for the modified Visual Analyzer output, which relocated the bottom

and then found the distance below the bottom where volume penetration dropped below a specified intensity level for a specified duration. The vertical extent of muck was then computed as the measured acoustic bottom thickness minus the "typical" acoustic bottom thickness, which was derived from 45 ground-validated catalog samples that were devoid of vegetation and characterized by the sand-sized sediments most commonly found in the Indian and Banana Rivers. Ground-validation revealed these acoustic estimates of muck thickness to be highly accurate, and provided the SJRWMD with a lagoon-wide inventory of the spatial and vertical extents of muck deposits for just the cost of post-processing. It also generated interesting trends related to the dynamics of muck deposition. There was a strong tendency for muck to accumulate in deep sinks, and a clear north-south gradient in the navigation channels, suggesting the headwaters of Indian River were a significant source of muck, as opposed to in-situ generation. The utility of this technique extends beyond finding muck. Presumably, it could be applied anywhere a surficial layer of unconsolidated sediments overlies a significantly harder substrate.

ABSTRACT

This chapter presents the results of a large-scale hydroacoustic survey conducted in April-May 2008. The objective of this study was to map the distribution and vertical extent of muck in the Indian River Lagoon, utilizing the data collected during a seasonal drift macroalgae survey. Indian River was surveyed from the Sebastian Inlet to its northernmost extent in the Titusville area. Banana River was surveyed from its convergence with the Indian River northward to the Federal Manatee Zone near Cape Canaveral. The survey vessel was navigated along pre-planned lines running east-west and spaced 200 m apart, except for when muck was indicated by the oscilloscope display, at which point a meandering path was adopted to demarcate the horizontal extent of muck. Hydroacoustic data were collected with a BioSonics DT-X echosounder and two multi-plexed digital transducers operating at 38 and 420 kHz. The vertical extent of muck was derived from the 38 kHz hydroacoustic signal, which was processed with Visual Analyzer, a fish-finding software package produced by BioSonics Inc. The software was adapted to integrate echo energy below the water-sediment interface, and a set of post-processing algorithms were developed to translate the sub-bottom echo energy profile into continuous scale estimates of muck thickness. In this manner 500,000+ 38 kHz pings were translated into 88,927 geo-located estimates of muck layer thickness, down to a minimum bottom depth of 1 m. Ground-truthing was conducted in July 2008 at twenty sites within the Indian River. The predictions of muck layer thickness were found to be accurate over the ground-truthed range of 0-3m (r^2 = 0.882, SE=0.52m). The vertical distribution of acoustically-predicted muck demonstrated the tendency for muck to accumulate in deeper areas of the lagoon. For the case of Indian River (excluding navigation channels), muck was not detected in depths shallower than 1.4m and rare in the range of 1.4-2.2 m (only 3.6% of records had a predicted muck thickness greater than 0.5 m). The frequency of muck plateaued between 2.2-3.4 m (9.6%) before making a sharp rise to 82% in the range of 4-5 m. As expected, the mean muck layer thickness was significantly greater within the navigation channels (0.56 m) than outside of them (0.08 m). A significant latitudinal trend of

muck thickness was detected within the Indian River navigation channels. The mean muck thickness decreased from 1.38 m at its northernmost origins to 0.83 m in the Titusville area before plateauing at approximately 0.4 m for the remainder of segments. Outside of the main ICW channels, 23 individual muck deposits were identified; 22 in the Indian River and 1 in the Banana River. Factors in descending order of co-occurrence were proximity to causeways or jetties, riverbed depressions, and proximity to shore and drainage channels. In conclusion, this study establishes that a single-beam acoustic survey is a cost-effective and accurate alternative for mapping the distribution and vertical extent of muck deposits in the shallow-water environment of the Indian River Lagoon. Moreover, the temporal consistency afforded by a digital transducer allows for direct and meaningful comparisons between successive surveys.

3.1. INTRODUCTION

The primary objective of the 2008 large-scale hydroacoustic survey was to map the distribution and biomass of seasonal drift macroalgae. This was achieved by processing the 38 and 420 kHz data within BioSonics Visual Bottom Typer seabed classification software, merging the two frequencies into a single dataset, and creating a supervised training catalog. In this study only the raw 38 kHz data was utilized for muck detection. The greater power output of the lower frequency transducer increased signal penetration into bottom sediments, both in terms of distance and proportion. The vertical extent of muck was quantified from the vertical profile of sub-bottom echo return intensity (db), obtained by processing the raw 38 kHz data with Visual Analyzer, a fish-finding software package developed by BioSonics Inc. Visual Analyzer was designed to integrate echo intensities across the water column, but by over-riding the bottom-picking algorithm it was possible to integrate across the entire range of depths, i.e. below the water-sediment interface. A series of novel post-processing algorithms were developed to translate the output of Visual Analyzer into continuous scale predictions of muck layer thickness. For this study, muck is loosely defined as accumulations of black, clay-sized, organic-rich sediments. The muck sediments may be depositional or formed *in-situ* from the decomposition of submerged aquatic vegetation. These muck deposits are easily disturbed, and the resulting plume can create localized nutrient overloads and high turbidity, both of which are detrimental to the health of seagrass habitats and biodiversity. Knowledge of the distribution and abundance of muck deposits is important for understanding the factors governing muck deposition, and for optimizing dredging projects aimed at removing muck from the lagoon.

3.2. METHODS AND MATERIALS

3.2.1 Survey Area

The acoustic survey was completed between the dates of April 1 - May 21, 2008. Indian River was surveyed from its origin in the Titusville area (28.7664^{o}) southward to Wabasso, just below the Sebastian Inlet (27.8743^{o}) (Appendix 3.A1). Banana River was surveyed from the Federal Manatee Zone near Cape Canaveral (28.4329^{o}) southward to its convergence with Indian River in the Melbourne area (28.1571^{o}). The survey vessel was navigated along pre-planned lines, running east-west and spaced 200 m apart, to a minimum depth of approximately 1 m. When the real-time oscilloscope display indicated the survey vessel was over muck, a meandering path was adopted to demarcate the horizontal extent of the muck deposit.

3.2.2 Sonar Equipment

The survey was conducted from a 7.5 m v-hull boat with a 0.5 m draft (Figure 2.1). Hydroacoustic data were acquired with a BioSonics DT-X echosounder and two multiplexed, single-beam digital transducers with full beamwidths of 10^{o} (38 kHz) and 6.4^{o} (420 kHz), operated at 5-Hz and 0.4 ms pulse duration. The 38 kHz data were utilized for muck detection and the 420 kHz data for bathymetry. The two transducers were located on a swing-arm mounted to the gunwale. The GPS antenna was mounted directly above the transducers for optimal integration of acoustical and positional data strings. Global positioning data were collected with a Trimble Ag132 dGPS, differentially corrected against the WAAS signal to achieve positioning accuracies less than 0.9 m horizontal dilution of precision. The dGPS signal was interfaced with HypackMax© to provide real-time monitoring of vessel position with respect to the 2004 DOQQ images and pre-planned survey lines. To avoid turbulence-induced signal contamination, evident as a rolling disturbance on the real-time oscilloscope display, vessel speed was adjusted to maintain a net speed (vessel+drift) of approximately 4.5 knots.

3.2.3 Data Processing

The 38 kHz hydroacoustic data were processed with BioSonics Visual Analyzer 4 software. Originally developed for determining fish sizes and densities, the settings were manipulated in such a manner as to adapt the program from a water column profiler to a sub-surface profiler. This included 'defeating' the bottom-picking algorithm of Visual Analyzer so that it would integrate the sub-bottom. This in turn required adding back a bottom-picking algorithm (discussed in section 3.2.5). Visual Analyzer integrates the echo intensity level (dB) for a grouping of successive pings, stratified by depth. This is illustrated in Figure 3.1.

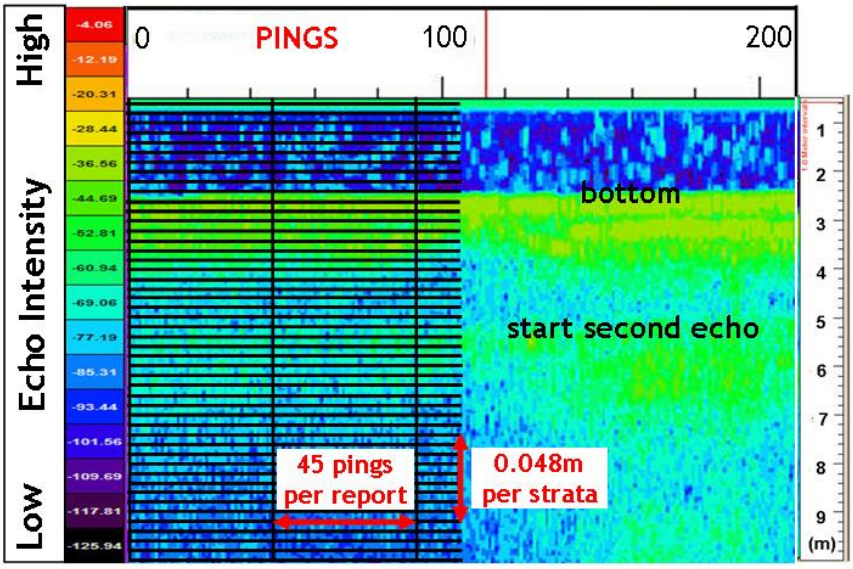

Figure 3.1 Echo integration in Visual Analyzer. Echo intensity is integrated for each box (black lines). Box dimensions are specified by user; 200 strata (=0.048 m) and 200 reports (=45 pings per report). Strata depth is the vertical resolution, i.e. the thinnest detectable layer. Frequency is the horizontal resolution, i.e. the traverse between reports (~ 20 m at 4.5 knots).

Each raw 30-minute data file, containing 9000 pings, was partitioned into 200 reports. At the 5 Hz sampling frequency, each report was therefore the average of (5 pings s^{-1}) · (60 s min^{-1}) · (30 min) = 9000 pings / 200 reports = 45 pings per report. At the average survey speed of 4.5 knots (2.3 m s^{-1}), the distance between reports was approximately (2.3 m s^{-1}) · (45 pings) / (5 pings s^{-1})

= 20 m. Each report was sliced into 200 strata (i.e. depth bins). The vertical extent of each stratum was (10m - 0.5m) · (200 strata - 1) = 0.04774 m per stratum. So for each 30-minute file, Visual Analyzer computed the average echo intensity within 40,000 boxes (200 reports long x 200 strata deep). Before discussing the rationale by which information about the muck layer was extracted from the 38 kHz signal, a brief review of basic hydroacoustic operational theory is presented.

3.2.4 Single-Beam Hydroacoustic Theory

3.2.4.1 Acoustic Impedance

Single-beam acoustic ground discrimination systems are routinely used for benthic habitat assessment, typically utilizing transducers in the range of 50-200 kHz. Transducers on the lower end of the frequency spectrum, such as the 38 kHz model used in this study, produce higher energy pings that are capable of significant penetration into unconsolidated sediments. Combined with low transmission losses (shallow depth) and low acoustic impedence (similar bulk densities), the 38 kHz signal was able to penetrate through water-muck interface unimpeded, until contacting the first sub-surface reflector (i.e. hard-packed river sediments). Figure 3.2 displays vertical profiles of 38 kHz signal intensity acquired over (i) a typical Indian River sand bottom and (ii) a thick muck layer over a sand bottom. In both examples the water column is characterized by low signal intensity, as most suspended particles are too small and diffuse to interact with the relatively large wavelength of the 38 kHz beam (λ = 4.04 cm). The water-sediment interface of the typical sand bottom is evidenced by a sudden increase in echo intensity, due to the large increase in wet bulk density from water to packed sand. The small proportion of energy that penetrated the boundary decays to baseline intensity within about a meter. In constrast, the water-sediment interface of a muck-covered bottom is evidenced.

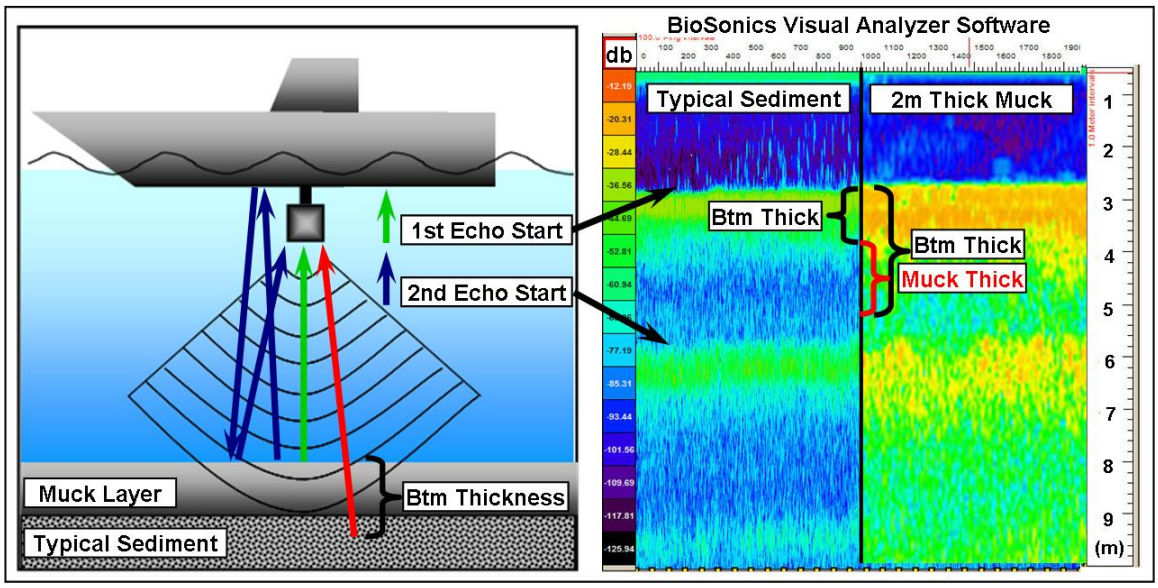

Figure 3.2 Illustration of muck thickness. (left) Specular return of first echo from the water-sediment interface (green arrow) and backscatter caused by signal penetration into muck layer (red arrow). The multi-path second echo (blue arrow) reflects off the air-water interface or vessel and back to the bottom before returning to the transducer. (right) BioSonics Visual Analyzer oscilloscope displays for a "typical" riverbed composed of sand-sized sediments and for a 2m thick deposit of muck. Muck thickness is computed as the difference between the measured acoustic bottom thickness and a constant value of "typical" acoustic bottom thickness.

3.2.4.2 Acoustic Bottom Thickness

As just discussed, there will always be some energy penetration into the unconsolidated sand-sized sediments that typify the lagoon. Quantifying the vertical extent of muck thus requires knowledge of the 'typical' acoustic bottom thickness, which is defined here as the sub-bottom depth over which the signal decays below a certain echo intensity threshold. The threshold was heuristically determined by observing the relationship between bottom composition and the real-time oscillioscope display.

3.2.4.3 Bottom Picking

BioSonics EcoSAV plant detection software and Quester Tangent's IMPACT seabed classification software both use the maximum rate of rise as a primary criterion for their bottom-picking algorithms. In this study, the maximum rate of rise between strata was used in a similar

fashion to define the bottom-pick. Locating the bottom within the output of Visual Analyzer was a critical step in the process of adapting it from a water-column fish-finder to a sub-surface profiler, i.e. from the design intent of looking up from the bottom to looking down from the bottom.

3.2.5 Quantifying Muck Thickness

The acoustic bottom thickness was calculated for each hydroacoustic record as the difference between the bottom depth (i.e. water-sediment interface) and the depth at which signal intensity dropped below -40 db (see the Introduction to Single-Beam AGDS for an explanation of why echo intensities are negative). There is no physical significance to -40 db; the value was simply arrived at by reviewing a large number of catalog samples. The bottom depth was defined as the maximum rate of rise in echo return intensity, computed as the maximum value of ($dB_n - dB_{n-1}$) for strata 1 through 200. The vertical extent of the muck layer was then calculated as the measured acoustic bottom thickness minus a constant value of "typical" acoustic bottom thickness (Figure 3.3). The typical acoustic bottom thickness was obtained from a sub-set of ground-validated catalog samples collected for the drift macroalgae project. 45 catalog samples, consisting of a 30-90 second hydroacoustic file and a concurrent drop-cam video file, were selected on the basis that they were generally devoid of epibenthic biota and constituted of the sand-sized particles typical of the majority of Indian and Banana River riverbeds. 33 of the catalog samples were collected during the Apr-May 2007 BioSonics trial and the remaining 12 were collected during the 2008 lagoon-wide survey. The 45 catalog files were processed in Visual Analyzer, yielding a total of 500 records, which was reduced to 329 after removing records that appeared either irregular or as if the bottom was too soft. The acoustic bottom thickness of the remaining records averaged 18 strata, or 0.86 m (Figure 3.3). A multiple linear regression ($r^2 = 0.044$, n=329) demonstrated that the acoustic bottom thickness was independent of bottom depth (p=0.001) and year of acquisition (p=0.041), coded as -1/1. Combined, these

observations validate the spatial and temporal consistency afforded by digital transducers, which will allow for direct and meaningful comparisons between successive surveys

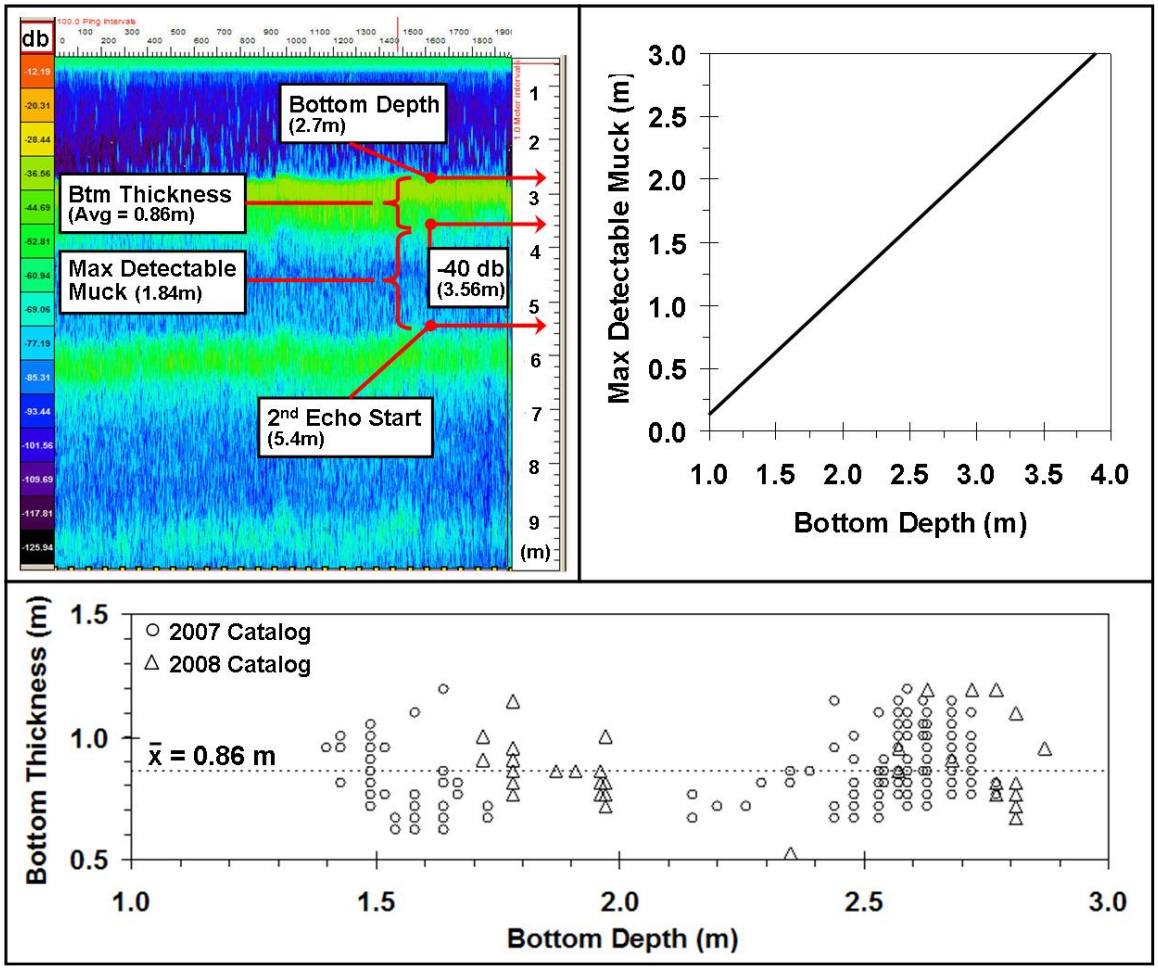

Figure 3.3 Maximum detectable muck thickness vs depth. (upper left) BioSonics Visual Analyzer display of a "typical" riverbed. Maximum Detectable Muck Thickness is equal to [Start of 2nd Echo - (Bottom Depth + Typical Bottom Thickness)]. (upper right) Maximum Detectable Muck Thickness as a function of Bottom Depth. (bottom) Computation of the average Acoustic Bottom Thickness from 45 sonar catalog samples collected in the Indian and Banana Rivers.

3.2.5.1 Maximum Detectable Muck Thickness

A second echo return is created when the first echo reflects off the survey vessel or air-water interface and contacts the bottom a second time before returning to the transducer (Figure 3.2). For this reason, the second echo returns at approximately twice the depth of the first echo. The

presence of the second echo imposed a constraint on the maximum vertical extent of muck that could be detected, i.e. it is possible for the first echo to still be reverberating from the muck layer when the second echo arrives at the transducer. The second echo starts at twice the depth of the first echo, so the maximum detectable muck thickness is equal to the depth at the start of the second echo, minus the sum of the bottom depth and the typical acoustic bottom thickness of 0.86 m (Figure 3.3, upper left). The maximum detectable muck layer thickness increases from 0.62 to 3.0 m as water column depth increases from 1. 5 to 4.0 m (Figure 3.3, upper right). The ratio of (detected muck thickness):(maximum detectable muck thickness) was calculated for each hydroacoustic report, to identify records where the reported muck thickness was constrained by water column depth.

3.2.6 Data Analysis

The 88,927 geo-located acoustic muck records were joined with a SJRWMD shapefile of Indian River Lagoon segments (IRL_Segments.shp) in ArcMap v 9.0. These records were further sub-divided by clipping to a SJRWMD shapefile of navigation channels (ICW.shp). The segment-average muck thickness was calculated as the simple average of records falling within a particular segment, either within or outside of navigation channels (any records acquired while demarcating muck deposits were removed, so as not to over-represent the abundance of muck). The vertical extent of muck was further described by computing the percentage of records falling into four ranges of thickness; 0.0-0.5, 0.5-1.0, 1.0-2.0, and > 3.0 m. The actual area surveyed within each segment was obtained by clipping the segment shapefile to a shapefile of the acoustic survey extent.

Polygons were drawn around individual muck deposits that (i) were located outside of the main ICW navigational channel, (ii) had an average acoustically-derived muck thickness greater than 0.5 m, and (iii) spanned multiple survey tracks (identified post-survey) or were demarcated

during the survey (identified in real-time from oscilloscope display). The perimeter of each deposit was estimated using the trackplots of acoustically-derived muck thickness and the 420 kHz bathymetry as guides. The average muck thickness and bottom depth was computed for each deposit as the simple average of records falling within the polygon (records acquired while demarcating muck deposits included). Images of each of deposit were exported from ArcMap at a scale of 1:10,000. Factors suspected to relate to the spatial distribution of muck were noted, including; proximity and orientation to the main navigation channel, causeways and jetties, spoil areas, and drainage outlets, and the nearest distance to the shore (without crossing the main navigation channel).

3.2.7 Ground Truthing

The acoustically-derived muck thickness was ground-truthed on July 17, 2008, with the assistance of scientists from SJRWMD (J. Steward, L. Morris, and L. Hall). Twenty sites of varying predicted muck thickness (0 to 3 m) were selected for ground-truthing, located within three clusters along the Indian River. The vertical extent of the muck layer was measured by probing the riverbed with a tee-handled, open-ended PVC pipe, calibrated in 1.0 cm increments. The pipe was driven through the muck layer at a near-normal angle of incidence until the consolidated sediment lying beneath could be felt. After pulling the pipe back on deck a thick coating of muck remained on the PVC pipe. The depth of the muck layer was recorded as the maximum interface between clean pipe and muck. Three replicate probings were taken at each site. The vessel was re-positioned to the target coordinates and the actual GPS coordinates were recorded for each replicate, just as the pipe was driven into riverbed. The three acoustically-derived muck thickness records nearest to the center-point of the three replicates were queried in ArcMap. The ground-truthed and acoustically-derived muck thicknesses were reported as the simple average of the three probings and the three acoustic records, respectively. The

performance of the acoustic method was evaluated by simple linear regression of the acoustic and ground-truthed averages, forcing the constant to zero.

3.3. RESULTS

3.3.1 Spatial Distribution of Muck

The 500,000+ 38 kHz pings were post-processed into 88,927 geo-located estimates of muck thickness and plotted over the 2004 DOQQ's (Appendices 3.A1-3.A5). The mean values of muck thickness by IRL segment, within and outside of navigation channels, are reported in Table 3.1 (off-track records acquired while demarcating muck deposits were removed, so as not to over-represent muck abundance). An independent samples t test was performed to assess whether a difference in mean muck thickness existed between (1) records from within the navigation channels versus records from outside of navigation channels, or (2) records from the navigation channels of Indian River versus records from the navigation channels of Banana River. The Levene test showed a significant difference between the variances of both comparisons, so the unequal variances version of the t test was used. The mean muck thickness was greater within the navigation channels (M=0.56m SD=0.62, n=5657) than outside (M=0.08m SD=0.30, n=81839), and the difference was found to be statistically significant ($p<0.001$, two-tailed). The 95% CI around the difference between these sample means ranged from 0.46 to 0.49m. The mean muck thickness within the navigation channels of Banana River (M=1.22m SD=0.97, n=347) was greater than that of Indian River (M=0.51m, SD=0.57, n=5310), and the difference was also found to be statistically significant ($p<0.001$, two-tailed). The 95% CI around the difference between these sample means ranged from 0.60 to 0.81m.

The author considers navigation channels to be ideal features for spatial comparisons of muck deposits. Their depth, orientation, and areal extent are generally consistent throughout the

lagoon, making them a natural sediment trap from which to base comparisons. There was a significant latitudinal trend in muck thickness within the navigation channels of Indian River (Figure 3.4). The mean muck thickness was 1.38 m within the northernmost segment (Mims) and 0.83 m in the adjacent segment (TitusvilleA North), compared to an average value of 0.42 m for the remaining Indian River segments. This suggests that the watershed within the Mims segment is a major source of muck sediments for Indian River.

Table 3.1 Summary of the muck layer thickness (MT) derived from the 38 kHz hydroacoustic signal, broken down by SJRWMD segments and by proximity to navigation channels. Excludes off-track records acquired while demarcating muck deposits.

Survey Area		Inside Navigation Channel								Outside Navigation Channel							
			Mean	Mean	% of Records With Muck Thickness in Range of				Survey		Mean	Mean	% of Records With Muck Thickness in Range of				Survey
Name	Segment	n	Depth (m)	MT (m)	0.5 - 1m	1 - 2m	2 - 3m	> 3m	Area (km²)	n	Depth (m)	MT (m)	0.5 - 1m	1 - 2m	2 - 3m	> 3m	Area (km²)
Mims	IR2	263	2.66	1.38	11.0	39.2	30.8		0.36	6588	1.38	0.007	0.2	0.2	0.0		33.60
TitusvillA North	IR3	164	2.86	0.83	13.4	29.9	10.4		0.28	1984	1.41	0.011	0.3	0.4			7.31
TitusvillB North	IR4	217	3.40	0.56	18.0	13.4	6.0		0.36	1899	1.68	0.116	4.5	4.0	0.3		5.12
Titusville South	IR5	366	2.70	0.43	30.3	11.2			0.98	8388	1.77	0.049	1.5	1.2	0.3		46.33
Port St. John	IR5	1224	2.57	0.57	24.6	22.7	0.5	0.1	1.40	10854	1.74	0.045	0.7	1.0	0.5	0.0	31.97
Cocoa	IR7	148	3.13	0.41	27.0	9.5			0.37	1781	2.09	0.185	6.7	2.2	0.8	0.4	5.85
Rockledge	IR8	434	2.94	0.70	21.0	26.3	4.8		0.80	4683	2.35	0.207	7.5	5.1	1.6		10.03
Pineda North	IR9	324	3.37	0.31	18.8	4.9			0.76	3743	2.51	0.123	4.6	0.8	0.3		9.56
Pineda South	IR10	261	3.31	0.31	17.6	8.0			0.69	6372	2.65	0.234	1.3	2.7	2.6	1.9	16.98
Eau Gallie	IR11	225	3.38	0.19	12.4	0.4			0.31	4415	2.35	0.112	2.1	4.3	0.1		11.80
Crane Creek Seg	IR12A	80	3.04	0.51	28.8	10.0	2.5		0.30	1826	2.01	0.064	3.6	1.2			6.55
Turkey Creek	IR12B	92	2.85	0.47	38.0	12.0			0.38	2544	2.03	0.026	0.5	1.2	0.0		8.90
Malabar	IR13A	242	2.73	0.42	27.3	12.8			0.40	4320	1.93	0.007	0.1	0.1			11.76
Grant	IR13B	385	2.52	0.21	9.6	4.2			0.57	1498	1.64	0.076	3.1	1.9	0.6	0.1	4.91
Sebastian Br C	IR14BRE	452	2.32	0.53	20.4	25.4	0.2		0.65	2746	1.45	0.027	0.5	0.4	0.1		9.51
Sebastian IR C	IR14IND	302	2.33	0.40	31.1	8.3			0.55	4007	1.45	0.018	0.5	0.5	0.0		11.68
Wabasso North	IR15	131	2.70	0.32	14.5	9.2			0.23	517	1.45	0.043	1.0	0.6			1.47
Cape Canaveral S	BR2	260	2.60	1.14	4.6	21.9	32.7		0.43	1741	1.81	0.021	0.5	0.7	0.1		4.25
Port Canaveral	BR3	87	2.82	1.47	5.7	25.3	41.4		0.12	3174	1.71	0.030	0.2	0.2			11.90
Cocoa Beach	BR4								0.00	1385	1.74	0.261	1.0	14.4			3.68
S. Cocoa Beach	BR5								0.00	6768	1.86	0.068	0.9	0.3	0.2	0.2	26.54
Satellite Beach	BR7								0.00	606	1.75	0.064	3.3	1.0			3.38
Total =>									10.0								283.1
Lagoon Average =>			2.77	0.56	21.2	15.6	4.1	0.0			1.89	0.08	1.52	1.39	0.39	0.15	

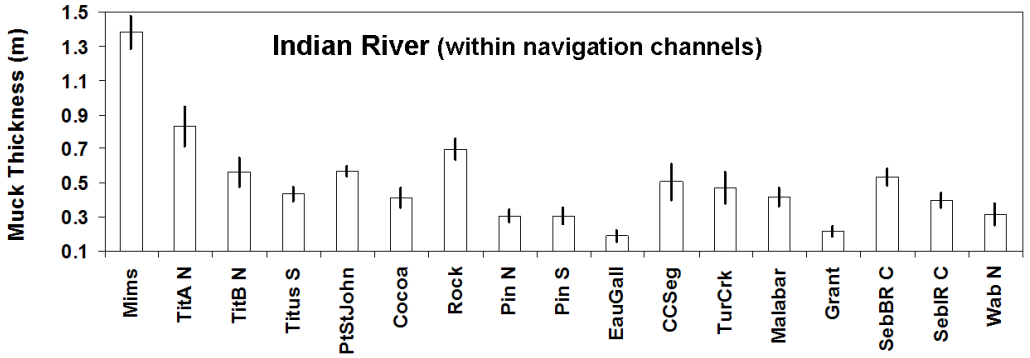

Figure 3.4 Mean values of acoustically-derived muck thickness acquired within the navigation channels of Indian River, broken down by SJRWMD segments. Error bars = 95% CI.

3.3.2 Vertical Extents of Muck

The vertical extents of muck deposits within the SJRWMD segments were further described by tallying the percentage of records falling within four ranges of muck thickness (Table 3.1). Within the navigation channels of Indian River, the Mims segment had the greatest percentage of records in the 2-3m category (30.8%), followed by the two adjacent segments TitusvillA North and TitusvillB North (10.4 and 6.0%, respectively). Of the 14 remaining Indian River segments, only four had any records in the 2-3m category, and only two were greater than 1%. The only two Banana River segments with navigation channels, Cape Canaveral S and Port Canaveral, also had high percentages of records in the 2-3m category, 32.7% and 41.4%, respectively.

3.3.3 Muck Deposits (Outside of Main Navigation Channels)

A total of 23 muck deposits were identified, demarcated and described (Table 3.2, Appendices 3.B1-B2). 22 of the deposits were located in the Indian River, and of these, only one small deposit was located south of Crane Creek. 16 of the 23 muck deposits were in close proximity to a causeway or jetty; of these 10 were north of the causeway or jetty and 6 were south. 12 of the deposits were located in a depression, and 9 of these were also in close proximity to a causeway or jetty. 11 deposits were within 500 m of the shore. 4 deposits were near drainage outlets, and only 2 deposits were in close proximity to spoil islands.

3.3.4 Muck versus Bottom Depth

It is reasonable to assume that muck tends to accumulate in the deeper areas of the lagoon, where it is less likely to be re-suspended by wind shear or boat traffic. Of the 23 muck deposits identified in the Indian and Banana Rivers, 12 were located in riverbed depressions (both man-made and natural). The tendency for muck to migrate towards sinks was further examined by quantifying the probability of encountering muck as a function of bottom depth, using the 69,000+ acoustic records from the Indian River (excluding navigation channels). This was

accomplished by dividing the number of records with a measured muck thickness greater than 0.5 m by the total number of records within a particular range of bottom depth (Figure 3.5). The records were binned into 21 bottom depth increments, ranging from 1.0 to 5.0 m. Muck was not detected at bottom depths less than 1.4 m. In the range of 1.4 – 2.2 m, the proportion of records with muck thickness greater than 0.5 m was only 3.6%. The proportion plateaued at roughly 10% for bottom depths in the range of 2.2 – 3.4 m before beginning a sharp upward trend. In the range of 4- 5 m, an average of 82% of acoustic records were classified as having muck greater than 0.5 m thick. These trends support the idea that muck sediments tend to accumulate in the deeper areas of the lagoon.

Table 3.2 Summary of muck deposits outside of main ICW navigation channel. Includes off-track records acquired while demarcating the horizontal extent of deposits.

Muck Deposit	Survey Area		Centerpoint of Muck Deposit		Avg Depth	Area	Avg Muck	Which Side of	Distance to Shore	In Pit?	Near Jetty/Causeway?			Near Spoil Area?		Near Drainage
Shapefile	Name	Segment	Lat	Lon	(m)	(km2)	(m)	ICW	(m)	Y / N	Y / N	Dir	(m)	Y / N	Dir	Outlet?
Muck01	TitusvillB North	IR4	28.6487	80.7916	2.06	0.0440	1.12	E	315	Y	Y	S	85	N		Y
Muck02	Titusville South	IR5	28.6185	80.7993	2.37	0.0363	0.90	W	220	N	Y	S	30	N		N
Muck03	Titusville South	IR5	28.5864	80.7948	2.41	0.0197	1.40	W	415	Y	N			N		N
Muck04	Titusville South	IR5	28.5611	80.7287	2.18	0.1550	0.88	E	765	N	N			N		Y
Muck05	Titusville South	IR5	28.5306	80.7622	2.86	0.0777	1.68	E	2900	Y	Y	N	265	N		N
Muck06	Port St. John	IR5	28.4854	80.7659	2.48	0.1458	1.30	W	340	Y	Y	S	420	N		N
Muck07	Port St. John	IR5	28.4676	80.7545	2.06	0.0251	0.88	W	620	N	Y	S	25	N		N
Muck08	Port St. John	IR5	28.4058	80.7332	2.47	0.0268	1.25	E	1265	Y	Y	N	210	Y	SW	N
Muck09	Rocklege	IR8	28.3553	80.7140	1.59	0.0364	0.60	E	545	N	Y	S	40	N		N
Muck10	Rocklege	IR8	28.3515	80.7206	2.15	0.0181	0.94	W	82	N	N			N		N
Muck11	Rocklege	IR8	28.3477	80.7130	2.15	0.0957	1.09	E	790	N	N			N		N
Muck12	Rocklege	IR8	28.3345	80.7085	2.80	0.0371	1.81	E	895	N	N			N		N
Muck13	Pineda North	IR9	28.2380	80.6715	2.01	0.0066	1.01	W	125	Y	N			N		N
Muck14	Pineda North	IR9	28.2081	80.6569	2.60	0.0064	1.64	W	445	Y	Y	N	200	N		N
Muck15	Pineda South	IR10	28.2041	80.6431	4.11	0.0528	3.14	E	375	Y	Y	S	135	N		N
Muck16	Pineda South	IR10	28.2004	80.6540	3.58	0.0266	2.58	W	525	Y	Y	S	400	N		N
Muck17	Pineda South	IR10	28.1355	80.6136	3.19	0.1173	1.33	E	990	N	Y	N	15	N		N
Muck18	Eau Gallie	IR11	28.1335	80.6101	2.66	0.2182	1.41	E	336	Y	Y	S	35	N		N
Muck19	Eau Gallie	IR11	28.0872	80.5854	2.58	0.0871	1.40	E	625	N	Y	N	5	N		N
Muck20	Crane Creek Seg	IR12A	28.0784	80.5928	2.41	0.2859	0.51	W	475	N	Y	S	15	N		Y
Muck21	Crane Creek Seg	IR12A	28.0842	80.5869	2.20	0.0307	1.25	E	1010	N	Y	S	60	N		N
Muck22	GRANT	IR13B	27.9674	80.5412	2.82	0.0090	1.25	W	100	Y	N			Y	SW	Y
Muck23	S. Cocoa Beach	BR5	28.2119	80.6321	4.03	0.0741	2.46	W	535	Y	Y	N	120	N		N
	Yes / North / East							12		12	16	6		2		4
	No / South / West							11		11	7	10		21		19

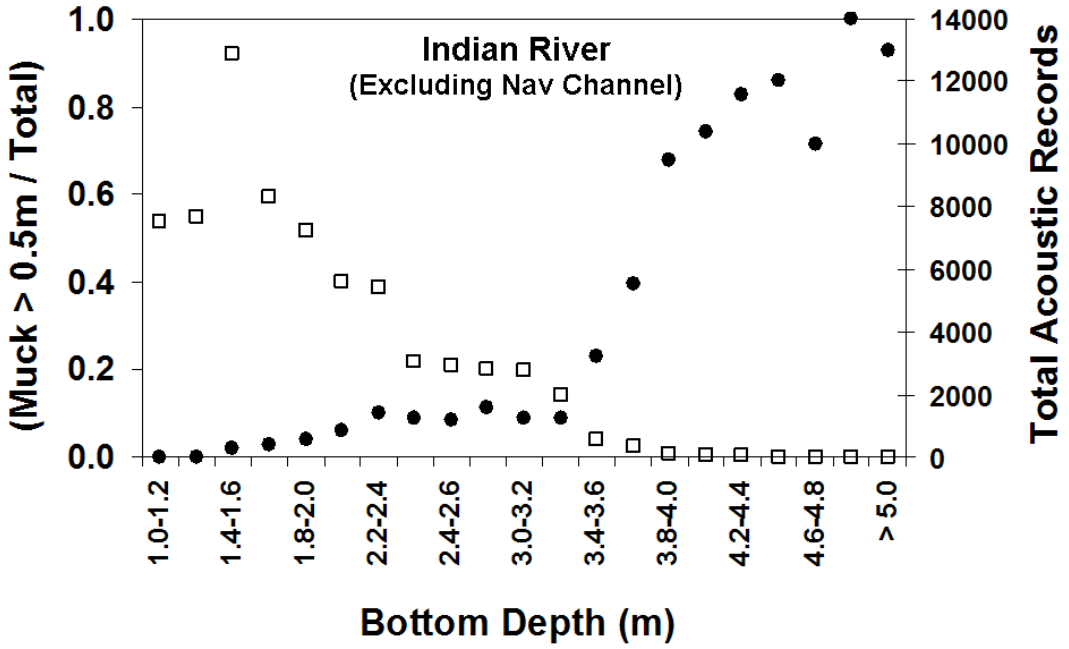

Figure 3.5 (●) Probability of encountering muck as a function of bottom depth, computed as the number of records with measured muck thickness greater than 0.5 m divided by the total number of records (within individual depth bins). (□) Total number of acoustic records within depth increments.

3.3.5 Ground-Truthing

The acoustically-derived muck thickness agreed closely with ground-truthing (n=20, r^2 = 0.882, SE=0.52m), and only slightly under-predicted the thickness of the muck layer (b=0.902) (Figure 3.6). Three of the five samples with the largest under-predictions (1, 11, 13) were constrained by bottom depth, i.e. the ratio of (detected muck thickness):(maximum detectable muck thickness) was close or equal to 1. In another of these samples (#16), the muck layer was capped by a thin layer of highly compacted sand. This caused a large portion of the signal to be reflected off the surficial layer, and the subsequent under-prediction of muck thickness.

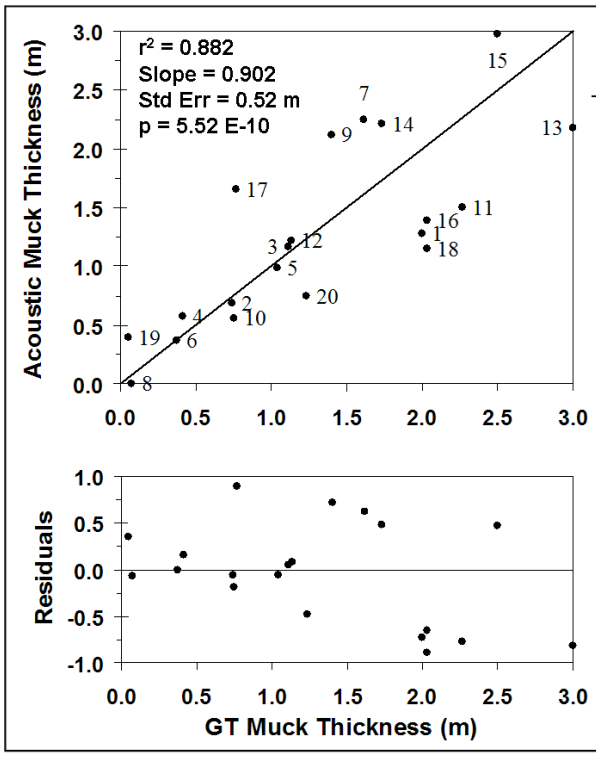

Sample	Sample Location Lat	Lon	Depth (m)	Muck Thickness GT	Acoustic	MT / MT_{Max}
1	28.3555	80.7149	2.15	2.00	1.27	0.988
2	28.3515	80.7201	2.18	0.74	0.68	0.525
3	28.3513	80.7204	2.26	1.11	1.16	0.829
4	28.3512	80.7211	2.37	0.41	0.57	0.374
5	28.3431	80.7130	3.50	1.04	0.99	0.374
6	28.3376	80.7117	3.67	0.37	0.37	0.130
7	28.3372	80.7099	3.13	1.62	2.24	0.993
8	28.3357	80.7066	0.85	0.08	0.00	0.000
9	28.3338	80.7082	2.97	1.40	2.12	1.000
10	28.3337	80.7076	2.28	0.75	0.56	0.390
11	28.2379	80.6713	2.36	2.27	1.50	1.000
12	28.2324	80.6624	3.20	1.13	1.22	0.521
13	28.2083	80.6571	3.04	3.00	2.18	1.000
14	28.2000	80.6543	3.21	1.73	2.21	0.940
15	28.1997	80.6539	3.94	2.50	2.98	0.963
16	28.0866	80.5886	3.09	2.03	1.38	0.618
17	28.0860	80.5898	3.17	0.77	1.66	0.717
18	28.0843	80.5954	2.07	2.03	1.15	0.948
19	28.0823	80.5943	1.91	0.05	0.40	0.299
20	28.0769	80.5932	2.25	1.23	0.75	0.540

Figure 3.6 Ground-truthing of muck layer thickness, accomplished by probing bottom sediments with a calibrated probe. MT/MT_{Max} is the acoustically-derived muck thickness divided by the maximum-detectable muck thickness. Ground-truthed muck thickness reported as the average of three replicates. Acoustic muck thickness reported as the average of the three records nearest the centerpoint of three ground-truthing replicates.

Chapter 4: Detecting end-member structural and biological attributes of a coral reef using an acoustic ground discrimination system

FORWARD

In Chapter 1 it was found that simple scatterplots of E1 and E2 at either 38 or 418 kHz discriminated between the LIDAR-derived benthic habitat classes, but that even after heavy filtering considerable overlap remained between classes. This indicated that more information was needed to reliably and unambiguously discriminate between benthic habitats. In Chapter 2, a multivariate classification scheme was developed to meet the demand for greater discriminatory power; the framework of the multi-pass discriminant analysis (DA) method was established for the simple three-group classification scheme of bare substrate, attached macroalgae, and drift macroalgae. In this chapter, lessons learned on the relict reefs of Palm Beach County, FL and the riverbeds of Indian River Lagoon were extended to a diverse coral reef in Palau. The ostensible purpose was to map topographic complexity as part of a parrotfish territory study, but the results presented in this chapter are focused on the developments that culminated in producing a thematic benthic habitat map from single-beam back-scatter.

This chapter builds on the multi-pass DA method developed for Chapter 2, with (necessarily) greater emphasis on arranging and grooming of the training dataset. In Chapter 2, the three pre-defined bottom classes (bare substrate, attached macroalgae, and drift macroalgae) were intuitive and clearly defined. Defining bottom classes on a diverse coral reef was not as simple. Initial attempts at classifying the training dataset failed because of the nature of the pre-defined categories; the 120+ training samples were initially divided among categories of sand, seagrass, rubble on flat hardbottom, sparse branching coral on flat hardbottom, sparse branching coral on rugose hardbottom, and abundant branching coral on rugose hardbottom. The problem was that all except the sand class were by definition “mixed”, e.g. rubble on flat hardbottom was rubble

and flat hardbottom. Similar to the heterogeneous training samples of Indian River Lagoon, a 30-ping training sample of rubble on flat hardbottom would likely consist mostly of pings encoding rubble, some encoding flat hardbottom, with the balance being some combination of rubble and flat hardbottom. Attempting to cluster a class constituted of two pure acoustic signatures and a mixture of those two is clearly doomed to fail. This problem was corrected by using the new pure-end member approach to cataloging; the 120+ samples constituting the training dataset were instead arranged into pure end-member categories of sand, seagrass, rubble, flat hardbottom, rugose hardbottom, and branching coral. The multi-pass DA algorithm was then used to refine the frequently heterogeneous training samples into their pure end-members by retaining only those records that classified correctly and exceeded a minimum probability of group membership.

The narrow beam-width (6.4^{o}) of the 418 kHz transducer made this single feature extraction approach possible. At the average survey depth of 10 m, the 6.4^{o} beam would ensonify a roughly-circular area with a diameter of 1.2 m. Even on a diverse coral reef, a ping ensonifying such a small area of seabed can be assumed to be fairly pure, i.e. sand, or coral, or hardbottom. This philosophy of utilizing narrow beam-widths to isolate micro-scale features is diametrically opposed to the common practice of utilizing wide beamwidths to ensonify an area larger than the horizontal scale of bottom roughness (e.g. sand ripples). Most AGDS employ beam-widths in the range of 12-55^{o} (Penrose et. al., 2005), similar to the 24-50^{o} range of beamwidths reported in the handful of coral reef studies (Hamilton et al., 1999, Moyer et al. 2005, Riegl and Purkis, 2005; Walker, Riegl, and Dodge, 2008; White et al., 2003). At 10 m, these 24 and 50^{o} beamwidths would ensonify roughly-circular areas with diameters of 4.2 and 9.3 m, respectively. These diameters are clearly above the scale of spatial heterogeneity on a typical coral reef, creating a calibration dilemma; either train the AGDS on homogeneous benthos and leave the heterogeneous benthos un-classified, or attempt to capture the many ‘mixed’ classes and overwhelm the discriminatory capability of the AGDS. In this study, the combination of shallow

depths, narrow beamwidth, a highly replicated training dataset arranged by pure end-member features, refined by multiple passes through DA classification algorithms circumvented this dilemma of scale.

ABSTRACT

A thematic map of benthic habitat was produced for a coral reef in the Republic of Palau, utilizing hydroacoustic data acquired with a BioSonics DT-X echosounder and a single-beam 418 kHz digital transducer. This paper describes and assesses a supervised classification scheme that used a series of three discriminant analyses (DA) to refine training samples into end-member structural and biological elements, utilizing E1′ (leading edge of 1st echo), E1 (trailing edge of 1st echo), E2 (complete 2nd echo), fractal dimension (1st echo shape), and depth as predictor variables. Hydroacoustic training samples were assigned to one of six predefined groups based on the plurality of benthic elements (sand, sparse SAV, rubble, pavement, rugose hardbottom, branching coral), visually estimated from spatially co-located ground-truthing videos. Records that classified incorrectly or failed to exceed a minimum probability of group membership were removed from the training dataset until only 'pure' end-member records remained. This refinement of 'mixed' training samples circumvented the dilemma typically imposed by the benthic heterogeneity of coral reefs, i.e. to either train the acoustic ground discrimination system (AGDS) on homogeneous benthos and leave the heterogeneous benthos un-classified, or attempt to capture the many 'mixed' classes and overwhelm the discriminatory capability of the AGDS. This was made possible by a conjunction of narrow beamwidth (6.4°) and shallow depth (1.2 to 17.5 m), which produced a sonar footprint small enough to resolve most of the microscale features used to define benthic groups. Survey data classified from the 3rd-Pass training DA were found to (i) conform to visually-apparent contours of satellite imagery, (ii) agree with the structural and biological delineations of a benthic habitat map created from visual interpretation of 2004 IKONOS imagery, and (iii) yield values of benthic cover that agreed closely with independent, contemporaneous video transects. The methodology was proven on a coral reef environment for which high quality satellite imagery existed, as an example of the potential for single-beam systems to thematically map coral reefs in deep or turbid settings where optical methods are unsatisfactory.

4.1. INTRODUCTION

Single-beam acoustic ground discrimination systems (AGDS) have been used in a variety of bottom-typing applications, due in large part to their low cost, compact size, ease of deployment, and modest data storage requirements relative to side-scan and multibeam sonar systems. The two most commonly used off-the-shelf AGDS are QTC-View (Collins et al., 1996) and RoxAnn (Chivers et al., 1990), which utilize disparate post-processing algorithms for characterizing echo return waveforms. QTC-IMPACT software decomposes digitized waveforms into 166 parameters (Fourier, wavelet, and shape analysis), reduces the highly collinear variables into three principal components, and divides them into classes using a Bayesian clustering algorithm (Legendre et al., 2002). RoxAnn hardware processes echo returns in real-time and outputs two acoustic energy parameters; E1 (time integral of the squared amplitude of the trailing edge of the 1st echo waveform) and E2 (complete 2nd echo). "E1 and E2 are often referred to as 'roughness' and 'hardness', implying measures of mechanical hardness and geometrical or physical roughness, but they are simply acoustic indices with some unknown relation to seabed conditions" (Hamilton et al., 1999).

A common application of AGDS has been characterization of sediment type as a surrogate indicator of benthic habitat. In this approach it is assumed that benthic community structure is closely correlated with particle size distribution. The AGDS is trained on granulometric parameters measured from sediment grab samples, but is presumed to respond to secondary attributes of particle size distribution, (e.g. acoustic backscatter is correlated with surficial texture (Burns et al., 1989; McKinney & Anderson, 1964), and echo shape is correlated with sediment compaction, via the degree of signal penetration (Ellingsen et al., 2002; Freitas et al., 2006; Hamilton et al., 1999). Numerous studies have assessed the potential for sediment classification by E1 and E2, obtained either directly from RoxAnn or from post-processing of digitized

waveforms, with varying degrees of success (Bax et al., 1999; Collier & Brown, 2005; Greenstreet et al., 1997; Hamilton et al., 1999; Kloser et al., 2001; Wilding et al., 2003). Greenstreet et al. (1997) noted that "RoxAnn was responding to other physical or biotic seabed features other than just particle size". Hamilton et al. (1999) similarly observed that "QTC bottom classes generally had consistent grain size and texture properties, and followed grainsize trends, but RoxAnn classes were difficult to define". Kloser et al. (2001) and Foster et al. (2009) reported that E1 and E2 relate to a combination of seabed hardness and roughness attributes, including the epibenthic biota. Other studies have shown that benthic community structures cannot be predicted by granulometric properties alone, suggesting other factors play a significant role in determining the distribution of infaunal and epifaunal biota (Anderson, 2008; Gray, 1974; Seiderer & Newell, 1999; Snelgrove & Butman, 1994). While these findings do not challenge the general utility of AGDS for mesoscale (10-100's of meters) mapping of sediment distribution, they do seriously undermine attempts to relate such mapping products to microscale (10-100's of centimeters) features of benthic habitats.

More recent efforts have sought to expand the utility of RoxAnn by directly classifying benthic habitats using the full suite of output parameters (E1, E2, depth, and a derived acoustic variability) within the IDRISI image-classification platform for loch (Brown et al., 2002; Foster-Smith & Sotheran, 2003) and coral reef (White et al., 2003) environments. White et al. (2003) assessed RoxAnn's capability to differentiate coral reef habitats by performing external accuracy assessments at four levels of resolution, moving up the dendrogram from highest similarity (k=10) to successively lower similarities (k= 5,4,3). RoxAnn could reliably discriminate habitats at intermediate resolution (e.g. mud, sand with sparse algae, sand with algae and sparse coral, and coral) but at the highest resolution (k=10), which included various combinations of substrate and coral elements, there was excessive overlap between classes. Halley & Bruce (2007) used RoxAnn-based parameters (E1, $S_{v,Max}$, E2) and SeaBed Mapper 4.0 to classify an area of granite

reef outcroppings into four classes; sand, hard sand, low- and medium-profile reefs. While these levels of resolution would likely satisfy many resource management requirements and would clearly be superior to simple bathymetry in areas inaccessible to optical imagery, achieving greater resolution of coral reef benthic habitats from an AGDS remains an attractive proposition. Foster-Smith & Sotheran (2003) posited that RoxAnn E1/E2 Cartesian plots are "very limited and not recommended for interpretation of AGDS data". Foster et al. (2009) performed a point-by-point comparison of data acquired from a BioSonics DT-X digital echosounder against a backdrop of LIDAR-delineated habitat classification, and found that E1/E2 plots at both 38 kHz and 418 kHz differentiated benthic habitats, although considerable overlap remained even after heavy filtering of E1 and E2 (20-80 percentile) and consolidation from eight to five habitat classes.

The present study adds the parameters E1′ (defined as the front part of the 1st echo waveform) and fractal dimension (a measure of shape irregularities of 1st echo waveform) to E1, E2, and depth for a single frequency (418 kHz) AGDS classification of a coral reef environment in Palau. A novel supervised classification scheme is used to refine heterogeneous training samples into end-member structural and biological elements by passing training data through a series of discriminant analysis algorithms.

4.2. METHODS

4.2.1 Study Area

An acoustic survey was conducted between April 24-28, 2006 on the fore reef slope and back reef lagoon of Ngaderrak, the inner barrier reef of a double barrier reef system located in Koror, Republic of Palau (Figure 4.1). The fore reef was surveyed from depths of 1.2 to 17.5 m, from the seaward edge of the reef crest down to the transition into sand. The mean slope angle of the

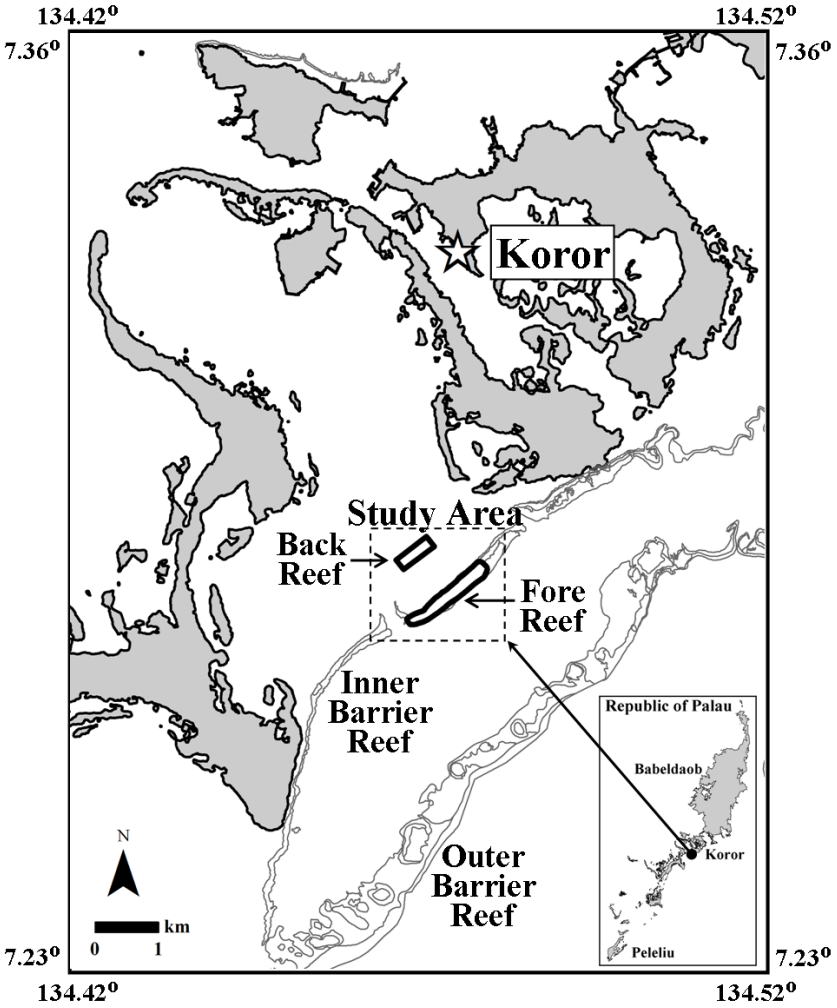

Figure 4.1 Study area in the Republic of Palau, located on the inner barrier reef offshore the island of Koror. Two areas were surveyed; one on the fore reef and another in the back reef lagoon, separated by an intertidal reef crest.

fore reef was approximately 3.7 degrees. The upper fore reef was characterized by well-developed spur and groove formations that transitioned into progressively lower rugosity aggregate reef, starting midway down the slope. These reef structures were separated by large expanses of flat pavement covered by a variably-thick layer of carbonate sand and variably-abundant rubble. The major geomorphological structures were generally contiguous over the scale of the study site, but at the scale of the sonar footprint the distribution of structural and biological components was characterized by a high degree of benthic heterogeneity. The dominant scleractinian taxa were branching forms of fine, densely branched *Millepora*, coarse,

open branched *Acropora*, and tabulate *Acropora* (Knudby & LeDrew, 2007). The back reef lagoon was surveyed from a depth of 1.9 m on the reef flat down to a depth of 9.0 m at the deepest part of the lagoon. The reef flat was primarily composed of flat pavement with scattered coral and rubble. The transition from reef flat to lagoon was sudden; depth decreased from roughly 2 to 7 m in just 50 m. The lagoon bottom gradually transitioned from a thin veneer of sand over pavement in the southwest to deep sand in the north-east. The portion of lagoon surveyed was primarily uncolonized carbonate sand with isolated patches of *Halophila* spp. along the northernmost extent. Within these patches the seagrass was typically 4 cm high and sparse (approximately 25% areal cover).

4.2.2 Hydroacoustic Survey

Hydroacoustic data was acquired with a BioSonics DT-X echosounder and a single-beam 418 kHz digital transducer with a full beamwidth of 6.4^{o}, which ensonified a roughly-circular area with a diameter equal to 11% of water depth. Hydroacoustic data were collected at a 5-Hz sampling frequency and 0.4 ms pulse duration, at an average net speed of 4 knots (vessel plus drift). Global positioning data were collected with a Trimble Ag132 dGPS operated in satellite mode. The dGPS signal was interfaced with navigational software to provide real-time monitoring of vessel position with respect to geo-referenced imagery and pre-planned survey lines, spaced 25 m apart. Within the fore reef study area, meandering tracklines were also surveyed while acquiring hydroacoustic samples for the training dataset. The total area surveyed was 0.30 and 0.14 km^2 on the fore and back reefs, respectively.

4.2.3 Data Processing and QA

Hydroacoustic data were processed with BioSonics Visual Bottom Typer (VBT) seabed classification software (v1.10) to obtain values of E1′ (time integral of the squared amplitude of the leading edge of the 1st echo waveform), E1 (2nd part of 1st echo), E2 (complete 2nd echo),

and FD (fractal dimension of 1st echo waveform), and depth (Burczynski, 1999). VBT computes FD as the Hausdorff dimension of the first echo (Mandelbrot, 1982), simplified by gridding the waveform into 'box' dimensions (Hastings & Sugihara, 1994). The authors of the FD method used by VBT proposed the fractal structure of the bottom surface would be reflected in the shape of the echo waveform, making FD a measure of topographic complexity (Lubniewski & Stepnowski, 1997). The E1′ sampling window was increased above the theoretical recommendation (equal to pulse duration) so that E1 would capture only the trailing edge of the first echo, thereby maximizing sensitivity to scattering components of the seabed. Other critical user-defined settings included a time-varied gain adjustment of 20log[Range] to compensate for spherical spreading and absorption losses, averaging of 5 pings for improved signal stability, and a minimum energy filter (50%) to preferentially select echoes contacting the seabed at angles closest to normal incidence. The acoustic energy parameters E1′, E1, and E2 were log-transformed to improve normality (Sokal & Rohlf, 1981). The current version of VBT does not normalize echo length to a reference depth, which can cause depth-biasing of the values of E1′, E1, E2, FD, and possibly E0 (Dommisse et al., 2005). To ameliorate the potential for depth contamination, log-transformed acoustic energy parameters and FD were empirically normalized to median survey depth. Median values of acoustic parameters were computed at fourteen ranges of depth and logarithmic polynomials were fit to the four acoustic parameters. Depth-normalization factors were applied to each hydroacoustic record, calculated as the ratio of model-predicted acoustic energy at actual depth divided by the model-predicted acoustic energy at median survey depth (Figure 4.2). Depth-normalized hydroacoustic records were constrained between 1.25-17.5 m and filtered by class-specific 1 and 99 percentiles of logE1′, logE1, logE2 and FD. Remaining outliers were identified from scatterplots of independent variables and de-selected from the training dataset prior to submitting to discriminant analysis. Outliers frequently result from intrusion of environmental and hardware factors, e.g. ship wakes, excessive pitch and

roll, co-mingling of echoes, and can be separated from the main data cloud by orders of magnitude.

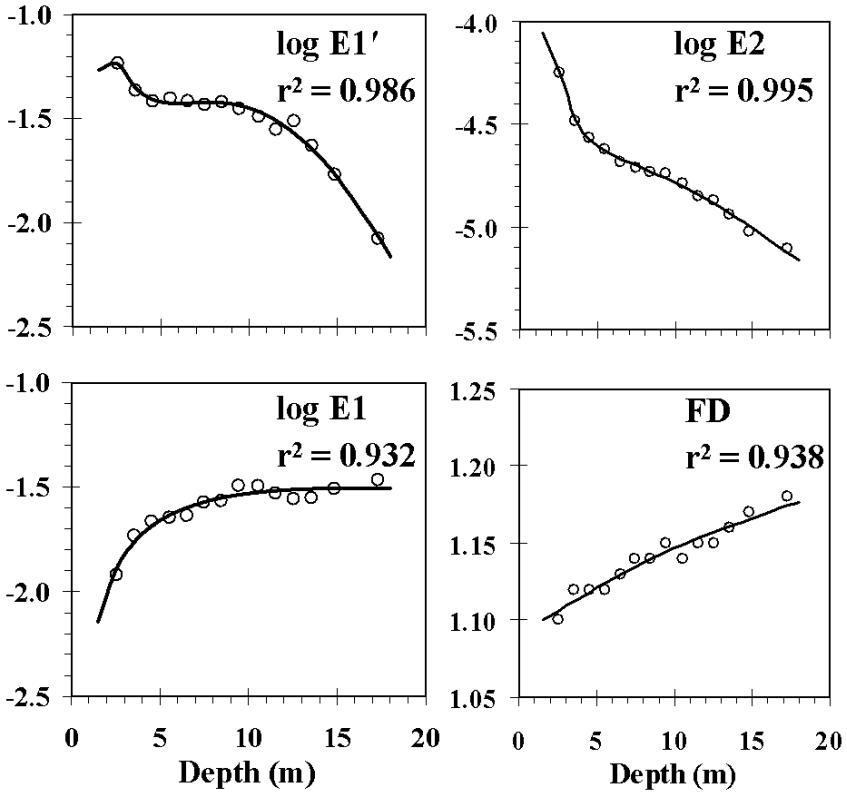

Figure 4.2 Empirical models used to normalize acoustic parameters to median survey depth, created from survey data collected over reefal zones within the study area (n=10859). High-order logarithmic polynomials (solid line) were fit to median values of acoustic parameters computed for 14 depth bins (○).

4.2.4 Training Dataset

Over 100 ground-validated hydroacoustic samples were collected within the study area, of which 65 were chosen for the training dataset. Samples were collected with the vessel drifting in idle or anchored over a target, and consisted of 30-120 seconds of concurrent hydroacoustic and video files; the latter were acquired with a drop camera trailing just behind the ensonified area. Videos were reviewed post-survey and assigned visually-apparent areal cover of structural (unconsolidated carbonate sand, rubble, pavement, rugose hardbottom) and biological elements (submerged aquatic vegetation (SAV), massive and sub-massive coral, branching coral). Areal

cover was used to assign training samples to an initial set of predefined groups; (1) sand, (2) sparse SAV, (3) rubble, (4) pavement, (5) rugose hardbottom, and (6) branching coral. The SAV group was mostly *Halophila spp*., approximately 4 cm high and 25% areal cover. The 'branching coral' group included several genera of varying form, ranging from the dense, fine branches of *Millepora spp*. to the open, large branches of *Acropora spp*. The 'rubble' group was primarily large, unconsolidated fragments of the aforementioned branching corals.

4.2.5 Multivariate Classification

Discriminant analysis (DA) is an eigenanalysis technique (i.e. matrix-based) that determines the linear combination of independent variables that maximizes discrimination between predefined groups. The independent variables logE1′, logE1, logE2, FD, and depth were entered stepwise with prior probabilities of group membership computed from group size. The classification workflow was divided into three major segments; (1) an exploratory DA to arrive at the most logical set of predefined groups and optimal number of acoustic classes to describe them, (2) a series of three descriptive DA's to refine the training dataset into end-member records and produce a set of classification functions, and (3) a predictive DA to classify survey records using the classification functions of the 3rd-Pass descriptive DA (Figure 4.3).

4.2.5a Exploratory DA - The most satisfactory arrangement of predefined groups (i.e. the number and defining features of groups, assignment of training samples to groups) was arrived at by a course of exploratory DA's. As a check against the subjective *a priori* assignments, an approximation of the optimum number of groups was obtained using one of the many stopping rules developed for clustering algorithms. Milligan & Cooper (1985) reported the variance ratio criterion (VRC) of Calinski & Harabasz (1974) to be amongst the best performers in a simulation study of 30 stopping rules. To compute the VRC, the 5 independent variables were normalized by $(x-\mu)/\sigma$ for equal weighting prior to submitting the training dataset to a principal

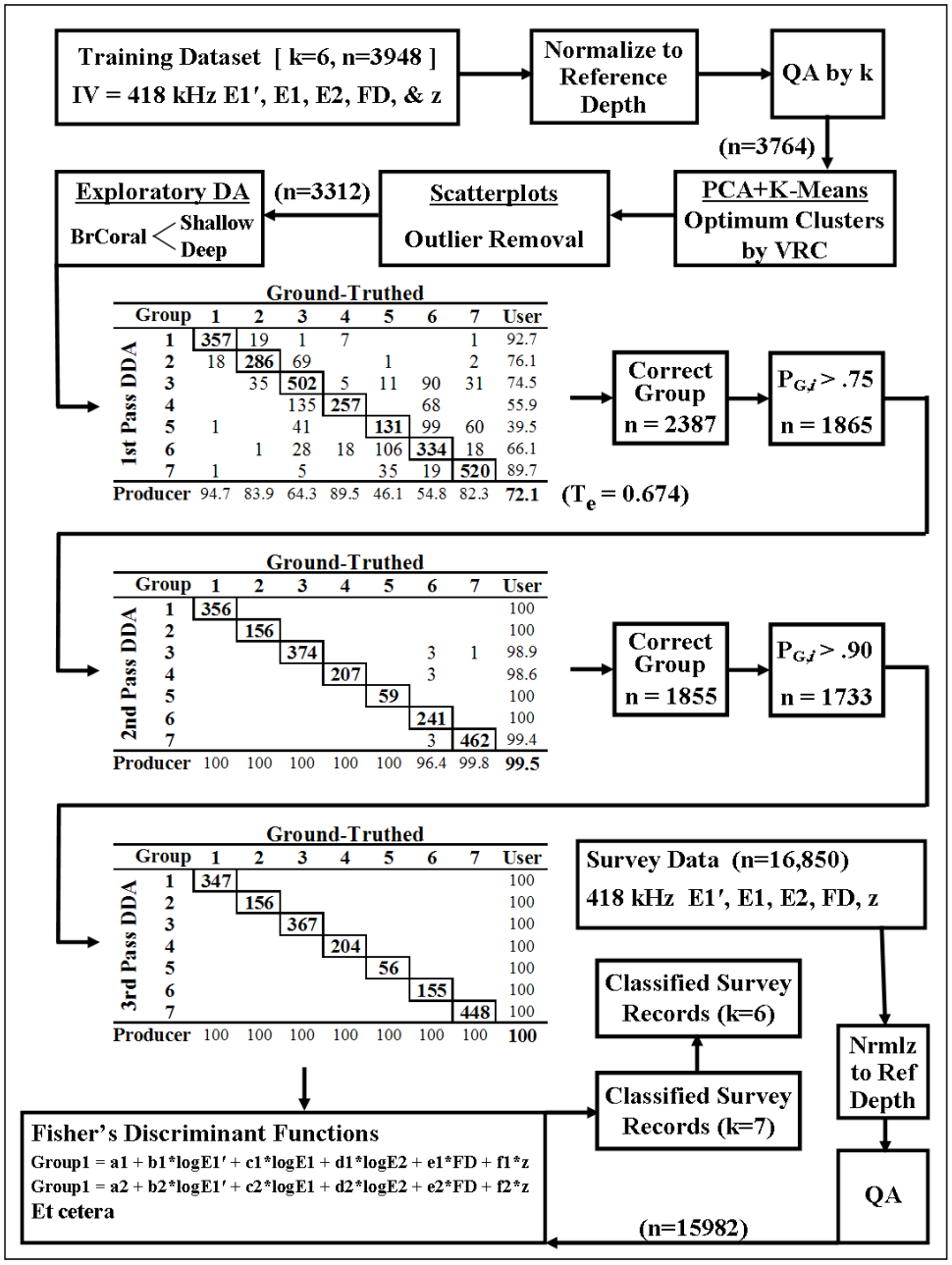

Figure 4.3 Workflow of classification scheme. 65 hydroacoustic samples were assigned to one of six *a priori* groups (n=3948). Log-transformed values of E1′, E1, E2, and FD were empirically normalized to depth. QA consisted of min/max depth and 1/99 percentile filters, calculated individually for each group, followed by outlier filtering. An exploratory discriminant analysis (DA) revealed seven acoustic classes constituted the six *a priori* groups. The training dataset was refined by passing through three descriptive DA's. Only those catalog records that (1) classified correctly and (2) exceeded a minimum probability for group membership were passed onto the next DA. The Fisher's Linear Discriminant Functions obtained from the 3rd-Pass DA were used to classify survey data into one of 7 acoustic classes, which were then consolidated into the six *a priori* benthic habitat groups.

components analysis. The first 5 principal components, which accounted for 100% of the variance, were then submitted to a K-means cluster analysis to separate the training data into homogenous groups. For each value of k, the VRC was computed as the maximum between-cluster variance divided by the minimum within-cluster variance. Calinski & Harabasz (1974) suggest that the first local maximum of VRC is an informal indicator of the optimal value of k.

4.2.5b Descriptive DA – Training records submitted to the 3rd-Pass descriptive DA were tested for critical DA assumptions because (i) ecological data frequently violate DA assumptions (Williams, 1983), e.g. skewed distributions commonly arise when values cannot be negative (Limpbert, Stahel, & Abbt, 2001), (ii) a primary objective was to assess the discriminatory power of individual hydroacoustic variables, judging by the canonical functions obtained from the descriptive DA, and (iii) unequal variance-covariance matrices distort plots of canonical functions (Krzanowski, 1977; Lachenbruch et al., 1973; Wahl & Kronmal, 1977; Williams, 1982). The assumption of normal multivariate distributions was assessed by ratios of skewness and kurtosis to their respective standard errors, recognizing that little is known about selecting proper significance levels for formal tests of normality (Afifi, Clark, & May, 2004). Homogeneity of variance and covariance was assessed by comparison of between-group variances and similarity of log determinants, respectively. Significance of the discriminant function was tested by a chi-square transformation of the Wilks' lambda score. The critical DA assumption of mutual exclusivity of groups was impinged upon by "mixed" training samples acquired over heterogeneous benthos, i.e. the group-defining structural/biological element exceeded 75% in only 26 of 65 training samples. For example, only 11 of the 15 samples comprising the 'sand' group were visually-estimated as 75% or greater sand, the balance being primarily rubble and branching coral. This violation was addressed by extracting end-member records from the mixed training samples in a series of three descriptive DA's. Only records that (1) correctly classed by

the discriminant analysis and (2) exceeded a minimum probability of group membership were passed onto the next DA (Figure 4.3). This process also removed any remaining outliers, to which DA is particularly sensitive.

4.2.5c Predictive DA - Discriminant analysis generates a set of Fisher's linear discriminant functions (FLDF) for each group, based on the linear combination of independent variables providing the best discrimination between groups. The FLDF from the 3rd-Pass descriptive DA of the training dataset were used to classify survey records. For each record, group scores were computed as the sum of the product of FLDF coefficients and independent variables plus a constant. Records were classified as the group with largest score.

4.2.6 Evaluating the Efficacy of Acoustic Classification

Ideally, an adequate number of ground-truthed hydroacoustic samples would have been withheld from the training dataset and used for an external accuracy assessment, since predictive accuracy will always be greater using the training dataset than for a new dataset (Huberty, 1994; Kachigan, 1986). However, the high degree of benthic heterogeneity encountered during the survey (i) necessitated more training replicates than anticipated (to demonstrate that heterogeneous samples could be refined into end-member structural and biological components), and (ii) rendered the most heterogeneous samples unusable (as the objective was to avoid "mixed" acoustic classes, which would result from ensonifying multiple structural/biological elements in a single ping). For these reasons the external accuracy analysis was abandoned in favor of using all applicable ground-truthing samples for creating a more diverse and robust training dataset. An internal accuracy assessment was conducted for each of the three descriptive DA's; overall accuracy, producer's accuracies, and user's accuracies were computed directly from the error matrices (Story & Congalton, 1986). Overall accuracy was adjusted to the number of benthic groups using the Tau coefficient for equal probability of group membership, T_e (Ma & Redmond, 1995). Tau

is a measure of the improvement of the classification scheme over a random assignment of polygons to categories, bounded between -1 (0% overall accuracy for 2 map categories) and 1 (100% accuracy for any number of categories).

In lieu of a conventional external accuracy analysis, the acoustic classification scheme was assessed by comparison to (i) independent, contemporaneous, spatially co-located video transects of the fore reef of Ngaderrak (Marcos, 2008) and (ii) a recent benthic habitat map (BHM) of the Palauan archipelago, produced for the National Ocean Services coral reef mapping, assessment, and monitoring program (Battista, Costa, & Anderson, 2007b). A synoptic characterization of the fore reef (i) was compiled from the average percent cover of video grabs obtained from a hull-mounted video camera, automatically classified using color and texture features (Marcos, 2008; Vergara, 2009). The video transects were limited to approximately 8 m depth by image resolution. The video transects were not run along the acoustic tracklines, so a 10 m buffer was used to select acoustic and video records, i.e. acoustic records within 10 m of a video record, and vice versa. The BHM (ii) was created through visual interpretation of 2004 multispectral IKONOS imagery using the NOAA Habitat Digitizer extension at a 1-acre minimum mapping unit, guided by a hierarchical classification scheme. Polygons were drawn around geographic zones, e.g. reef flat, lagoon, and further sub-divided on the basis of biological and structural features. Biological cover assignments were made by stepping through the following categories until 10% or more cover was encountered; live coral, seagrass, macroalgae, coralline algae, turf, uncolonized. The predictive accuracy of the NOAA BHM at the detailed levels of geomorphological structure and biological covers detailed biological cover was 90.0% and 79.9%, respectively (Battista et al., 2007b). The acoustic interpretation of the NOAA BHM was quantified by tallying acoustic classifications within each BHM polygon. The general fit of acoustic classification was judged by superimposing classified trackplots and spatially-continuous contour plots onto the IKONOS imagery. Contour plots were created with radial-basis

interpolation functions (ArcMap v9.2), which are exact and deterministic and make no assumptions about the data.

4.3. RESULTS

4.3.1 Data Processing and Exploratory DA

Quality analysis reduced the number of training dataset records from 3,948 to 3,764 and outlier removal reduced the final number to 3,312 (Figure 4.3). A series of exploratory DA's revealed the most satisfactory arrangement of predefined groups to be; (1) sand, (2) sparse SAV, (3) rubble, (4) pavement, (5) rugose hardbottom, (6) branching coral (deep), and (7) branching coral (shallow). The need to divide the 'branching coral' group into shallow ($P_{50,depth}$ = 4.1 m) and deep ($P_{50,depth}$ = 9.0 m) acoustic classes was evident in scatterplots of DF1/DF2, E1/E2, and E1/FD. There were no apparent physical factors other than depth to account for the division; both the deep and shallow classes had various branching morphologies in common, including finely and densely branched *Millepora*, coarsely and open branched *Acropora*, and tabulate *Acropora*. Based on previous observations of lower than expected values of E2 over rough seabeds (Foster et al., 2009; Hamilton et al., 1999; Riegl et al., 2007), it is inferred that at shallow depths the colonies of branching corals scattered the signal to such an extent that a large proportion of the signal did not return to the transducer, reducing the values of all acoustic energy parameters, but particularly the multi-path E2, relative to the same coral colonies occurring at deeper depths (Figure 4.4d).

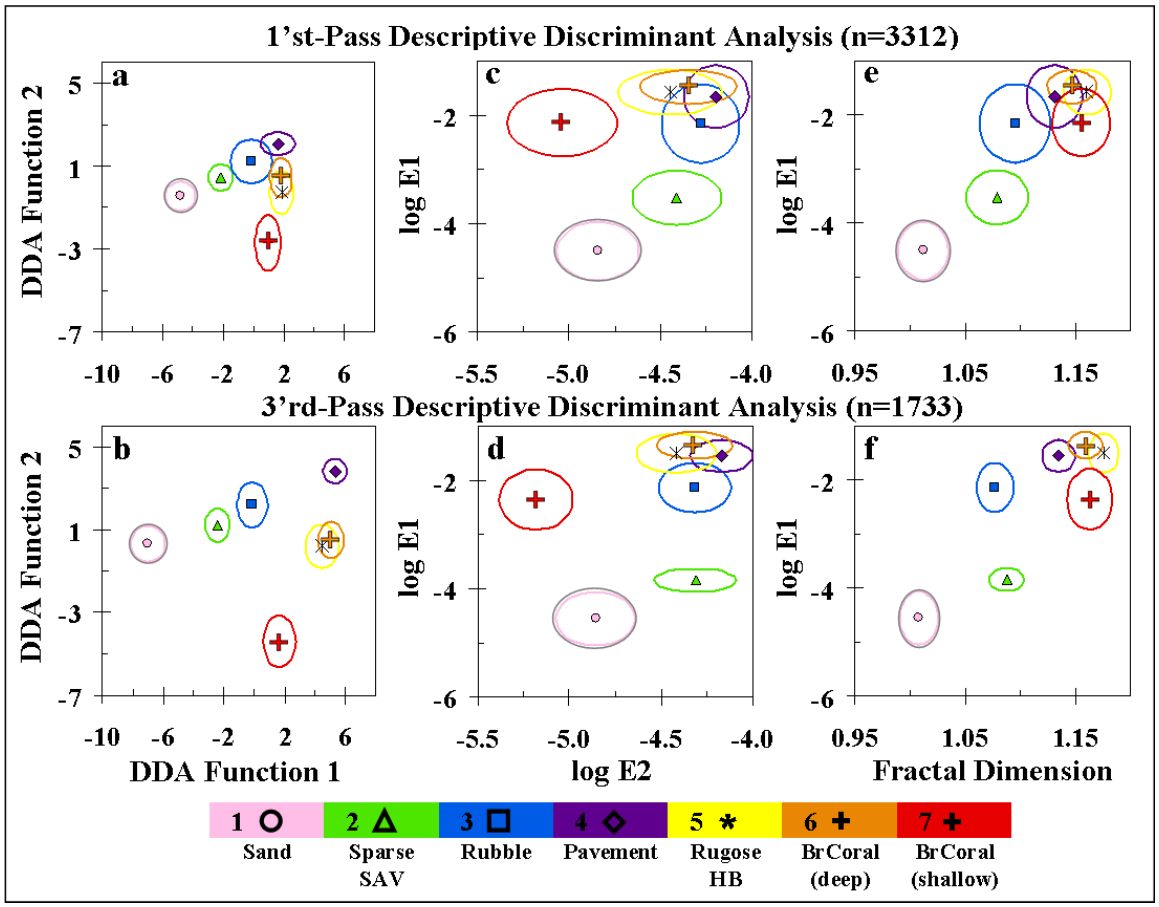

Figure 4.4 Scatterplots of supervised classification and refinement of training dataset. Centerpoints denote cluster averages, ellipses are dispersion (1 standard deviation) about x and y. Discriminant functions 1 and 2 (of 5) of training data submitted to the 1st (a) and 3rd-Pass (b) descriptive DA (DDA), using predictor variables logE1', logE1, logE2, fractal dimension (FD) and depth. Shown for comparison are the log E1vsE2 (c-d) and logE1vsFD (e-f) scatterplots of the DDA training records.

Median values of the four acoustic parameters were calculated for each of the seven acoustic classes (Table 4.1). The partitioning of E1′ and E1 bottom sampling windows had the desired effect of discriminating topographic complexity by constraining E1 to trailing edge of the first echo waveform, which is primarily comprised of incoherent backscatter reflected from a combination of rough seabed surfaces and epibenthic biota. The contribution of E1 to the total integrated area of the first echo waveform [E1/(E1′/E1)] ranged from 0.001 for 'sand' to 0.939 for 'branching coral (deep)'.

Table 4.1 Median values of predictor variables of refined training dataset (after 3rd DDA, n=1733) computed for the 7 acoustic classes. Also included are the 5, 50, and 95th percentiles of bottom depth. SAV = submerged aquatic vegetation. HB = hardbottom. BrCoral = branching coral.

Acoustic Class		Median Values Training Dataset					Depth Percentiles (m)					
		E1′	E1	E1	E2	FD	Training Data			Survey Data		
		$x10^{-3}$	$x10^{-3}$	(E1′+E1)	$x10^{-5}$	$x10^{1}$	P_5	P_{50}	P_{95}	P_5	P_{50}	P_{95}
1	Sand	29.9	0.03	0.001	1.44	1.007	5.3	5.4	7.4	2.2	7.0	12.3
2	SAV (sparse)	58.3	0.15	0.003	4.70	1.086	5.6	5.7	5.7	2.0	2.8	10.1
3	Rubble	49.8	6.99	0.123	4.87	1.082	2.9	8.4	14.3	2.5	6.8	12.4
4	Pavement	65.5	29.6	0.312	6.55	1.137	14.0	14.4	14.6	10.1	13.6	17.6
5	Rugose HB	39.1	36.3	0.482	4.50	1.176	2.4	6.9	7.3	2.2	5.8	8.8
6	BrCoral (deep)	2.89	44.3	0.939	5.02	1.159	8.3	9.0	15.4	6.4	9.8	13.8
7	BrCoral (shallow)	1.00	3.17	0.760	0.57	1.166	3.6	4.1	4.4	2.0	5.1	9.1

The first local maxima of the VRC criterion, obtained from a PCA + K-means clustering of the training dataset, suggested the optimum number of clusters was 8. Table 4.2 is a comparison matrix of exploratory DA groups (k=7) versus PCA + K-means clusters (k=8).

Table 4.2 Comparison matrix of training dataset records, alternatively classified by the exploratory DA (columns) and the PCA+K-means cluster analysis (rows). The latter was used as an independent verification of the appropriate number of acoustic classes, using the variance ratio criterion as a guide. Going across rows, 6 of 8 K-means clusters are dominated by a single DA Group, validating the number of *a priori* groups.

	DA Group Assignment								
K-Means Cluster	1	2	3	4	5	6	7	n	%
1			240	260		60		560	89.3
2		31	328		6	97	21	483	67.9
3	360	15	2	7			1	385	93.5
4					3	6	355	364	97.5
5		1	119		204	175	33	532	93.6
6	1		23		68	72	220	384	57.3
7	16	294	57		2		2	371	79.2
8			12	20	1	200		233	85.8
								3312	

Going across rows, it can be seen that 6 of the 8 K-means clusters were dominated by a single DA group. Given the diametrically-opposed design of the two algorithms, i.e. maximizing between-group variation of predefined groups (DA) versus minimizing within-cluster variation of undefined groups (K-means), this level of agreement is strong evidence that the 7 groups identified by the exploratory DA captured the full extent of acoustic diversity present within the training dataset. It also suggests further discrimination of the seabed was not warranted, given the samples constituting the training dataset.

4.3.2 Multi-Pass Descriptive DA

The seven-group training dataset was submitted to a series of three descriptive DA's to refine the predominantly heterogeneous samples into end-member records. The overall internal classification accuracy was 72.1% for the 1st Pass DA, 99.5% for the 2nd Pass DA, and 100.0% for the 3rd Pass DA. The proportion of records rejected by the three DA's was equitably distributed among individual training samples, which suggests the independent variables represented spatially and temporally consistent seabed characteristics of the predefined groups (Figure 4.5).

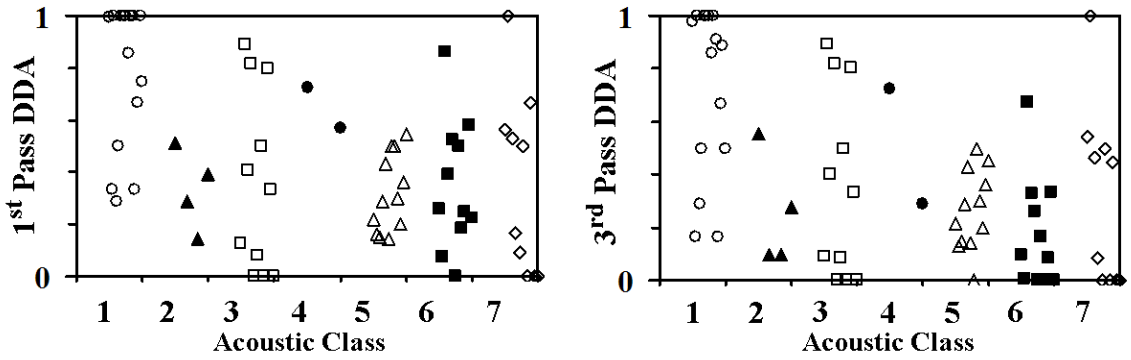

Figure 4.5 Proportion of training dataset records that (1) classified correctly and (2) exceeded the minimum probability of group membership following the 1st (upper) and 3rd (lower) descriptive DA. Each symbol represents one of the 65 catalog samples comprising the seven-class raining dataset, divided into seven acoustic classes; 1=sand, 2=sparse SAV, 3=rubble, 4=pavement, 5=rugose hardbottom, 6=branching coral (deep), and 7=branching coral (shallow). The equitable rejection of records among individual training samples suggest suggests the independent variables represented spatially and temporally consistent seabed characteristics of the seven acoustic classes.

4.3.3 Predictive DA

The 15982 survey records that passed QA were classified into 1 of 7 acoustic classes using the Fisher's linear discriminant functions obtained from the 3rd-Pass descriptive DA. The deep and shallow branching coral classes (6 and 7) were consolidated into a single 'Branching Coral' group for mapping, as the distinction appeared to be based solely on signal properties and not on any apparent ecological properties. The classified acoustic trackplots and interpolated surfaces are shown superimposed onto IKONOS imagery, with delineations of geographic zone as described by the NOAA benthic habitat map (BHM) (Figure 4.6a&c). The location and acoustic class designation of training samples are shown in Figure 4.6b. The biological cover and geomorphological structure assignments of the NOAA BHM are shown in Figure 4.6d-e.

4.3.4 Evaluating the Efficacy of Acoustic Classification

4.3.4a Qualitiative Assessment - The distribution of acoustic classifications conformed closely to the visually-apparent contours of IKONOS imagery and to the delineations of NOAA BHM structural and biological classifications. In the fore reef area the acoustics accurately detected the reef edges and correctly concentrated the 'branching coral' classifications on the seaward edge of the shallow spur and groove and aggregate reef formations (Figure 4.6a). Furthermore, the acoustics correctly placed most of the 'rugose hardbottom' classifications on the well-developed, shallow aggregate reef polygons (BHM polygons 18 and 16 in Figure 4.6d). The acoustics also correctly classified the deep hardbottom (polygons 22 and 21) as 'pavement', with a small amount of 'branching coral' along the edges. The acoustic classification of the shallower portion of polygon 21 correctly reflected a transition to more 'rugose hardbottom' and 'branching coral'. At the time of the survey, this acoustic characterization was a more accurate description of the deep hardbottom features than that of the NOAA BHM, which classified the deep hardbottom as 'aggregate reef with 90-100% coral cover'. In the back reef area the acoustics accurately detected the break between reef flat and lagoon, correctly classified the lagoon as predominantly 'sand'

with a small amount of 'rubble' (Figure 4.6a&c), and placed 'branching coral' along the edge of the reef flat (polygon 10, 90-100% coral on pavement). Other than polygon 10, the majority of classifications on the reef flat were 'sparse SAV', which generally agrees with the BHM biological cover assignments. The acoustics incorrectly classified polygon 7 (BHM = 90-100% seagrass) as 'rugose hardbottom', which is surprising given the separation of these two classes in discriminant function space (Figure 4.4).

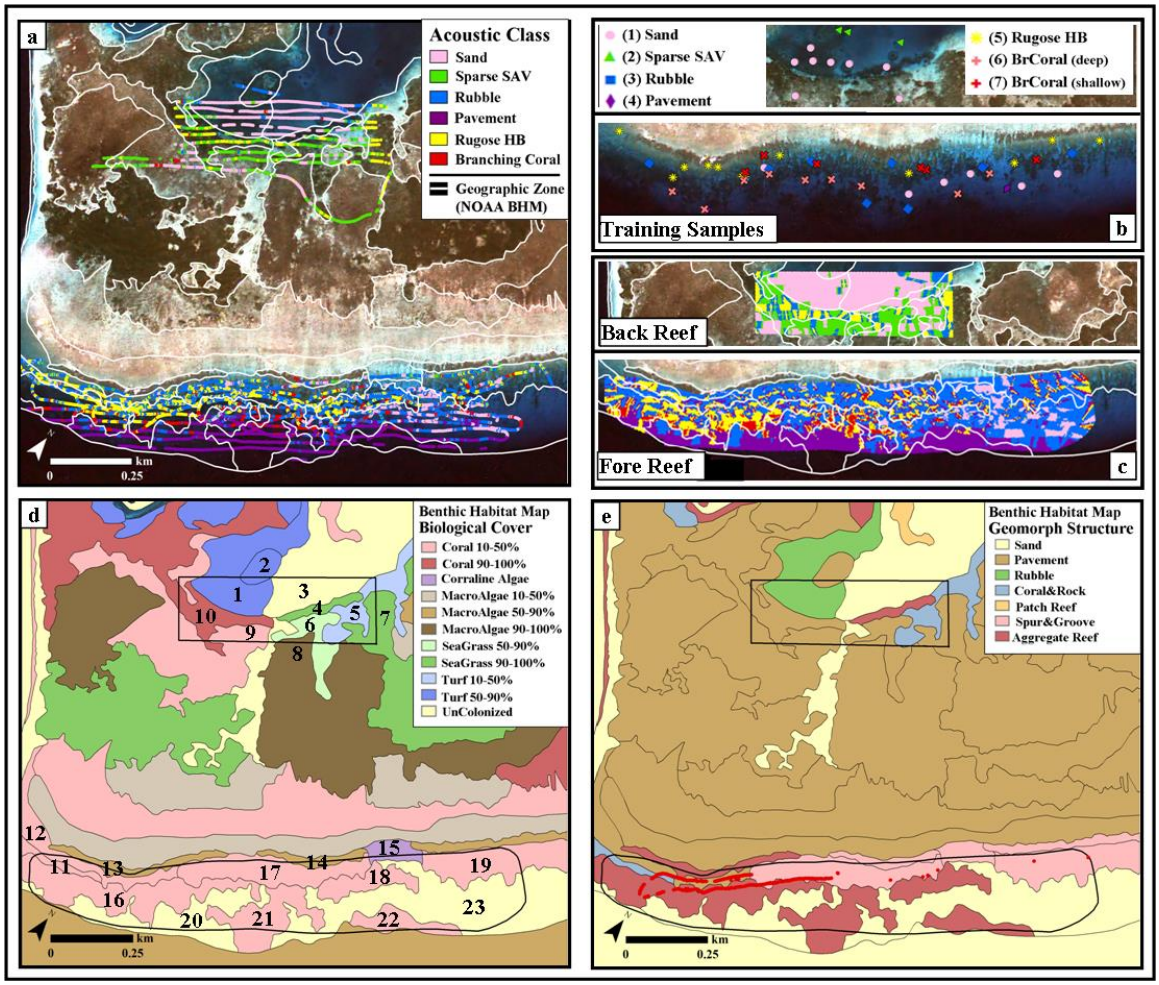

Figure 4.6 (a) Classified hydroacoustic trackplot of survey data, using the Fisher's linear discriminant functions obtained from 3rd-Pass descriptive DA superimposed on IKONOS imagery (with NOAA BHM delineations of geographic zone), (b) locations of training dataset samples, (c) interpolated map of classified survey trackplot, (d) NOAA benthic habitat map of biological cover with alias ID's of NOAA polygons (see Table 4.4) and (e) geomorphological structure. Black outlines in d-e indicate the boundaries of interpolated classification maps. Red circles in (e) denote video transect points within a 10 m buffer of the hydroacoustic trackplot.

4.3.4b Quantitative Assessment – The acoustic classification scheme was quantitatively assessed by comparison to (i) independent, contemporaneous, spatially co-located video transects on the fore reef of Ngaderrak and (ii) the NOAA BHM. The average percent cover computed from video transect records was in very close agreement with the acoustic classifications, computed from the 310 still images and 1,592 acoustic records that fell within 10 m of each other (Figure 4.6e, Table 4.3).

Table 4.3 Synoptic Characterization of Ngadeerak Fore-Reef: Comparison of acoustic classification of survey data to automated classification of still images obtained from an independent, contemporary video transect. Acoustic and image records are co-located within a 10 m buffer (see Figure 4.6e).

	n	Sand & Pav	Rubble	Rugose HB	Sp. SAV	BrCor
Acoustic	1592	4.5%	37.6%	41.3%	6.5%	10.1%
Video	310	3.6%	35.1%	37.7%	n/a	23.7%

The only discrepancy was 'branching coral', which the acoustics estimated as 10.1%, versus the 23.7% obtained from still images. This discrepancy diminishes if the acoustically-predicted 'sparse SAV' cover (6.5%) is added to 'branching coral' (10.1% + 6.5% = 16.6%, which is close to 23.7%). There are reasons to suspect that branching coral was mis-classified as SAV, given (i) there was no SAV observed on the fore reef, and (ii) the acoustic SAV predictions tended to be in places where coral would be expected. Comparison to the NOAA BHM was achieved by tallying acoustic survey records falling within each BHM polygon and computing the percent membership of acoustic classes (Table 4.4). For ease of comparison, the BHM polygons were sorted into 6 major groupings (BHM1-6) of structural and biological attributes. The acoustic interpretation of the BHM groupings was generally consistent and rational. To cite a few examples, the two BHM coral groupings, BHM1 (rugose reef) and BHM2 (pavement), acoustically classified as 13.1% and 10.5% 'branching coral', compared to just 3.9%, 4.0%, and 1.5% for the non-coral groups

(BHM3-5). The two uncolonized sand and pavement BHM groupings (BHM5 and 6) acoustically classified as 54.5% and 51.0% 'sand + pavement', compared to 31.0% and 28.9% for the pavement with SAV and pavement with coral groupings (BHM4 and 2), and just 9.5% and 13.4% for the rugose reef groupings (BHM1 and 3).

Table 4. 4 Summary of acoustically-classified survey records falling within NOAA benthic habitat map (BHM) polygons. For each polygon, the percent membership to the 6 predefined groups was computed for survey records falling within that polygon, as well as the 5th, 50'th, and 95'th percentiles of the 418 kHz depth picks. For ease of comparison, the BHM polygons were sorted into 6 major groupings (BHM1-6) of structural and biological attributes.

NOAA Benthic Habitat Map						Acoustic Classification (%)							Depth (m)		
Polygon ID		Geomorphology		Biology		Records	Sand	SpSAV	Rub	Pav	RHB	BrCor	Percentile		
NOAA / Alias		Zone / Structure		Type/Cover		(#)	1	2	3	4	5	6+7	P5	P50	P95
BHM1: Rugose Reef with Branching Coral															
1434	19	Fore Reef	S&G	Coral	10-50%	1052	14.4	11.5	41.7	0.0	21.9	10.6	2.4	4.6	7.7
1363	17	Fore Reef	S&G	Coral	10-50%	1907	9.2	5.8	42.9	0.0	31.1	10.9	2.4	4.9	7.0
1356	18	Fore Reef	AgRf	Coral	10-50%	1677	4.7	3.7	43.7	0.4	32.5	15.0	4.6	6.8	9.1
1361	16	Fore Reef	AgRf	Coral	10-50%	2279	2.7	4.1	31.5	6.8	39.0	15.8	4.7	7.3	10.9
						Avg =	7.7	6.3	40.0	1.8	31.1	13.1			
BHM2: Pavement with Branching Coral															
5918	9	Reef Flat	Pav	Coral	10-50%	382	29.8	45.8	7.6	0.0	6.8	9.9	1.9	2.2	2.5
1426	10	Reef Flat	Pav	Coral	90-100%	309	5.8	48.2	6.8	0.0	36.6	2.6	2.0	2.6	4.8
1365	12	Fore Reef	Pav	Coral	10-50%	605	6.0	15.0	36.4	0.0	35.0	7.6	2.2	3.1	5.7
1401	11	Lagoon	SCRUS	Coral	10-50%	491	9.4	8.8	45.0	0.0	32.6	4.3	4.1	5.1	6.3
1358	21	Fore Reef	AgRf	Coral	10-50%	909	1.0	1.4	20.1	41.6	12.2	23.7	7.2	11.0	16.2
1357	22	Fore Reef	AgRf	Coral	10-50%	304	2.0	0.0	5.3	77.6	0.0	15.1	12.0	15.8	18.0
						Avg =	9.0	19.9	20.2	19.9	20.5	10.5			
BHM3: Rugose Reef without Branching Coral															
1364	13	Fore Reef	AgRf	MA	50-90%	64	9.4	15.6	53.1	0.0	18.8	3.1	2.2	2.6	3.1
1432	15	Fore Reef	S&G	CCA	10-50%	86	17.4	14.0	55.8	0.0	8.1	4.7	2.6	3.6	4.3
						Avg =	13.4	14.8	54.5	0.0	13.4	3.9			
BHM4: Pavement with Abundant SAV															
5921	7	Reef Flat	Pav	SG	90-100%	146	17.5	46.2	4.8	0.0	26.7	4.8	1.9	2.1	2.4
1424	6	Reef Flat	Pav	SG	50-90%	193	11.8	70.8	5.2	0.0	10.1	2.1	2.0	2.6	3.3
5920	8	Reef Flat	Pav	MA	90-100%	192	35.9	49.0	5.2	0.0	7.8	2.1	1.9	2.2	2.6
1362	14	Fore Reef	S&G	MA	50-90%	91	33.0	24.2	28.6	0.0	3.3	11.0	2.0	2.4	3.3
1419	4	Reef Flat	AgRf	SG	90-100%	74	56.8	25.7	12.2	0.0	5.4	0.0	4.5	6.3	7.2
						Avg =	31.0	43.2	11.2	0.0	10.7	4.0			
BHM5: Uncolonized Sand and Pavement (BackReef)															
1420	5	Reef Flat	SCRUS	Turf	10-50%	190	38.4	40.5	13.2	0.0	6.3	1.6	2.1	2.4	4.2
1472	2	Lagoon	Pav	Turf	50-90%	127	39.4	7.1	48.8	0.0	3.1	1.6	5.0	5.9	7.3
1471	1	Lagoon	Rub	Turf	50-90%	342	78.4	4.1	14.9	0.0	0.9	1.8	5.0	6.7	7.5
5952	3	Lagoon	Sand	UnCol	90-100%	645	61.9	0.9	35.5	0.0	0.8	0.9	6.5	8.4	8.9
						Avg =	54.5	13.2	28.1	0.0	2.8	1.5			
BHM6: Uncolonized Sand and Pavement (ForeReef)															
1367	23	Fore Reef	Sand	UnCol	90-100%	2677	22.9	4.6	33.2	22.0	5.9	11.4	7.0	10.8	14.9
1359	20	Fore Reef	Sand	UnCol	90-100%	1025	6.1	2.6	23.0	51.0	4.0	13.2	8.9	11.9	17.3
						Avg =	14.5	3.6	28.1	36.5	5.0	12.3			
						Average of Back Reef =	35.5	24.6	21.8	0.0	14.8	3.2			
						Average of Fore Reef =	9.8	5.4	34.4	14.9	22.1	13.4			

4.3.5 Testing DA Assumptions

Critical DA assumptions were tested on the training records submitted to the 3rd-Pass descriptive DA. The assumption of normal multivariate distributions can generally be accepted if the ratios of skewness/SE and kurtosis/SE fall between ±1.96 (p=0.05 two-tail). Of the 35 tests for normality, the number of violations totaled 18 and 9 for skewness and kurtosis, respectively (Figure 4.7a-b). The most numerous and serious violations came from the depth variable; not all predefined groups were sampled evenly with respect to depth, which resulted in n-modal and leptokurtic frequency distributions. Tabachnick & Fidell (2007) reported that DA significance testing is robust against violations of normality provided it is caused by skewness and not outliers. Since the latter is an unlikely contributor, given the pre-screening of outliers and subsequent three-pass descriptive DA, the results should be interpretable in spite of the number of violations of normality. The dispersion of variances was found to be homogenous for all independent variables (except depth), as judged by the relative similarities of between-group variances (Figure 4.7c). The dispersion of covariances was found to be heterogeneous by Box's M ($p<0.001$), but this finding was disregarded since small differences between covariance matrices can be found significant when sample sizes are large (Tabachnick and Fidell 1997). The dispersion of covariances was instead judged by the relative similarity of log determinants (Figure 4.7d). By that criteria the dispersion of covariances was found to be homogenous; the 95% CI of the 42 comparisons [k*(k-1)] of log determinants, computed as LD_i/LD_j, was 1.04±0.09. The degree of multicollinearity between independent variables was low, judging by values of pooled within-groups correlation coefficients from the 3rd-Pass descriptive DA (Table 4.5). The magnitude of r averaged 0.147 and spanned a range of 0.025 (LogE2 vs Depth) to -.353 (logE1′ vs FD). The assumption of low multicollinearity can generally be accepted if no single value of r exceeds 0.90 and if a small number of r's exceed 0.75.

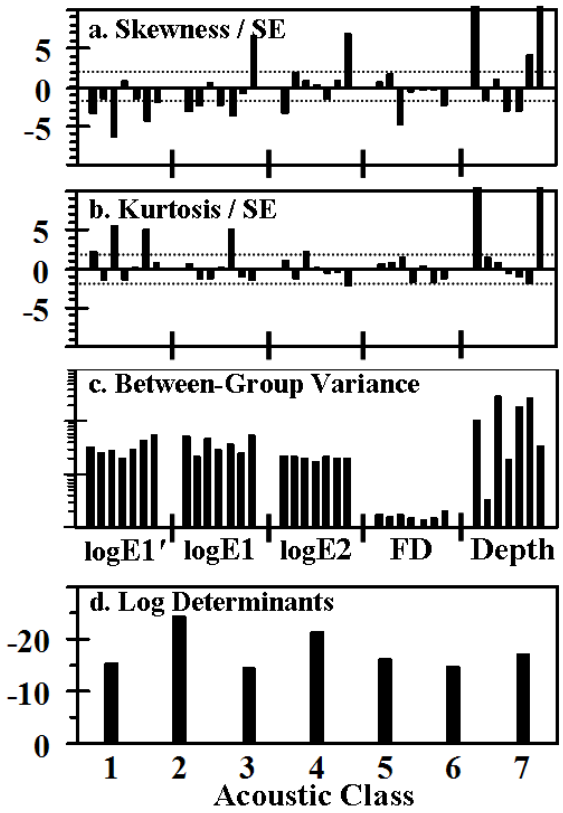

Figure 4.7 Tests of critical assumptions for discriminant analysis (DA) performed on the five independent variables submitted to the 3rd-Pass descriptive DA; (a-b) normal multivariate distributions, judged by ratios of skewness and kurtosis to standard error for the seven acoustic classes, (c) homogeneity of variance, and (d) homogeneity of covariance among the seven acoustic classes.

Table 4.5 Degree of multicollinearity between the independent variables of the training dataset, indicated by the pooled within-groups correlation coefficients of the 3rd-Pass descriptive DA. Coefficients may range from -1 to +1, i.e. perfect negative and positive collinearity.

Variable	logE1	logE2	FD	Depth
logE1'	-0.064	0.036	-0.353	0.105
logE1		0.209	0.169	-0.284
logE2			-0.058	0.025
FD				-0.170

4.3.6 Testing for Significance

All five independent variables (logE1′, logE1, logE2, FD, and depth) were found to be significant by forward stepwise DA, using Mahalanobis distance (MD) as the criteria and the probability of F

for entry and removal (p= 0.05 and 0.10, respectively). The MD is the distance of a case from the centroid of a group, in units of standard deviations, measured in n-dimensional attribute space (n=5). The 3rd-Pass descriptive DA model was found to be statistically significant ($p<0.001$) based on the chi-square transformation Wilks' Lambda. The magnitude of Wilks' Lambda for the 5 discriminant functions (DF) utilized in the model was 0.0012, i.e. only 0.12% of the total variance in DF scores was not explained by differences among the groups.

4.3.7 Back-Classifying the Training Dataset

If the multi-pass descriptive DA procedure truly refined heterogeneous training samples into "pure" structural and biological elements, the Fisher's linear discriminant functions (FLDF) obtained from the 3rd-Pass descriptive DA should classify the unrefined training dataset into proportions similar to those estimated from ground-truthing videos. That was precisely what happened for the 'sand', 'rubble', 'rugose hardbottom', and 'branching coral' groups (Figure 4.8). For example, the eleven samples constituting group 3 (rubble) ground-truthed as 69.6% rubble, 21.5% pavement, 7.0% branching coral, and 1.9% rugose hardbottom. The distribution of acoustic classifications was very similar; 66.6% 'rubble', 21.1% 'pavement', 6.4% 'sparse SAV', 2.2% 'branching coral', and 3.7% 'rugose hardbottom'. The SAV was an obvious misclassification, and a reminder that acoustic classes can be best likened to localized centers of gravity along a continuum of n-dimensional hyperspace (similar to the concept of a species as a cluster of phenotypic traits along an n-dimensional continuum).

The back-classification of groups 2 (sparse SAV) and 4 (pavement) were the exceptions, and point to a limit on the resolution of small-scale seabed features resulting from the sliding scale of a depth-dependent sonar footprint across a backdrop of benthic heterogeneity. Group 2 was ground-truthed as 25% SAV and 75% sand, but classed acoustically as 81.5% 'sparse SAV'. The

SAV patchiness was at the level of individual shoots, considerably smaller than the diameter of the sonar footprint (0.64 m at the group-average depth of 5.7 m). As cataloged, it was not

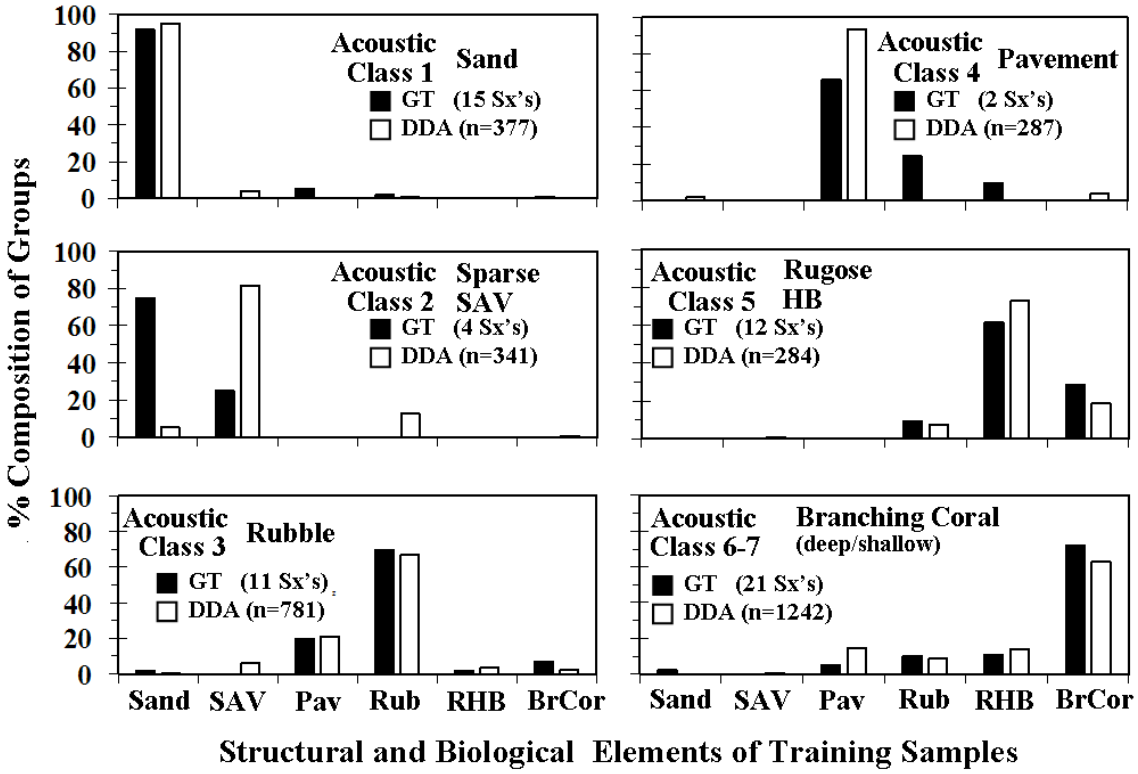

Figure 4.8 Back-classification of unrefined training dataset (k=7, n=3312) using the Fisher's linear discriminant functions obtained from the 3rd-Pass descriptive DA. (■) Average ground-validated composition of bottom classes, estimated from videos of training samples and weighted by number of records per hydroacoustic sample. (□) Composite 3rd-Pass DDA acoustic classification of unrefined training dataset. SAV = submerged aquatic vegetation, RHB = rugose hardbottom, BrCoral = branching coral.

possible to resolve SAV from the underlying sand and so group 2 was a 'mixed' class of sparse SAV in sand. Similarly, the training samples constituting group 4 (pavement) ground-truthed as 66% pavement, 24% rubble, and 10% rugose hardbottom, but classed acoustically as 93% 'pavement'. At the group-average depth of 14.4 m the sonar footprint was 1.61 m in diameter, and it was clear in the videos that most pings would have included some rubble and/or rugose hardbottom. Thus, group 4 was also a "mixed" class that would be more correctly defined as 'deep pavement with sparse rubble'. The same phenomenon can be observed in the preferential rejection of deep 'rubble' records (group 3). Of the 781 'rubble' records in the unrefined training

dataset, 250 had a depth greater than 12 m. 230 of these records were rejected in the 1st and 2nd-Pass descriptive DA's (out of a total of 414 rejected records). Of these 230 records, 177 were rejected due to mis-classification (as opposed to low probability of group membership). Of these 177 records, 93% were classified as 'pavement', i.e. 'deep pavement with sparse rubble'. The general lesson is that for a given beamwidth, the likelihood of ensonifying a 'pure' class will diminish with increasing depth, due to the increasing diameter of the conically spreading signal.

4.3.8 Interpretation of Descriptive DA

A discriminant function (DF) is similar in form to a multiple regression equation, although in the case of DA the coefficients are computed to maximize discrimination between predefined groups, based on the values of independent variables. When there are fewer independent variables than groups, as in this study, the number of DF's equals the number of independent variables. The first DF accounts for the greatest amount of between-group variance, with each successive function contributing less than the preceding one. The standardized DF coefficients (SDFC) are weighted to the magnitudes of the independent variables and are used to assess the relative contribution of each independent variable to a DF. As partial coefficients they reflect the unique contribution of each independent variable, controlling for the other independents in the model. However, they do not indicate which groups the functions discriminate between. Between-group discrimination can be visualized by scatterplots of individual scores for two given DF's, or by mean values of DF's for each group, i.e. functions at group centroids (FGC). The spread of mean FGC scores discriminant scores indicates the extent to which a particular pair of DF's discriminate between groups. The discriminatory character of independent variables, i.e. which variables discriminated by which groups, was assessed by synthesizing information from the SDF coefficients and FGC's.

4.3.8a Standardized discriminant function coefficients (SDFC)

The first two DF's accounted for 62.8 and 28.7% of between-group variance within the 3rdPass descriptive DA training dataset (Figure 4.9). The first DF was informed primarily by FD and logE1, and to a lesser extent, depth. The second DF was informed primarily by logE2, log E1′ and depth. Neither the magnitudes nor rankings of the SDFC's of the first and second DF's changed appreciably from the 1st to 3rdPass DA. This was not the case for the third, fourth, and fifth DF's, for which the magnitudes, signs, and rankings of most SDFC's changed appreciably after the 1stPass descriptive DA (Figure 4.9).

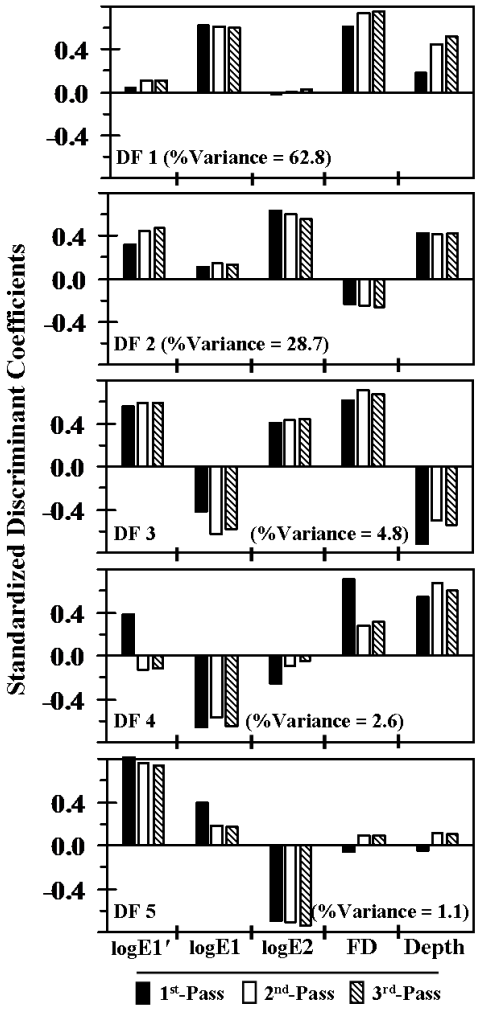

Figure 4.9 Standardized discriminant function coefficients of the 1st, 2nd, and 3rd-Pass descriptive DA, reflecting the relative contributions of independent variables within each of the five discriminant functions.

4.3.8b Functions at group centroids (FGC)

The first DF divided the 7 acoustic classes into two major groupings of geomorphology; reef (acoustic classes 4-7) and non-reef (acoustic classes 1-3). This can be seen across the x-axis of the DF1 vs DF2 scatterplot (Figure 4.4b) and in the relative values of FGC (Table 4.6, first column). The second DF primarily discriminated between the more topographically complex habitats, forming three groupings of clusters; (i) 'branching coral (shallow)', (ii) 'branching coral (deep)' and 'rugose hardbottom', and (iii) 'pavement' and 'rubble'. The third-to-fifth DF's explained only a small proportion of the between-group variance (8.4%), but were critical for differentiating between the most similar acoustic classes. For example, 'rugose hardbottom' and 'branching coral (deep)' were poorly differentiated by the first two discriminant functions (Figure 4.4b), but are clearly differentiated in the scatterplots of the third, fourth, and fifth discriminant functions (Figure 4.10). That the magnitudes and rankings of standardized coefficients of the first and second DF's did not change markedly between the 1st and 3rd-Pass descriptive DA's, but those the third-fifth DF's did, indicate that the multi-pass descriptive DA refinement served largely to make these finer distinctions between similar habitats.

Table 4.6 Mean scores of discriminant functions (i.e. functions at group centroids) of 3rd-Pass descriptive DA (for the 7 acoustic classes of the training Dataset). The spread of mean scores down a column indicates which groups, and to what degree, a discriminant function distinguishes between.

Acoustic Class	Functions at Group Centroids				
	1	2	3	4	5
1	-7.00	0.31	-0.72	0.47	0.11
2	-2.43	1.23	3.03	0.66	-0.57
3	-0.13	2.19	-0.28	-1.39	-0.03
4	5.32	3.82	-0.45	1.16	0.72
5	4.46	0.18	2.83	-1.04	0.92
6	5.05	0.49	-1.01	0.43	-1.39
7	1.65	-4.40	-0.06	-0.01	0.17

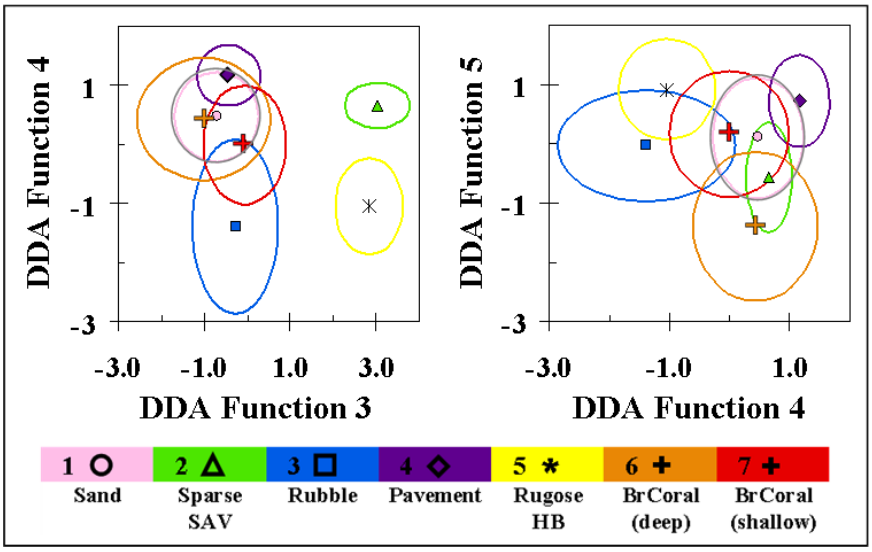

Figure 4.10 3rd-Pass descriptive DA (n=1733). Utility of higher order discriminant functions was splitting the most similar geomorphological groups, e.g. rugose reef hardbottom from deep branching coral, and sparse SAV from rubble. Centerpoints denote cluster averages, ellipses are dispersion (1 standard deviation) about x and y.

Synthesizing standardized DF coefficients and FGC revealed the rankings and functions of independent variables to be in accord with the general principles of AGDS seabed classification. FD and E1 were the largest contributors to between-group discrimination, differentiating reef and non-reef habitats. The second largest contribution came from E2, followed closely by E1' and depth, providing discrimination between individual reef habitats, i.e. 'pavement', 'rugose reef', and 'branching coral (shallow and deep)'. The finding that E1 differentiated sand (flat/soft/smooth) from reef (rugose/hard/rough) agrees with the general empirical rationale for seabed classification, which posits that a rougher seabed surface creates more scattering of the transmitted echo contacting the seabed at an oblique angle of incidence, increasing the proportion of signal returning to the transducer in the second half of the first echo (Burczynski, 1999; Burns et al., 1989). And given that FD was designed as a metric of topographic complexity (Lubniewski & Stepnowski, 1997), computed from the first echo but effectively independent of E1 (Table 4.5), it is not surprising to find it complementing E1. That E2 contributed most to

discriminating between reef habitats would at first seem to unlikely, as E2 is generally considered an indicator of seabed 'hardness' and the groups it differentiated were all 'hard' carbonate structures. Further, Hamilton et al., (1999) found E2 to be an unreliable classifier over rocky rough habitats, oscillating between very low and very high value. However, a previous study using the same AGDS demonstrated the 418 kHz E2 to be significantly and negatively correlated with a LIDAR-derived metric for topographic complexity, and that the stability of E2 was not diminished over rocky habitats compared to sand habitats, but simply smaller (Foster et al., 2009). E2 can thus be understood to be more sensitive to very rough surfaces by virtue of it being a multi-path echo, i.e. E2 experiences a greater proportion of signal loss over rough terrain than the first echo waveform. Similarly, Riegl et al. (2007) reported lower E2 values over 'rough/hard' reef facies than 'soft/flat' sand.

4.4. DISCUSSION

4.4.1 Critical Review of Multi-Pass DA Classification

The final mapping product of a supervised classification scheme is predicated by the nature of the training dataset, which in turn is influenced by spatial factors (e.g. benthic heterogeneity, depth zonation) and hardware factors (e.g. AGDS design, operating frequency). When applied to coral reefs, conventional approaches to AGDS training are likely to produce unsatisfactory results, in particular due to the high degree and small scale of benthic heterogeneity. A training dataset consisting solely of homogeneous benthos will leave heterogeneous portions of the map un-classified or mis-classified (Foster-Smith & Sotheran, 2003), and cataloging the many 'mixed' classes can overwhelm the discriminatory potential of AGDS (Hutin et al., 2005). This study presents a novel alternative to the dilemma, capitalizing on a small sonar footprint resulting from a conjunction of shallow depth (1.2 to 17.5 m) and narrow beamwidth (6.4^{o}), which made resolution of most micro-scale features possible. The method of sample acquisition was equally

important, as the co-located drop-video allowed explicit benthic characterization of each 30-120 second hydroacoustic sample, avoiding the pitfalls associated with the use of buffers around sampling stations (Foster-Smith & Sotheran, 2003). The heterogeneous training dataset was refined into end-member structural and biological elements by multiple passes through descriptive DA's, rejecting records that were incorrectly classified or failed to exceed a minimum probability of group membership. This also allowed for direct computation of acoustically-predicted percent cover of sand, sparse SAV, rubble, pavement, rugose hardbottom, and branching coral.

Because an external accuracy analysis was not performed, the efficacy of the classification scheme was instead assessed by a summation of the evidence pertaining to the training catalog and the final mapping products. After taking all the following evidence into consideration, it was found reasonable to assert that (i) the critical requirements of DA were sufficiently met to accept conclusions regarding the relative importance and function of predictor variables, (ii) the multi-pass DA oriented the acoustic classes in discriminant function space in accordance with the general empirical rationale of seabed classification, and (iii) the multi-pass DA classification scheme yielded an accurate depiction of the benthos, judging by the visually-apparent fit with IKONOS imagery and general agreement with independent characterizations of the study area.

4.4.1a Descriptive DA Statistics

The critical assumptions of discriminant analysis were tested and largely met, including; (i) skewness and kurtosis, (ii) homogeneous dispersion of variances and covariances, and (iii) a low degree of multicollinearity (Figure 4.7 and Table 4.5). All five independent variables were found to be significant by forward stepwise entry to the 3rd-Pass descriptive DA. An independent assessment of optimum clusters validated the arrangement of the training dataset into six groups, and the seven acoustic classes required to describe them (Table 4.2).

4.4.1b Depth Contamination

Depth contamination was observed in the raw values of E1′, E1, E2, and FD, although the ultimate cause differed from those observed for RoxAnn E1 and E2 parameters (Bax et al., 1999; Greenstreet et al., 1997; Kloser et al., 2001; Voulgaris & Collins, 1990). BioSonics VBT compensates for absorption and spreading losses but does not normalize echo length to a reference depth, whereas RoxAnn normalizes to reference depth but does compensate for absorption and spreading losses (Hamilton et al., 1999). The trends of the acoustic energy parameters with depth appeared sensible. That E2 decreased with depth could be explained by greater absolute deflection, for a given grazing angle. That E1′ decreased and E1 increased with depth could be explained by the echo dilating along the time axis, shifting proportionally more echo energy from E1′ to E1. In this study the four acoustic parameters were empirically normalized to a reference depth using logarithmic polynomials fit to median values at 14 ranges of depth. It appears this treatment of depth contamination was successful, because; (i) depth was not a major predictor variable (Figure 4.9), (ii) depth was not strongly correlated with other predictor variables (Table 4.5), and (iii) the depth range of habitat classes was greater for the predictive DA of survey data than it was for the descriptive DA of training data, i.e. depth as an independent variable did not place an artificial constraint on classification.

4.4.1c Orientation of Habitats

The orientation of the ‘sand’, ‘sparse SAV’, ‘rubble’, and ‘pavement’ classes along a diagonal within E1:E2 space (Figure 4.4d) agreed with the general empirical rationale for seabed classification, which posits that E1 increases with seabed roughness and E2 increases with seabed hardness (Chivers et al., 1990; Heald & Pace 1996; Orlowski, 1984), provided surfaces are flat (Burczynski, 1999). Similar diagonal arrangements have been observed for sediment classes (Bax et al., 1999; Greenstreet et al., 1997; Magorrian et al., 1995), and coral reef benthic

habitat classes (Foster et al., 2009; White et al., 2003). The position of 'sparse SAV' to the right of the diagonal is a predictable outcome given SAV's requirement of a solid attachment surface, i.e. carbonate rock underlying the thin sand veneer would act as a subsurface reflector, amplifying the value of E2 (Foster et al., 2009; Greenstreet et al., 1997). Topographically complex habitats 'branching coral (deep)' and 'rugose hardbottom' lay to the left of the diagonal, in accordance with previous observations of lower than expected values of E2 over rough seabeds (Foster et al., 2009; Hamilton et al., 1999; Kloser et al., 2001). The 'branching coral (shallow)' class had a diminished E1 and a greatly reduced E2, a logical extension of the former argument, assuming signal scatter and resultant signal losses would be exacerbated over shallow colonies of branching coral. Confidence in the efficacy of the DA classification scheme is bolstered by the observation that the ordering of acoustic classes in DF1/DF2 space is (i) the same as E1/E2 and E1/FD space, and (ii) consistent with the visually-apparent features of the classes.

4.4.1d Multi-Pass DDA Refinement

Refinement of heterogeneous training samples into end-member elements by multiple-passes through descriptive DA's succeeded for most of the benthic groups, judging by the correspondence between ground-truthed and acoustically-predicted proportions of structural and biological elements (Figure 4.8). The 'sparse SAV' and 'pavement' classes illustrated limitations of resolution. The patchiness of 'sparse SAV' was at the level of individual shoots, well below the resolving power of the 6.4^{o} beam, as was the scale of rubble deposits co-occurring in the deeper 'pavement' class.

4.4.1e Final Mapping Product

There are three lines of direct evidence supporting the validity of the acoustic classification scheme; (i) the general fit of the acoustic classifications to the visually-apparent features of the IKONOS imagery (Figure 4.6a&c), (ii) the close agreement of acoustically-predicted cover of

rubble and branching coral to a contemporaneous, co-located video survey (13.3 vs 16% branching coral and 39.3 vs 40% rubble, respectively), and (iii) the consistent, logical acoustic interpretation of NOAA benthic habitat map classifications. While the confusion matrices of Figure 4.3 are internal, the large number of samples (65) collected over the relatively small area (0.44 km^2), combined with the generally equitable proportion of records passing through the 3 descriptive DA's (Figure 4.5), supports the conclusion that the DA's were keying on true seabed characteristics and not simply on chance anomalies of independent variables.

4.4.2 Applicability to Future Work

While there are obvious benefits to automated real-time classification of AGDS output, the requirement of *a priori* group assignments can be problematic due to the difficult and time-consuming process of matching acoustic signatures to desired seabed characteristics. Even the task of defining groups is far from straightforward on a coral reef (Foster-Smith & Sotheran, 2003), as evidenced in this study by (i) the necessity to divide the 'branching coral' group into the shallow and deep acoustic classes, and (ii) the realization that rubble could not be resolved from the underlying pavement beyond the depth where the sonar footprint eclipsed the scale of patchiness and created a 'mixed' class of pavement and rubble. The amount of time required to glean this level of detail from an AGDS dataset would usually prove cost-prohibitive for an off-site survey. The more economic approach is to collect digitized waveforms that can be processed and deciphered post-survey. In this study there were additional benefits to a post-processing approach, including the ability to; (i) experiment with VBT settings to optimize between-group discrimination, especially the partitioning of E1′ and E1, (ii) experiment with different training categories and assignments *a posteriori*, as it became clear what the AGDS could and could not discriminate, (iii) perform a thorough and custom-fitted quality analysis of the training dataset, which allowed the 1st-Pass descriptive DA to correctly locate the initial cluster centroids, and (iv) add, remove, transform, or modify independent variables.

Expanding the multiple-echo predictor dataset beyond the standard E1 and E2 and utilizing an n-dimensional classification algorithm were also essential steps for moving beyond a soft/smooth soft/rough hard/smooth hard/rough categorization (Kloser et al., 2001; Riegl & Purkis, 2005). DA is designed to maximize between-group discrimination; this is evident by comparison of the DF1/DF2 scatterplot to those of E1/E2 and E1/FD (Figure 4.4). The higher-order discriminant functions allowed for differentiation of the most similar habitats (Figure 4.10), in-line with the observation of Foster-Smith & Sotheran (2003) that E1/E2 Cartesian plots are "very limited and not recommended for interpretation of AGDS data". Given the wide gaps between benthic groups in discriminant function space, it is assumed that more bottom types could have been described with (i) an expanded training dataset, and (ii) the addition of a duplicate set of independent variables acquired at the lower end of AGDS frequencies.

By recognizing and adapting to the limitations of the single-beam acoustic ground discrimination system, it was possible to produce a useful thematic benthic habitat map of a shallow and highly heterogeneous coral reef environment. Refining the training dataset into end-member structural and biological elements allowed for direct computation of acoustically-predicted percent cover, which could be a useful contribution to the decision-making processes of conservation and resource management. The methodology was proven on a coral reef environment for which high quality satellite imagery existed, as an example of the potential for single-beam systems to thematically describe coral environs that cannot be fathomed by image-based remote sensing techniques.

ACKNOWLEDGEMENTS

We thank the GEF Coral Reef Targeted Research project for funding and the Palau International Coral Reef Center for great logistical support.

Chapter 5: Using hydroacoustics to create a benthic map of the potential for drift macroalgae attachment

FORWARD

The objective of this study was to identify areas of seafloor most likely to support a seasonal drift macroalgae bloom, in the waters offshore Sanibel Island, FL and within San Carlos Bay. For a drift macroalgae bloom to reach nuisance levels, there must be adequate expanses of rough, stable substrate onto which the drifting colonies can attach and grow. Exposed rocky substrata are most commonly associated with macroalgae, but drift macroalgae have also been observed growing on consolidated shell hash, seagrass, pen shells, and worm tubes. The seabed offshore Sanibel Island and within San Carlos Bay is predominantly a mixture of unconsolidated silt and sand-sized sediments with variably abundant quantities of broken bi-valve shell debris, unsuitable for macroalgae attachment. The premise of this project was to acoustically discriminate between these "smooth" unconsolidated habitats and the "rougher" areas of consolidated shell hash and exposed live hardbottom.

Unlike the preceding chapters, which pushed the limits of what could be detected and classified with a single-beam AGDS, this study was more akin to a typical sediment classification application. But with that said, the relative ease with which this study was completed bore testimony to the efficacy of the methodological development that preceded it. Both the Indian River Lagoon and Palau classification schemes required numerous iterations; the former due to the difficulty of detecting the diminutive SAV targets and the latter due to the difficulties associated with the subjective coral reef categories. This study was completed with far less intervention. This was due in part to the visual and acoustic distinctiveness of the bottom categories, and in part to additions made to the classification process. These additions sought to automate the otherwise subjective processes of arranging and grooming the training dataset prior

to classification. The first addition was a method for strategically removing outlier records. After quality analysis (QA) and merging the 38 and 418 kHz data, the training dataset was submitted to a principle components analysis (PCA) and the principle components were then partitioned into homogeneous groups using K-Means clustering. The number of clusters was intentionally set very high (k=16); the few disproportionately small clusters were identified as outliers and removed from the training dataset. The remaining records were again submitted to PCA+K-means analysis and the percent membership amongst the 16 K-means clusters was computed for each training sample and submitted to a multidimensional scaling analysis. Training samples found to be outliers in the 2D MDS plot were rejected outright, and others were re-assigned if (1) they were located among another bottom class in the 2D MDS plot, and (2) the initial visually-apparent class assignment could reasonably be overturned to the class indicated by the MDS plot. In every study, fastidious grooming of the training dataset has been the key to successful classification, and these additions helped to guide and automate that process.

The acoustic surveys revealed two areas of high acoustic roughness and large spatial extents that had not been previously mapped; one was an area of exposed consolidated shell hash on either side of a large sand spit, and other was an area of exposed live hardbottom within San Carlos Bay. Coupled with shallow depths and close proximity to the outflow of the Caloosahatchee River, these nearshore areas have the right combination of substrate and environmental factors to host a large-scale drift macroalgae bloom event.

ABSTRACT

Beginning In the winter of 2003-2004, several episodes of red drift macroalgae blooms resulted in massive amounts of macroalgae washing ashore the beaches of Sanibel Island, Bonita Springs, and Ft Meyer Florida. A study conducted after the first event supported a link to increasing land-based nutrient enrichment. A large-scale program was initiated in May 2008, with the primary goal of further defining the possible roles and sources of nutrient enrichment with respect to nuisance macroalgae blooms. This study reports the results of the hydroacoustic mapping component of this program. The goal of this study was to identify areas of substrate suitable for supporting a macroalgae bloom. Areas within San Carlos Bay and offshore Sanibel Island, FL were hydroacoustically surveyed from nearshore to about 11 km offshore during the periods of October 6-10, 2008 and May 10-22, 2009. The hydroacoustic data was acquired with a BioSonics DT-X echosounder and a multiplexed single-beam digital transducers operating at 38 and 418 kHz. Eleven acoustic parameters derived from the 38 and 418 kHz signals were utilized to classify the survey data into 5 ascending categories of visually-apparent seabed roughness. Classes 1 and 2 were both primarily constituted of unconsolidated silt and sand-sized sediments, unsuitable for a bloom. Class 3 is a marginal substrate for a bloom, consisting of packed sand and large intact shell debris. Classes 4 and 5 offer the best attachment sites for a bloom, consisting of consolidated shell hash, live hardbottom, and submerged aquatic vegetation. The majority (~ 80%) of acoustic classifications were of soft bottom sediments (classes 1-2), but there were two significant expanses of rough seabed suitable for macroalgae attachment. These two areas covered a total of 19 km^2, within which ~ 56% of the hydroacoustic records classified as "rough" (classes 3-5). The first was a large area of seagrass beds and live hardbottom in the mouth of San Carlos Bay, where large amounts of macroalgae were variably present during the April-May 2009 surveys. The second was offshore Lighthouse Point, near the mouth of San Carlos Bay, situated near a large sand spit that extended from the beach to approximately 6 km offshore. Along the west side of the sand spit there were substantial areas of moderate to high

bottom roughness, mostly in the form of consolidated shell hash. The average depths of these two acoustically-rough areas were only 5.0 and 4.0 m, so sufficient irradiance to initiate a bloom could be assumed. These textured and shallow areas on or near the mouth of San Carlos Bay are presumably potential sources for macroalgae attachment and growth, which could easily be transported onto the beaches under some storm conditions given the close proximity to the shoreline. In contrast, the areas in open Gulf of Mexico waters were classified predominantly as soft sediments with low bottom roughness. The site offshore Redfish Pass had a moderate (~22%) proportion of "rough" classifications out to 5km offshore, but from 5-10km offshore the bottom classified as >95% soft sediments. The other two Gulf of Mexico sites classified as >95% soft sediments from nearshore to 11 km offshore. Independent, concurrent video transects indicated there were small areas with large amounts of shell and live hard bottom that occurred sporadically greater than 10km offshore, but all things considered the open Gulf waters around Sanibel Island may not be a major source of drift macroalgae.

.

5.1. INTRODUCTION

In the winter of 2003/2004, massive amounts of red drift macroalgae washed ashore the beaches of Sanibel Island, Bonita Springs, and Fort Meyers, all located in Lee County, FL. Several episodic recurrences have created a nuisance for these beach communities, affecting the aesthetic quality of the beach and necessitating expensive removal programs. A two-phase water sampling study, conducted first in August 2004, prior to Hurricane Charley, and again in October 2004, after months of elevated freshwater discharge from the Caloosahatchee River, supported a link to increasing land-based nutrient enrichment (Lapointe and Bedford, 2006). The October 2004 survey documented enrichment of N and P extending to at least 26 km from shore. The questions now facing resource managers concern the anthroprogenic sources of the blooms, and what can be done to ameliorate their frequency and impact.

The hydroacoustic survey presented in this study was one component of a larger project initiated by the City of Sanibel and the Lee County DEP to identify the sources and possible causes of the drift algae blooms. The primary focus of the larger study was the availability of nutrients and their role in generating large-scale macroalgae blooms within the waters of Lee County, FL. The primary focus of the hydroacoustic survey was to identify areas of substrate conducive to attachment and propagation of drift macroalgae, since the limiting factor of macroalgae abundance in the eastern Gulf of Mexico is the availability of rocky substrata (Humm, 1973). The seabed offshore Sanibel Island and within San Carlos Bay is predominantly unconsolidated silt and sand with variably abundant quantities of bi-valve shell debris. The challenge was to utilize a single-beam acoustic ground discrimination system (AGDS) to identify areas suitable for macroalgae attachment. Combined with the other streams of information generated by the larger project, e.g. nutrient gradients and light availability, the most-likely sources of drift macroalgae blooms can be identified and observed.

Single-beam AGDS have been used in a variety of bottom-typing applications, due in large part to their low cost, compact size, ease of deployment, and modest data storage requirements relative to side-scan and multibeam sonar systems. A common application of AGDS has been characterization of sediment type as a surrogate indicator of benthic habitat. Most studies have utilized the E1 (time integral of the squared amplitude of the trailing edge of the 1st echo waveform) and E2 (complete 2nd echo) acoustic energy parameters. "E1 and E2 are often referred to as 'roughness' and 'hardness', implying measures of mechanical hardness and geometrical or physical roughness, but they are simply acoustic indices with some unknown relation to seabed conditions" (Hamilton et al., 1999). In a typical bottom-typing study, the AGDS is trained on granulometric parameters measured from sediment grab samples, but is presumed to respond to secondary attributes of particle size distribution, (e.g. acoustic backscatter is correlated with surficial texture (Burns et al., 1989; McKinney & Anderson, 1964), and echo shape is correlated with sediment compaction, via the degree of signal penetration (Ellingsen et al., 2002; Freitas et al., 2006; Hamilton et al., 1999). Numerous studies have assessed the potential for sediment classification by E1 and E2 with varying degrees of success (Bax et al., 1999; Collier & Brown, 2005; Greenstreet et al., 1997; Hamilton et al., 1999; Kloser et al., 2001; Wilding et al., 2003). Greenstreet et al. (1997) noted that "RoxAnn was responding to other physical or biotic seabed features other than just particle size". Hamilton et al. (1999) similarly observed that "QTC bottom classes generally had consistent grain size and texture properties, and followed grainsize trends, but RoxAnn classes were difficult to define". Kloser et al. (2001) and Foster et al. (2009) reported that E1 and E2 relate to a combination of seabed hardness and roughness attributes, including the epibenthic biota.

More recent efforts have sought to expand the utility of RoxAnn by directly classifying benthic habitats using the full suite of output parameters (E1, E2, depth, and a derived acoustic

variability) within the IDRISI image-classification platform for loch (Brown et al., 2002; Foster-Smith & Sotheran, 2003) and coral reef (White et al., 2003) environments. Foster et al. (2009) performed a point-by-point comparison of data acquired from a BioSonics DT-X digital echosounder against a backdrop of LIDAR-delineated habitat classification, and found that E1/E2 plots at both 38 kHz and 418 kHz differentiated benthic habitats, although considerable overlap remained even after heavy filtering of E1 and E2 (20-80 percentile) and consolidation from eight to five habitat classes.

In this study a total of eleven acoustic parameters (E0, E1′, E1, E2, and fractal dimension at 38 and 418 kHz, plus the 418 kHz bottom depth) were used to classify the seabed offshore Sanibel Island and within San Carlos Bay. The two additional acoustic energy parameters complete the compartmentation of the first echo waveform; E0 is the pre-bottom backscatter and E1′ is the leading edge of 1st echo. The fractal dimension (FD) is a measure of shape irregularities of 1st echo waveform. A novel supervised classification scheme was used to refine the training dataset into end-member structural and biological elements by passing training samples through a series of discriminant analysis algorithms. The hydroacoustic survey data was classified into one of five categories of ascending bottom roughness, as an indication of the potential for drift macroalgae to attach to the seabed. The large-scale patterns of acoustically-predicted roughness, along with depth as a proxy for available irradiance, were used to identify areas with the greatest potential to generate a bloom of drift macroalgae.

5.2. METHODS

5.2.1 Study Area

Hydroacoustic surveys were conducted in the nearshore waters of Sanibel Island, FL. Six areas encompassing the local diversity of benthic habitats were surveyed, including sites offshore

Sanibel Island and within San Carlos Bay. The surveys were conducted in two segments; a methods-development exercise conducted October 6-8, 2008 and a larger-scale survey on May 10-22, 2009. Three areas were surveyed in 2008; a 7x2 km plot alongshore Lighthouse Point (400m spacing), a 6x1 km plot offshore Redfish Pass (200m spacing), and a 1,500m meander through seagrass in Pine Island Sound (Figure 5.1). Five areas were surveyed in 2009; an additional 7x2 km plot adjacent to the 2008 Lighthouse Point plot, a 10x5 km plot offshore Ft Meyers Beach (1600m spacing), a 10 km transect offshore Tarpon Bay Road, a 9x1.6 km plot offshore Dinkins Bayou (800m spacing), and a 9x3.2 km plot within San Carlos Bay (800m spacing).

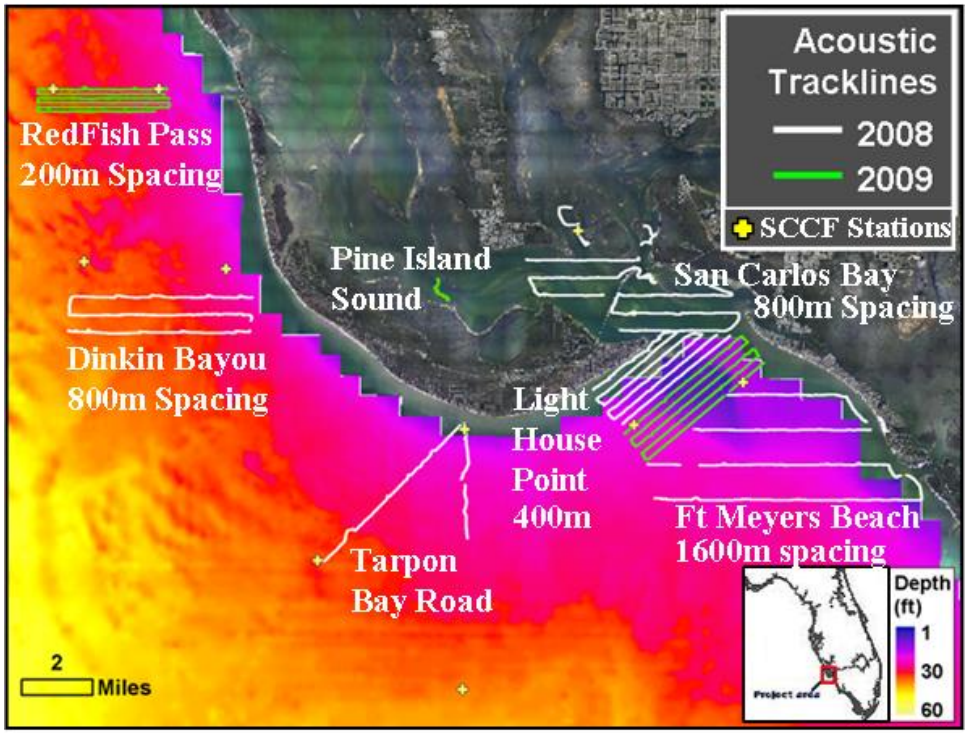

Figure 5.1 Trackplots of hydroacoustic surveys, conducted during the periods of October 2008 and May 2009. Yellow Crosses denote the location of benthic stations monitored by the Sanibel-Captiva Conservation Foundation.

5.2.2 Hydroacoustic Survey

The survey was conducted from a 7.5 m v-hull boat with a 0.5 m draft, an average net speed of

4.5 knots (vessel plus drift). Hydroacoustic data was acquired with a BioSonics DT-X echosounder and two multiplexed, single-beam digital transducers with full beamwidths of 10^{o} (38 kHz) and 6.4^{o} (418 kHz), operated at 5-Hz sampling frequency and 0.4 ms pulse duration (Figure 2.1). The 38 and 418 kHz transducers ensonified a roughly-circular area of seabed with diameters equal to approximately 17% and 11% of water depth, respectively. The Transmit Power Reduction (-9.1 db) option within the BioSonics Visual Acquisition (VisAcq) software was used to reduce the onset of reverberation at the shallowest depths. Global positioning data were collected with a Trimble Ag132 dGPS, differentially corrected against a WAAS signal to achieve positioning accuracies less than 0.9 m horizontal dilution of precision. The dGPS signal was interfaced with navigational software to provide real-time monitoring of vessel position with respect to geo-referenced imagery and pre-planned survey lines.

5.2.3 VBT Processing (Acoustic Energy and Shape Parameters)

Hydroacoustic data were processed with BioSonics Visual Bottom Typer (VBT) seabed classification software (1.0) to obtain values of E1′ (time integral of the squared amplitude of the leading edge of the 1st echo waveform), E1 (2nd part of 1st echo), E2 (complete 2nd echo), E0 (pre-bottom backscatter of 1^{st} echo), and FD (fractal dimension, a measure of shape irregularities of 1^{st} echo waveform), as per Burczynski (1999). The VBT bottom sampling windows were set to 50, 30, 90, and 180 samples for E0, E1′, E1, and E2, respectively. The E1′ setting was adjusted so that E1 would capture only the trailing edge of the first echo, maximizing its sensitivity to scattering components of the seabed. Other user-defined settings include; time-varied gain=20logR, minimum data processing threshold= -80dB, 5 pings per report, and energy filter=50%. VBT computes FD as the Hausdorff dimension of the first echo (Mandelbrot 1982), simplified by gridding the waveform into ‘box’ dimensions (Lubniewski & Stepnowski, 1997). The acoustic energy parameters E0, E1′, E1, and E2 were log-transformed to improve normality (Sokal & Rohlf, 1981).

5.2.4 Normalizing to Reference Depth

The current version of VBT does not normalize echo length to a reference depth, i.e. adjust the sampling rate to effectively adjust the width of E1′ and E1 bottom sampling windows (in units of samples) to maintain a consistent first echo division as the echo stretches and flattens with increasing depth (Dommisse et al., 2005). Purely from the standpoint of echo length, E2 should not require normalization to a reference depth provided the bottom sampling gate is adequately wide to capture the entire second echo across the range of depths. But as it turned out, all acoustic parameters except E0 were significantly correlated with depth. To ameliorate the effect of depth contamination, the log-transformed acoustic energy parameters and FD were empirically normalized to median survey depth. The raw VBT output of individual survey sites dominated by unconsolidated sediment, e.g. Redfish Pass, were sorted by depth and median values of acoustic parameters were computed for each block of 1,000 records. This allowed for comparison of site-specific depth trends and provided a check for temporal consistency, i.e. October 2008 versus May 2009 datasets. These sites were characterized by relatively flat, sedimentary, uncolonized seabeds. This made it reasonable to assume that depth was the main factor affecting echo shape. Sorting by depth and taking the median value 1000 record blocks served to randomize the survey datasets, minimizing the potential for within-site spatial variability to intrude upon the observed depth trends. Median values were likewise computed for selected training samples, ground-validated as uncolonized sand, to (i) fill-out the coverage of bottom depths, and (ii) validate the methodology. Examples are shown in Figure 5.2 for the E1 and FD parameters. The curves of Figure 5.2 were then binned into 18 ranges of depth and logarithmic polynomials were fit to each of the acoustic parameters (Figure 5.3). The rationale for binning the 1000-record blocks was to further homogenize the datasets, making it easier to visualize the depth trends and the resultant fitted curves. Depth-normalization factors were applied to each hydroacoustic record, calculated as the ratio of model-predicted acoustic energy at actual depth divided by the model-predicted

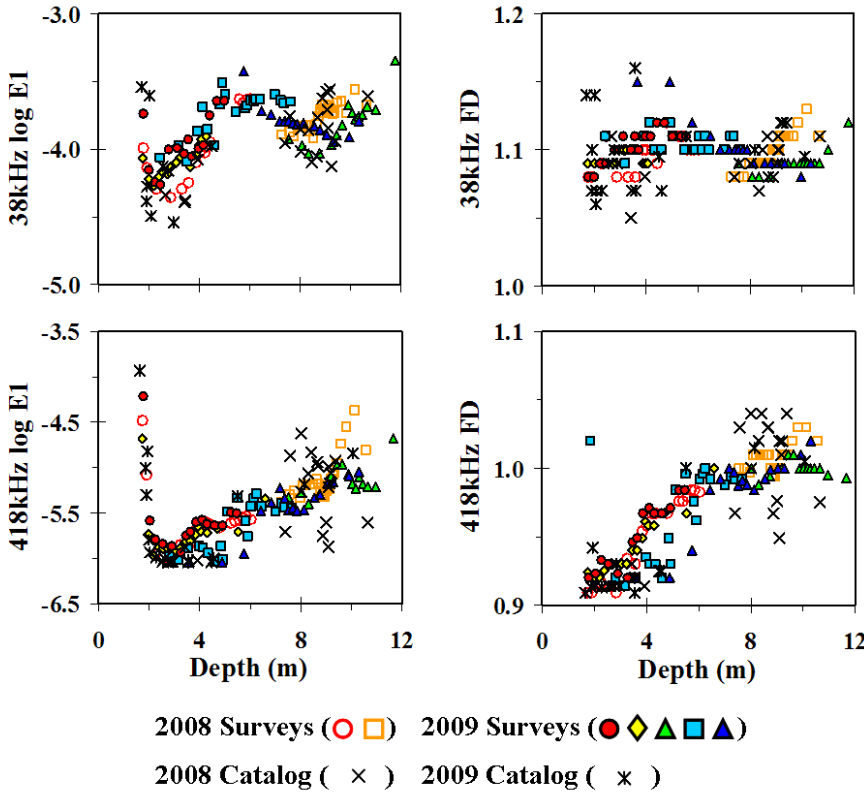

Figure 5.2 Examples of datasets used for creation of depth-normalization models, all ground-validated as uncolonized, unconsolidated sediments. (i) median values of acoustic parameters for blocks of 1,000 survey records (colored symbols), and (ii) median values of selected training catalog samples (x and *).

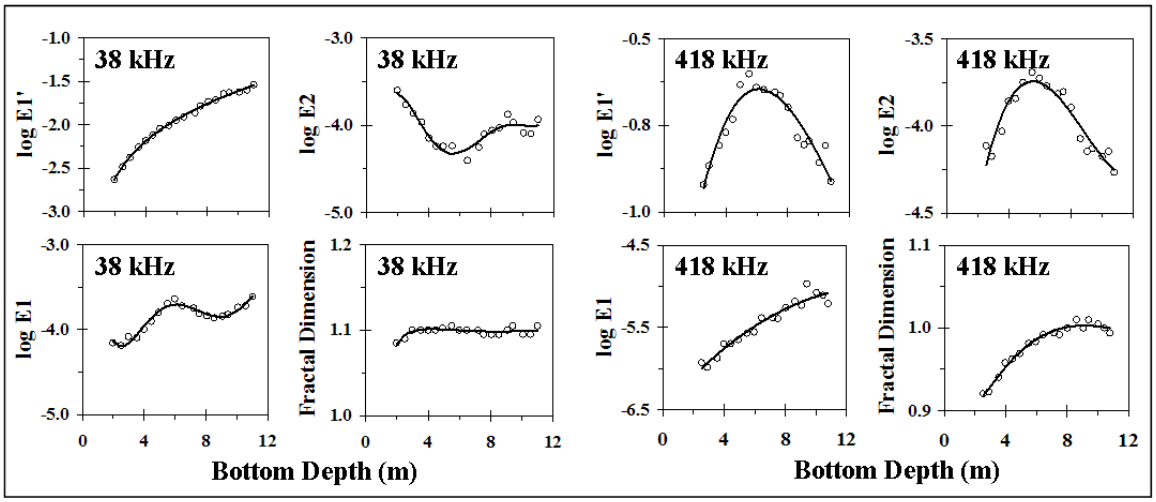

Figure 5.3 Empirical models (solid line) used to normalize acoustic parameters to median survey depth. These high-order logarithmic polynomials were fit to the median values of acoustic parameters at 18 bins of depth (○), computed from the data in Figure 5.2.

acoustic energy at median survey depth. The E1 of both frequencies had inflection points around 2m, with very steep slopes on the shallow side of the curve (Figure 5.3). To avoid the high degree of uncertainty associated with the inflection point and steep slope, the depth-normalization models were constrained to depths greater than 1.75m, and survey data shallower than 1.75m were rejected during quality analysis.

5.2.5 Quality Analysis

The log-transformed and depth-normalized hydroacoustic survey records were subjected to a series of QA filters to identify and remove "irregular" hydroacoustic returns. The following QA process was conducted individually for each survey site so as to emphasize removal of anomalous within-site records, so as not to key on genuine between-site variation. The first filter checked the differential depth between successive pings, removing waveforms that contacted the seabed at shallow angles, typically caused by excessive vessel roll. The next filter removed records with depths less than 1.75m or greater than the 99.5 percentile. The 99.5 percentile setting rejected the anomalously deep records within a survey site, which are frequently the result of misshapen waveforms. The final filter addressed outliers by removing records for which either of the ten acoustic parameters fell beyond either the 1 or 99 percentile.

5.2.6 Training Dataset

62 ground-validated hydroacoustic samples were collected within the study area for the training dataset, collected with the vessel drifting in idle (Figure 5.4a). Each sample consisted of 30 seconds of concurrent hydroacoustic and video files, acquired with a drop camera trailing just behind the ensonified area. Videos were reviewed post-survey and assigned visually-apparent areal cover of structural (mud, sand, shell, hardbottom) and biological elements (turf, macroalgae, seagrass, scleractinians, alcyonaceans, pen shells, and worm tubes). Areal cover was used to assign training samples into one of five categories of visually-apparent seabed roughness, ranging

from low to high and intended to represent the potential for macroalgae attachment (Table 5.1). For example, the "low" roughness areas (Classes 1 and 2), mainly represented by smooth soft sediment (mud/sand mixtures) with little or no shell or small rocks, had little hard substrate suitable for attachment and growth of macroalgae. In contrast, the "high" roughness areas (Classes 4 and 5), represented by hard, rocky bottoms or seagrasses, had substantial amounts of substrate suitable for macroalgae.

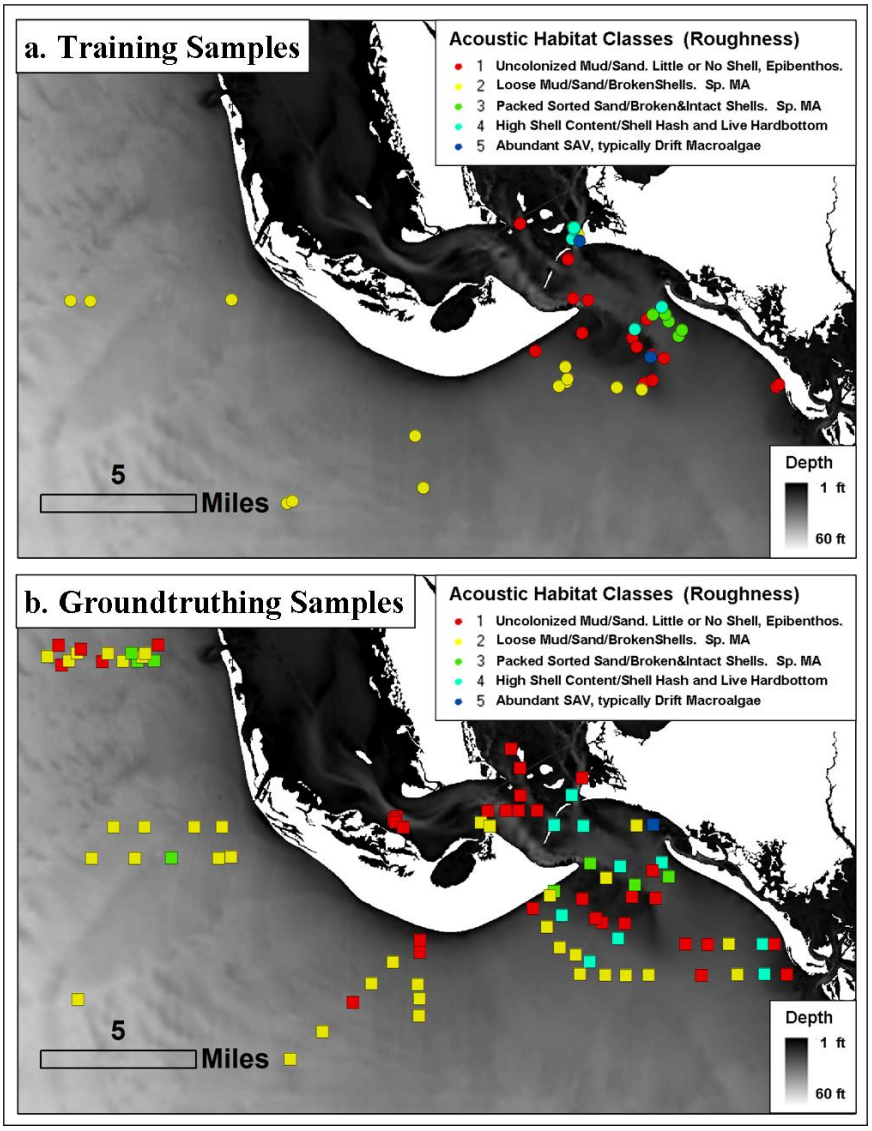

Figure 5.4 Locations of (a) training and (b) groundtruthing hydroacoustic + video samples.

Table 5.1 Bottom roughness scheme for classifying hydroacoustic data.

Bottom roughness
Class 1 = low = soft sediments (sand, mud) with no or little bi-valve shell debris, rock, epibenthic organisms; vertical structure < 5 cm in most of area
Class 2 = low = mainly mud/sand mixtures with variable amounts of bi-valve shell debris, rock, epibenthos; vertical structure variable, < 10 cm in most of area
Class 3 = moderate = mainly packed shell debris and scattered rubble/rock with variable amounts of mud/sand mixtures, epibenthos variably abundant, vertical structure < 10 cm in most of area
Class 4 = high = intact bi-valve shells and hard bottom, mostly exposed bedrock, epibenthos typically abundant, vertical structure typically > 10 cm.
Class 5 = high = abundant drift macroalgae, or seagrasses, typically with attached macroalgae and other epibenthos, vertical structure > 10 cm

5.2.7 Multivariate Classification

Discriminant analysis (DA) is an eigenanalysis technique (i.e. matrix-based) that determines the linear combination of independent variables that maximizes discrimination between predefined groups. The supervised classification workflow was divided into four major segments; (1) a series of multivariate analyses [Principle Components Analysis (PCA) → K-means clustering → multidimensional scaling (MDS)] to refine the assignment of each training sample to one of the five classes, and to remove outlying hydroacoustic records, (2) an exploratory DA to arrive at the final class assignment of training samples, and to reject training samples that did not conform to their assigned class, and (3) a series of three descriptive DA's to refine the training dataset into end-member records and produce a set of classification functions, and (4) a predictive DA to classify survey records using the classification functions of the 3rd-Pass descriptive DA (Figure 5.5). The eleven independent variables (38 and 418 kHz log E0, logE1′, logE1, logE2, FD, and 418 kHz depth) were entered stepwise into the DA with prior probabilities of group membership computed from group size.

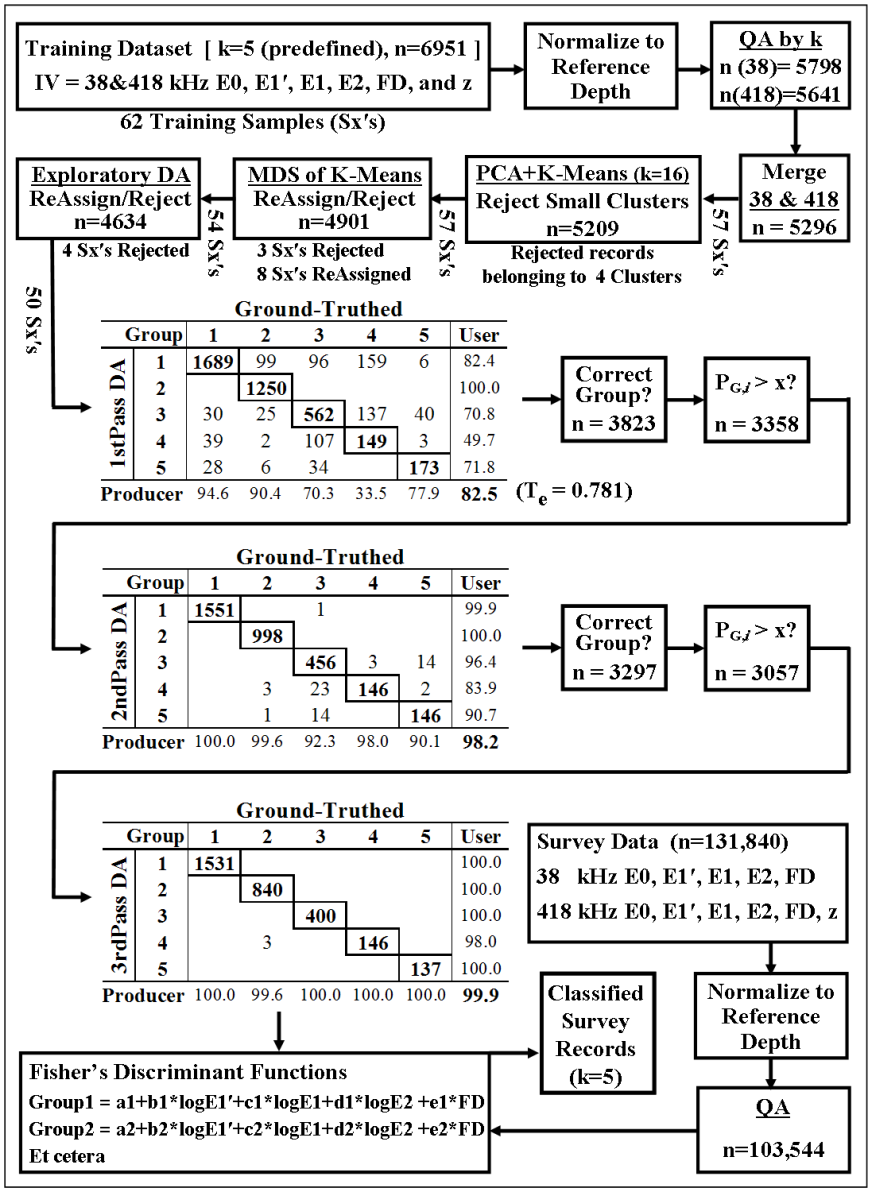

Figure 5.5 Classification workflow. Hydroacoustic training samples were assigned to one of five a priori bottom classes. Acoustic parameters were normalized to average survey depth, using empirical models created from survey and select training data. Quality analysis consisted of a max depth span, min/max depth, and 1/99 percentile filters (calculated individually for each training group), followed by PCA/K-means/MDS outlier filtering and class re-assignment. The final membership of training dataset was determined using an exploratory discriminant analysis (DA). The training dataset was refined by passing through three DA's. Only those training records (1) classifying correctly and (2) exceeding a minimum probability for group membership passed onto the next DA. The Fisher's Linear Discriminant Functions obtained from the 3rd DA were used to classify survey data into one of five a priori bottom classes.

5.2.7.1 PCA + K-means + MDS of Training Dataset

The 62 hydroacoustic samples comprising the training dataset was submitted to the same series of QA filters as the survey data. Next, the individual 38 and 418 kHz datasets were merged into a single dataset (57 of the original 62 samples remained after QA/Merge). The final form of the training dataset was arrived at using a series of multivariate techniques, in which some samples were rejected outright and others were re-assigned to another acoustic bottom class (Figure 5.5). First, the eleven independent variables were standardized by $(x-\mu)/\sigma$ for equal weighting and submitted to a PCA. The first 10 Principle Components (PC), accounting for 98.3% of variance, were submitted to a K-means clustering algorithm to separate the training data into 16 clusters (a number arrived at by trial and error). Records belonging to disproportionately small clusters were regarded as outliers and removed from the training dataset. The remaining records were then submitted to another PCA+K-means analysis (again, k=16). For each of the 57 training samples the proportion of records falling into each of the 16 clusters was computed (hypothetically, a training sample might have 25% of its records fall into cluster 4, 25% into cluster 12, and 50% into cluster 16). This matrix (columns = K-means cluster membership, rows = training samples) was submitted to an MDS analysis (obtained from a Bray-Curtis similarity matrix). Training samples judged to be outliers in the 2D MDS plot were rejected outright (i.e. samples that not only grouped apart from other samples of the same bottom class, but also from the samples as a whole). Training samples were re-assigned if (1) they were located among another bottom class in the 2D MDS plot, and (2) the initial visually-apparent class assignment could reasonably be overturned to the class indicated by the MDS plot.

5.2.7.2 Exploratory DA

The final arrangement of the training dataset was achieved by an exploratory DA, using the post-MDS training dataset. As a check against the number of subjectively chosen *a priori* groups, an approximation of the optimum number of groups was obtained using one of the many stopping

rules developed for clustering algorithms. Milligan & Cooper (1985) reported the variance ratio criterion (VRC) of Calinski & Harabasz (1974) to be amongst the best performers in a simulation study of 30 stopping rules. To compute the VRC, the first 5 PC of the last PCA analysis were submitted to K-means cluster analysis. For each value of k, the VRC was computed as the maximum between-cluster variance divided by the minimum within-cluster variance. Calinski & Harabasz (1974) suggest that the first local maximum of VRC is an informal indicator of the optimal value of k.

5.2.7.3 Descriptive DA

The post-exploratory-DA training dataset was submitted to a series of three descriptive DA's to (i) refine the heterogeneous training samples into "pure" structural and biological elements, (ii) examine how the independent variables contribute to discrimination between groups, and (iii) generate a set of Fisher's linear discriminant functions (FLDF) for classification of survey records into one of the five pre-defined bottom classes. Training records submitted to the 3rd-Pass descriptive DA were tested for critical DA assumptions because (i) ecological data frequently violate DA assumptions (Williams 1983), (ii) it is useful to assess the discriminatory power of individual hydroacoustic variables, judging by the canonical functions obtained from the descriptive DA, and (iii) unequal variance-covariance matrices distort plots of canonical functions (Krzanowski 1977; Lachenbruch et al., 1973; Wahl & Kronmal, 1977; Williams 1982). The assumption of normal multivariate distributions was assessed by ratios of skewness and kurtosis to their respective standard errors. Homogeneity of variance and covariance was assessed by comparison of between-group variances and similarity of log determinants, respectively. Significance of the discriminant function was tested by a chi-square transformation of the Wilks' lambda score. The critical DA assumption of mutual exclusivity of groups was impinged upon by "mixed" training samples acquired over heterogeneous benthos. This violation was addressed by extracting end-member records from the mixed training samples in a series of three descriptive

DA's. Only records that (1) correctly classed by the discriminant analysis and (2) exceeded a minimum probability of group membership were passed onto the next DA. This process also removed any remaining outliers, to which DA is particularly sensitive. Outliers frequently result from intrusion of environmental and hardware factors, e.g. ship wakes, excessive pitch and roll, co-mingling of echoes, and can be separated from the main data cloud by orders of magnitude.

5.2.7.4 Predictive DA

Discriminant analysis generates a set of Fisher's linear discriminant functions (FLDF) for each group, based on the linear combination of independent variables providing the best discrimination between groups. The FLDF from the 3rd-Pass descriptive DA of the training dataset were used to classify survey records. For each record, group scores were computed as the sum of the product of FLDF coefficients and independent variables plus a constant. Records were classified as the group with largest score.

5.2.8 Accuracy Assessment

An external accuracy assessment was conducted using only samples that were not included in the training dataset, since predictive accuracy will always be greater using the training dataset than for a new dataset (Huberty 1994; Kachigan 1986). A total of 117 ground-validation samples were collected in-line with the survey by intermittently slowing to idle speed, deploying a weighted video camera overboard, and simultaneously recording sonar and video for a period of 30-60 seconds. The Trimble dGPS latitude and longitude and UTC time were burned onto the recorded video for post-survey synchronization with hydroacoustic data. As with the training dataset samples, videos were reviewed post-survey and assigned visually-apparent areal cover of structural (mud, sand, shell, hardbottom) and biological elements (turf, macroalgae, seagrass, scleractinians, alcyonaceans, pen shells, and worm tubes). Areal cover was used to assign

training samples into one of five categories of visually-apparent seabed roughness (Table 5.1). The ground-validation data was subjected to the same VBT post-processing, depth-normalization, and quality assurance as described previously for the survey data. Of the 117 in-line ground-validation samples collected, 89 remained for accuracy assessment. These 89 samples were constituted of a total of 3,398 individual hydroacoustic records (approximately 45 records per sample). Each of the 3,398 records were classified into one of the five bottom classes of Table 5.1 using the same Fisher's linear discriminant functions that used to classify the survey data. The ground-validated class of each of the 89 samples was then computed as the mode of the DA-predicted class.

The overall accuracy, producer's accuracies, and user's accuracies were computed directly from a confusion matrix of ground-validated (columns) versus DA-predicted (rows) classifications (Story & Congalton, 1986). The overall accuracy (Po) was calculated as the sum of the major diagonal, i.e. correct classifications, divided by the total number of ground-validation samples. Overall accuracy was adjusted to the number of groups using the Tau coefficient for equal probability of group membership, T_e (Ma & Redmond, 1995). Tau is a measure of the improvement of the classification scheme over a random assignment of samples to categories, bounded between -1 (0% overall accuracy for 2 map categories) and 1 (100% accuracy for any number of categories). Each diagonal element was divided by the column total to yield a producer's accuracy and by the row total to yield a user's accuracy. The producer's and user's accuracies provide different perspectives on classification accuracy. The producer's accuracy (omission/exclusion error) indicates how well the mapper classified a particular category, i.e. the percentage of times that substrate known to be class 1 was correctly classified as class 1. The user's accuracy (commission/inclusion error) indicates how often map categories were classified correctly, i.e. the percentage of times that a sample classified as class 1 was actually class 1 and not one of the other four classes.

5.3. RESULTS

5.3.1 QA of Training Dataset

Of the 62 (n=6951) ground-validated hydroacoustic training samples collected within the study area, 57 (n=5296) remained after QA and merging of the 38 and 418 kHz hydroacoustic datasets (Figure 5.5). Most were rejected because they did not exceed the minimum depth filter of 1.75m. Remaining outliers were removed by performing a PCA+K-means clustering analysis (k=16) and rejecting records belonging to four disproportionately small clusters, which accounted for only 0.26-0.62% of the total records. The membership of the remaining fourteen clusters ranged from 1.3 to 22.9% of the total records. Following PCA+K-means outlier removal, 5209 records belonging to 57 hydroacoustic samples remained in the training dataset.

5.3.2 Final Arrangement of the Training Dataset

The initial assignment of the 62 training samples was done on the basis of visually-apparent seabed characteristics, after reviewing the accompanying video files. Prior to submitting the training dataset to the multi-pass descriptive DA, these bottom type assignments were re-evaluated in two steps. First, the eleven independent variables of the 5,209 records passing the PCA+K-means outlier removal step were again submitted to PCA, and the first ten PC were clustered into homogeneous groups (k=16) using a K-means algorithm. The percent membership amongst the 16 K-means clusters was computed for each of the 57 samples. This matrix (columns = K-means cluster membership, rows = training samples) was submitted to an MDS analysis, obtained from a Bray-Curtis similarity matrix (Figure 5.6a).

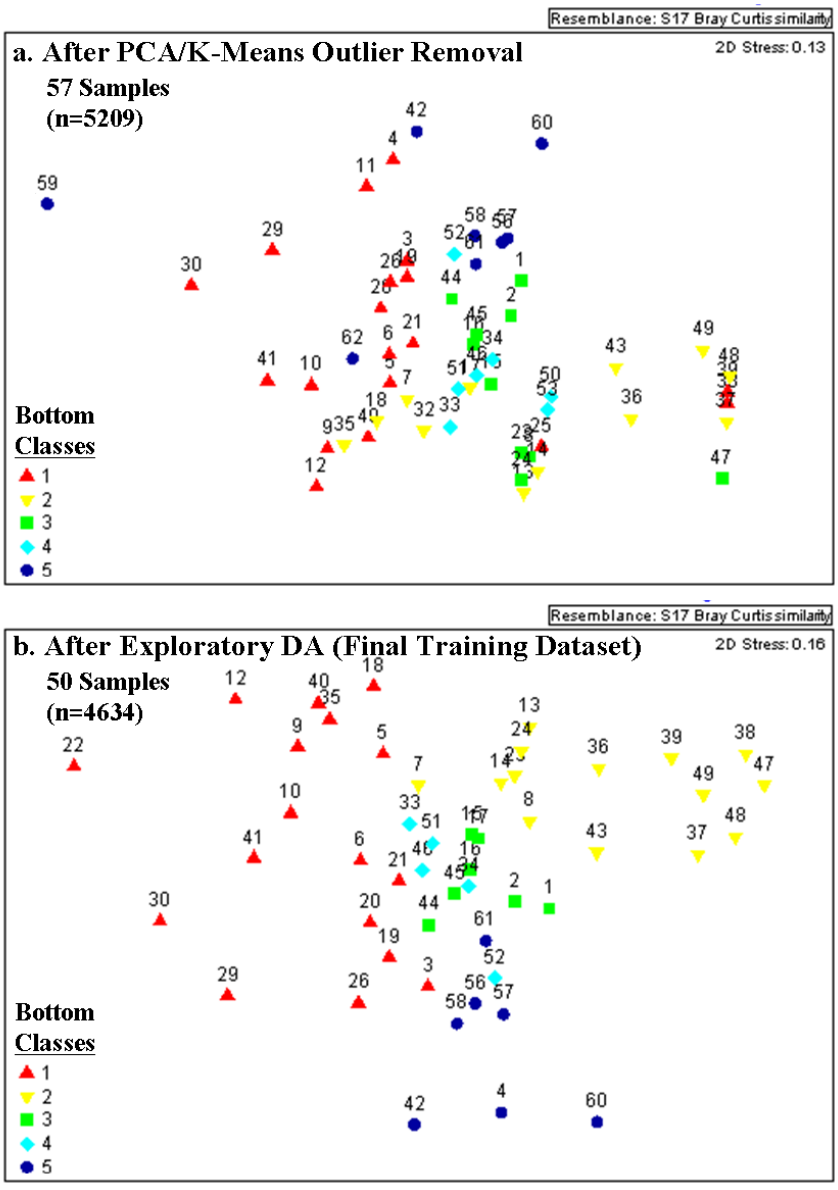

Figure 5.6 2D MDS plots of training dataset constructed from Bray-Curtis similarity matrix after (a) rejecting four disproportionately small PCA+K-means clusters, and after (b) final rejection/reassignment of training records/samples following the exploratory discriminant analysis.

Three training samples (#'s 25, 59, and 62) were found to (i) lie far outside their respective class groupings, and (ii) bear no resemblance to the bottom class with which they comingled in 2D MDS space. Since their location within the MDS plot could not be reconciled with their visually-apparent characteristics, these samples were rejected outright from the training dataset. It is interesting to note that the substrate of all three samples was visually classified as being 100%

mud. It will later be seen that other samples with high mud contents were found to have extreme values of certain acoustic parameters, suggesting that a separate "mud" class could have been warranted (see '*E2 Skew and Kurtosis')*. Eight of the remaining 54 training samples were found to comingle among other classes (#'s 7, 8, 23, 24, 35, 38, 39, 47). Because the initial visually-assigned class and the class with which they comingled differed by only one unit, and the definition of these classes was subjective and somewhat arbitrary, these eight samples were re-assigned. Second, the newly arranged training dataset (54 samples, n=4901) was submitted to an exploratory DA as a final check prior to multi-pass descriptive DA. Four samples (#'s 11, 32, 50, 53) were rejected from the training dataset due to gross mis-classification. The remaining 50 training samples (n=4634) were submitted to the multi-pass descriptive DA.

5.3.3 (VRC) Optimum Number of Classes

As a check against the number of subjectively chosen *a priori* groups, an approximation of the optimum number of groups was obtained using the variance ratio criterion (VRC), one of the many stopping rules developed for clustering algorithms. For each value of k, ranging from 3-20, the VRC was computed as the maximum between-cluster variance divided by the minimum within-cluster variance. Calinski & Harabasz (1974) suggest that the first local maximum of VRC is an informal indicator of the optimal value of k. The first local maximum, and hence the suggested optimum number of groups, was observed at k=4 (Figure 5.7).

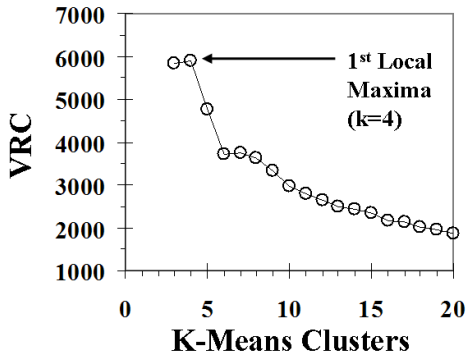

Figure 5.7 Trend of the variance ratio criterion.

However, the plot of VRC also suggests that k=5 is a reasonable number of groups, as this was the last value of k prior to the beginning of a monotonic decline beyond k=6.

5.3.4 Exploratory DA versus K-means Clustering

The first local maxima of the VRC criterion suggested the optimum number of clusters was 4, or less favorably, 5. Table 5.2a is a comparison matrix of the exploratory DA classifications (k=5) versus the PCA+K-means clusters (k=5). In other words, the exploratory DA classification (bottom classes 1-5) of each training record is compared to the PCA+K-means cluster, obtained from the VRC optimum clusters analysis. For ease of interpretation, the comparison matrix was standardized to a constant number of 100 exploratory DA cases (Table 5.2b).

Table 5.2 (a) Comparison matrix of training dataset records classified by DA into 5 bottom roughness classes and by a PCA+K-means into 5 clusters, and (b) the same data standardized to 100 cases per class (to remove bias of unequal sample sizes). Going across rows it can be seen that 4 of 5 K-Means Clusters were dominated by a single DA Group, while the other was mostly classes 3/4, validating the VRC's recommendation of 4 (or to a lesser extent 5) optimum classes.

a. Comparison Matrix of Training Dataset

		Exploratory DA					
		1	2	3	4	5	n
K-Means	1	184	0	2	6	45	237
	2	1372	71	102	36	0	1581
	3	0	0	0	0	34	34
	4	506	14	636	243	181	1580
	5	76	1307	30	54	2	1469
	n	2138	1392	770	339	262	4901

b. Standardized to 100 Cases per Class

		Exploratory DA						
		1	2	3	4	5	n	%
K-Means	1	9	0	0	2	17	28	60.7
	2	64	5	13	11	0	93	68.8
	3	0	0	0	0	13	13	100
	4	24	1	83	72	69	249	62.2
	5	4	94	4	16	1	119	79.0
	n	100	100	100	100	100	500	

Going across rows, it can be seen that 4 of the 5 K-means clusters were dominated by a single DA bottom class. The standardized comparison matrix suggests that bottom classes 1, 2, and 5 are all unique classes, and that bottom classes 3 and 4 form a fourth class. This reinforces the suggestion of the VRC criterion of an optimum number of 4 groups. But given the diametrically-opposed design of the two algorithms, i.e. maximizing between-group variation of predefined

groups (DA) versus minimizing within-cluster variation of undefined groups (K-means), this level of agreement is strong evidence that the 5 pre-defined bottom types of Table 5.1 approaches an optimal balance between the number of bottom types and the capability of the hydroacoustics to differentiate between them.

5.3.5 Multi-Pass Descriptive DA (Supervised Training Catalog)

The five-group training dataset was submitted to a series of three descriptive DA's to (i) refine the heterogeneous training dataset in "pure" end-member structural and biological elements, (ii) examine how the independent variables contribute to discrimination between groups, and (iii) generate a set of Fisher's linear discriminant functions (FLDF) for classification of survey records into these "pure" classes. The overall (internal) classification accuracy was 82.5% for the 1st-Pass DA (n=4634), 98.2% for the 2ndPass DA (n=3358), and 99.9% for the 3rdPass DA (n=3057) (Figure 5.5). The proportion of rejected records was equitably distributed amongst the individual training samples comprising the five classes, suggesting the independent variables represented spatially and temporally consistent seabed characteristics of the predefined groups (Figure 5.8). If the proportion of rejected records had not been equitably distributed amongst training samples, i.e. if a few samples within a class passed through the three DA's unscathed while most others were heavily filtered, it would follow that the acoustics were not keying in on the diagnostic structural and biological elements but rather some superfluous and unrecognized variable. The proportion of rejected records was not equitably distributed between bottom classes, as evidenced by the range of 1st-PassDA producers accuracies. The high predictive accuracies of classes 1 and 2 was presumably due to the relatively homogeneous nature of these habitats compared to the "rougher" classes, i.e. large expanses of uncolonized mud and sand were common, whereas hardbottom or SAV tended to be patchy (see section 4.2.6). This necessitated the use of variable thresholds of probabilities of group membership ($P_{G,i}$) in the multi-pass DA workflow (Figure

5.5), tightening the constraints on classes 1-2 and relaxing those of 3-5, to prevent over-prediction of the "purer" classes.

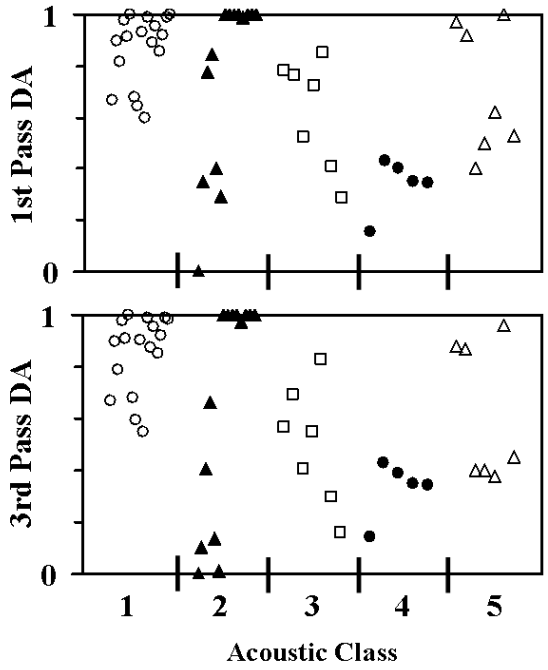

Figure 5.8 Equitable rejection of records among individual training samples suggest suggests the independent variables represented spatially and temporally consistent seabed characteristics of the five acoustic classes. Proportion of training dataset records that (1) classified correctly and (2) exceeded the mininum probability of group membership following the 1st (upper) and 3rd (lower) descriptive DA. Each symbol represents one of the 50 catalog samples comprising the five-class training dataset.

5.3.6 Predictive DA (Classified Survey Trackplots)

The 103,544 survey records that passed QA were classified into 1 of 5 acoustic bottom classes using the Fisher's linear discriminant functions obtained from the 3rd-Pass descriptive DA. The classified acoustic trackplots are shown overlying bathymetry obtained by the South Florida Water Management District (Figure 5.9). The five classes are arranged in ascending order of roughness, and hence greater potential for acting as a drift macroalgae attachment site. Figure 5.10 displays the supervised classification of video transects collected independently in May 2009, alongside the acoustic classifications. The video and acoustic classifications are in general agreement, although there appears to be a calibration bias regarding classes 1 and 2. In the

offshore Gulf of Mexico sites, what was acoustically classified as class 2 was judged to be class 1 in the video transect. But this is a minor difference, as both classes are soft bottom sediments unsuitable for macroalgae settlement. There were two areas within San Carlos Bay where the acoustic and video trackplots crossed (Figure 5.10, insets A-B). The two methodologies can be seen to generally agree on the transitions from smooth to rough bottom classifications.

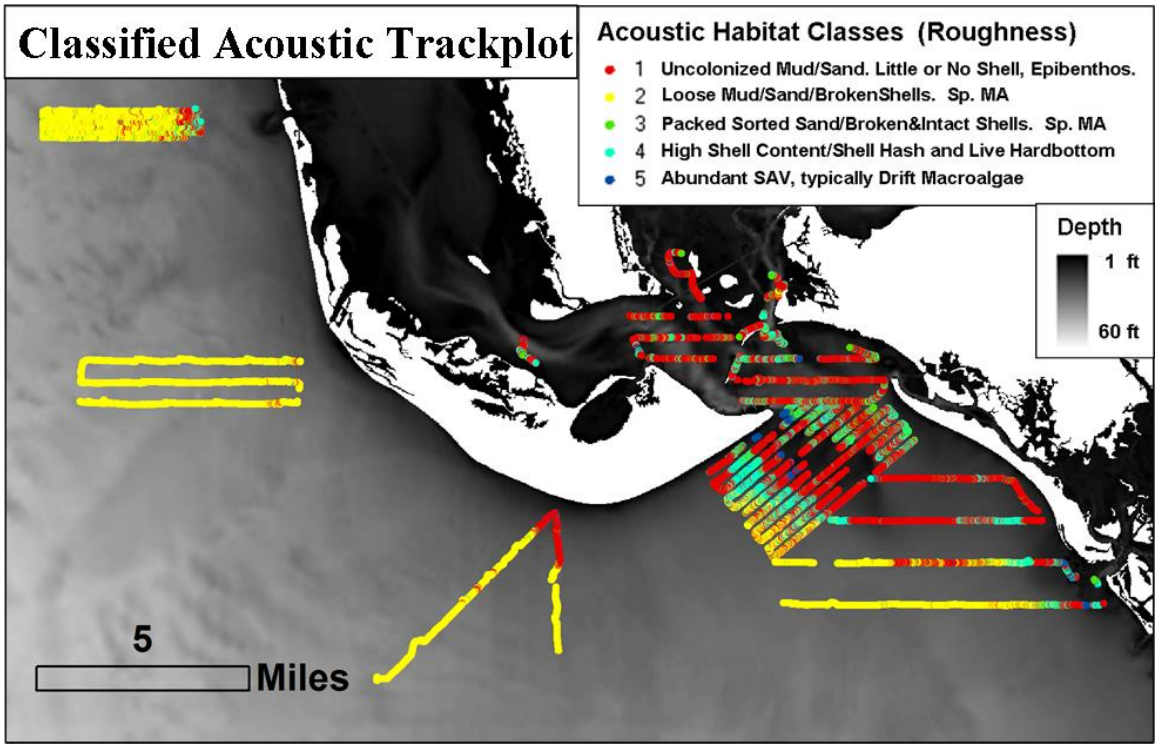

Figure 5.9 Classified hydroacoustic trackplot, using the using Fisher's linear discriminant functions obtained from 3rd-Pass descriptive DA.

5.3.7 Between-Site Comparisons

Factors influencing an areas potential to produce a large-scale drift macroalgae event include seabed texture (availability of attachment sites for drifting macroalgae), spatial expanse (adequate surface area to generate required biomass), irradiance at depth, and nutrient availability. The hydroacoustic survey directly addressed the first two factors; the supervised classification scheme utilized a training dataset categorized by visually-apparent "roughness", and the classified

trackplots allowed for demarcation of acoustically rough areas. The hydroacoustic survey indirectly addressed irradiance by providing bathymetry along with estimations of seabed roughness (the attenuation coefficient of photosynthetically-active radiation being the missing part of the equation). And distance from the mouth of the Caloosahatchee can be used a rough indication of nutrient availability (excepting possible contributions from submarine groundwater discharge).

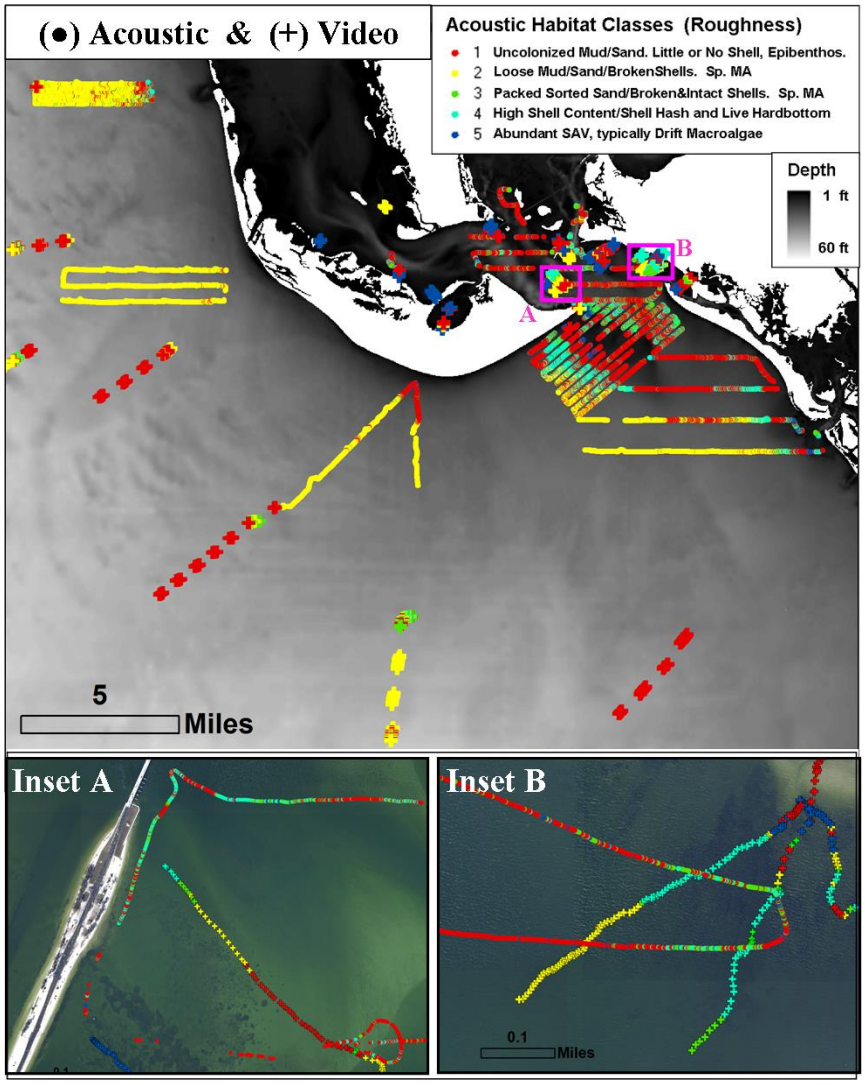

Figure 5.10 Classified hydroacoustic trackplot and classified video transects. (Insets A-B) Areas where the hydroacoustic and video transects intersected, allowing for casual comparison of the two methodologies.

General trends of acoustic roughness are evident in the classified trackplots (Figure 5.9). These visual trends were quantified by computing the proportions of acoustically-derived roughness and bathymetry for each of the six hydroacoustic survey sites (Figure 5.11).

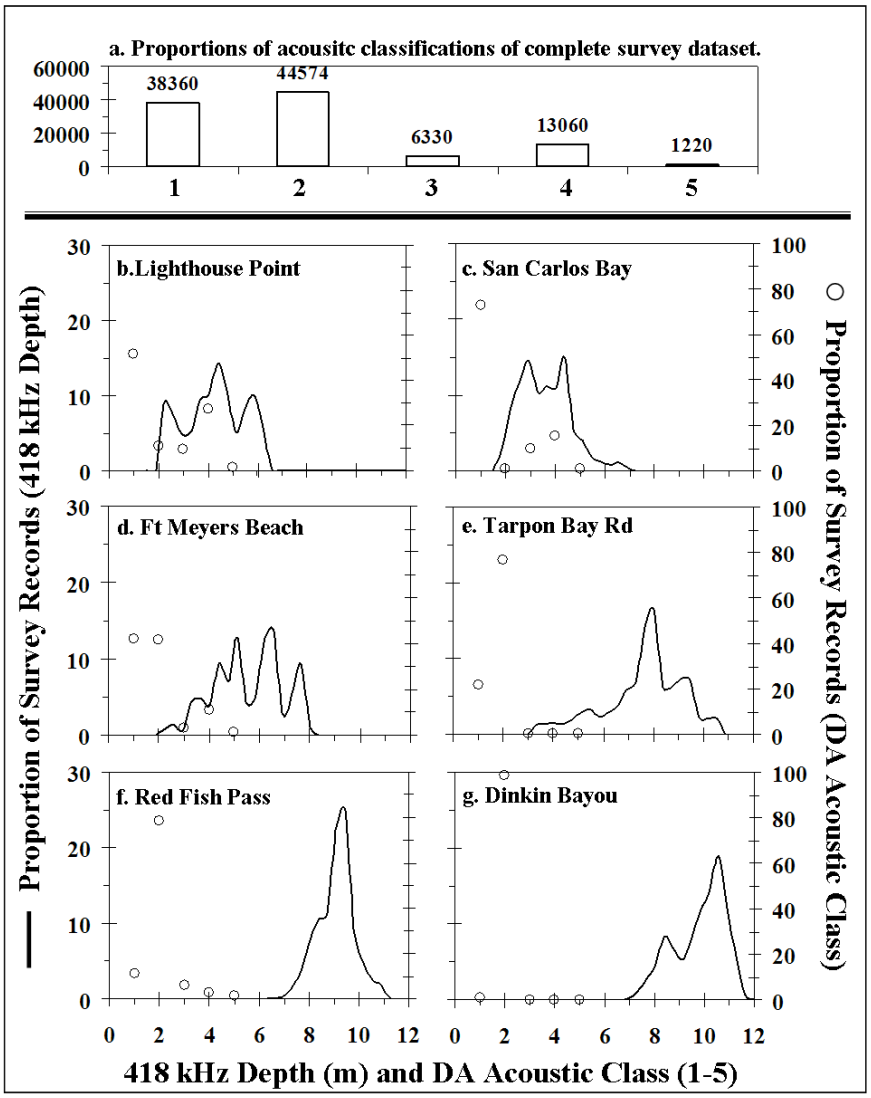

Figure 5.11 Bathymetric and acoustic class profiles of survey sites. (a) Distribution of hydroacoustic survey records among the five bottom classes for the complete survey, and (b) histograms of 418 kHz bottom depth (solid line) and distribution of survey records among the five bottom classes (○) for each survey site.

The sites within San Carlos Bay and offshore Lighthouse Point have the largest proportions of "rough" acoustic classifications (classes 3-5). Inside the Bay, the rough areas consisted mainly of

seagrass beds and areas of live hardbottom. Large amounts of macroalgae were variably present during the April-May 2009 surveys. Offshore Lighthouse Point, there were substantial areas with moderate to high bottom roughness, mostly in the form of bivalve shell debris, on both sides of the large sand spit extending from the beach to approximately 6 km offshore. The requirements for a macroalgae bloom appear to be met in both of these areas. The San Carlos Bay and Lighthouse Point sites are both characterized by relatively shallow depths; the average depth of records classified as "rough" (classes 3-5) was only 4.0m for San Carlos Bay and 5.0m for the Lighthouse Point site. Both sites are situated along the outflow of the Caloosahatchee River, which would presumably satisfy the nutrient requirements for a bloom event. And if a bloom were to occur in these areas, the macroalgae could be easily transported to the beaches, given the close proximity to the shoreline.

In contrast, the sites in the open Gulf of Mexico waters (offshore Redfish Pass, Tarpon Bay Road, and Dinkin Bayou) were characterized as uncolonized or sparsely vegetated mud and sand sediments in relatively deeper waters, out to a distance of 11 km (acoustic) and 24 km (video) offshore. The site offshore Redfish Pass had a moderate (~22%) proportion of "rough" classifications out to 5km offshore, but from 5-10km offshore the bottom classified as >95% soft sediments. The other two Gulf of Mexico sites classified as >95% soft sediments from nearshore to 11 km offshore. The homogenous habitats of unconsolidated sediments suggests that the open Gulf waters around Sanibel-Captiva may not be a major source of drift macroalgae.

5.3.8 Back-of-the-Envelope Calculations

To be the source of a drift macroalgae event, a site must provide an area of rough seabed large enough to produce adequate biomass, in addition to adequate attachment sites, irradiance, and nutrients. For this example, two acoustically-rough areas (classes 3-5) were demarcated and their areas were computed within a GIS environment (Figure 5.12). These areas were the backside of

the sand spit offshore Lighthouse Point (7.1 km^2) and an area within the mouth of San Carlos Bay (12.0 km^2). The hydroacoustic records within these two areas classified as 62 and 52% "rough", compared to just 19% for the other records lying outside these areas (Figure 5.12). For the example of the Lighthouse Point site, if drift macroalgae covered 33% of the delineated area (2.3 km^2), and 10% of that algae washed ashore, the total coverage would be 0.23 km^2 of drift macroalgae (at the *in situ* density). This is approximately equal to the area of exposed beach between Lighthouse Point and Tarpon Bay Road (7km x 35m = 0.24 km^2).

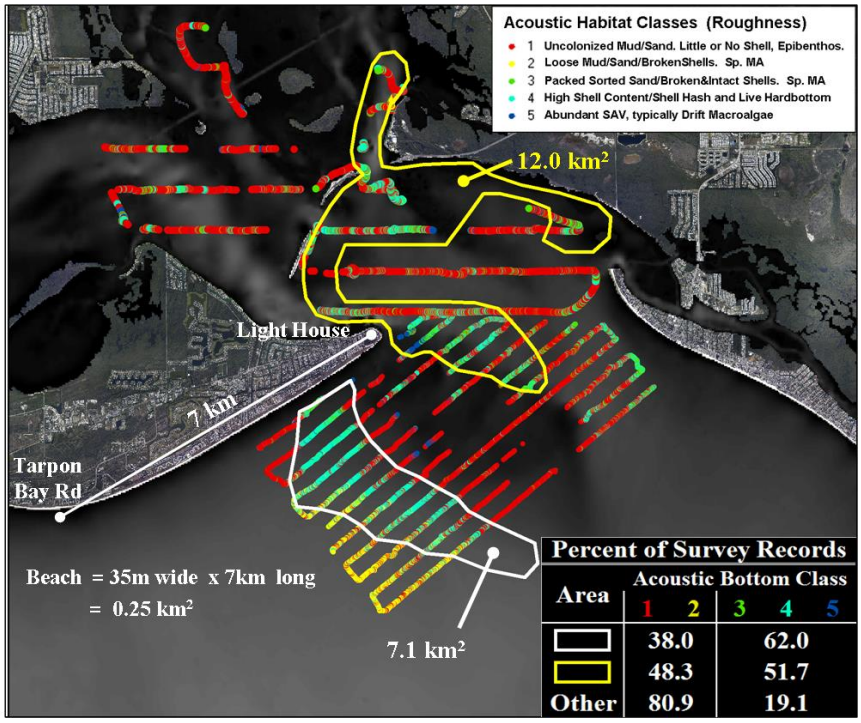

Figure 5.12 Assessing the potential for Lighthouse and San Carlos Bay sites to generate a nuisance MA bloom. Classified hydroacoustic trackplot of the San Carlos Bay and Lighthouse Point surveys. Demarcations denote areas of high acoustic roughness (i.e. high proportion of bottom classes 3-5). (Inset Bottom-Right) Distribution of hydroacoustic survey records among the five bottom classes within the two rough areas, compared to the other records lying outside of the rough demarcations.

5.3.9 Accuracy Assessment

Accuracy assessment was conducted using samples withheld from the training dataset, since predictive accuracy will always be greater using the training dataset than for a new dataset

(Huberty 1994; Kachigan 1986). A total of 117 ground-validation samples were collected in-line with the survey by intermittently slowing to idle speed, deploying a weighted video camera overboard, and simultaneously recording sonar and video for a period of 30-60 seconds. Of the 117 in-line ground-validation samples collected, 89 remained for accuracy assessment. Samples were rejected from the accuracy assessment for a number of reasons, including; (i) depths less than the 1.75m minimum, (ii) not passing the quality analysis filters, or (iii) the seabed did not fit neatly into one of the five predefined bottom types. It was for the first reason that class 5 (abundant SAV) was not included in the accuracy assessment, as all but one sample was too shallow. The overall predictive accuracy (P_o) for the 89 ground-truthing samples was 80.0% for the four seabed classes (Table 5.3). The Tau coefficient for equal probability of group membership (Te) was 0.73, i.e. the rate of misclassifications was 73% less than would be expected from random assignment of hydroacoustic records to one of the four classes.

Table 5.3 Confusion matrix of acoustically-predicted (MAP) versus ground-validated (TRUTH) classifications of the 89 samples passing QA. Class 5 was omitted due to most samples being rejected by the minimum depth filter

		TRUTH					
	Group	**1**	**2**	**3**	**4**	**row**	**User**
MAP	**1**	**28**	2			30	93.3
	2	5	**29**	3	1	38	76.3
	3		1	**5**		6	83.3
	4	1	5	0	**9**	15	60.0
	column	34	37	8	10	**89**	
	Producer	82.4	78.4	62.5	90.0	P_o =	**0.80**
						T_e =	**0.73**

5.3.10 Verifying Temporal and Spatial Consistency

A supervised classification scheme requires temporal consistency of predictor variables over the duration of data acquisition. Classification accuracy would diminish if baseline values of acoustic parameters shifted due to instrument drift or the intrusion of environmental factors.

Temporal consistency is clearly evident in the data used to construct the empirical depth-normalization models (Figure 5.2). For the examples of E1 and FD, it can be seen that October 2008 data are in line with May 2009 data, for both the survey data and the individual training samples.

5.3.11 Testing DA Assumptions

The canonical functions generated by DA can be useful for interpreting the roles that the different independent variables play in discriminating between the various groups, provided critical assumptions are not seriously violated. For this reason, critical DA assumptions were tested on the training records submitted to the 3rd-Pass descriptive DA.

5.3.11.1 Skew and Kurtosis

The assumption of normal multivariate distributions can generally be accepted if the ratios of skewness/SE and kurtosis/SE fall between ±1.96 (p=0.05 two-tail). Of the 50 tests for normality (E0/E1′/E1/E2/FD x 5 classes x 2 frequencies = 50 tests of skewness and 50 tests of kurtosis), the number of violations for the data submitted to the 3rdPass descriptive DA totaled 31 and 28 for skewness and kurtosis, respectively, distributed nearly equally between the 38 and 418 kHz frequencies (Figure 5.13). With the exception of E0, most violations were not excessive, and examination of histograms of independent variables (Figures 5.14-5.15) shows that most violations were due to skew, which DA is robust against, and not outliers, which it is not (McCune and Grace, 2002). It is also evident that the multiple DA passes improved the normality of the training dataset, as the number of violations for the unrefined (1stPass DA) training dataset totaled 41 and 36 for skewness and kurtosis, respectively (Figure 5.13).

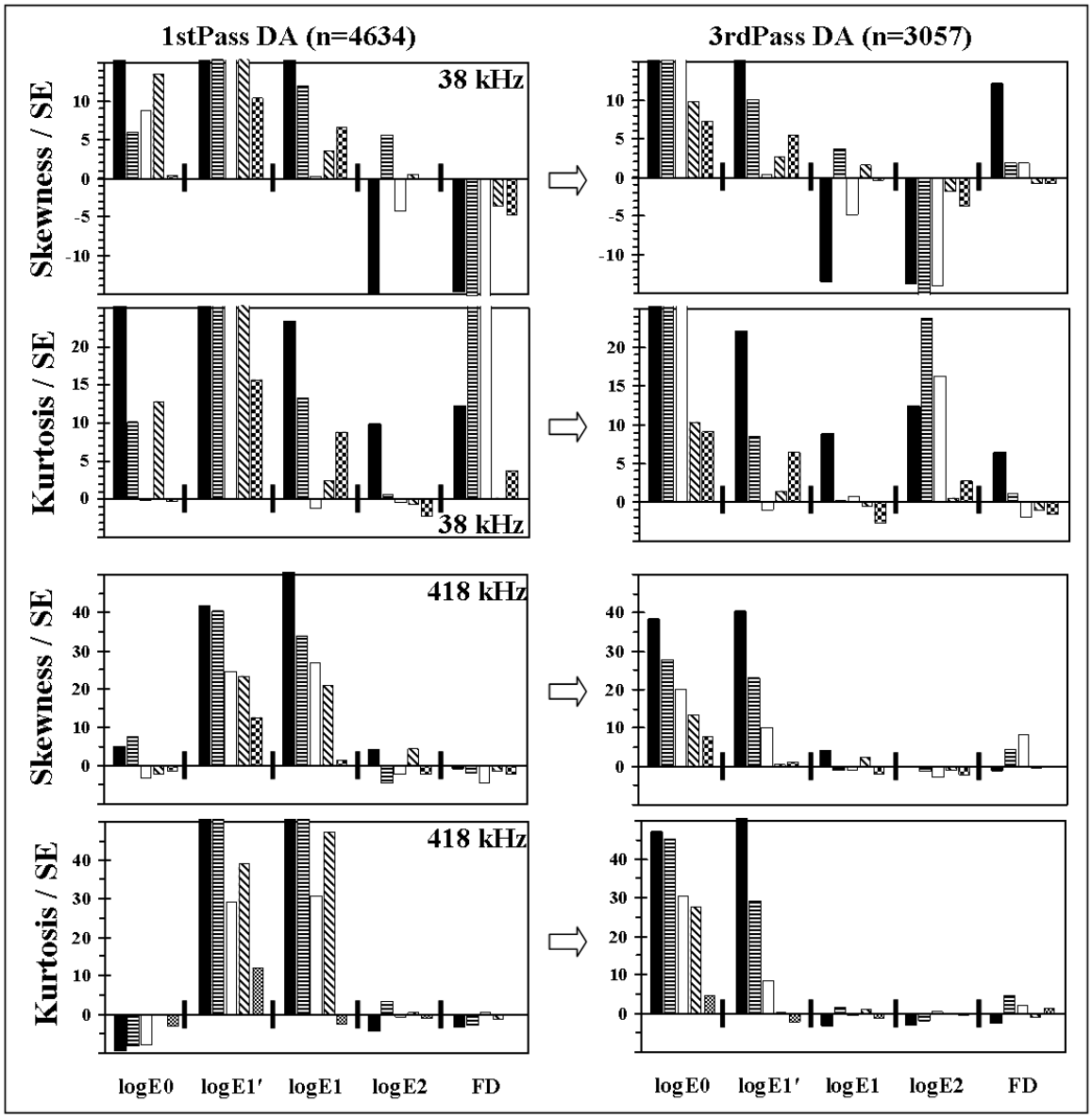

Figure 5.13 Tests of normal multivariate distributions performed on the independent variables submitted to the 1st-Pass (left) and 3rd-Pass descriptive DA, computed for the five bottom classes.

5.3.11.2 E0 Skew and Kurtosis

The most numerous and serious violations came from the E0 parameter, which accounted for 34% of the total violations. The authors of VBT intended for E0 to be primarily a measure of sediment thickness for heterogeneous bottoms, e.g. a thin veneer of unconsolidated sediment overlying a compacted bottom (Burczynski 1999). E0 would not be expected to function as such

in this study, as the seabeds tended to be vertically homogeneous, e.g. an acoustically-deep layer of unconsolidated sand. The authors of VBT speculated that E0 could also function as a measure of SAV thickness, which the pattern of E0 violations appears to support. The magnitude of violations was greatest for groups 1-3 (SAV absent to sparse), slightly less for group 4 (variably abundant SAV), and approaching normality for group 5 (abundant SAV). The presumed cause for this trend is bimodality of groups 1-3, e.g. E0 is typically near zero with occasional non-zero values coincident with sparse SAV. Histograms of 38 and 418 kHz E0 support this scenario; groups 1-4 are "peaked" with gradually diminishing low-magnitude right-tails (Figures 5.14-5.15), which is a preferable outcome since DA is robust against skew but not outliers (McCune and Grace, 2002). The histograms also suggest E0 functions primarily as discriminating group 5 from groups 1-4, particularly at 418 kHz. A similar frequency-dependent sensitivity to epibenthic biota was also observed Chapter 5, where the 418 kHz E0 was found to be sensitive to the presence of gorgonians whereas the 38 kHz E0 was not.

5.3.11.3 Dispersion of Variances and Covariances

The dispersion of variances was found to be generally homogenous, except for the E0 of both frequencies, as judged by the relative similarities of between-group variances (Figure 5.16). The dispersion of variances was also found to be heterogeneous in the Broward County field experiments. The dispersion of covariances was found to be heterogeneous by Box's M ($p<0.001$), but this finding was disregarded since small differences between covariance matrices can be found significant when sample sizes are large (Tabachnick and Fidell 1997). The dispersion of covariances was instead judged by the relative similarity of log determinants (Figure 5.16). By that criteria the dispersion of covariances was found to be homogenous; the 95% CI of the k*(k-1) = 20 comparisons of log determinants, computed as LDi/LDj, was 1.08±0.08. Unlike skewness and kurtosis, the dispersion of variances and covariances were not much affected by multiple DA passes.

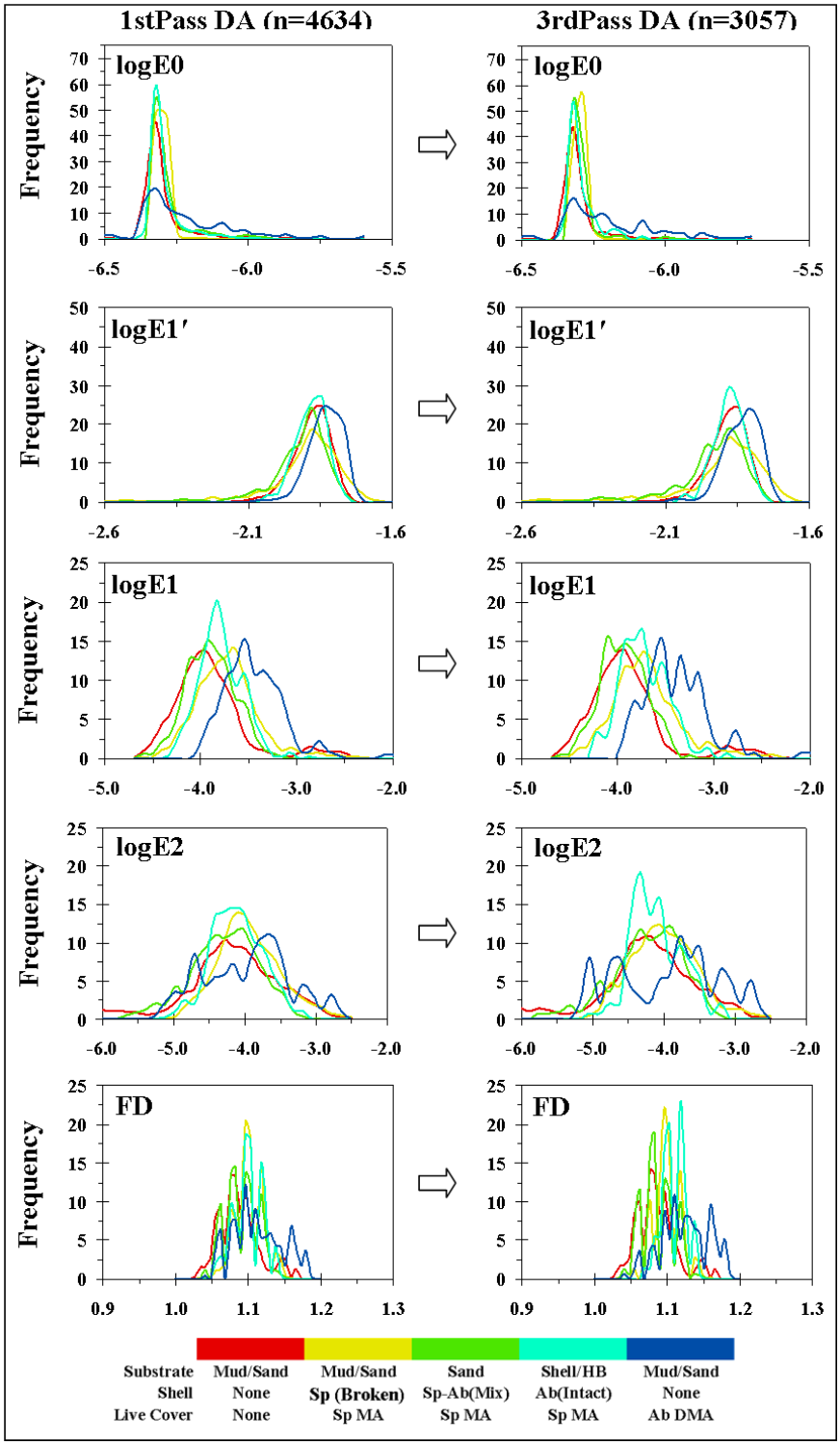

Figure 5.14 Histograms of independent variables of 38 kHz training dataset submitted to (left) 1st-Pass and (right) 3rd-Pass descriptive DA.

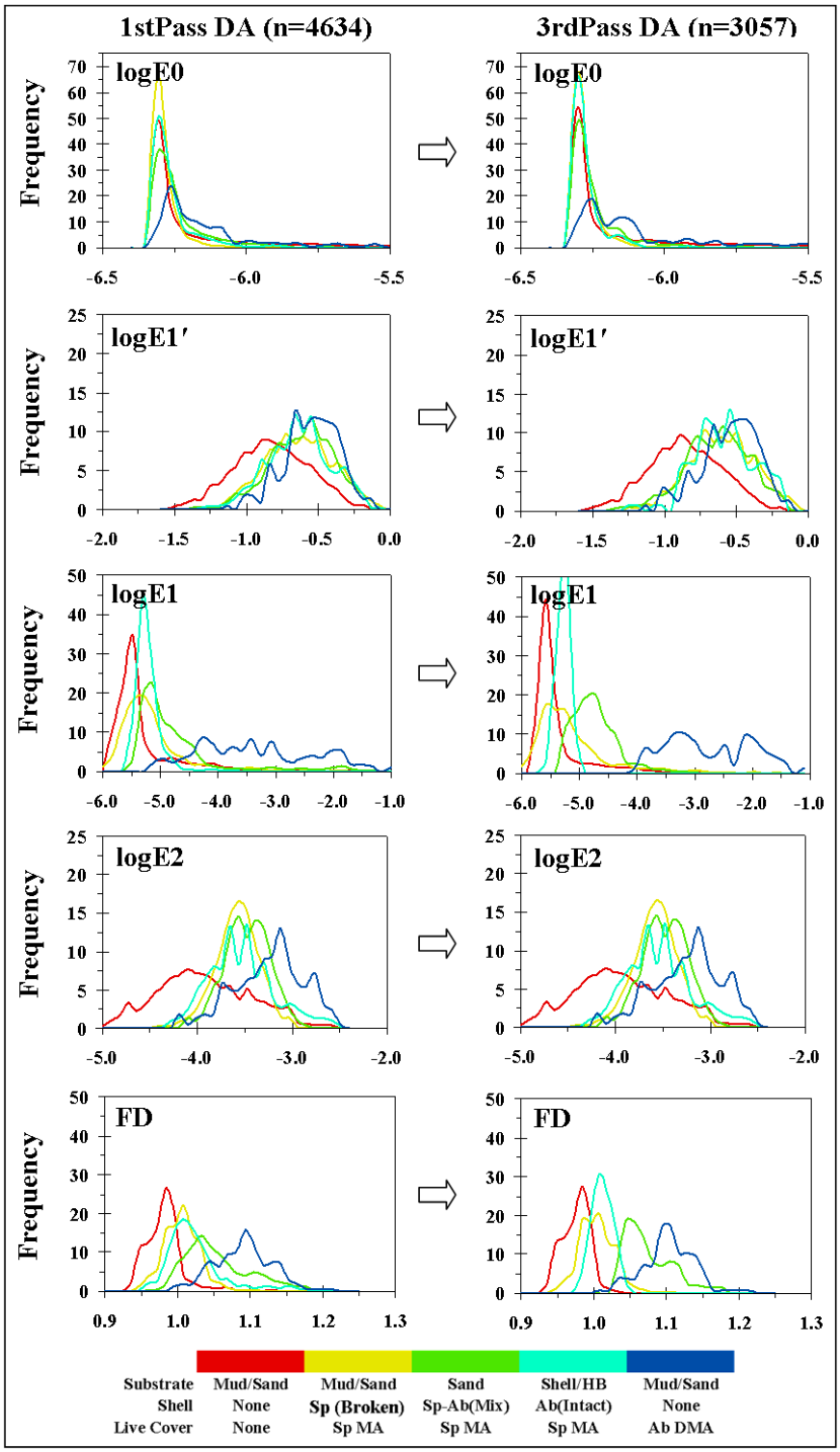

Figure 5.15 Histograms of independent variables of 418 kHz training dataset submitted to (left) 1st-Pass and (right) 3rd-Pass descriptive DA.

5.3.11.4 Group 4 Between-Group Variance

With the exception of E0, the only other variables that were flagged by the dispersion of variances plots were the 418 kHz E1 and FD of group 4, which had markedly lower covariances than the other four groups (Figure 5.16). The most likely explanation appears to be spatial clustering of the five training samples constituting group 4 (Figure 5.4a). Being a rarely encountered bottom-type, the five samples came from only two areas. Within San Carlos Bay, three group 4 samples were collected within 575m of each other. Offshore Ft Meyers beach, the remaining two group 4 samples were collected 1,800m apart from each other, along the same across-shore survey line. The two affected variables, E1 and FD, are both measures of topographic complexity, further suggesting that the low covariance resulted from relative under-sampling of seabed "roughness" characterizing group 4.

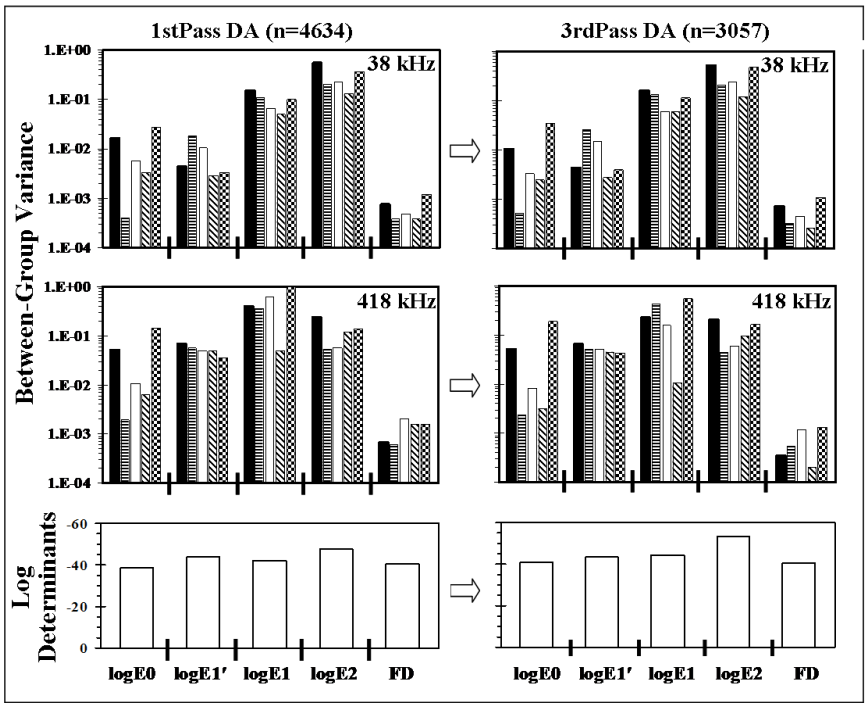

Figure 5.16 Testing of critical assumptions for discriminant analysis, performed on the independent variables submitted to the (left) 1st-Pass and (right) 3rd-Pass descriptive DA. Testing for homogeneity of variance (between-group variance), and homogeneity of covariance (log determinants of independent variables).

5.3.11.5 Multicollinearity

The assumption of low multicollinearity can generally be accepted if no single value of r exceeds 0.90 and if a small number of r's exceed 0.75 (SPSS 2001). The degree of multicollinearity between independent variables was low by this criteria, judging by values of pooled within-groups correlation coefficients from the 3rd-Pass descriptive DA (Table 5.4). The magnitude of r averaged 0.130 and spanned a range of -0.001 (38 kHz E1′ vs FD) to 0.501 (38 kHz E1 vs FD). Two informative trends emerge from examination of rankings of correlation coefficient magnitudes, the first expected, the second unexpected; (1) within a frequency, parameters associated with similar seabed properties are amongst the most intercorrelated, and (2) the same parameters of different frequencies are amongst the least intercorrelated. These observations are elaborated upon below.

5.3.11.6 Most Intercorrelated Variables

Out of the 55 pair-wise comparisons, the most and 3rd-most intercorrelated pairs of variables were 38 kHz E1-FD and the 418 kHz E1-FD (Table 5.4b). E1 and FD are both measures of topographic complexity, independently derived from the first bottom echo (Burczynski 1999). The 2nd- and 4th-most intercorrelated pairs of variables were the 418 kHz E1′-E2 and 38 kHz E1′-E2. These parameters are both associated with bottom "hardness" (Burczynski 1999), provided the bottom surface is flat, as was generally the case for the sedimentary-dominated habitats of this study. That acoustic parameters associated with the same seabed features would show up as the most intercorrelated variables can be viewed as an affirmation of rational acoustic discrimination of bottom types.

5.3.11.7 Least Intercorrelated Variables

Out of the 55 pair-wise comparisons, the 54th-least intercorrelated pair of variables were the 38 and 418 kHz E1, the 47th-least were the 38 and 418 kHz E1′, and the 46th-least were the 38 and

418 kHz FD (Table 5.4b). This is a strong endorsement for multi-frequency surveying, as it suggests that a given acoustic parameter offered unique interpretations at different frequencies.

able 5.4 Degree of multicollinearity between the independent variables of the training dataset, indicated by the pooled within-groups correlation coefficients of (a) data submitted to the 1st-Pass and (b) 3rd-Pass descriptive DA. Coefficients may range from -1 to +1, i.e. perfect negative and positive collinearity.

a. 1st-Pass DA of Training Dataset

Pooled Within-Groups Correlation Coefficients Between Independent Variables

Variable	38E1′	38E1	38E2	38FD	418E0	418E1′	418E1	418E2	418FD	418z
38E0	0.018	0.114	0.032	0.216	0.154	-0.003	0.038	0.022	-0.029	-0.039
38E1′		0.112	0.366	-0.011	-0.025	0.022	-0.047	0.071	-0.069	-0.156
38E1			0.007	0.443	0.208	-0.109	0.007	-0.166	-0.054	-0.048
38E2				-0.038	-0.124	0.035	-0.044	0.098	-0.125	0.086
38FD					0.282	-0.046	0.040	-0.071	0.006	-0.151
418E0						0.009	0.063	0.055	0.022	-0.079
418E1′							0.123	0.435	0.115	-0.099
418E1								0.248	0.552	-0.101
418E2									0.171	-0.158
418FD										-0.133

b. 3rd-Pass DA of Training Dataset

Pooled Within-Groups Correlation Coefficients Between Independent Variables

Variable	38E1′	38E1	38E2	38FD	418E0	418E1′	418E1	418E2	418FD	418z
38E0	0.008	0.085	0.046	0.170	0.085	-0.044	-0.021	-0.063	-0.013	0.009
38E1′		0.126	0.359	-0.001	-0.030	0.014	-0.066	0.058	-0.058	-0.193
38E1			0.026	0.501	0.218	-0.158	0.002	-0.267	-0.052	-0.104
38E2				-0.031	-0.141	0.046	-0.070	0.102	-0.183	0.187
38FD					0.316	-0.124	-0.009	-0.225	-0.016	-0.130
418E0						0.010	-0.004	0.050	0.029	-0.107
418E1′							0.164	0.447	0.150	-0.217
418E1								0.298	0.424	-0.179
418E2									0.180	-0.266
418FD										-0.253

5.3.12 Testing for Significance

All eleven independent variables (38 and 418 kHz logE0, logE1′, logE1, logE2, and FD, 418 kHz depth) were found to be significant by forward stepwise DA, using Mahalanobis distance (MD) as the criteria and the probability of F for entry and removal (p= 0.05 and 0.10, respectively).

The MD is the distance of a case from the centroid of a group, in units of standard deviations, measured in n-dimensional attribute space (n=11 in this case). The 3rd-Pass descriptive DA model was found to be statistically significant ($p<0.001$) based on the chi-square transformation Wilks' Lambda. The magnitude of Wilks' Lambda for the 4 discriminant functions (DF) utilized in the model was 0.016, i.e. only 1.6% of the total variance in DF scores was not explained by differences among the groups.

5.3.13 Interpretation of Descriptive DA

A discriminant function (DF) is similar in form to a multiple regression equation, although in the case of DA the coefficients are computed to maximize discrimination between predefined groups, based on the values of independent variables. When there are more than two groups, the number of DF's equals the smaller of (i) the number of groups minus 1, or (ii) the number of variables, so in this study there were four DF's. The first DF accounts for the greatest amount of between-group variance, with each successive function contributing less than the preceding one. The standardized DF coefficients (SDFC) are weighted to the magnitudes of the independent variables and are used to assess the relative contribution of each independent variable to a DF. As partial coefficients they reflect the unique contribution of each independent variable, controlling for the other independents in the model. However, they do not indicate which groups the functions discriminate between. Between-group discrimination can be visualized by scatterplots of individual scores for two given DF's, or by mean values of DF's for each group, i.e. functions at group centroids (FGC). The spread of mean FGC scores discriminant scores indicates the extent to which a particular pair of DF's discriminate between groups. The discriminatory character of independent variables, i.e. which variables discriminated by which groups, was assessed by synthesizing information from the SDF coefficients and FGC's.

5.3.13.1 Standardized discriminant function coefficients (SDFC)

The first two DF's accounted for 68.1 and 25.2% of between-group variance within the 3rd-Pass descriptive DA training dataset (Figure 5.17). The first DF was informed mostly by depth, followed by and 418 kHz FD and E2. The second DF was dominated by the 418 kHz FD. The third DF was informed primarily by the 418 kHz E1 and FD. The fourth DF was informed primarily by the 418 kHz E2 and the 38 kHz FD, followed by the 418 kHz E0 (presumably an SAV signature). The effect of refining the training dataset can be seen as relatively minor adjustments to the magnitudes of SDFC's from the 1st to 3rd-Pass descriptive DA's.

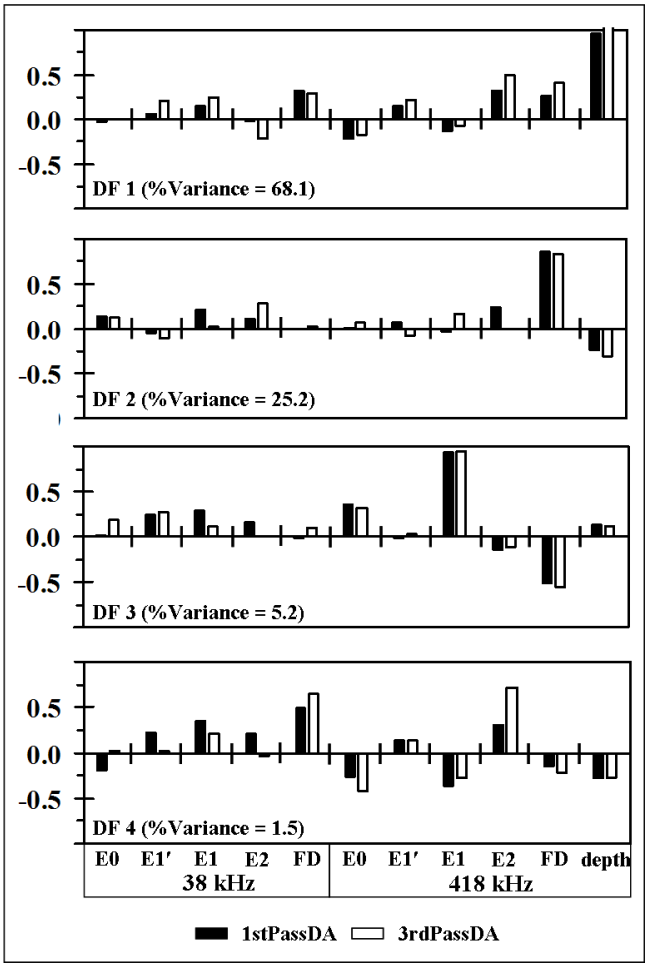

Figure 5.17 Standardized discriminant function coefficients of the 1st and 3rd-Pass descriptive DA, reflecting the relative contributions of independent variables within each discriminant function.

5.3.13.2 Functions at group centroids (FGC)

The first DF divided the five bottom classes into three major groupings; class 1 (uncolonized mud/sand), class 2 (sparsely vegetated mud/sand with low shell content), and the "rougher" classes 3-5. This can be seen across the x-axis of the DF1 vs DF2 scatterplot (Figure 5.18b) and in the relative values of FGC (Table 5.5, first column). The second DF primarily discriminated between the "rougher" classes 3-5, but did not discriminate between the structurally-similar classes 1 and 2. The third DF mainly broke-out class 5 (abundant drift macroalgae) from the other four classes. The fourth and final DF explained only a small proportion of the between-group variance (1.5%), but made the fine distinction between classes 3 and 4. As observed in previous studies (Chapters 2, 4, 6), an important function of the multi-pass descriptive DA can be seen as improved discrimination between the most similar classes.

Table 5.5 Mean scores of discriminant functions, i.e. functions at group centroids, for the 5 acoustic classes. The spread of mean scores down a column indicates which groups a discriminant function distinguishes between, and to what degree.

	Functions at Group Centroids (3rdPass DA)			
Bottom Class	Discriminant Function			
	1	2	3	4
1	-2.43	-0.72	0.09	-0.08
2	4.12	-0.99	0.19	-0.05
3	0.65	2.83	-1.38	-0.29
4	-0.19	0.52	-0.69	1.79
5	0.08	5.29	2.58	0.10

5.3.13.3 Synthesizing SDFC and FGC

The rankings and discriminatory functions of E1 and E2 were found to be in accord with the general principles of AGDS seabed classification. And the discriminatory functions of the non-traditional parameters (E0, E1′, FD) were consistent with their definitions. The top

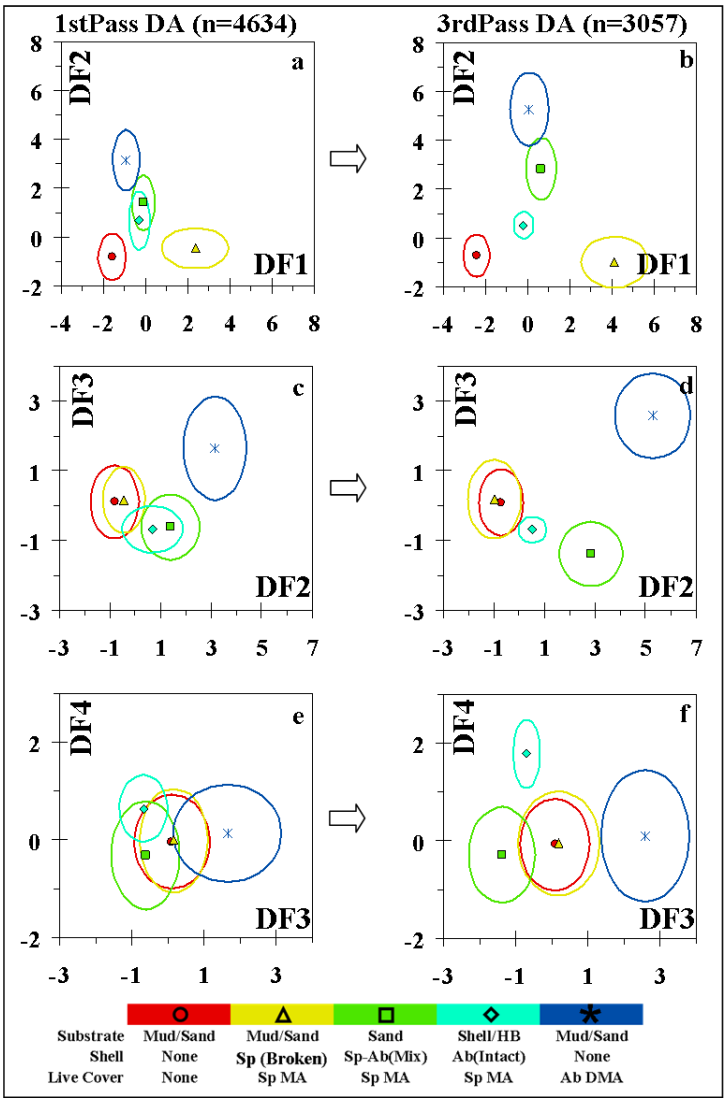

Figure 5.18 Scatterplots of discriminant functions from supervised classification of training dataset into five bottom classes by multi-pass discriminant analysis. Centerpoints denote cluster averages, ellipses are dispersion (1 standard deviation) about x and y. (left) Data submitted to 1st descriptive DA and (right) 3rd-Pass descriptive DA.

discriminatory contributors were the 418 kHz FD, depth, E1, and E2. This is also clear in the confusion matrices of dual-frequency versus single-frequency classification of the training data submitted to the 1st-Pass DA (Table 5.6). It is somewhat surprising that the 418 kHz signal so thoroughly dominated the 38 kHz signal. The first two bottom classes were both composed

primarily of soft bottom sediments, the only difference being the presence of sparse bi-valve debris in class 2. Yet, the producer's accuracies at 38 kHz were nearly identical to those at 418

Table 5.6 Internal accuracies of 1st-Pass discriminant analysis of training dataset utilizing (a) 38 and 418 kHz E1′, E1, E2, and FD, (b) 418 kHz only, and (c) 38 kHz only.

a. 38 & 418 kHz

DA Class	Ground-Validated 1	2	3	4	5
1	**1689**	99	96	159	6
2	0	**1250**	0	0	0
3	30	25	**562**	137	40
4	39	2	107	**149**	3
5	28	6	34	0	**173**
Producer's	94.6%	90.4%	70.3%	33.5%	77.9%

Overall Accuracy (P_o) 82.5%

Tau (Te) = 0.796 ± 0.013

b. 418 kHz

DA Class	Ground-Validated 1	2	3	4	5
1	**1694**	113	116	210	6
2	1	**1203**	0	0	0
3	41	60	**542**	153	66
4	27	1	80	**82**	3
5	23	5	61	0	**147**
Producer's	94.8%	87.0%	67.8%	18.4%	66.2%

Overall Accuracy (P_o) 79.2%

Tau (Te) = 0.757 ± 0.014

c. 38 kHz

DA Class	Ground-Validated 1	2	3	4	5
1	**1635**	124	793	437	146
2	0	**1257**	0	0	0
3	7	1	**3**	2	0
4	36	0	2	**2**	7
5	108	0	1	4	**69**
Producer's	91.5%	91.0%	0.4%	0.4%	31.1%

Overall Accuracy (P_o) 64.0%

Tau (Te) = 0.580 ± 0.016

kHz (Table 5.6). The 38 kHz signal thoroughly failed to discriminate the rougher classes (again, surprising since these should have varied in hardness). For the case of E1, it could be argued that using the same settings for bottom sampling windows could have favored the 418 kHz frequency. But for the cases of E2 and FD there are no such uncertainties, given that (i) the E2 sampling gates of both frequencies were more than ample to capture the entire second echo, and (ii) the computation of FD does not involve subjective settings. The parameters that most frequently showed up as minor contributors were the E1′ of both signals, and the 38 kHz E0 and E2 parameters. That E1′ would rank among the lowest contributors is self-evident from the erratic values seen in the acoustic trackplots acquired near Lighthouse Point (Appendices 5.A1-A2). The cause of this erratic behavior is presumed to be due to the fact that E1′ results from the specular (i.e. normal incidence) reflection from the bottom, making it very sensitive to vessel pitch and roll. The low ranking of the 38 kHz E0 suggests the 38 kHz frequency did not interact with epibenthic biota as the 418 kHz evidently did.

DF1: The E1, E2, and FD parameters of both frequencies detected the subtle differences between class 1 (mud/sand) and class 2 (mud/sand with low shell content), correctly ranking class 2 as slightly "rougher" and "harder" than class 1 (Appendices 5.B1f,h and B2f,h). But depth was the major contributor to DF1, due mainly to the non-overlapping depth ranges of classes 1 and 2 in the training dataset (Figure 5.19a). This in turn was the result of a general cross-shore zonation that existed between classes 1 and 2, which was reflected in the training dataset.

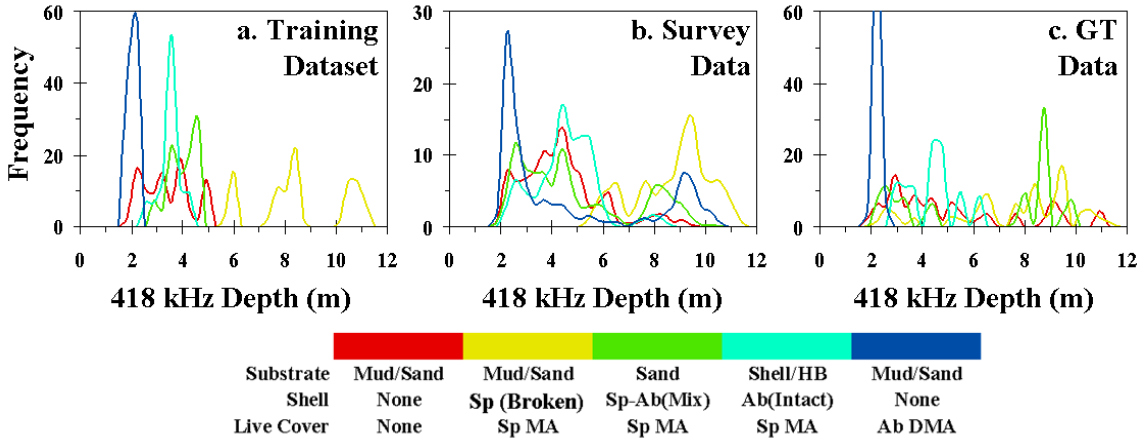

Figure 5.19 Histograms of bottom depth for each of the five bottom classes for (a) training data submitted to the 3rd-Pass descriptive DA, (b) classified survey records, and (c) ground-truthing records.

DF2: The second discriminant function discriminated between the 3 acoustically roughest classes (3-5), with the 418 kHz FD standing out as the largest information provider (Appendix 5.B2h). As FD (fractal dimension) is a measure of the shape irregularities of 1st echo waveform, it is not unexpected that it would play an important role in making the cut between the acoustically rough classes. As for frequency selection, the 418 kHz FD clearly provided more discriminatory power than did the 38 kHz FD (Appendix 5.B1h).

DF3: The third discriminant function differentiated class 5 (abundant drift macroalgae) from the other 4 classes, relying heavily upon the 418 kHz E1 and FD, with smaller but notable

contributions from the 418 and 38 kHz E0. The contribution of E0 (pre-bottom backscatter) indicates that it is functioning as an SAV-detection parameter in this study (and not as a sediment-over-hardbottom detector, as was it's primary design intent).

DF4: The final discriminant function differentiated class 4 (shell and hardbottom with variably abundant SAV) from the other 4 classes, and was informed primarily by the 418 kHz E2 and 38 kHz FD, and to a lesser extent the 418 kHz E0. Again, it appears the 418 kHz E0 was functioning as an SAV-detection parameter, and by inference, that the 38 kHz E0 was not. As for the role of the other parameters, there is no apparent explanation, beyond the obvious statement that adding meaningful independent variables improves discriminatory power, irrespective of whether their function is understood.

5.4 DISCUSSION

The success of a remotely-sensed classification scheme is most objectively judged from the confusion matrix of ground-validated versus predicted classes, compiled from a properly planned and executed accuracy assessment (AA) (Story & Congalton, 1986). The confusion matrix constructed from the 89 hydroacoustic samples passing QA confirmed that classes 1 through 4 could be accurately predicted throughout the study area (Table 5.3). Unfortunately, the shallow depths of class 5 (abundant SAV) resulted in most class 5 AA samples being rejected by the minimum depth QA filter. However, class 5 was clearly the most easily distinguished class within the training dataset (Figure 5.18), so it would not be unreasonable to presume the predictive accuracy of class 5 would at a minimum be on par with the other four classes.

Another concern with the AA was the low number of ground-validated class 3 and 4 samples (8 and 10, respectively). This resulted from the AA being conducted in-line with the survey (i.e.,

haphazard instead of stratified), in combination with the rarity of survey records acoustically classified as class 3 and 4 (6.1 and 12.6% of survey records, respectively). While there are no rigid guidelines for minimum sampling intensity, 25 samples per class has been adopted for NOAA's benthic habitat mapping programs (Battista et al., 2007a, Battista et al., 2007b). Therefore, for the purpose of judging the efficacy of the final acoustic product it is prudent to consider all the supporting evidence, as a supplement to the confusion matrix. The lack of serious violations of normality, the rational orientation of habitats in scatterplots of acoustic parameters, the generally equitable proportion of records passing through the 3 descriptive DA's, and the conformation of acoustic predictions to local topography all support the conclusion that the DA keyed in on true seabed characteristics and not simply on chance anomalies of independent variables. These observations are discussed in greater detail below.

5.4.1 Casual Review of Acoustic Classification

The descriptive statistics that accompanied the DA analyses provided objective measures of the of the normality of the independent variables and their relative contributions to differentiating between the 5 pre-defined bottom classes. As useful as these statistics were for understanding and critiquing the classification scheme, they do not provide a simple picture of how a multivariate classification scheme might be expected to work. For this purpose, trackplots of acoustic parameters are shown alongside the acoustically-classified trackplot for the area offshore Lighthouse Point (Appendices 5.A1-A2). This allows for a casual comparison of the patterns of acoustic parameters with the final acoustic bottom classifications. One of the most interesting features is the area of bivalve shell debris on the west side of the large sand spit, categorized as bottom class 4 in this study. This area is delineated in white in each plot of Appendices 5.A1-A2. As previously discussed in the *Synthesizing SDFC and FGC* section, it was the fourth discriminant function that differentiated class 4 from the other four bottom classes, and it was the 418 kHz E2 and 38 kHz FD that provided most of the discriminatory power. Irrespective of how

or why these two parameters are reacting to this particular bottom type, it is evident that they are working in concert to detect bottom class 4. And this reinforces the extra discriminatory power afforded by multiple parameters at multiple frequencies. For example, the shallow sand spit was interpreted as acoustically "hard" by the 418 kHz E2 but not by the 38 kHz E2. And the extreme west end of the survey area was observed to by mud with numerous worm tubes (with attached macroalgae). Curiously, the 418 kHz signal detected this transition as marked decrease in E2, whereas the 38 kHz did not. This suggests the mud layer was thin, i.e. the 38 kHz signal penetrated to a subsurface reflector whereas the 418 kHz signal did not.

5.4.2 Critical Review of Multi-Pass DA Classification

The final mapping product of a supervised classification scheme is predicated by the nature of the training dataset, which in turn is influenced by spatial factors (e.g. benthic heterogeneity, depth zonation) and hardware factors (e.g. AGDS design, operating frequencies). When an AGDS is used in environments more complicated than the relatively homogeneous lagoonal systems in which they were first applied, a conventional approach to supervised classification is likely to produce unsatisfactory results, in particular due to a high degree and small scale of benthic heterogeneity. A training dataset consisting solely of homogeneous benthos will leave heterogeneous portions of the map un-classified or mis-classified (Foster-Smith & Sotheran, 2003), and cataloging the many 'mixed' classes can overwhelm the discriminatory potential of AGDS (Hutin et al., 2005). This study presents a novel alternative to the dilemma, capitalizing on a small sonar footprint resulting from a conjunction of shallow depth (1.75 to 12m) and narrow beamwidths (6.4^{o} and 10^{o}), which made resolution of most micro-scale features possible. The method of sample acquisition was equally important, as the co-located drop-video allowed explicit benthic characterization of each 30 second hydroacoustic sample, avoiding the pitfalls associated with the use of buffers around sampling stations (Foster-Smith & Sotheran, 2003). The heterogeneous training dataset was refined into end-member structural and biological

elements by multiple passes through descriptive DA's, rejecting records that were incorrectly classified or failed to exceed a minimum probability of group membership.

Even though an external accuracy analysis was performed, the efficacy of the classification scheme can be further assessed by a summation of the evidence pertaining to the training catalog and the final mapping products. After taking all the following evidence into consideration, it was found reasonable to assert that (i) the critical requirements of DA were sufficiently met to accept conclusions regarding the relative importance and function of predictor variables, (ii) the multi-pass DA oriented the acoustic classes in discriminant function space in accordance with the general empirical rationale of seabed classification, and (iii) the multi-pass DA classification scheme yielded an accurate depiction of the benthos.

5.4.2.1 Descriptive DA Statistics

The critical assumptions of discriminant analysis were tested and largely met, including; (i) skewness and kurtosis (Figure 5.13), (ii) homogeneous dispersion of variances and covariances (Figure 5.16), and (iii) a low degree of multicollinearity (Table 5.4). All eleven independent variables were found to be significant by forward stepwise entry to the 3rd-Pass descriptive DA. An independent assessment of optimum clusters (VRC) supported partitioning the training dataset into five classes.

5.4.2.2 Removing Depth Contamination

Depth contamination of the raw values of E1′, E1, E2, and FD was evident (Figure 5.3), and expected, due to the lack of echo length normalization in the BioSonics VBT v1.10 software. Empirically normalizing acoustic parameters to a reference depth appeared to have resolved the issue. Firstly, depth was not strongly correlated with other predictor variables, as would be expected if depth contamination persisted (Table 5.4). Secondly, the class-specific depth ranges

of the survey dataset extended beyond those of the training dataset, i.e. depth as an independent variable did not place an artificial constraint on classification. For example, while class 1 was not cataloged deeper than 5 m (Figure 5.19a), of the 38,360 survey records that classified as class 1, 27% were deeper than 5 m (Figure 5.19b).

5.4.2.3 Understanding Depth as Predictor Variable

The 418 kHz bottom depth was used as a predictor variable because it was available and its inclusion improved the predictive accuracy. But with respect to the efficacy of acoustic classification, the role of depth as predictor variable warrants further consideration. Although it is a fact depth was the major predictor variable in the first discriminant function (DF1)\, a summation of evidence suggests the acoustic classification was not depth contaminated. The influence of depth as an independent variable is instead viewed as having been predicated by (1) the natural depth-zonation of some bottom classes, and (2) not sampling all bottom types across their range of depths. Regarding the first condition, bottom classes 1 and 2 exhibited a cross-shore zonation that was reflected in both the training and ground-truthing datasets (Figure 5.19a,c). Bottom classes 1 and 2 were both uncolonized mud/sand sediments, the only difference being that bottom class 2 included a small portion of shell debris. The nearshore break observed between these classes, by both acoustic classification and ground-truthing, is presumed to result from the platy shell debris being more easily transported out of the nearshore zone than ovoid-shaped mud/sand grains (Wang, Davis, and Kraus, 1998). As an example of the second condition, the depth range of bottom class 4 was much narrower in the training dataset than observed in ground-truthing (Figure 5.19a,c). This explains why depth played a large role as predictor variable. The question of how the classification would be affected by excluding depth as a predictor variable is addressed below.

5.4.2.4 Excluding Depth as Predictor Variable

Merging bottom classes 1 and 2 significantly reduced the importance of depth as a predictor variable (Figure 5.20a). This was confirmed by comparing the magnitudes of the standardized canonical DF coefficients, obtained by submitting the unrefined (1stPass) training dataset to a DA, with and without merging classes 1 and 2. This confirms that the natural depth zonation of these two classes, reflected in the training dataset, was indeed responsible for the preeminence of depth in DF1 (Figure 5.17). However, excluding depth as a predictor variable did not cause substantial confusion between classes 1 and 2, as can be seen in the comparison matrix of predicted class membership of training dataset records, obtained by running the DA with and without depth as a predictor variable (Figure 5.20b). As indicated by the producer's accuracies, over 80% of both the class 1 and class 2 records classed identically, with or without depth. This indicates that other acoustic parameters "picked up the slack", i.e. the importance of depth in DF1 was simply a matter of circumstance and not one of necessity.

a. (1stPassDA) Standardized Canonical Discriminant Function Coefficients of the first discriminant function, with original 5 bottom classes and after merging classes 1-2.

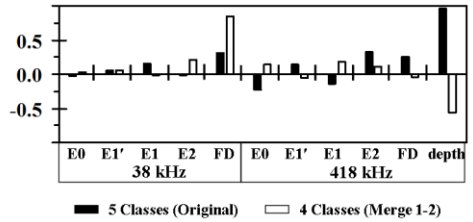

b. (1stPassDA) Comparison matrix of acoustic classifications, (columns) with depth as an independent variable and (rows) without.

1stPass DA with Depth as IndVar

	Group	1	2	3	4	5	User
Without	1	**1713**	170	15	0	0	90.3
	2	333	**1021**	169	297	11	55.8
	3	3	37	**594**	0	14	91.7
	4	0	6	0	**3**	0	33.3
	5	0	16	16	0	**216**	87.1
Producer		83.6	81.7	74.8	1.0	89.6	**76.5**

Figure 5.20 Evaluating predictive role of depth. Depth at first appeared as an important predictor variable judging by (a) the magnitude of the SCDF depth coefficient of the 1st-Pass DA. Merging bottom classes 1 and 2 significantly reduced the SCDF depth coefficient, but (b) excluding depth as an independent variable did not cause undue confusion between bottom classes 1 and 2, supporting the observation of a natural cross-shore zonation from class 1 to class 2.

However, the comparison matrix further revealed that bottom class 4 was indeed dependent on depth as a predictor variable. Without depth, 99% of the class 4 records mis-classified as class 2. This is foreshadowed by the co-location of classes 2 and 4 within the acoustic parameter scatterplots of both frequencies (Figures 15-16). One possible interpretation is that the heterogeneous bottom class 4 produced a "mixed" acoustic signature similar to the homogeneous bottom class 2, with the tie being broken by depth. Another possible interpretation is that same combination of acoustic parameters (418 kHz E2 & E0 and 38 kHz FD) occurred for both classes 2 and 4 in the training dataset, with the tie again broken by depth. Unfortunately there is insufficient information to discern between these two possibilities (and attempting to do so would be a major undertaking). Whichever scenario was at work, the depth-dependency of classes 2 and 4 could likely have been resolved by either sampling class 4 across its entire range of depth, or by a slight adjustment to the E1′ bottom sampling window (to maximize capture of incoherent backscatter at the depth of class 4). Furthermore, this lesson reinforces the reality that seabeds with clearly differing physical properties will not necessarily produce mutually exclusive acoustic signatures.

5.4.2.5 Orientation of Habitats

The five bottom classes were pre-defined in order of visually-apparent surficial roughness, with the purpose of identifying areas most likely to provide attachment points for drift macroalgae. Therefore, if the acoustic parameters do indeed represent visually discernible features of the seabed, the orientation of the classes within scatterplots of variables would be expected to form sensible patterns. While not a prerequisite for success (the accuracy assessment is the ultimate acid test), such a finding would bolster confidence in acoustic classification and make the entire process of acoustic classification more tangible. For example, bottom types assembling themselves into a sensible order would support the type of supervised classification practiced in this study, with the caveat of appropriate checks. Otherwise, the researcher would be forced to

accept that the acoustic interpretations are inaccessible, and thus relinquish full control of supervised classification to clustering algorithms.

The orientation of bottom classes did generally agree with the visually-apparent properties of the seabed at 418 kHz, but less so at 38 kHz. This agrees with the observation that teh 418 kHz parameters played a larger role in between-group discrimination than the 38 kHz parameters (Figure 5.17). This does not discount the value of the 38 kHz signal; the relative magnitudes of the SCDFC unequivocally demonstrate the discriminatory role played by the 38 kHz parameters (Figure 5.17). It does suggest that 418 kHz signal senses the seabed, via scattering, in accord with how we see the seabed, e.g. surficial texture, epibiota. Conversely, it also suggests the 38 kHz signal senses the seabed, via volume absorption, in a way very different than our perceptual experience.

At 418 kHz the orientation of class 1 (mud/sand), class 2 (mud/sand/sparse shells), and class 3 (sand/abundant shells) along a diagonal of E1:E2 space (Appendix 5.B2f) agreed with the general empirical rationale for seabed classification, which posits that E1 increases with seabed roughness and E2 increases with seabed hardness (Chivers et al., 1990; Heald & Pace 1996; Orlowski 1984), provided surfaces are flat (Burczynski 1999), which they were in this study. The underlying assumption is that an increasing content of shell debris translates into an acoustically rougher and harder surface. The orientation in 418 kHz E1:FD space also ordered the bottom classes along a diagonal (Appendix 5.B2h). The positive correlation of E1 and FD agrees with the fact that both parameters are metrics of topographic complexity, derived from very different aspects of the first echo waveform. The position of class 5 (abundant drift macroalgae) in 418 kHz E1:E2 space is less congruous with expectations. The high value of E1 was expected, resulting from scattering within canopy of drift

macroalgae. However, E2 should have diminished for the same reason, as less signal would be expected to complete the multi-path circuit after having been effectively scrambled within the drift macroalgae. The reason for the higher-than-expected E2 was presumably an artifact of empirical depth normalization; class 5 was not cataloged beyond 2.5 m (Figure 5.19a) and the slope of E2 below 4 m was very steep (Figure 5.3).

5.4.2.6 Multi-Pass DDA Refinement

The multi-pass DDA was intended to refine the variably-heterogeneous training samples into end-member elements by only passing through training records that classified correctly and exceeded a minimum threshold of probability of group membership. While quantifying the degree of spatial heterogeneity for each training sample was beyond the scope of this study (this would have required on-the-ground physical measurements of individual training samples), it is possible to make generalizations about the training videos as a whole. Bottom class 1 (mud/sand) was generally very homogeneous; rarely was anything other than mud or sand observed in the 17 training videos. Class 2 (mud/sand/sparse shells) was only slightly less homogenous, due to the latitude involved in assessing the proportion of "sparse" shells. Class 3 (sand/abundant shells) was more heterogeneous, due to the greater between- and within-sample variability concomitant with higher shell content, e.g. the shell content of a training sample categorized as 50% shell could vary from 0% to 100% throughout the video. Class 4 (shell and hardbottom with variably abundant SAV) was even more heterogeneous, as a result of patchy substrate (exposed hardbottom dispersed in sand/shell) and variably-present SAV. Class 5 (abundant drift macroalgae) was generally homogeneous, as the percent cover exceeded 75% for the majority of training samples. This general trend of visually-apparent heterogeneity was faithfully reproduced in the trend of producer's accuracy for the 1stPass DDA confusion matrix (Figure 5.5). Only small percentages of class 1 and 2 were mis-classified (5.4 and 9.6%, respectively), in accordance with their low degrees of spatial heterogeneity. The rates of mis-classification jumped to 29.7%

for class 3 and 66.5% for class 4, in accordance with their relatively higher degrees of spatial heterogeneity. And the rate of mis-classification dropped down to 22.1% for class 5. These trends support the idea that the multi-pass DDA did indeed refine the training dataset into pure end-member records.

5.4.2.7 Final Mapping Product

Beyond the objective confirmation of accuracy conferred by the confusion matrix (Table 5.3), the trackplots of classified hydroacoustic data formed patterns of bottom types that were rational on a number of accounts. The spatial distribution of acoustic classification was far from random, but instead formed large-scale patterns of contiguous bottom types (Figure 5.9). The validity of these patterns is supported by a casual comparison to the patterns formed by the intensive cataloguing and groundtruthing within the survey areas (Figure 5.4). Moreover, the patterns are in accord with the topography, hydrology, and ecology of the area. For example, the offshore Gulf of Mexico sites (Redfish Pass, Dinkin Bayou, Tarpon Bay Road) were a monotonous tract of class 2 (mud/sand/sparse shell) with nearshore class 1 (mud/sand). The nearshore transition to class 1 was consistently confirmed by groundtruthing and makes sense from a sediment transport standpoint, as the platy shell debris would be more likely to be transported out of the nearshore zone than ovoid-shaped mud/sand particles. Another example is the transition from class 1 to class 4 along the cross-shore lines offshore Ft Meyers Beach (Figure 5.21). In Figure 5.21 the classified acoustic trackplot is displayed over bathymetric contours created from the 418 kHz bottom depth. Class 1 (mud/sand) extends along the shoreface sands to a depth of 4-4.5m, where there is an abrupt transition to class 4 (abundant shell) coincident with a acoustically-verified increase in slope. At the bottom of the slope, the acoustically-predicted bottom type gradually transitions to class 1 (mud/sand) and then class 2 (mud/sand/sparse shells). The existence of this acoustically-predicted shell feature along the shelf break is supported by groundtruthing, and can be understood as either a depositional or erosional feature, similar to the shell deposits observed

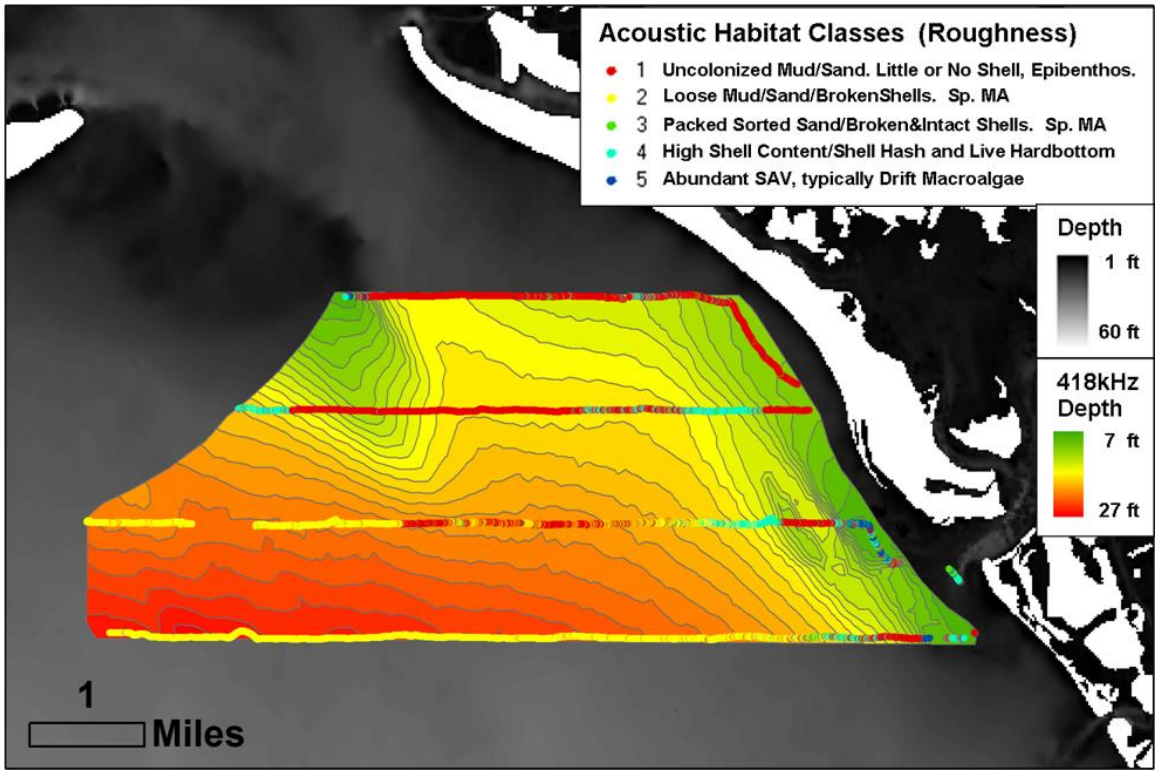

Figure 5.21 Classified acoustic trackplot displayed over 418 kHz bathymetric contours. Class 1 (mud/sand) extends along the shoreface sands to a depth of 4-4.5m, where there is an abrupt transition to class 4 (abundant shell) coincident with the steep slope. At the bottom of the slope, the acoustically-predicted bottom type gradually transitions to back to class 1 (mud/sand) and then class 2 (mud/sand/sparse shells). This acoustically-predicted shell feature along the shelf break is supported by groundtruthing, and can be understood as either a depositional or erosional feature, similar to the shell deposits observed around the sand spit offshore of Lighthouse Point.

around the sand spit offshore Lighthouse Point. The conformation of acoustic predictions to local topography, the high overall accuracy seen in the confusion matrix, the generally equitable proportion of records passing through the 3 descriptive DA's, the rational orientation of habitats in acoustic parameter scatterplots, and the lack of serious violations of normality all support the conclusion that the DA keyed in on true seabed characteristics and not simply on chance anomalies of independent variables.

5.4.3 Applicability to Future Work

While there are obvious benefits to automated real-time classification of AGDS output, the requirement of *a priori* group assignments can be problematic due to the difficult and time-consuming process of matching acoustic signatures to desired seabed characteristics. The task of defining acoustically-discernible bottom classes from the continuum of seabed types was far from straightforward, as was the assignment of individual samples to groups based on visually-apparent characteristics. This study demonstrated that such a supervised classification is possible, provided group membership is scrutinized and data carefully filtered prior to classification. And these preparatory steps yield the additional benefit of greater confidence in the resultant classification scheme. The amount of time required to glean this level of detail from an acoustic dataset would usually prove cost-prohibitive for an off-site survey. The more economic approach is to collect digitized waveforms that can be processed and deciphered post-survey. In this study there were additional benefits to a post-processing approach, including the ability to; (i) experiment with VBT settings to optimize between-group discrimination, especially the partitioning of E1′ and E1, (ii) experiment with different training categories and assignments *a posteriori*, (iii) perform a thorough and custom-fitted quality analysis of the training dataset, which allowed the 1st-Pass descriptive DA to correctly locate the initial cluster centroids, and (iv) add, remove, transform, or modify independent variables.

Expanding the multiple-echo predictor dataset beyond the standard E1 and E2 and utilizing an n-dimensional classification algorithm were also essential steps for moving beyond a soft/smooth vs vs soft/rough vs hard/smooth vs hard/rough categorization (Kloser et al., 2001; Riegl & Purkis, 2005). DA is designed to maximize between-group discrimination; this is evident by comparison of the DF1/DF2 scatterplot to those of E1/E2 and E1/FD (Figures 15-16 versus Figure 5.18). The higher-order discriminant functions allowed for differentiation of the most similar habitats (Figure 5.18), in-line with the observation of Foster-Smith & Sotheran (2003) that E1/E2

Cartesian plots are "very limited and not recommended for interpretation of AGDS data". The use of multiple frequencies improved the discriminatory power, although it was clear that the 418 kHz signal provided the most information. The main contribution of the 38 kHz signal was discriminating class 4 from the other four bottom classes, in which the 38 kHz FD played a major role in the fourth discriminant function. It is possible that the dominance of the 418 kHz signal was to some degree due to tuning the VBT bottom sampling windows using the 418 kHz signal, and using the same settings for the 38 kHz signal.

In spite of the limitations and difficulties associated with interpreting multiple-frequency single-beam acoustic data, it was possible to produce a useful thematic benthic map of ascending bottom roughness. That being said, several lessons gleaned from this study would inform future endeavors. Ideally, depth should not be a significant predictor variable. The discriminatory power should come from solely from the acoustic energy and shape parameters. This could possibly have been achieved by ensuring that each bottom class was adequately sampled across its entire depth range, with a large degree of replication. The constraint is time, as this would have required collecting far more training samples, as many would be discarded once the final arrangement of bottom classes was arrived at post-survey. Another potential improvement would be to tune the VBT settings individually for each signal, rather than using the same settings for both, to maximize the information contained within the echoes of all frequencies. That being said, adding additional frequencies, e.g. 200 and 1000 kHz, would almost certainly add discriminatory power, though at extra capital expense, logistical difficulties, and greater post-processing time.

Chapter 6: Mapping *Acropora cervicornis* and gorgonian abundance using an acoustic ground discrimination system

FORWARD

It was first recognized in Chapter 1 that erect colonies of gorgonians could be detected by the first echo pattern-recognition algorithms of BioSonics EcoSAV software. These heuristic-based algorithms look for "direct evidence" of plant features between the near-field and the trailing edge of the first echo, e.g. pre-bottom backscatter. It was also noted that the 418 kHz signal appeared to more reliably detect gorgonians than the 38 kHz signal. There is a physical basis for the frequency-dependent detection of gorgonians; presumably, the longer wavelength of the 38 kHz signal (4.04 versus 0.37 cm at 418 kHz) allows it to more frequently pass through the relatively open architecture of the gorgonian canopy. This chapter was initially conceived as a controlled field verification of these observations. The survey vessel would be anchored over (i) gorgonians and (ii) adjacent bare pavement, and the shape of 38 and 418 kHz echo envelopes would be compared for evidence of the gorgonian canopy encoded in the waveforms. The scope was later expanded to include the branching coral *Acropora cervicornis*. This prompted an additional phase of data acquisition; in addition to the anchored samples, two areas of nearshore hardbottom were also surveyed along tightly-spaced pre-planned navigation lines. Within these sites, small patches of *A. cervicornis* had previously been delineated and the percent cover had been determined by NCRI scientists. This offered an excellent backdrop for assessing the efficacy of *A. cervicornis* detection. However, the addition of *A. cervicornis* also introduced a new wrinkle to the detection methodology; the initial objective of demonstrating acoustic detection of gorgonians was expanded to both detecting and differentiating between the canopies of gorgonians and *A. cervicornis*.

Two main post-processing approaches were taken. In the first approach, the heuristic-based algorithms of BioSonics EcoSAV plant-detection software were re-tuned for gorgonians and *A. cervicornis* (which presented very different targets compared to the blades of *Zostera* spp. for which the software was designed). As previously observed in Chapter 1, the 418 kHz signal detected gorgonians more reliably than did the 38 kHz signal. While anchored over gorgonians, 69.7% of 418 kHz pings detected the canopy, versus 38.4% at 38 kHz. While anchored over *A. cervicornis*, the 38 and 418 kHz signals detected *A. cervicornis* similarly well (72.5 and 82.2% of pings, respectively). EcoSAV also provided accurate measurements of canopy height for both gorgonians and *A. cervicornis*. If the population of gorgonians and *A. cervicornis* differed markedly in canopy height, it would be reasonable to use the acoustically-predicted canopy height to differentiate between the taxa. However, the canopy height *A. cervicornis* in the study area (0.6 m) lies squarely in the middle of the range of gorgonian canopy height (0.2-1.3 m). An accurate map of undifferentiated gorgonian and *A. cervicornis* abundance would still be a valuable product, and ground-validation of the largest patches could reveal the dominant constituents. But obviously, a remote method would produce a more value-added mapping product, and provide greater confidence in the platform as a whole. The frequency-dependent detection of gorgonians and frequency-independent detection of *A. cervicornis* provided a means for doing so. Recall that EcoSAV outputs estimates of canopy height and areal cover; these values are computed as the average of a block of 10 pings. For non-zero values of 418 kHz EcoSAV cover, if the ratio of 38:418 kHz EcoSAV cover was greater than 0.55 (0.384/0.697), the 418 kHz EcoSAV cover was designated as *A. cervicornis*. If the ratio was less than 0.55, the 418 kHz EcoSAV cover was designated as gorgonian.

In the second approach, the output of BioSonics Visual Bottom Typer software was submitted to the same dual-frequency, multi-pass discriminant analysis (DA) scheme used in Chapters 4 and 5 (and the single-frequency multi-pass DA of Chapter 2). The survey data was classified as sand,

bare pavement, gorgonians, or *A. cervicornis* using a training dataset compiled from the Scooter and FTL6 sites, using a combination of anchored and hand-picked survey data. This main appeal of this approach was the potential for direct differentiation between gorgonian and *A. cervicornis* canopies, based on the linear combination of 38 and 418 kHz acoustic parameters E0, E1′, E1, E2, and fractal dimension (compared to the straightforward but simplistic above-bottom feature-detection of EcoSAV). This generally proved true, as the DA-predictions within the FTL6 and Scooter patches were almost exclusively *A. cervicornis*. However, the DA over-predicted *A. cervicornis* cover outside of *Acropora* patches. This over-prediction was ameliorated by using the EcoSAV predictions of canopy height as a final check in the classification process; if DA predicted class was either *A. cervicornis* or gorgonian, but the EcoSAV predicted canopy height was zero, the DA prediction was reclassified as bare pavement.

The main objective of this chapter, to unambiguously demonstrate that single-beam AGDS can reliably detect the canopies of epibiota such as gorgonians and *A. cervicornis*, was more of a formality than true exploration. Less anticipated was the utility of independent metrics for resolving taxa (38 vs 418 kHz EcoSAV gorgonian detection) and for reducing false positives (EcoSAV canopy-height modifier of DA classifications). The two hybrid classification schemes presented in this chapter are just a preview of the myriad acoustic combinations that could be wielded to improve the accuracy and scope of acoustic classifications. Furthermore, as evidenced by the K-Means versus DA comparison matrices of previous chapters, the reoccurring theme is that the choice of a classification algorithm is of secondary importance to the need for a logically arranged and properly groomed training dataset.

ABSTRACT

This study presents the results of methods developed for acoustic remote sensing of *Acropora cervicornis*, a threatened species of scleractinian sporadically occurring on the nearshore hardbottom of Southeast Florida. The objective was to develop techniques for mapping isolated *Acropora* patches on a scale larger than what is feasible using on-the-ground methods. A time-series of *A. cervicornis* cover could inform resource managers about the fate of such patches, e.g. do they appear and vanish, creep by extension from a central point, or leap by colony fragmentation. The main challenge to acoustically mapping *A. cervicornis* was distinguishing it from gorgonians occupying the same habitat. Hydroacoustic surveys were conducted in October 2009 at two nearshore sites in Broward County, FL utilizing a BioSonics DT-X echosounder and multiplexed single-beam digital transducers operating at frequencies of 38 and 418 kHz. NCRI scientists have monitored the spatial extent and percent cover of *A. cervicornis* within these sites, providing an ideal background against which to calibrate the hydroacoustic predictions. Two approaches were evaluated. The first approach utilized BioSonics EcoSAV post-processing software, designed to predict areal cover and canopy height of submerged aquatic vegetation using a series of heuristic pattern-recognition algorithms. Anchored over *A. cervicornis*, the 38 and 418 kHz signals performed similarly well. Anchored over gorgonians, the 38 kHz signal detected the canopy roughly half as frequently as the 418 kHz signal. Undifferentiated 418 kHz EcoSAV cover was allocated to either *A. cervicornis* or gorgonians exploiting this frequency-dependent detection. The second approach utilized the acoustic energy (E0, E1′, E1, and E2) and shape (fractal dimension) parameters obtained from BioSonics Visual Bottom Typer software. A dual-frequency training dataset was used to classify records as sand, bare pavement, gorgonians, or *A. cervicornis*. Both approaches yielded promising results, based on a number of metrics, unambiguously demonstrating that single-beam AGDS are capable of reliably detecting *A. cervicornis* and gorgonians under controlled conditions.

6.1. INTRODUCTION

Ephemeral patches of *Acropora cervicornis*, a protected species of scleractinian coral, are known to occur along the nearshore hardbottom habitats of Southeast Florida. Little is known about the ecology of these patches; in particular, how their extents might vary temporally and spatially. Several scenarios are possible; (i) they may simply appear and vanish, (ii) sparse patches may coalesce into dense patches, (iii) patches might "creep" by extension along an environmental gradient, or (iv) patches might "leap" by means of colony fragmentation. In June 2008, NCRI scientists initiated an on-the-ground monitoring program to begin providing answers to these questions. The boundaries of two *A. cervicornis* patches within Broward County, FL were delineated by a diver towing a dGPS and the percent cover of *A. cervicornis* within and just outside of the patches has been assessed at a frequency of approximately twice per year. Percent cover was visually estimated by divers swimming a 7 m radial transect around the nodes of a 23m (Scooter) and 30 m (FTL6) grid. While this on-the-ground technique is cost-effective for assessing cover within relatively small patches (FTL6 = 7,680 km^2, Scooter = 11,020 km^2), it becomes prohibitively expensive for surveying beyond the perimeter of the delineated patches.

This study presents the results of hydroacoustic surveys in the areas of the FTL6 and Scooter patches. The surveys were conducted in October 2009 using a BioSonics DT-X echosounder and multi-plexed single-beam 38 and 418 kHz digital transducers. In addition to the survey lines, training samples of bare pavement, *A. cervicornis*, and gorgonians were collected by anchoring the survey vessel directly over the target. The main objective of this study was to develop a method for reliably detecting the areal cover of *A. cervicornis*. Given that erect colonies of gorgonians (i) occupy the same habitats as *A. cervicornis* in Broward County, (ii) are far more common, and (iii) could be expected to present a similar acoustic target, i.e. a high degree of backscatter, it was necessary to develop a method for discriminating between *A. cervicornis* and

gorgonians. Two main approaches were evaluated; (1) direct detection of the tall (>0.5 m) epibenthic canopy, and (2) supervised classification of the 38 and 418 kHz acoustic energy and shape parameters into categories of sand, bare pavement, gorgonian, and *Acropora*, using the dual-frequency multi-pass discriminant analysis (DA) method developed in previous chapters.

The first approach involved processing the 38 and 418 kHz data (anchored and survey) using BioSonics EcoSAV (v2.0) software. EcoSAV was designed to predict the areal cover and canopy height of submerged aquatic vegetation (SAV), based on a series of heuristic pattern-recognition algorithms that identify plant features between the near-field and the trailing edge of the first echo envelope (Guan et al., 1999; Sabol and Melton, 1996). The first step was to tune the EcoSAV algorithms for both the 38 and 418 kHz signals, using the anchored training samples as a guide. The second and more challenging step was to identify a means by which to differentiate *A. cervicornis* cover from gorgonian cover. The most satisfactory method evolved from observations made from the training samples; the 418 kHz signal detected *Acropora* and gorgonians similarly well, whereas the 38 kHz reliably detected *Acropora* but frequently failed to detect gorgonians. This phenomenon was exploited to allocate the undifferentiated 418 kHz EcoSAV cover to either *Acropora* or gorgonians.

The second approach utilized the same multi-pass discriminant analysis (DA) methodology successfully applied to mapping a coral reef habitat in Palau, estimating drift macroalgae biomass in the Indian River Lagoon, and bottom-typing seabed roughness in Sanibel. A training catalog of sand, bare pavement, *A. cervicornis*, and erect gorgonians was acquired by anchoring the survey vessel directly over targets within and just outside of the FTL6 patch. A total of ten acoustic variables were obtained by processing the 38 and 418 kHz training samples within BioSonics VBT (v2.0) software. Training samples were refined by passing through a series of DA, retaining only those records that (i) classified correctly and (ii) exceeded a threshold for

probability of group membership. The Fisher's linear discriminant functions obtained from classifying the training dataset were then used to classify the survey data.

A secondary objective of this study was to unequivocally demonstrate that a single-beam AGDS can detect epibenthic biota such as *Acropora* and gorgonians. This objective required controlling as many environmental variables as possible. This dictated the method of triple-anchoring over the targets and demarcating the ensonified boundaries. The intrusion of depth-contamination was controlled by acquiring the anchored training samples at identical depths. The intrusion of variable substrate composition was controlled for by acquiring the training samples within very close proximity to each other. These precautions allowed for an unambiguous assessment of the influence of colonies of *A. cervicornis* and erect gorgonians on the resultant echo envelopes.

6.2. METHODS

6.2.1 Study Area

The hydroacoustic surveys were conducted on October 1-16, 2009 on the nearshore hardbottom off of Sunrise Blvd, in Ft. Lauderdale, FL (Figure 6.1). The FTL6 *A. cervicornis* patch is located on colonized pavement at a depth of 4.8 m. The Scooter patch is approximately 700 m east of FTL6, on the ridge complex habitat at a depth of 3.9 m. Within the FTL6 and Scooter delineations, cover is almost exclusively monospecific stands of *A. cervicornis*. The FTL6 patch appears to be the more mature of the two, as the current living coral is attached to a framework of consolidated *Acropora* rubble that is itself attached to the underlying pavement. Where cover exists within FTL6, it is generally contiguous on a scale of several meters. The Scooter patch is primarily individual colonies (typically ~0.3 meter) attached directly to the pavement. The

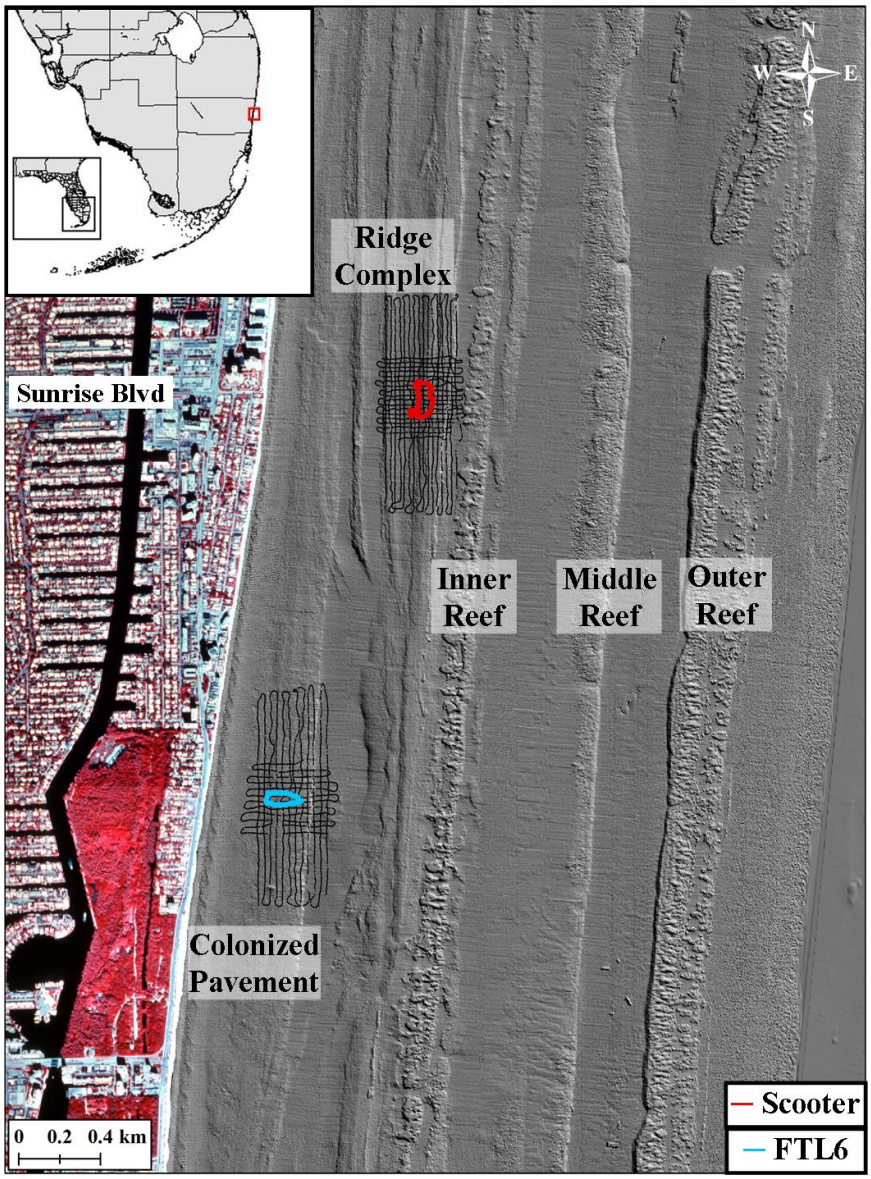

Figure 6.1. ***Acropora*** **and gorgonian study area offshore Ft. Lauderdale, FL. FTL6 (blue) and Scooter (red)** ***Acropora cervicornis*** **delineations and October 2009 hydroacoustic trackplots (black) are displayed over 2002 LADS bathymetry.**

colonies within Scooter have yet to coalesce into the large expanses of cover observed within FTL6. Cover within Scooter is greatest in the southwest portion of the patch. *A. cervicornis* exists beyond the FTL6 and Scooter delineations as sparse distributed individual colonies. The predominant cover (besides turf and macroalgae) is *Palythoa caribaeorum* and erect colonies of gorgonians. The gorgonians can be divided into two major categories on the basis of colony

height; (i) tall gorgonians with a typical canopy height of 0.8-1.3 m, constituted primarily of *Pseudopterogorgia* and *Plexaura spp*., and (ii) short gorgonians with a typical canopy height of 0.2-0.8 m.

6.2.2 Hydroacoustic Survey

The survey was conducted from a 7.5 m v-hull boat with a 0.5 m draft, at an average net speed of 4 knots (vessel plus drift). Hydroacoustic data was acquired with a BioSonics DT-X echosounder and two multiplexed, single-beam digital transducers with full beamwidths of 10^{o} (38 kHz) and 6.4^{o} (418 kHz), operated at 5-Hz sampling frequency and 0.4 ms pulse duration (Figure 2.1). At the average survey depth of 4.8 meters, the 38 and 418 kHz transducers ensonified a roughly-circular area of seabed with diameters of 0.84 and 0.54 meters, respectively. Global positioning data were collected with a Trimble Ag132 dGPS operated in beacon mode, correcting to the local WAAS signal. The dGPS signal was interfaced with navigational software to provide real-time monitoring of vessel position with respect to geo-referenced imagery and pre-planned survey lines (1 km N-S and 0.5 km E-W). Line spacing was 23 meters (Scooter) and 30 meters (FTL6), coinciding with the grid node-spacing previously established for on-the-ground areal cover analysis.

6.2.3 Training Dataset

The purpose for collecting a training dataset was three-fold. It was used for the supervised classification of survey data using the multi-pass discriminant analysis method, for guiding EcoSAV tuning, and for a controlled assessment of the acoustic interpretation of epibenthic biota. The training dataset was constituted of (i) hydroacoustic samples collected with the survey vessel anchored over targets, and (ii) hand-picked survey records. The survey vessel was triple-anchored over three bottom types; pavement without epibenthic biota, pavement with *A. cervicornis*, and pavement with erect gorgonians (Figure 6.2b-d). The anchored-samples were all

within 80 meters of each other, in or near the FTL6 *Acropora* patch (Figure 6.3). After ensuring the vessel was stationary, a weighted line was suspended from the transducer arm, midway between the two transducers, to verify they were directly over the target. The canopy height of *A. cervicornis* and gorgonian colonies were computed as the average of eight field measurements, taken a distance of 1 meter from the centerpoint at 45 degree increments. The areal cover of *A. cervicornis* was 100%. The gorgonian canopy was more open than the *A. cervicornis* canopy, but due to its greater height still approached 100% cover in planar view. Hydroacoustic data was acquired over the anchored targets for a period of 10 minutes.

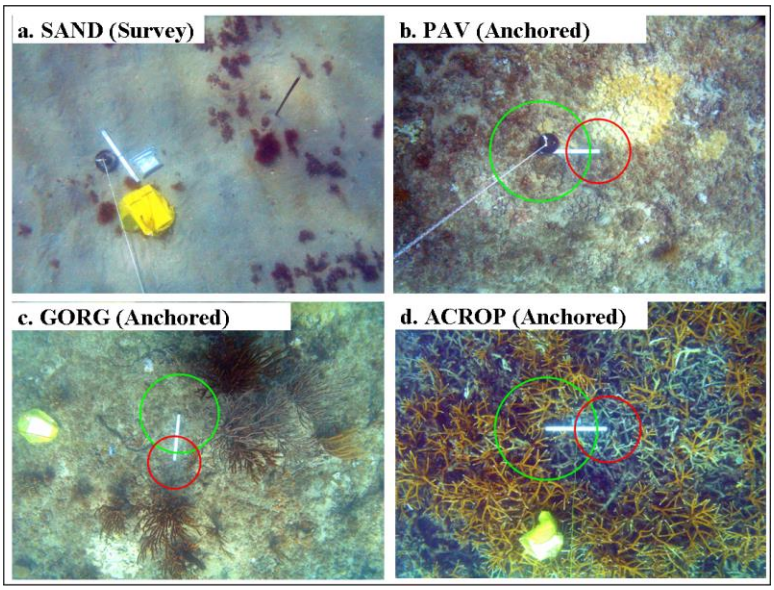

Figure 6.2. Planar photographs of training catalog sites, including (a) survey pings from an contiguous area of sand off the western edge of FTL6, and anchored sites (b-c) outside of and (d) within the FTL6 patch. The area ensonified by the 38 kHz (green) and 418 kHz (red) transducers are indicated for the anchored samples. Note: Photos taken after data acquisition - vessel had drifted off the dense cluster of gorgonians at the end of sampling.

The anchored training dataset was supplemented by handpicking records from the survey datasets. Survey records falling within the FTL6 and Scooter *Acropora* patches were added to the ACROP training dataset. Additional gorgonian samples were obtained by selecting survey records within 1 meter of EcoSAV predictions of canopy height ≥ 0.8 meter and predicted cover

> 30% (as will be shown later, these are the limits which best define the break between EcoSAV-detected colonies of ACROP and GORG). A SAND group, defined as unconsolidated carbonate sand with variably present and sparse colonies of unattached fleshy macroalgae (Figure 6.2a) was added to the training dataset by selecting ground-validated records from the westernmost region of the FTL6 survey area (Figure 6.3). This region was verified to be approximately 18 cm of sand over consolidated rubble. Throughout this document these combined anchored-plus-survey datasets are referred to as SAND, PAV, ACROP, and GORG.

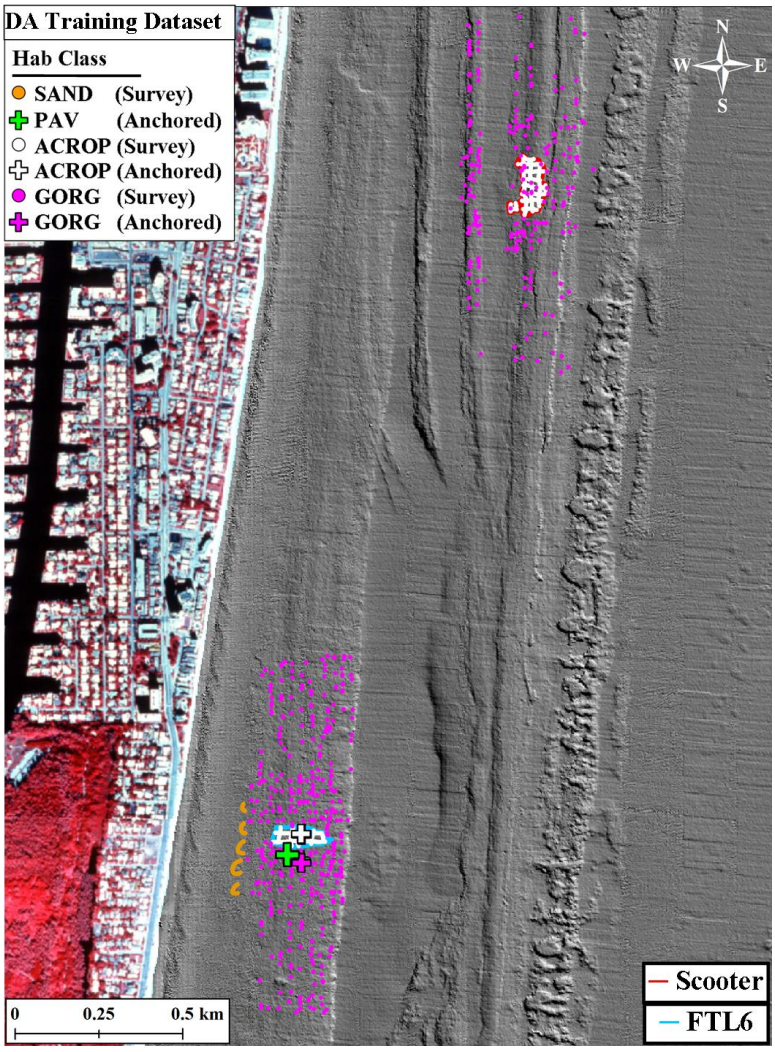

Figure 6.3. Location of samples constituting the training dataset. (crosses) Bare Pavement, *A. cervicornis*, and gorgonians samples collected with the survey vessel anchored over target. (circles) Survey records hand-picked for the training dataset.

6.2.4 EcoSAV Processing (Pattern Recognition Algorithms)

EcoSAV generates predictions of plant presence/absence and plant height for each ping by extracting features from each echo envelope and evaluating them in a series of algorithms. EcoSAV has 24 user-defined settings that can be adjusted to fine-tune the algorithms to the particular combination of equipment and environmental factors present within the study. The three main echo envelope features that EcoSAV infers as evidence of SAV are plant height, bottom thickness, and an ultra-quiet zone close to the bottom. EcoSAV computes areal coverage as the number of pings classified as "plant" divided the number of good quality pings in a sequential set of ten pings. EcoSAV first examines the 1st echo envelope to determine if it is BARE, defined as a positive finding for any of the three following criteria; (1) the plant is too short, i.e. the distance from the top of the potential plant to the declared bottom depth (designated as the primary plant feature) is less than the Plant Height Detection Threshold (PHDT), (2) the bottom is not too thick; i.e. the bottom is narrower than the Bottom Thickness Threshold (BTT), or (3) there is an ultra-quiet zone (UQZ) close to the bottom. The distances in the above statements refer to points along the x-axis of the echo envelope where intensity rises above or falls below user-defined settings. The default values of the PHDT and BTT are conservatively high (e.g. -60 dB), but under conditions of low background noise they can be set to lower values to increase sensitivity (as was done in this study). For a rough surface, the width of the first echo (time between echo intensity rising above and then falling below the threshold value) is much greater at -75 dB than at -60 dB, whereas there is little difference for a smooth surface. If a record is not found to be BARE, EcoSAV checks if it meets the definition of PLANT. This requires a negative result for the first BARE criteria, and then either a negative result for the second BARE criteria (i.e. a "thick" bottom) or a positive result for the secondary plant feature (another set of time/intensity thresholds being greater than the PHDT).

The two most critical settings in this study were the PHDT and the BTT. Starting values of PHDT and BTT were arrived at by reverse-engineering the plant detection algorithms, i.e. recording the intensity (y-axis) and distance (x-axis) values of 45 survey echo envelopes, ground-validated as either bare pavement or *A. cervicornis*. The final EcoSAV settings were arrived at by an iterative perturbation analysis of PHDT and BTT settings, using the anchored PAV, ACROP, and GORG datasets. In this study, the optimum setting of PHDT was loosely defined as the mid-point of where (i) decreasing PHDT only slightly increased the predicted cover of the ACROP and GORG datasets but greatly increased the frequency of false-positives in the PAV dataset, and (ii) increasing PHDT caused a precipitous drop of predicted cover in the ACROP and GORG datasets. This procedure was performed independently for the 38 and 418 kHz frequencies.

6.2.5 VBT Processing (Energy and Shape Parameters)

Hydroacoustic data were processed with BioSonics Visual Bottom Typer (VBT) seabed classification software (2.0) to obtain values of E1′ (time integral of the squared amplitude of the leading edge of the 1st echo), E1 (2nd part of 1st echo), E2 (complete 2nd echo), E0 (pre-bottom backscatter of 1st echo), and FD (fractal dimension, a measure of shape irregularities of 1st echo envelope), as per Burczynski (1999). The E1′ setting was adjusted so that E1 would capture only the trailing edge of the first echo, maximizing its sensitivity to scattering components of the seabed. VBT normalized echo length to average survey depth, to compensate for geometric spreading of the echo waveform. Other user-defined settings included; time-varied gain=20logR, minimum data processing threshold=-80dB, 5 pings per report, and energy filter=50%. VBT computed FD as the Hausdorff dimension of the first echo (Mandelbrot 1982), simplified by gridding the echo envelope into ‘box’ dimensions (Lubniewski & Stepnowski, 1997). The acoustic energy parameters E0, E1′, E1, and E2 were log-transformed to improve normality (Sokal & Rohlf, 1981).

6.2.6 VBT Quality Analysis

The processed acoustic data were subjected to a series of QA filters to identify and remove "irregular" hydroacoustic returns. The first filter checked the differential depth between successive pings, removing pings that contacted the seabed at angles exceeding normal-incidence, typically caused by excessive vessel roll. The next filter removed records with depths less than or greater than the 1 and 99 percentiles of depth, typically the result of misshapen echo envelopes. The final filter removed outliers by removing records for which any of the ten acoustic parameters fell beyond either the 1 or 99 percentile.

6.2.7 Multivariate Classification (DA)

Discriminant analysis (DA) is an eigenanalysis technique (i.e. matrix-based) that determines the linear combination of independent variables that maximizes discrimination between predefined groups. The independent variables logE0, logE1′, logE1, logE2, and FD were entered stepwise with prior probabilities of group membership computed from group size. The classification workflow was divided into two major segments; (1) a series of two descriptive DA's to refine the training dataset into end-member records and produce a set of classification functions, and (2) a predictive DA to classify survey records using the classification functions of the 2nd-Pass descriptive DA (Figure 6.4).

6.2.7.1 Descriptive DA

Training records submitted to the 2nd-Pass (final) descriptive DA were tested for critical DA assumptions because (i) ecological data frequently violate DA assumptions (Williams, 1983), e.g. skewed distributions commonly arise when values cannot be negative (Limpbert, Stahel, & Abbt, 2001), (ii) a primary objective was to assess the discriminatory power of individual hydroacoustic variables, judging by the canonical functions obtained from the descriptive DA, and (iii) unequal

variance-covariance matrices distort plots of canonical functions (Krzanowski, 1977; Lachenbruch et al., 1973; Wahl & Kronmal, 1977; Williams, 1982). The assumption of normal multivariate distributions was assessed by ratios of skewness and kurtosis to their respective standard errors. Homogeneity of variance and covariance was assessed by comparison of between-group variances and similarity of log determinants, respectively. Significance of the discriminant function was tested by a chi-square transformation of the Wilks' lambda score.

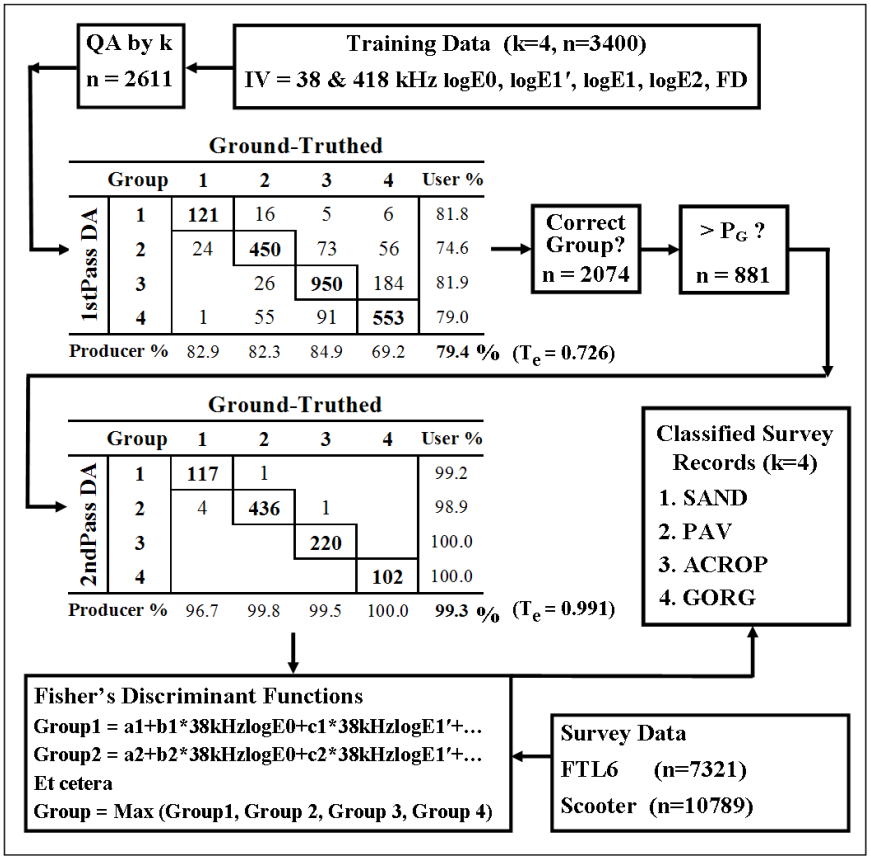

Figure 6.4 Workflow for multi-pass supervised discriminant analysis classification. Hydroacoustic samples were assigned to one of four *a priori* bottom classes. Quality analysis consisted of a differential depth filter (excessive pitch/roll), 1/99 percentile depth filter, and 1/99 percentile filters of the acoustic parameters. The training dataset was refined by passing through two DA's. Only those training records (1) classifying correctly and (2) exceeding a minimum probability for group membership passed onto the next DA. The Fisher's Linear Discriminant Functions obtained from the 2nd DA were used to classify survey data into one of the four *a priori* bottom classes.

6.2.7.2 Predictive DA

Discriminant analysis generates a set of Fisher's linear discriminant functions (FLDF) for each group, based on the linear combination of independent variables providing the best discrimination between groups (SAND, PAV, ACROP, GORG). The FLDF from the 2nd-Pass descriptive DA of the training dataset were used to classify survey records. For each record, group scores were computed as the sum of the product of FLDF coefficients and independent variables plus a constant. Records were classified as the group with largest score.

6.2.8 Accuracy Assessment

An external accuracy assessment was conducted by comparing the acoustic predictions of *Acropora* cover against the results of the most recent semi-annual monitoring; on October 14-15, NCRI researchers swam 7 m radial transects around 31 stations at Scooter and 32 stations at FTL6, visually estimating the percent cover of live and dead *Acropora* colonies within the entire 14 m diameter circle (Larson, unpublished data). Hydroacoustic records falling within the perimeters of the radial transects were selected and the acoustically-predicted cover was computed for both point-by-point and overall comparisons.

6.3. RESULTS

SECTION I. ECOSAV PROCESSING

6.3.1 Starting EcoSAV Settings (Reverse-Engineering)

The three echo envelope features that EcoSAV infers as evidence of SAV are plant height, bottom thickness, and an ultra-quiet zone close to the bottom. An ultra-quiet zone (UQZ) was not observed in this study; EcoSAV was found to be completely insensitive to the intensity and distance settings of this parameter. The absence of the UQZ criterion was not a fatal error, since

the plant detection algorithms operate on an IF/OR basis, i.e. a record is classified as BARE if there is no UQZ, or if plant height is less than the plant height detection threshold (PHDT), or if bottom thickness is less than the bottom thickness threshold (BTT). Starting values of PHDT and BTT were determined as the mean of reverse-engineered values of PHDT and BTT obtained from two sets of 45 survey echo envelopes, ground-validated as bare pavement and *Acropora*. This allowed for computation of the normal variate distributions (Z) of EcoSAV plant height and bottom thickness for bare pavement and *Acropora* (Figure 6.5a-b). The overlap of bare pavement and *Acropora* distributions in Figure 6.5a-b are in effect the *a priori* prediction of classification errors. These plots were used to estimate the starting values of PHDT and BTT, which were subsequently refined in the following perturbation analysis.

6.3.2 Final EcoSAV Settings (Perturbation Analysis)

Perturbation analysis suggested "optimum" values of PHDT and BTT values of 0.49 and 0.95m at 418 kHz and 0.81 and 3.82 m at 38 kHz, respectively (Figure 6.5c-f). At these combinations of settings, EcoSAV slightly under-predicted *Acropora* cover at both frequencies. The actual *Acropora* cover of the anchored site was 100%, whereas the EcoSAV predicted cover was 72.5% at 418 kHz and 82.2% at 38 kHz. The under-prediction was due primarily to the conservative BTT settings, which were necessary to prevent excessive false predictions of cover.

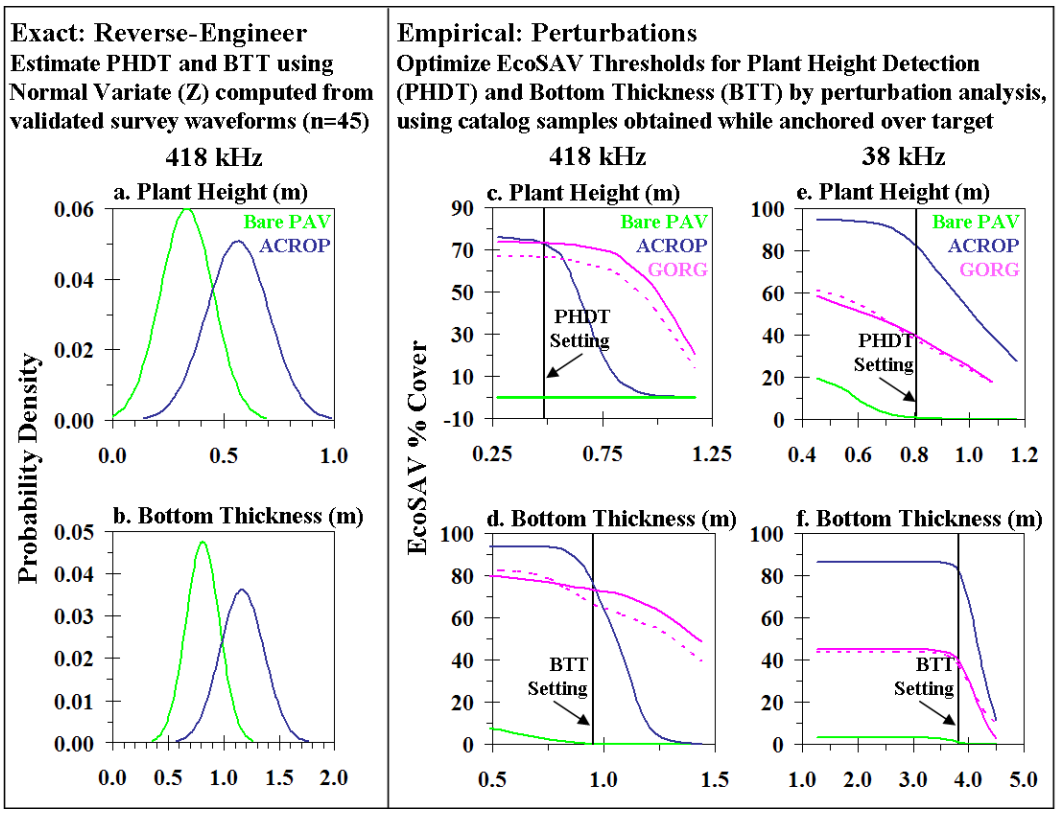

Figure 6.5 Results of reverse-engineering EcoSAV (a) plant height and (b) bottom thickness settings using 45 echo envelopes ground-validated as either bare pavement or *A. cervicornis*. Approximate EcoSAV settings were inferred from the probability density plots. Final EcoSAV plant height (c,e) and bottom thickness (d,f) were determined by perturbation analysis of anchored training samples.

6.3.3 Frequency-Dependent Detection of Gorgonians

An important finding of the EcoSAV tuning was the observation of frequency-dependent detection of gorgonians. At 418 kHz, the EcoSAV-predicted cover of the anchored ACROP and GORG training samples were approximately equal (Figure 6.5c-d, Table 6.1).

Table 6.1. EcoSAV predictions of cover for anchored training samples at the final plant height detection threshold and bottom thickness threshold settings. The low rate of 38 kHz gorgonian detection was used to allocate the 418 kHz Cover to either gorgonians or *A. cervicornis*, on the basis of the ratio of 38:418 kHz EcoSAV Cover.

Frequency (kHz)	PHDT (m)	BTT (m)	EcoSAV %Cover ACROP	GORG
418	0.49	0.95	72.5	69.7
38	0.81	3.82	82.2	38.4

At 38 kHz, the EcoSAV-predicted cover of the anchored GORG training samples was only about half that of ACROP training sample (Figure 6.5e-f, Table 6.1). Backscattering is the forte of higher frequencies, so the general superiority of the 418 kHz signal is no surprise. Presumably, the longer wavelength of the 38 kHz signal and the relatively open architecture of the *Plexaura* colonies in the anchored GORG sample allowed a larger proportion of the 38 kHz signal to pass through the canopy. Irrespective of the cause, this observed differential sensitivity of the 38 and 418 kHz signals to gorgonians was exploited to differentiate between gorgonians and *Acropora*.

Throughout this document, two types of EcoSAV cover are reported. The 418 kHz EcoSAV total cover is the raw output of EcoSAV using the optimum settings reported above (PHDT = 0.49 m and BTT = 0.95 m). This is the total cover of epibiota with a 418 kHz canopy height greater than 0.49 m. Each non-zero value of 418 kHz EcoSAV cover was then designated as either ACROP or GORG using the frequency-dependent rates of detection observed for the anchored samples. Recall that EcoSAV outputs estimates of canopy height and areal cover for a set of 10 pings. If the ratio of 38:418 kHz EcoSAV cover (for the set of 10 pings) was greater than 0.55 (0.384/0.697, Table 6.1), the 418 kHz EcoSAV cover was designated as *A. cervicornis*. If the ratio was less than 0.55, the 418 kHz EcoSAV cover was designated as gorgonian.

6.3.4 EcoSAV Processing of Survey Data

Trackplots of the 418 kHz EcoSAV total cover and the 418vs38 EcoSAV *Acropora* cover are shown in Appendices 6.A1c-d (FTL6) and B1c-d (Scooter). Spatially continuous surfaces created using ordinary point kriging are displayed in Appendices 6.A2c-d and B2c-d.

6.34.1 FTL6 predicted cover

The krig of 418 kHz EcoSAV total cover corresponded precisely with the ground-validated boundary of the *Acropora* patch (Appendix 6.A2c). Application of the 418vs38 ratio improved the fit of acoustic predictions; outside of the patch most of the cover was allocated to gorgonians, whereas inside the patch almost all the cover was allocated to *Acropora* (Appendix 6.A2d). The allocation of 418 kHz EcoSAV total cover records to *Acropora* and gorgonians is quantified in Table 6.2. Of the 117 records within the FTL6 patch with non-zero 418 kHz EcoSAV total cover, 104 (88.9%) were assigned to *Acropora*. That proportion is probably very close to the actual split between tall gorgonians and *Acropora* within FTL6. Conversely, of the 1757 records outside of the FTL6 patch with total cover greater than zero, only 1102 (62.7%) were assigned to *Acropora*. Again, that proportion is probably very close to the actual split between tall gorgonians and *Acropora* outside of FTL6.

Table 6.2. Proportion of survey records with non-zero 418 kHz EcoSAV Cover allocated to A. cervicornis and gorgonian, using the ratio of 38:418 kHz EcoSAV Cover. Proportionally more records were allocated to A. cervicornis inside the patch than outside of the patch.

Location	418 kHz EcoSAV Tot Cvr > 0	# of Records Assigned To… ACROP	GORG	%ACROP
Inside FTL6	117	104	13	88.9
Outside FTL6	1757	1102	655	62.7

6.3.4.2 Scooter predicted cover

The krig of the 418 kHz EcoSAV total cover corresponded closely with the ground-validated boundary of the southwestern portion of the patch, but did not accurately reflect the abundance of *Acropora* in the northeastern portion (Appendix 6.B2c). *Acropora* cover is slightly thinner in the north (35%) than in the south (45%) (Figure 6.6), but the greater dispersion of colonies in the northeastern most likely made them apparent to echosounding. Application of the 418vs38 ratio improved the acoustic predictions; again, the majority of 418 kHz total cover outside of the patch

was correctly allocated to gorgonians, whereas inside the patch almost all the cover was allocated to *Acropora*.

6.3.5 EcoSAV Accuracy Assessment

A synoptic comparison of acoustic versus ground-truthed *Acropora* cover was compiled by averaging the entirety of hydroacoustic records falling within the 7m cylinders of the radial transects (Figure 6.6). The EcoSAV-predicted cover was less than the ground-truthed cover at both sites, more so for Scooter than FTL6. The average 38vs418 EcoSAV *Acropora* cover of the 215 hydroacoustic records that fell within FTL6 was 32.4%, compared to 49.7% by ground-truth. The average EcoSAV-predicted *Acropora* cover of the 229 hydroacoustic records falling within Scooter was 15.0%, compared to 39.1% by ground-truth. A point-by-point accuracy assessment was conducted by averaging the predicted cover of records falling within each 7m cylinder (Figures 6.7-6.8). The EcoSAV-predicted cover was consistently low at both sites, as evidenced by the number of EcoSAV predictions lying below the identity line of the Figures 6.7-6.8.

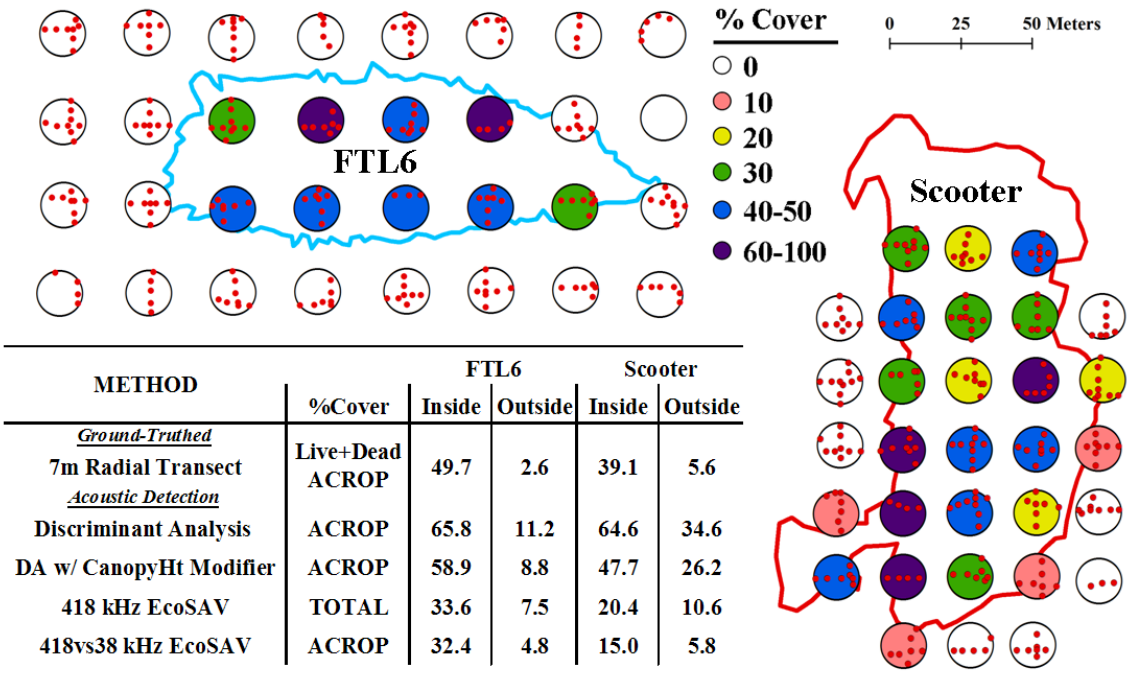

METHOD		FTL6		Scooter	
	%Cover	Inside	Outside	Inside	Outside
Ground-Truthed					
7m Radial Transect	Live+Dead ACROP	49.7	2.6	39.1	5.6
Acoustic Detection					
Discriminant Analysis	ACROP	65.8	11.2	64.6	34.6
DA w/ CanopyHt Modifier	ACROP	58.9	8.8	47.7	26.2
418 kHz EcoSAV	TOTAL	33.6	7.5	20.4	10.6
418vs38 kHz EcoSAV	ACROP	32.4	4.8	15.0	5.8

Figure 6.6 Synoptic ground-truthing of the FTL6 and Scooter sites, comparing the total *A. cervicornis* cover estimated from the Oct2009 7m radial transects to classified survey points falling within the 7m cylinder.

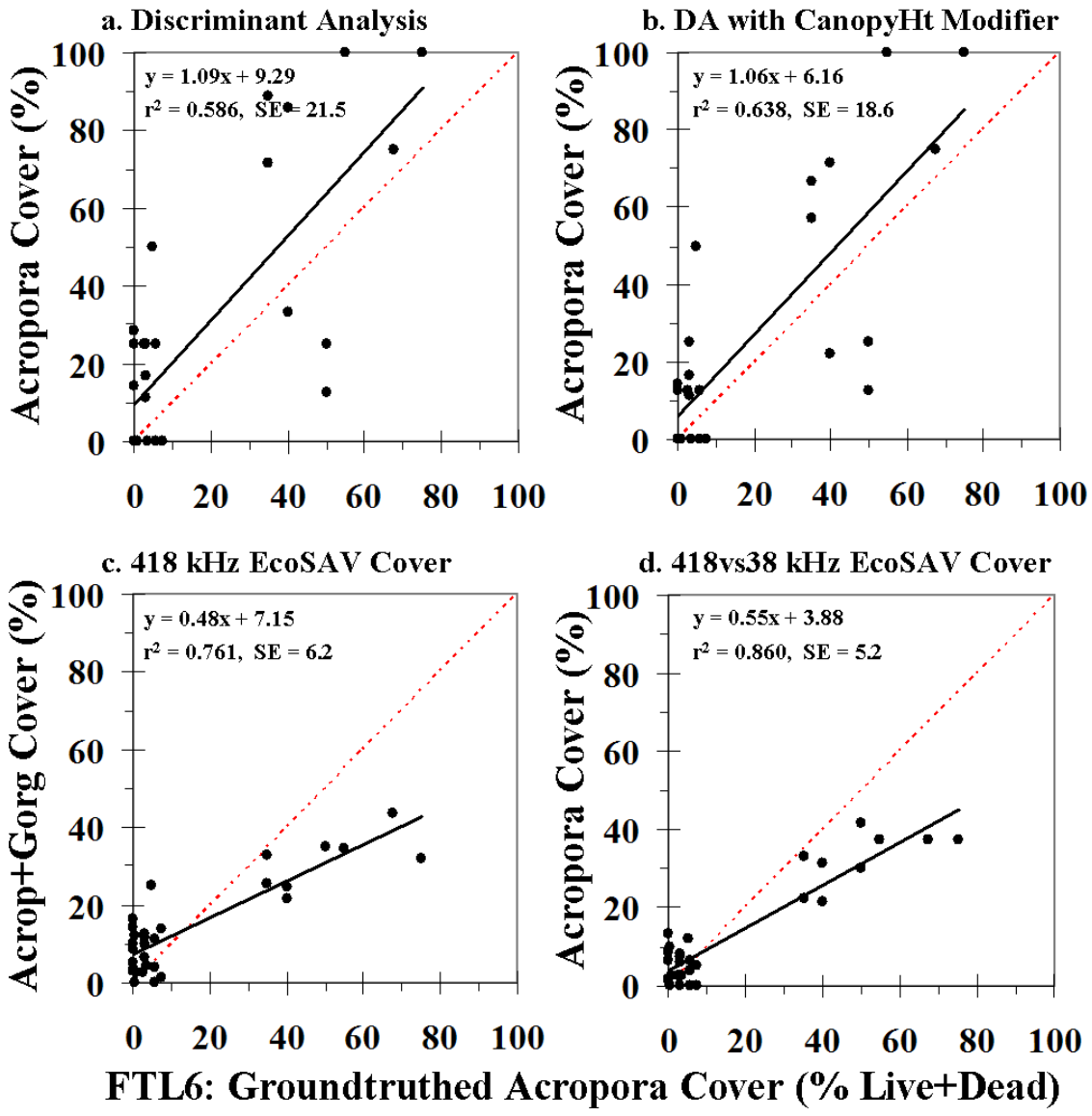

Figure 6.7 Point-by-point ground-truthing of FTL6 site, comparing the total *A. cervicornis* cover estimated from the Oct2009 7m radial transects to classified survey points falling within each 7m cylinder.

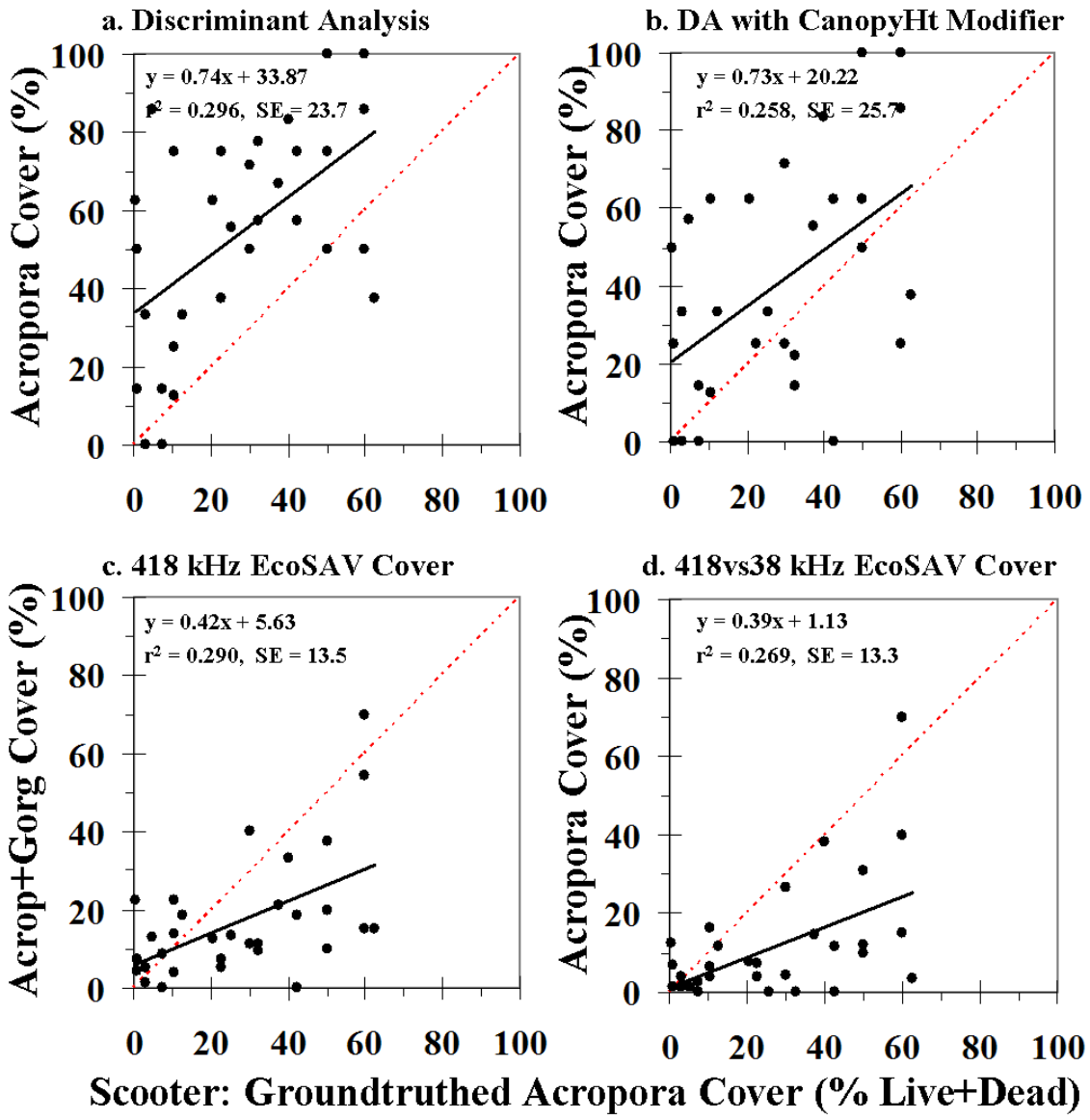

Figure 6.8 Point-by-point ground-truthing of Scooter site, comparing the total *A. cervicornis* cover estimated from the Oct2009 7m radial transects to classified survey points falling within each 7m cylinder.

6.3.6 EcoSAV Canopy Height

EcoSAV generates predictions of canopy height, computed as the difference between the predicted "true" bottom depth and the above-bottom depth at which the echo intensity rises above a specified intensity for a specified period of time. If the EcoSAV prediction of canopy height were found to be accurate, it could be a useful tool for describing epibiotic taxa. Using the

"optimum" PHDT and BTT of 0.49 and 0.95 m, histograms of the EcoSAV-predicted canopy height and areal coverage were computed from the 418 kHz signal of the ACROP and GORG training samples (Figure 6.9a-b), acquired while anchored over colonies of *A. cervicornis* and *Plexaura spp*., respectively (Figure 6.2c-d).

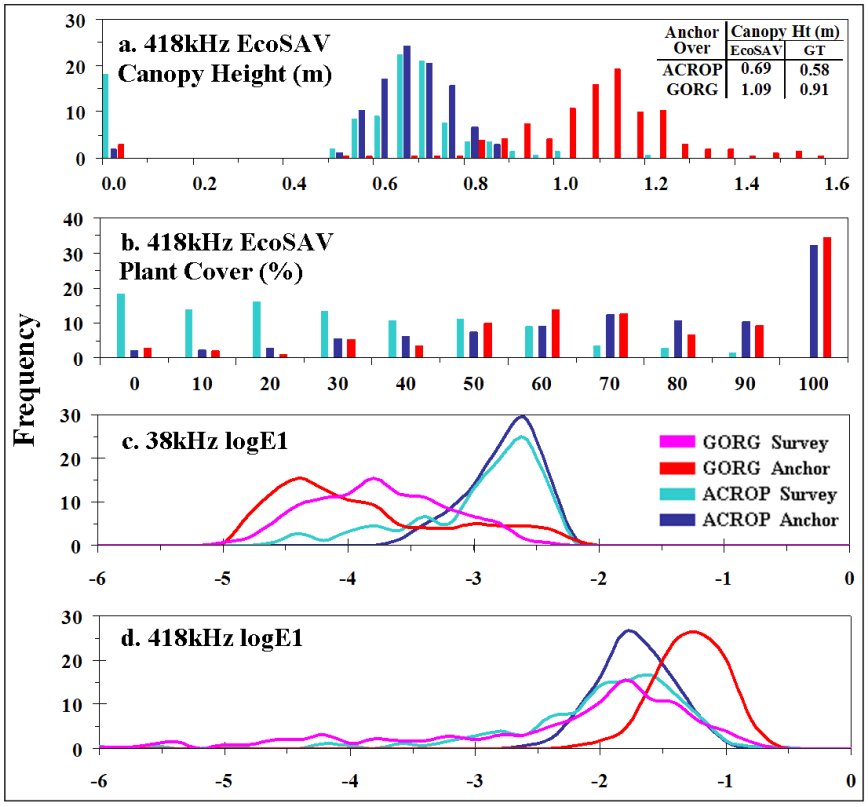

Figure 6.9 Frequency distributions of gorgonian (anchored) and A. cervicornis (anchored & survey) training samples, for (a) 418 kHz EcoSAV canopy height, and (b) areal cover. Frequency distributions of E1 acoustic energy parameter computed for gorgonian (anchored & survey) and *A. cervicornis* (anchored & survey) training samples, at (c) 418 and (d) 38 kHz.

Median values of EcoSAV-predicted canopy height agreed closely with field measurements for both *Acropora* and gorgonians; 0.69 versus 0.58 m (ACROP) and 1.09 versus 0.91 m (GORG), respectively (Figure 6.9a). The predicted canopy height of survey records within the FTL6 patch (ACROP – Survey) agreed closely with the anchored dataset. These findings suggest it may be possible to differentiate between *Acropora* and gorgonians based on EcoSAV canopy height,

though in reality most gorgonians in the study area were not as tall as those in the GORG – Anchored training sample.

SECTION II. VISUAL BOTTOM TYPER PROCESSING

6.3.7 Trends of VBT Acoustic Parameters

Although the output of discriminant analysis includes a measure of the relative contribution of each independent variable, the median values of training dataset groups can provide a simple and quick look at the relationships between bottom features and acoustic parameters. Median values of the ten acoustic parameters were calculated for the four training dataset groups (Table 6.3), using the data submitted to the 2nd-Pass DA (includes both anchored and hand-picked survey records).. Trackplots of acoustic parameters are shown overlaid on LIDAR hill-shaded surfaces in Appendices 6.C1-C5.

6.3.7.1 E0 (pre-bottom backscatter of 1st echo)

E0 is the energy reflected prior to the main beam prior to making contact with the true bottom, i.e. pre-bottom backscatter. It can result either from low bulk-density sediments overlying a harder "true" seabed or by the presence of epibiota. In this study, only the 418kHz GORG training dataset exhibited an elevated value of E0. This was also manifested as gorgonian canopy being mistaken for the true bottom by the VBT depth-pick algorithm at 418 kHz (Table 6.4).

Table 6.3. Median values of the ten acoustic parameters for the refined training dataset (submitted to 2ndPass DA), computed for the four classes of the training dataset. Composite of anchored and hand-picked survey records.

Acoustic Class	Median 418kHz Depth (m)	Median Values (38kHz)						Median Values (418kHz)					
		E0	E1′	E1	E1	E2	FD	E0	E1′	E1	E1	E2	FD
		$x10^{-6}$	$x10^{-3}$	$x10^{-3}$	(E1′+E1)	$x10^{-5}$	$x10^{1}$	$x10^{-6}$	$x10^{-3}$	$x10^{-3}$	(E1′+E1)	$x10^{-5}$	$x10^{1}$
SAND	5.03	0.52	7.65	0.07	0.009	7.20	1.08	0.52	94.30	0.00	2.2E-05	3.30	0.97
PAV	4.78	0.54	4.99	0.09	0.018	2.49	1.13	0.53	67.70	0.02	2.6E-04	4.61	1.00
ACROP	4.82	0.60	2.22	2.99	0.574	3.16	1.18	0.57	43.10	24.80	0.365	2.47	1.12
GORG	4.81	0.61	5.92	0.19	0.032	1.25	1.11	1.94	13.75	42.55	0.756	2.09	1.10

Table 6.4. Median depths of selected training samples submitted to 1stPass DA, obtained from processing 38 and 418 kHz signals in VBT (ACROP-survey and GORG-survey not included). At 418 kHz, the VBT bottom-picking algorithm mistook the gorgonian canopy for the true bottom.

Acoustic Class	Median Depth (m)		delta
	38kHz	418kHz	(m)
Sand - Survey	5.14	5.06	0.08
PAV - Anchor	4.90	4.78	0.11
ACROP - Anchor	5.06	4.92	0.13
GORG - Anchor	4.78	4.18	0.60

6.3.7.2 E1 (trailing edge of 1st echo)

The partitioning of E1′ and E1 bottom sampling windows had the desired effect of discriminating topographic complexity by constraining E1 to the trailing edge of the first echo envelope (primarily incoherent backscatter reflected from a combination of rough seabed surfaces and epibenthic biota). At 418 kHz the contribution of E1 to the total integrated area of the first echo envelope [E1/(E1′/E1)] ranged from less than 0.001 for SAND and PAV, 0.365 for ACROP, and 0.756 for GORG (Table 6.3). This trend was similar at 38 kHz, with the exception of the GORG group. A E1 value indicated a weak interaction of the 38 kHz signal with the gorgonian canopy, consistent with the lower rates of detection using EcoSAV.

6.3.7.3 E1′ (leading edge of 1st echo)

As expected, E1′ was negatively correlated with E1 (Figure 6.10). Going from bare sand/pavement to dense *Acropora*/gorgonians, a large proportion of echo energy shifted from E1′

to E1. Moreover, the total first echo energy (E1′ + E1) decreased with increasing E1, i.e. as bottom roughness increased, more signal was deflected to the extent that it did not return to the transducer.

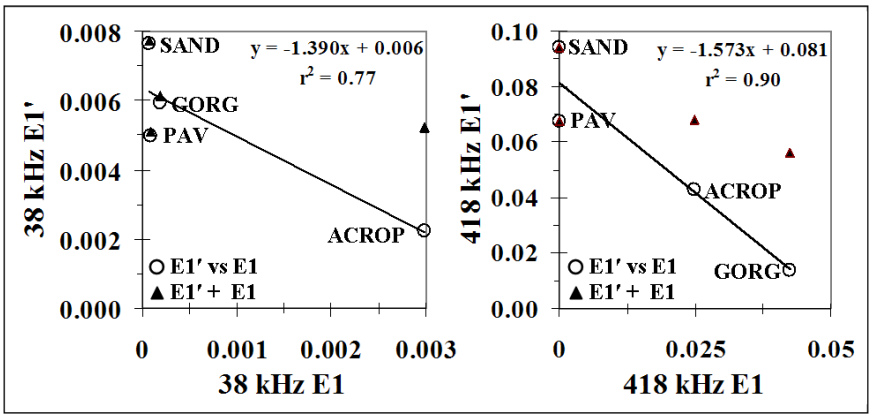

Figure 6.10 (○) Trends of median values of E1 versus E1′ for the four classes of the training dataset, taken from Table 6.3 (composite of anchored and hand-picked survey records submitted to 2ndPass DA) for (a) 38 and (b) 418 kHz signals. (▲) Trend of E1 plus E1′ (total first echo energy) versus E1, suggesting a trend of increasing signal loss with increasing bottom roughness.

6.3.7.4 E2 (complete 2nd echo)

The potential for the harder substrata of the reefal habitats to produce large values of E2 was overshadowed by a diminishing of E2 resulting from a greater proportion of incoherent backscatter produced by the combined contribution of seabed roughness and epibenthic biota. Stated another way, signal reflecting off gorgonians or rough pavement at obtuse angles is unlikely to complete the multi-path circuit of E2.

6.3.7.5 FD (fractal dimension of 1st echo)

The FD of both frequencies rationally arranged the four habitat classes. At 38 kHz, FD differentiated between SAND, PAV & GORG, and ACROP. As seen with E1 and E2, the gorgonians did not make a strong impression on the shape of the 38 kHz echo envelope, as

quantified by FD. At 418 kHz, FD differentiated between SAND, PAV, and ACROP & GORG, i.e. *A. cervicornis* and gorgonians similarly convoluted the 418 kHz echo envelope.

6.3.8 Multi-Pass Descriptive DA

The four-group training dataset was submitted to a series of two descriptive discriminant analysis (DA) classification routines (Figure 6.4). The overall internal classification accuracy was 79.4% for the 1stPass DA (n=2611) and 99.3% for the 2ndPass DA (n=881). The proportion of rejected records was equitably distributed among groups, as evidenced by the generally similar producers accuracies of the 1stPass DA. Going down the columns of the confusion matrix, it can be seen that the classification errors were not random (i.e. equally distributed amongst the other classes), but rather concentrated among the adjacent classes. Given that the training samples were pre-arranged in order of increasing visually-apparent roughness, this is reminder that acoustic classes can be best likened to localized centers of gravity along a continuum of n-dimensional hyperspace (similar to the concept of a species as a cluster of phenotypic traits along an n-dimensional continuum).

6.3.8.1 Training Dataset: Anchored versus Survey

The anchored training dataset was supplemented with handpicked records from the survey datasets. Survey records falling within the FTL6 and Scooter *Acropora* patches were added to the ACROP training dataset. Additional gorgonian samples were obtained by selecting survey records within 1 meter of EcoSAV predictions of canopy height $\geq$ 0.8 meter and predicted cover > 30%. To verify the efficacy of using a "mixed-bag" of training samples, the frequencies of log-transformed values of E1 were computed for the anchored and survey ACROP and GORG training datasets (Figure 6.9c-d). E1 is the 'backscatter' acoustic energy parameter and hence a leading contributor to the detection of epibiota, as revealed by the standardized discriminant function coefficients (Figure 6.11).

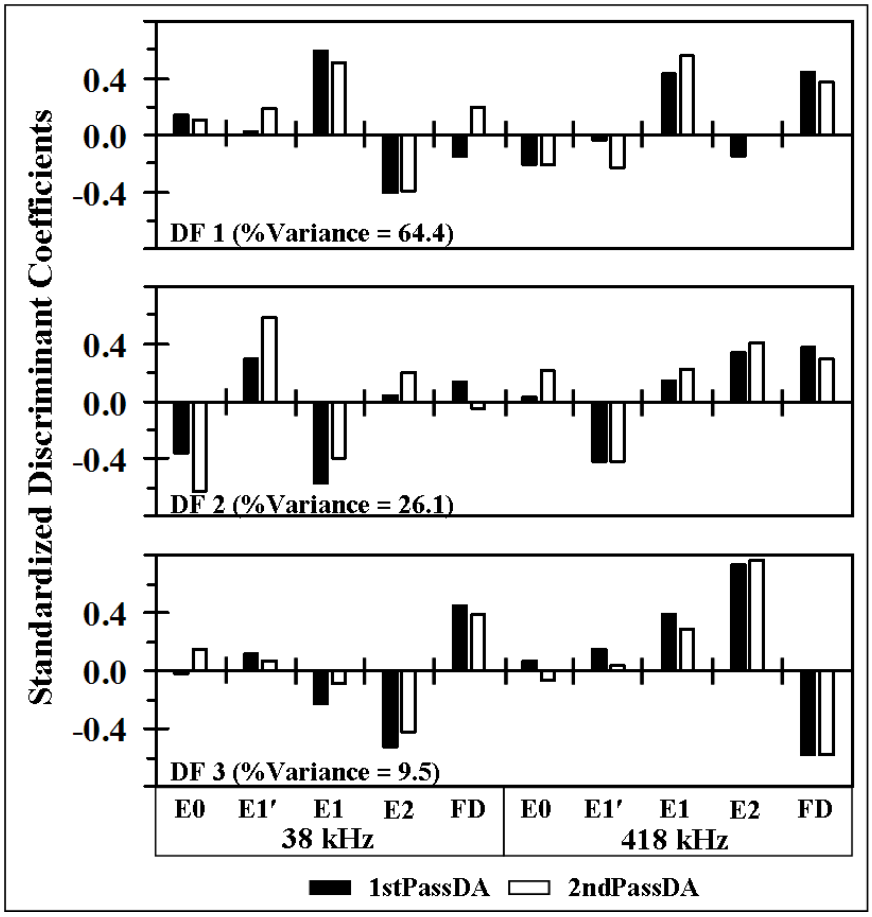

Figure 6.11 Standardized discriminant function coefficients of the 1st and 2nd-Pass descriptive DA, reflecting the relative contributions of independent variables within each discriminant function.

At both frequencies, the distributions of E1 were generally similar for the anchored and survey datasets, indicating the anchored and survey training samples are compatible. This indicates the acoustic energy parameters are not affected by vessel speed (in the range of drifting in idle to 4 knots under power). It further suggests the distinctive echo envelope signatures of the anchored datasets represented true acoustic diversity, and not just anomalous between-site variations in the benthos.

6.3.9 Predictive DA

The 18110 survey records that passed QA were classified into 1 of 4 acoustic classes (sand, bare pavement, *Acropora*, and gorgonian) using the Fisher's linear discriminant functions obtained from the 2nd Pass descriptive DA. Classified trackplots are shown in Appendices 6.A1a (FTL6) and B1a (Scooter). Spatially continuous surfaces were created using ordinary point kriging (Appendices 6.A2a and 6.B2a), obtained by coding DA-assigned classes as either 1 (DA class *Acropora*) or 0 (DA classes sand, bare pavement, or gorgonian). With respect to locating *Acropora* within the patch delineations, both the trackplots and krigs of DA-predicted *Acropora* cover appear satisfactory for both sites. Within the Scooter site, the DA-predicted *Acropora* cover is concentrated in the southern portion of the patch, as observed for the EcoSAV predictions. Within the FTL6 site, the trackplot and krig of DA-predicted *Acropora* cover corresponded precisely with the ground-validated boundary of the *Acropora* patch, also consistent with EcoSAV predictions. However, the DA method over-predicted *Acropora* cover outside of the Scooter patch and gorgonian cover outside of the FTL6 patch. A more highly replicated training dataset would undoubtedly improve the performance of the DA method.

6.3.10 DA Classification with Canopy Height Modifier

The problem of over-prediction was ameliorated using EcoSAV predictions of canopy height in the decision making process of class assignment. If the DA-assigned class was either a 3 (*Acropora*) or 4 (gorgonian), but the EcoSAV-predicted canopy height of the same hydroacoustic record was zero, that record was reassigned to a 2 (bare pavement). This had the effect of greatly reducing the over-prediction of *Acropora* cover outside of the patch at Scooter and the over-prediction of gorgonian cover outside of the patch at FTL6, without affecting the predictions within either patch. This is evident in both the classified acoustic trackplots (Appendices 6.A1b, 6.B1b) and krigs (Appendices 6.A2b, 6.B2b).

6.3.11 Testing DA Assumptions

Critical DA assumptions were tested on the training records submitted to the 2nd-Pass descriptive DA. The assumption of normal multivariate distributions can generally be accepted if the ratios of skewness/SE and kurtosis/SE fall between ±1.96 (p=0.05 two-tail). Of the 40 tests for normality, the number of violations totaled 24 and 16 for skewness and kurtosis, respectively (Figure 6.12a-d). The most numerous and serious violations came from the logE0 parameter, which accounted for 40% of the total violations. As previously discussed in the "Trends of VBT Acoustic Parameters" section, the only training group for which E0 registered significantly non-zero values was GORGS at 418 kHz. Hence, the distribution was strongly bimodal. The dispersion of variances was found to be homogenous for all independent variables (except logE0), as judged by the relative similarities of between-group variances (Figure 6.12e-f). The dispersion of covariances was found to be heterogeneous by Box's M ($p<0.001$), but this finding was disregarded since small differences between covariance matrices can be found significant when sample sizes are large (Tabachnick and Fidell 1997). The dispersion of covariances was instead judged by the relative similarity of log determinants (Figure 6.12g). By that criteria the dispersion of covariances was found to be homogenous; the 95% CI of the 12 comparisons [k*(k-1)] of log determinants, computed as LD_i/LD_j, was 1.04±0.16.

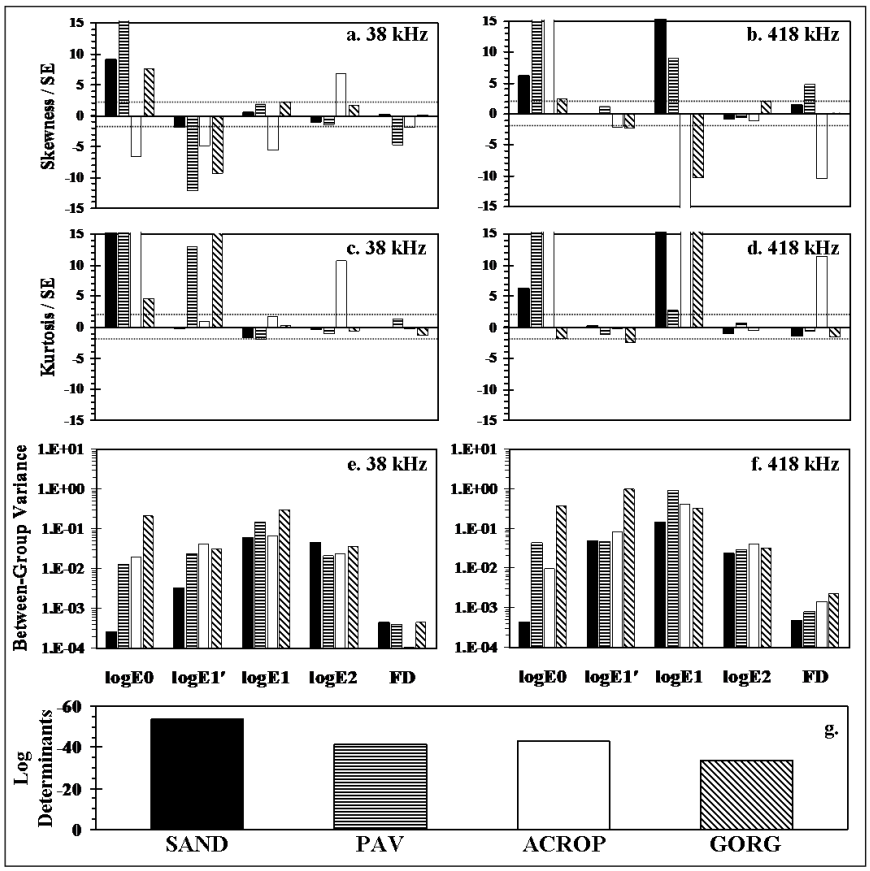

Figure 6.12 Testing of critical assumptions for discriminant analysis, performed on the independent variables submitted to the 2ndPass descriptive DA. Testing for (a-d) normal multivariate distributions, (e-f) homogeneity of variance (between-group variance), and (g) homogeneity of covariance (log determinants of independent variables).

The assumption of low multicollinearity can generally be accepted if no single value of r exceeds 0.90 and if a small number of r's exceed 0.75 (SPSS 2001). The degree of multicollinearity between independent variables was low by these criteria, judging by values of pooled within-groups correlation coefficients from the 2nd-Pass descriptive DA (Table 6.5). The magnitude of r averaged 0.149 and spanned a range of 0.002 (38E2 vs 418E1) to 0.704 (418E1 vs 418FD). That the 418 kHz E1 and FD were the most highly intercorrelated variables was not surprising, given that both are strongly associated with topographical complexity. Recall from the "Trends of VBT Acoustic Parameters" section that median values of E1 and E1′, computed for the four training categories (SAND, PAV, ACROP, GORG) were found to significantly correlated, especially at

418 kHz (Figure 6.10). However, the pooled within-groups correlation coefficient of the 418 kHz E1′ vs E1 comparison was below the 65'th Percentile of values within Table 6.5, and the 38 kHz E1′ vs E1 comparison was below the 18'th Percentile. Therefore, although a central measure of dispersion (median) suggested an intercorrelation, the pooled within-groups correlation coefficients did not.

Table 6.5. Degree of multicollinearity between the independent variables of the training dataset, indicated by the pooled within-groups correlation coefficients of data submitted to the 2nd-Pass descriptive DA. Coefficients may range from -1 to +1, i.e. perfect negative and positive collinearity.

Pooled Within-Groups Correlation Coefficients Between Independent Variables									
Variable	**38E1′**	**38E1**	**38E2**	**38FD**	**418E0**	**418E1′**	**418E1**	**418E2**	**418FD**
38E0	**-0.230**	**0.228**	**-0.024**	**0.128**	**0.600**	**-0.341**	**0.062**	**0.108**	**0.268**
38E1′		**-0.046**	**0.133**	**-0.183**	**-0.165**	**0.212**	**-0.140**	**-0.129**	**-0.259**
38E1			**-0.072**	**0.141**	**0.054**	**-0.220**	**-0.033**	**0.031**	**0.099**
38E2				**0.073**	**-0.049**	**-0.034**	**0.002**	**0.050**	**-0.021**
38FD					**0.098**	**-0.142**	**0.094**	**0.079**	**0.215**
418E0						**-0.029**	**-0.031**	**0.069**	**0.049**
418E1′							**-0.164**	**-0.051**	**-0.378**
418E1								**0.207**	**0.704**
418E2									**0.284**

6.3.12 Testing for Significance

All ten independent variables (38 and 418 kHz logE0, logE1′, logE1, logE2, and FD) were found to be significant by forward stepwise DA, using Mahalanobis distance (MD) as the criteria and the probability of F for entry and removal (p= 0.05 and 0.10, respectively). The MD is the distance of a case from the centroid of a group, in units of standard deviations, measured in n-dimensional attribute space (n=10). The 2nd-Pass descriptive DA model was found to be statistically significant ($p<0.001$) based on the chi-square transformation Wilks' Lambda. The magnitude of Wilks' Lambda for the 3 discriminant functions (DF) utilized in the model was 0.0071, i.e. only 0.71% of the total variance in DF scores was not explained by differences among the groups.

6.3.13 Interpretation of Descriptive DA

A discriminant function (DF) is similar in form to a multiple regression equation, although in the case of DA the coefficients are computed to maximize discrimination between predefined groups, based on the values of independent variables. When there are more than two groups, the number of DF's equals the smaller of (i) the number of groups minus 1, or (ii) the number of variables, so in this study there were three DF's. The first DF accounts for the greatest amount of between-group variance, with each successive function contributing less than the preceding one. The standardized DF coefficients (SDFC) are weighted to the magnitudes of the independent variables and are used to assess the relative contribution of each independent variable to a DF. As partial coefficients they reflect the unique contribution of each independent variable, controlling for the other independents in the model. However, they do not indicate which groups the functions discriminate between. Between-group discrimination can be visualized by scatterplots of individual scores for two given DF's, or by mean values of DF's for each group, i.e. functions at group centroids (FGC). The spread of mean FGC scores discriminant scores indicates the extent to which a particular pair of DF's discriminate between groups. The discriminatory character of independent variables, i.e. which variables discriminated by which groups, was assessed by synthesizing information from the SDF coefficients and FGC's.

6.3.13.1 Standardized discriminant function coefficients (SDFC)

The first two DF's accounted for 64.4 and 26.1% of between-group variance within the 2nd-Pass descriptive DA training dataset (Figure 6.11). The first DF was informed primarily by the 38 and 418 kHz E1's, followed by the 418 kHz E2 and FD. The second DF was informed primarily by the 418 kHz E0 and E1′, followed by the 38 kHz E1′ and E2 and the 418 kHz E1. The third DF was informed primarily by the 38 kHz E2 and FD, then by the 418 kHz E2 and FD. The effect of

refining the training dataset can be seen as relatively minor adjustments to the magnitudes of SDCF's from the 1st to 2nd-Pass descriptive DA's.

6.3.13.2 Functions at group centroids (FGC)

The first DF divided the four acoustic classes into three major groupings of biological cover; (1) uncolonized (SAND and PAV), (2) ACROP, and (3) GORG. This can be seen across the x-axis of the DF1 vs DF2 scatterplot (Figure 6.13b) and in the relative values of FGC (Table 6.6, first column). The second DF primarily discriminated GORG from SAND, PAV, and ACROP. The third DF explained only a small proportion of the between-group variance (9.5%), but was critical for differentiating between SAND and PAV, the two most similar bottom types (Figure 6.13d).

Table 6.6. Mean scores of discriminant functions, i.e. functions at group centroids, for the 4 acoustic groups. The spread of mean scores down a column indicates which groups a discriminant function distinguishes between, and to what degree.

Functions at Group Centroids (2ndPass DA)			
Group	Function		
	1	2	3
SAND	-3.75	0.84	2.64
PAV	-1.77	0.45	-0.99
ACROP	5.06	1.20	0.36
GORG	1.09	-5.51	0.30

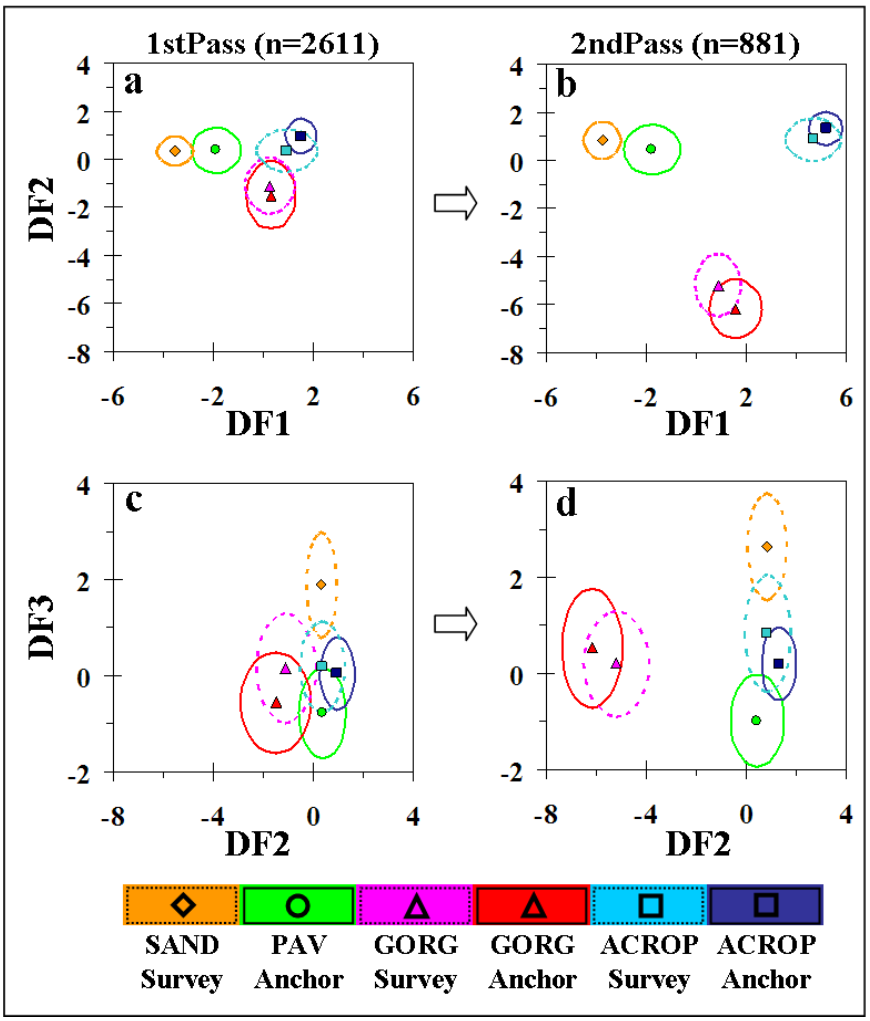

Figure 6.13 Supervised classification of training dataset into six acoustic classes by multi-pass discriminant analysis. Centerpoints denote cluster averages, ellipses are dispersion (1 standard deviation) about x and y. Discriminant functions 1 and 2 (of 3) of (a) 1st and (b) 2nd-Pass descriptive DA, and discriminant functions 2 and 3 of (c) 1st and (d) 2nd-Pass descriptive DA.

6.3.13.3 Synthesizing SDFC and FGC

The rankings and discriminatory functions of independent variables were found to be in accord with the general principles of AGDS seabed classification (concerning E1 and E2), and consistent with the functions of the other non-traditional parameters (E0, E1, FD) inferred from their definitions. E1 and FD were the largest contributors to between-group discrimination (DF1), in terms of the percentage of between-group variance explained, by splitting uncolonized seabed (SAND and PAV) from seabed colonized by tall epibiota (ACROP and GORG). The finding

agrees with the general empirical rationale for seabed classification, which posits that a rougher seabed surface creates more scattering of the transmitted echo contacting the seabed at an oblique angle of incidence, increasing the proportion of signal returning to the transducer in the second half of the first echo (Burczynski 1999; Burns et al., 1989). And given that FD is a metric of topographic complexity, computed from the first echo but effectively independent of E1 (Table 6.5), it is not surprising to find it complementing E1.

The second largest contribution (DF2) came from the 418 kHz E0 and E1′, which split GORG from the other three groups. Recall that the 418 kHz E0 rose above its baseline value only for the GORG class, and that there was an associated false bottom detection resulting from the high degree of pre-scatter (Table 6.4). The 418 kHz E1′ was an important GORG parameter, as it was disproportionately reduced by the strong interaction of the 418 kHz signal with the gorgonian canopy, which shifted the echo returns from E1' to E1.

The third largest contribution (DF3), though small in terms of variance explained, was nonetheless critical for making the split between the two most similar classes, SAND and PAV. The 38 kHz E2 and then FD contributed the most information, followed distantly by the 418 kHz E2 and FD. The 38 kHz FD correctly identified PAV as the rougher surface, and the 38 kHz E2 identified SAND as the harder surface. While the latter may at first seem contradictory, the SAND sample was characterized as approximately 18 cm of unconsolidated sand over flat hardbottom. The smoother surface of SAND meant that less 38 kHz signal was lost to incoherent backscatter, compared to PAV. In combination of the depth-penetrating capability of the 38 kHz signal and the presence of the underlying flat pavement acting as a subsurface reflector, a greater value of E2 over SAND compared to PAV can be understood. This was not observed at 418 kHz (Table 6.4), as the 418 kHz signal would have penetrated the unconsolidated sand insufficiently to be reflected back, resulting in an E2 less than that acquired over the rougher but harder PAV.

Similarly, Riegl et al. (2007) reported lower E2 values over 'rough/hard' reef facies than 'soft/flat' sand

6.4. DISCUSSION

6.4.1 Echo Envelopes of Anchored Datasets

Representative pings were selected from the anchored training samples by identifying hydroacoustic records for which E0, E1, E1′, E2, and FD were all within the respective 37.5-62.5 percentiles, computed individually for each anchored dataset at both frequencies (Figure 6.14-15).

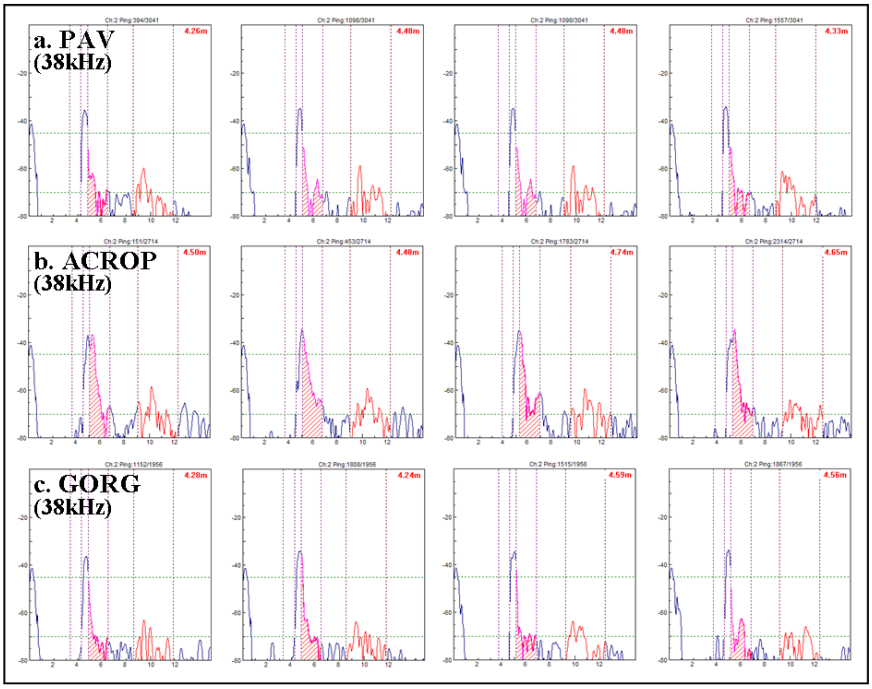

Figure 6.14 Representative 38 kHz echo envelopes selected from the training datasets, acquired while anchored over (a) bare pavement, (b) *A. cervicornis*, and (c) gorgonians. Viewed within BioSonics Visual Bottom Typer classification software.

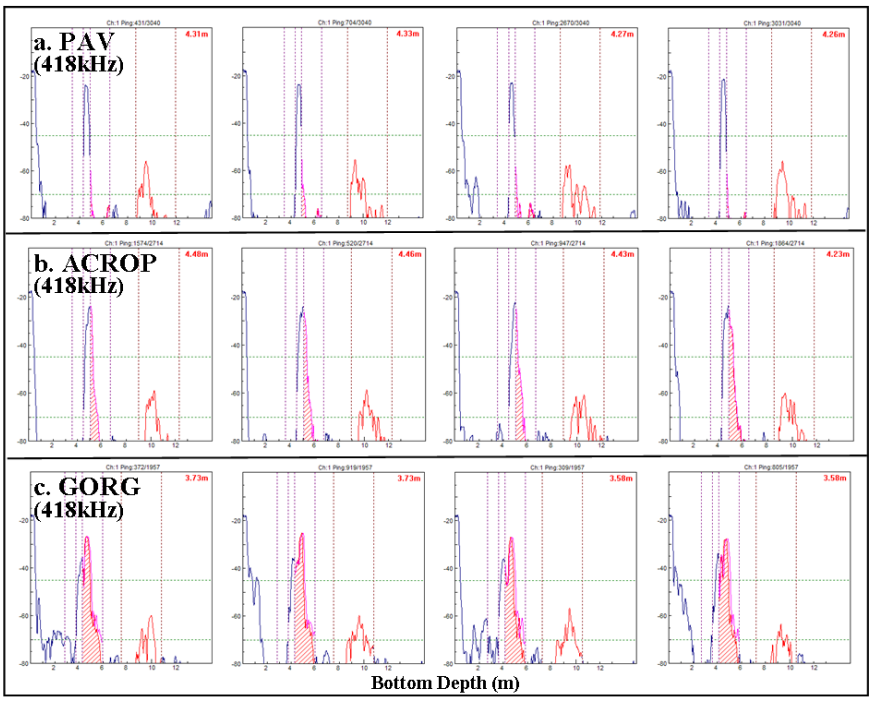

Figure 6.15 Representative 418 kHz echo envelopes selected from the training datasets, acquired while anchored over (a) bare pavement, (b) *A. cervicornis*, and (c) gorgonians. Viewed within BioSonics Visual Bottom Typer classification software.

The purpose was to understand how the presence of *Acropora* and gorgonians were reflected in the shape of echo envelopes. The 418 kHz echo envelopes clearly illustrate that the higher frequency signal better discriminates bare pavement from pavement colonized by *Acropora* or gorgonians than does the 38 kHz signal, in agreement with the general principles of acoustic classification (higher frequencies are better for discriminating rough surfaces). At 418 kHz, the most obvious influence of epibiota was a dramatic increase in the proportion of signal returning in the trailing edge of the first echo, as quantified in Table 6.3. The shape of the trailing edge of the 418 kHz echo envelopes was also telling. The trailing edges of the echo envelopes acquired over bare pavement (PAV) were smooth, and generally specular (i.e. a mirror image of the first part of the echo). In contrast, the trailing edges of the ACROP and GORG echo envelopes had shoulders with saw-tooth patterns, an apparent artifact of incoherent backscatter from the canopies. This was more exaggerated for the GORG echo envelopes, consistent with the greater

elevation of E1 (Table 6.3), i.e. more backscatter equated to a greater E1 and a "rougher" echo envelope. Another consistent artifact was the shape of the peak. At 418 kHz, the PAV echo envelopes were characterized by a single sharp peak, whereas the ACROP and GORG samples tended to have multiple peaks that occurred later in echo envelope. Given that the PAV and GORG samples were separated by only 8 meters, and the only apparent difference between the two was the presence of gorgonians, the acoustic "roughness" indicated by the split peaks and saw-toothed shoulders must have resulted from the presence of gorgonians. The general empirical rationale for seabed classification posits that a rougher seabed surface creates more scattering of the transmitted echo contacting the seabed at an oblique angle of incidence, increasing the proportion of signal returning to the transducer in the second half of the first echo (Burczynski, 1999). The substitution of epibiota for bottom surface is an extension of this rationale, in agreement with the findings of Kloser (2001), who reported that echo energies relate to a combination of seabed hardness and roughness attributes, including epibenthic biota.

The mechanism by which epibiota imparts a temporal shift of echo energy from E1′ to E1 is an increased path length caused by incoherent backscatter off a rough surface. Following this line of reasoning, the temporal shift of an echo return should be more apparent in the multi-patch E2 parameter. Visual Bottom Typer automatically sets the beginning of the E2 sampling window at twice the value of the depth pick, assuming a perfectly specular (i.e. mirror-image) vertically-incident echo should make two round trips from transducer to bottom in exactly twice the amount of time for a single round trip. It would follow that the gap between the E2 starting gate and the point at which the echo intensity crosses the noise threshold could be interpreted as the degree to which the echo deviated from a perfectly specular return. This in turn could be interpreted as the degree of backscatter from the combined contribution of surficial roughness and epibiota. In Figure 6.15, a clear and consistent progression can be seen in the appearance of echo returns within the E2 sampling window, from PAV to ACROP to GORG. This is the same order of

training samples indicated by E1′ vs E1, and indicates that the temporal shifts of E1 and E2 are indeed causally linked. On a side note, another indication of the 418 kHz signal interacting more strongly with the canopy of the GORG training sample is that the VBT depth-pick falsely interpreted the gorgonian canopy as the bottom, but was not similarly misled by the *Acropora* canopy (Table 6.4). Taken together, this evidence suggests that a partitioning of the E2 window, similar to the first-echo E1′/E1 method, could be a useful addition for detection of, and possibly discrimination between, epibenthic biota.

6.4.2 EcoSAV vs VBT – Selecting the "Best" Method

Two post-processing software platforms were utilized for detection of *A. cervicornis*, EcoSAV and VBT. Four methods were adapted to the output of these two pieces of software (see below). Further testing, particularly with respect to short gorgonian (0.2-0.8 m) detection, will be required before a definitive judgment can be made, but for know the 418vs38 kHz EcoSAV *Acropora* Cover method gets the nod. This method achieved the best balance between *A. cervicornis* detection, discrimination between *Acropora* and gorgonians, and avoidance of false positive detection. The four methods developed in this study are described below:

1. DA Classification - Supervised classification using results of multi-pass DA into categories of sand, bare pavement, *Acropora*, or gorgonian.
2. DA Classification with Canopy Height Modifier - Same as above, except records classified as *Acropora* or gorgonian were re-classified as bare pavement if the 418 kHz EcoSAV cover was equal to zero, i.e. both DA and EcoSAV methods had to agree.
3. 418 kHz EcoSAV Total Cover – The raw output of EcoSAV. Percentage of records for which a "plant" feature was detected, out of a stack of 10. The EcoSAV Plant Height Detection Threshold setting of 0.49 m should theoretically cause a large portion of the gorgonian cover to go undetected.

4. 418vs38 kHz EcoSAV *Acropora* Cover – Same as above, except records with cover greater than zero were assigned to either *Acropora* or gorgonian on the basis of the ratio of the 38:418 kHz EcoSAV cover.

The differences and similarities of these four methods are visually apparent in the classified trackplots and krigs of Appendices 6.A-B. A semi-quantitative analysis was performed by computing the average classifications for the four methods within three zones of FTL6 (Table 6.7); within the *Acropora* patch (Zone A), pavement outside the patch (Zone B), and the adjacent depression of sand (uncolonized by epibiota) with occasional exposed pavement (Zone C).

Table 6.7 Acoustically predicted cover, computed for the four methods (a-d), within three zones of FTL6; within the *Acropora* patch (Zone A), pavement outside the patch (Zone B), and the adjacent depression of sand (uncolonized by epibiota) with occasional exposed pavement (Zone C). Total *A. cervicornis* cover within FTL6 (Zone A) was estimated as 49.7% by the Oct2009 7m radial transects.

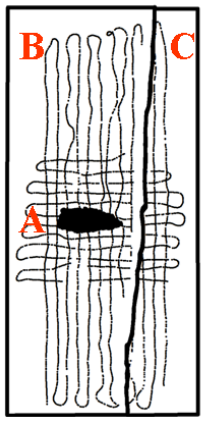

a. Discriminant Analysis Cover

Zone	n	Sand	Pav	Acrop	Gorg
A	145	0	12	74	14
B	3304	3	46	10	41
C	1067	51	30	3	16

b. DA Cover (CanopyHt Modifier)

Zone	n	Sand	Pav	Acrop	Gorg
A	145	0	26	63	11
B	3304	3	70	6	21
C	1067	51	44	2	3

c. 418 kHz EcoSAV Cover

Zone	n	Sand	Pav	Acrop	Gorg
A	143	70		30	
B	3114	92		8	
C	1068	98		2	

d. 418vs38 kHz EcoSAV Cover

Zone	n	Sand	Pav	Acrop	Gorg
A	143	70		26	4
B	3114	92		5	3
C	1068	98		2	0

The composite *Acropora* cover within FTL6 was computed as 49.7%, based on the October 2009 7m radial transects (Figure 6.6). Zone B was not thoroughly ground-truthed for this study, but video reconnaissance suggests an approximate cover of 1-2% A. cervicornis, 5-10% short gorgonians (0.2-0.8 m), and 2% tall gorgonians (0.8-1.3 m). Points lying along the edge of Zones B and C, characterized as broken pavement, boulders, rubble, and massive corals, were falsely

classified as epibiota and were withheld from these computations. The results of the four methods are discussed below:

1. DA Classification – Correctly concentrated *Acropora* within Zone A, but grossly over-predicted epibiotic cover in Zones B&C. Zone B ACROP+GORG ~50%, compared to only 14% on the high-end ground-truthed estimates.
2. DA Classification with Canopy Height Modifier – Improved predictions in Zones B&C (decreased roughly by half) while maintaining high predicted cover within Zone A.
3. 418 kHz EcoSAV Total Cover – Correctly concentrated *Acropora* within Zone A. Zone B&C predictions of epibiotic cover agreed with ground-truthing.
4. 418vs38 kHz EcoSAV *Acropora* Cover – Correctly allocated most (87%) Zone A cover to *Acropora*.

The selection of the 418vs38 kHz EcoSAV *Acropora* cover method was primarily informed by the point-by-point comparison of ground-truthed versus acoustically-predicted *Acropora* cover in Figures 8-9. Focusing on FTL6, the more developed of the two sites, the 418vs38 kHz EcoSAV *Acropora* Cover was judged to be the best performer, with a standard error ~3.5-4x less than the DA methods. A downside of the EcoSAV method is that it under-predicted *Acropora* cover, but at least it consistently under-predicted cover so that a correction factor could easily be applied to correct the bias. The final judgment awaits the extensive ground-truthing that will accompany the 2010-11 hydroacoustic survey of Miami-Dade County.

6.4.3 Edge Effects

As can be seen in the classified acoustic trackplots of all four methods at both sites, there was an obvious concentration of high acoustically-predicted cover along the edge features (pavement to sand transition). These edges were could be generally characterized as near-vertical relief of 3

meters, constituted of broken-up pavement, boulders, and rubble, and colonized by variably abundant massive corals and gorgonians. As judged by drop-video, the gorgonian areal cover along these edges was generally around 5-10%, considerably less than the 40-100% predicted by the most conservative model (38vs418 EcoSAV *Acropora*). The disparity becomes even greater taking into consideration the 38vs418 EcoSAV *Acropora* model under-predicted *Acropora* cover within FTL6 by 35% and Scooter by 60% (Figure 6.6). It is presumed the over-prediction resulted primarily from high slope. The spreading cone would contact the shallow plateau and the deeper sand at different times, creating the illusion of high incoherent backscatter (DA method) or high pre-bottom backscatter (EcoSAV method). To better understand these edge effects, fourteen drop-video samples at the Scooter site were classified by bottom type, *Acropora* cover, and short and tall gorgonian cover and plotted over the krigs of 418 kHz EcoSAV Total Cover and 418vs38 kHz EcoSAV *Acropora* Cover (Figure 6.16). Of the 14 samples, four were selected for discussion; two samples were located on an edge (sites 3-4) and two were not (sites 1-2). The analysis below reinforced the proposal that the false-positive detections of epibiotic cover were caused by the topographically complex substrate typifying these edges.

Site 1 - The first site was located approximately 25 meters from the edge, and characterized as pavement lightly colonized by short and tall gorgonians (~10-15%, total). The 418 kHz EcoSAV Total Cover was in very close agreement, predicting 10-20% cover. The 418vs38 method correctly allocated the majority of this cover to gorgonians.

Site 2 - The second site was characterized as flat pavement colonized by short gorgonians (30-50%). The 418 kHz EcoSAV Total Cover underestimated the cover, predicting 10-20%. The 418vs38 method correctly allocated the 418 kHz EcoSAV Total cover to gorgonians.

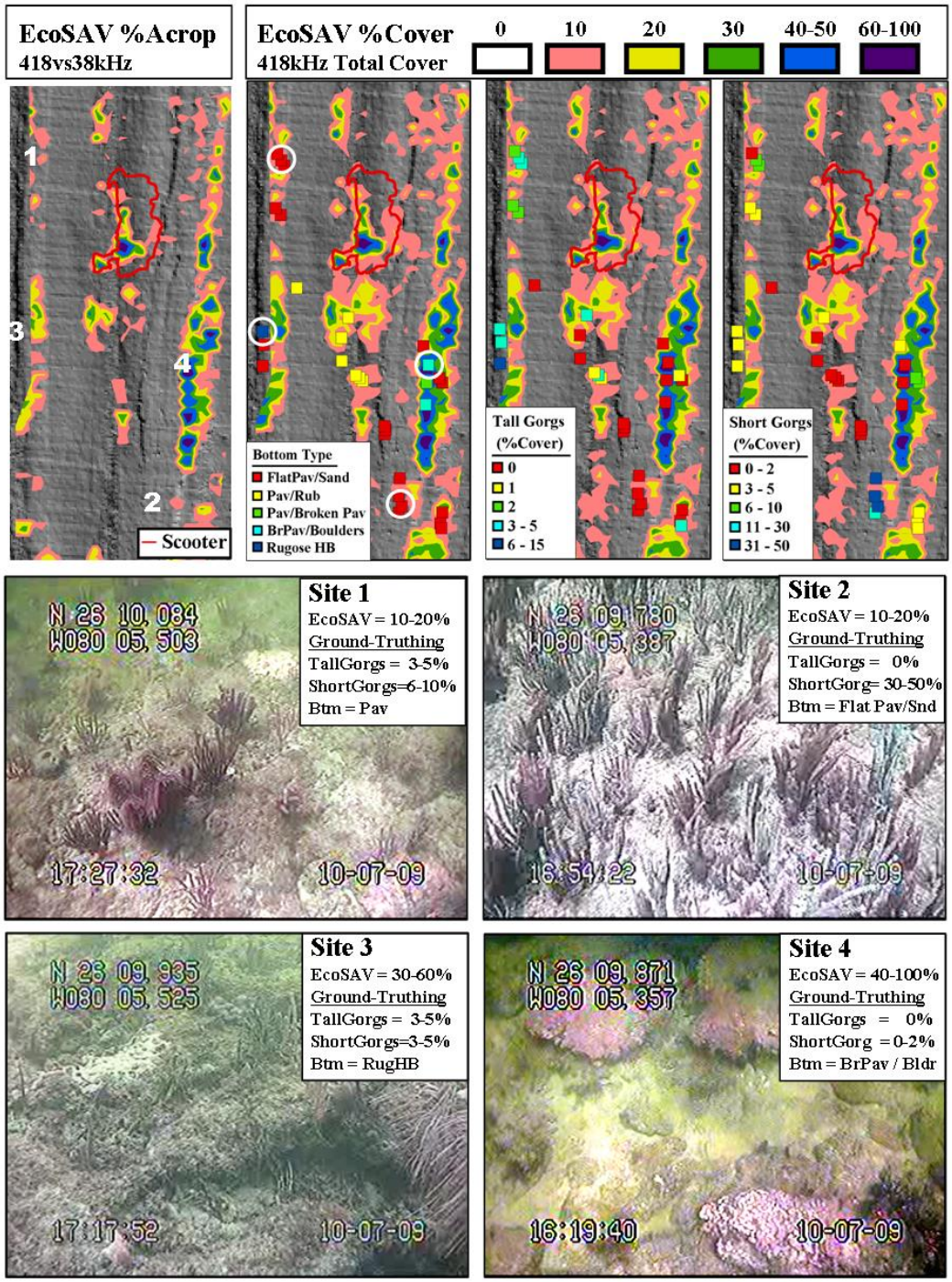

Figure 6.16 Scooter drop-video ground-truthing samples displayed over krigs of (left) 418vs38 EcoSAV *Acropora* cover and (right) 418 kHz EcoSAV Total Cover. Four ground-truthing samples were selected to illustrate the role of topographic complexity on false-positive predictions of cover. Sites 1 and 2 were of low topographic complexity, and acoustic predictions (418kHz EcoSAV Total cover) matched ground-truthed cover. Sites 3 and 4 were of high topographic complexity, and acoustic predictions matched ground-truthed cover.

Site 3 – The third site was located on an edge, and characterized as rugose hardbottom with equal proportions of short and tall gorgonians (~10-15%, total). The 418 kHz EcoSAV Total Cover method grossly overestimated the cover, predicting 30-60% cover. The 418vs38 method correctly allocated the majority of this cover to gorgonians.

Site 4 - The fourth site was located on an edge, and characterized as highly rugose broken pavement and boulders with a light cover of short gorgonians (~2%). The 418 kHz EcoSAV Total Cover method grossly overestimated the cover, predicting 40-100% cover.

6.4.4 Path Forward

The 418vs38 EcoSAV *Acropora* cover method appears to be the preferred approach for mapping *A. cervicornis*. The output of this method includes both an estimate of undifferentiated epibiotic cover (418 kHz EcoSAV cover) and an allocation of this cover to either *Acropora* or gorgonian, based on the frequency-dependent sensitivity to the gorgonian canopy. Having the ground-truthed *Acropora* patch delineations allowed for a clear demonstration of this methods capability of accurately detecting *A. cervicornis*. More ground-truthing of the FTL6 and Scooter sites is required to similarly assess the capability of discriminating between *A. cervicornis* and gorgonians outside of the *Acropora* patches. In addition, the anchored samples need to be replicated. In particular, the frequency-dependent detection of gorgonians requires further testing. And because EcoSAV does not normalize echo length to a reference depth, the additional anchored samples should be stratified by depth so the intrusion of depth contamination can be closely examined.

CHAPTER 2 APPENDIX

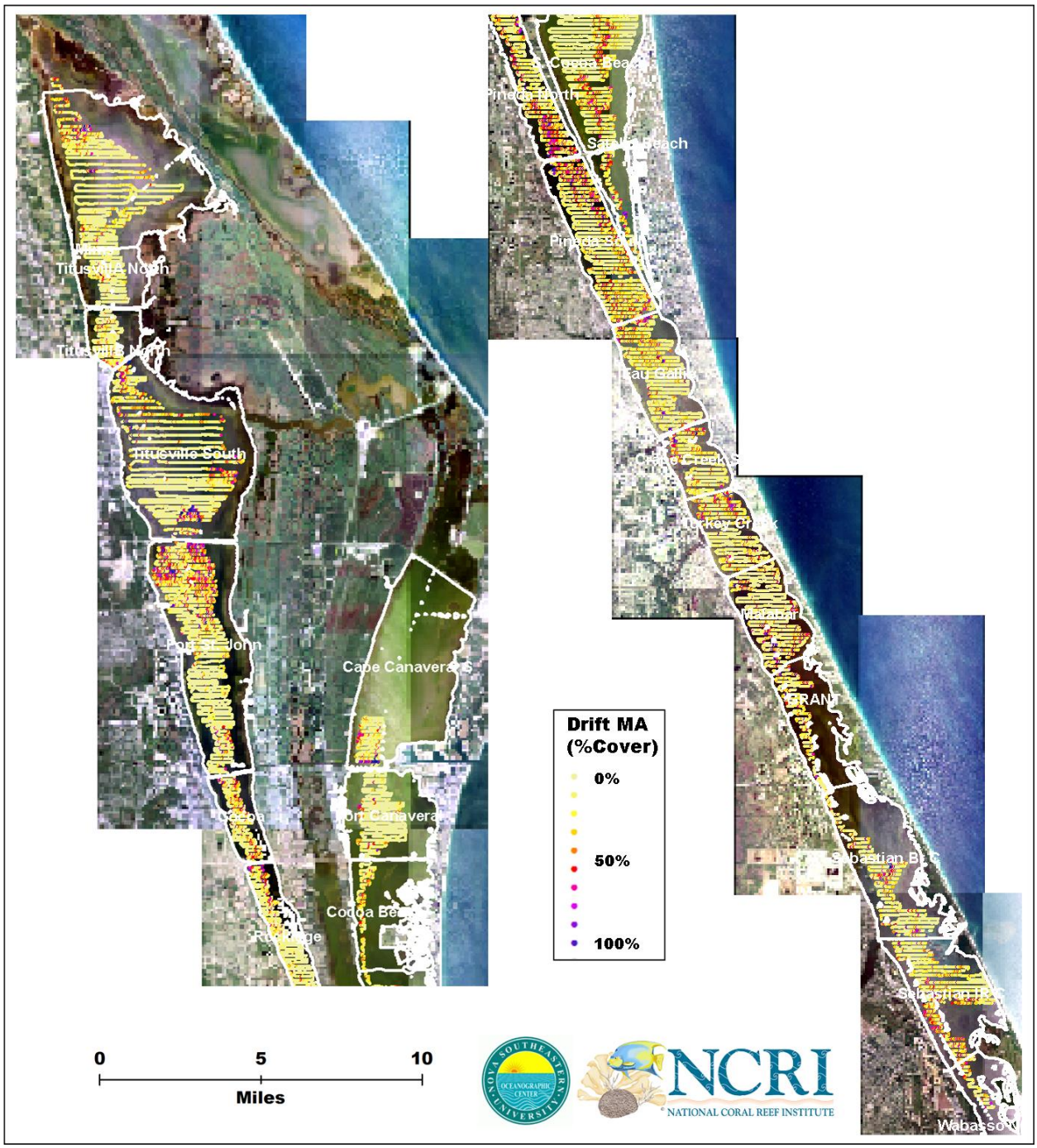

Appendix 2.A1. Extent of the 2008 acoustic survey of Indian River Lagoon, displaying the trackplot of the acoustically-derived percent cover of drift macroalgae. The boundaries of SJRWMD segments are displayed for reference.

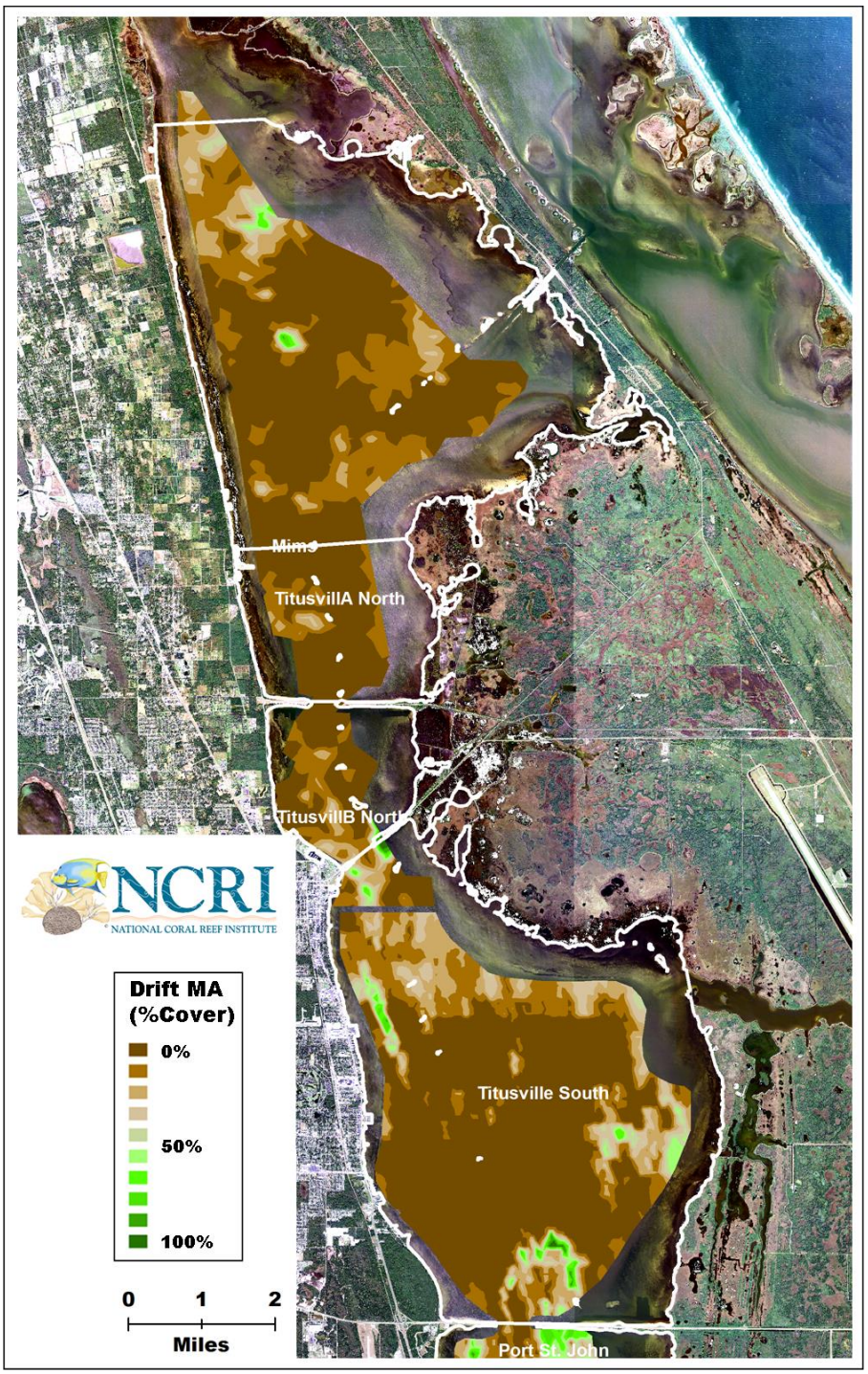

Appendix 2.A2. (Mims to Titusville) Kriged contour plot of acoustically-predicted drift macroalgae cover. The boundaries of SJRWMD segments are displayed for reference.

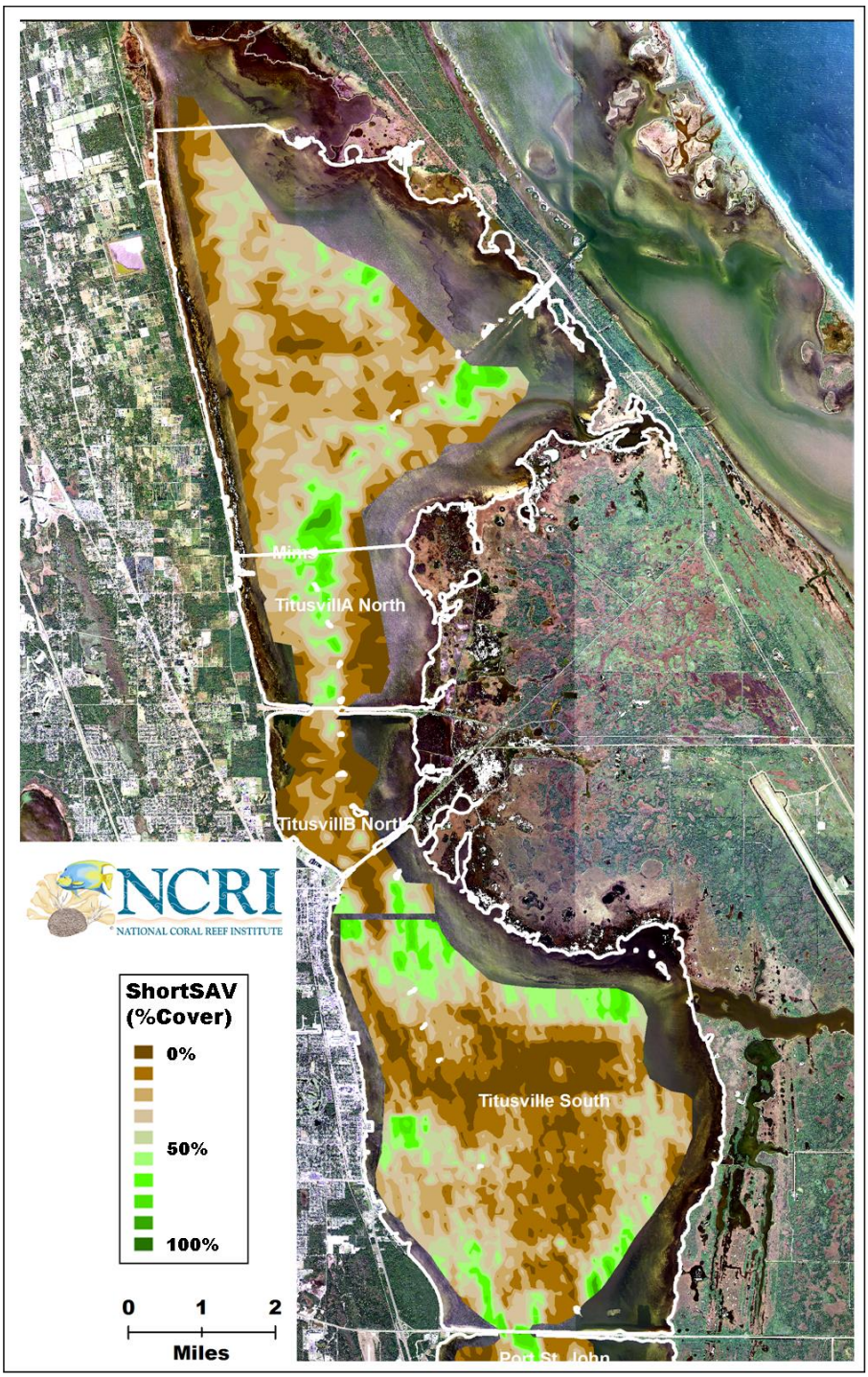

Appendix 2.A3. (Mims to Titusville) Kriged contour plot of acoustically-predicted short SAV cover (~10cm<). The boundaries of SJRWMD segments are displayed for reference.

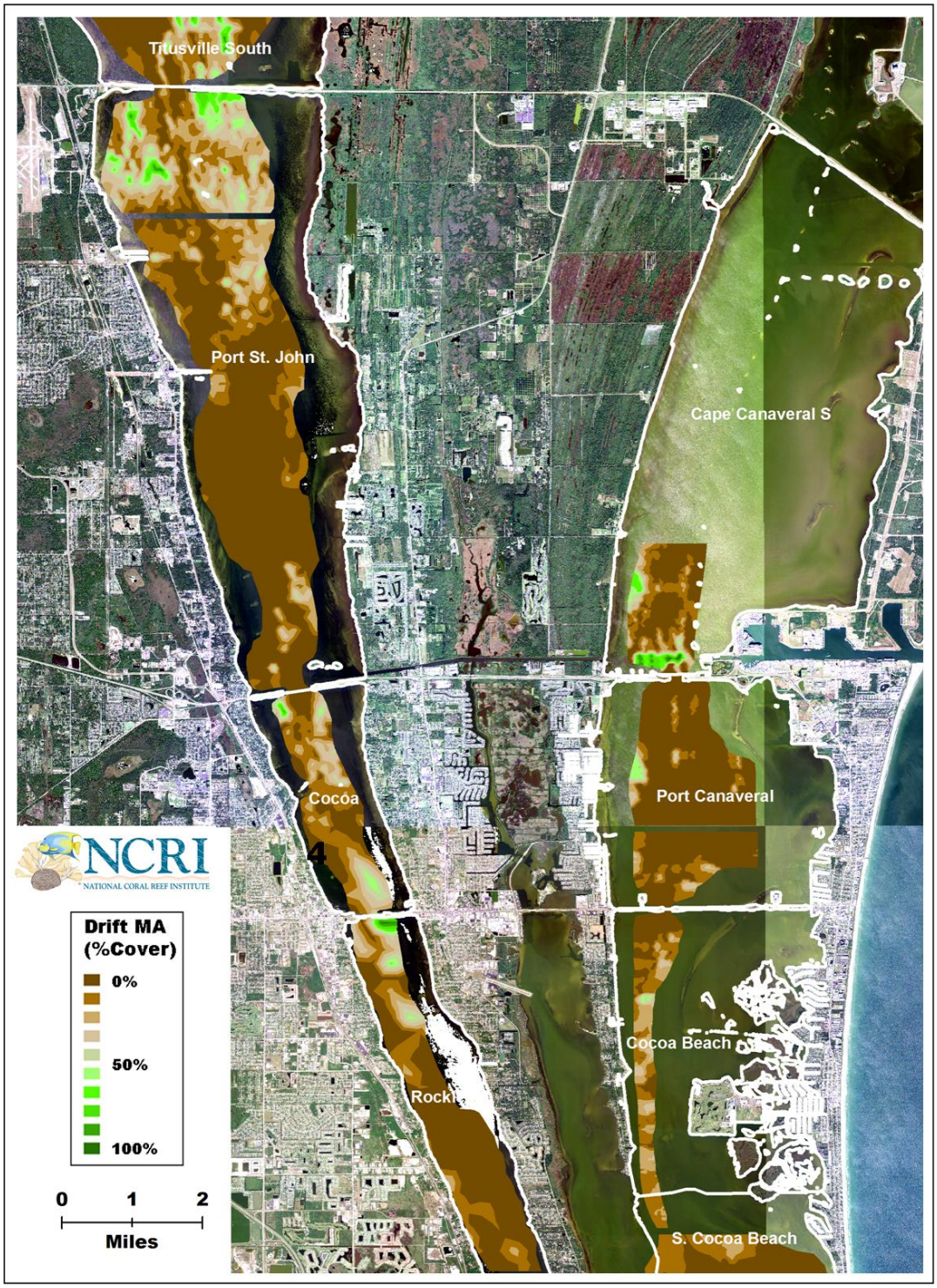

Appendix 2.A4. (Port St John to Rockledge) Kriged contour plot of acoustically-predicted drift macroalgae cover. The boundaries of SJRWMD segments are displayed for reference.

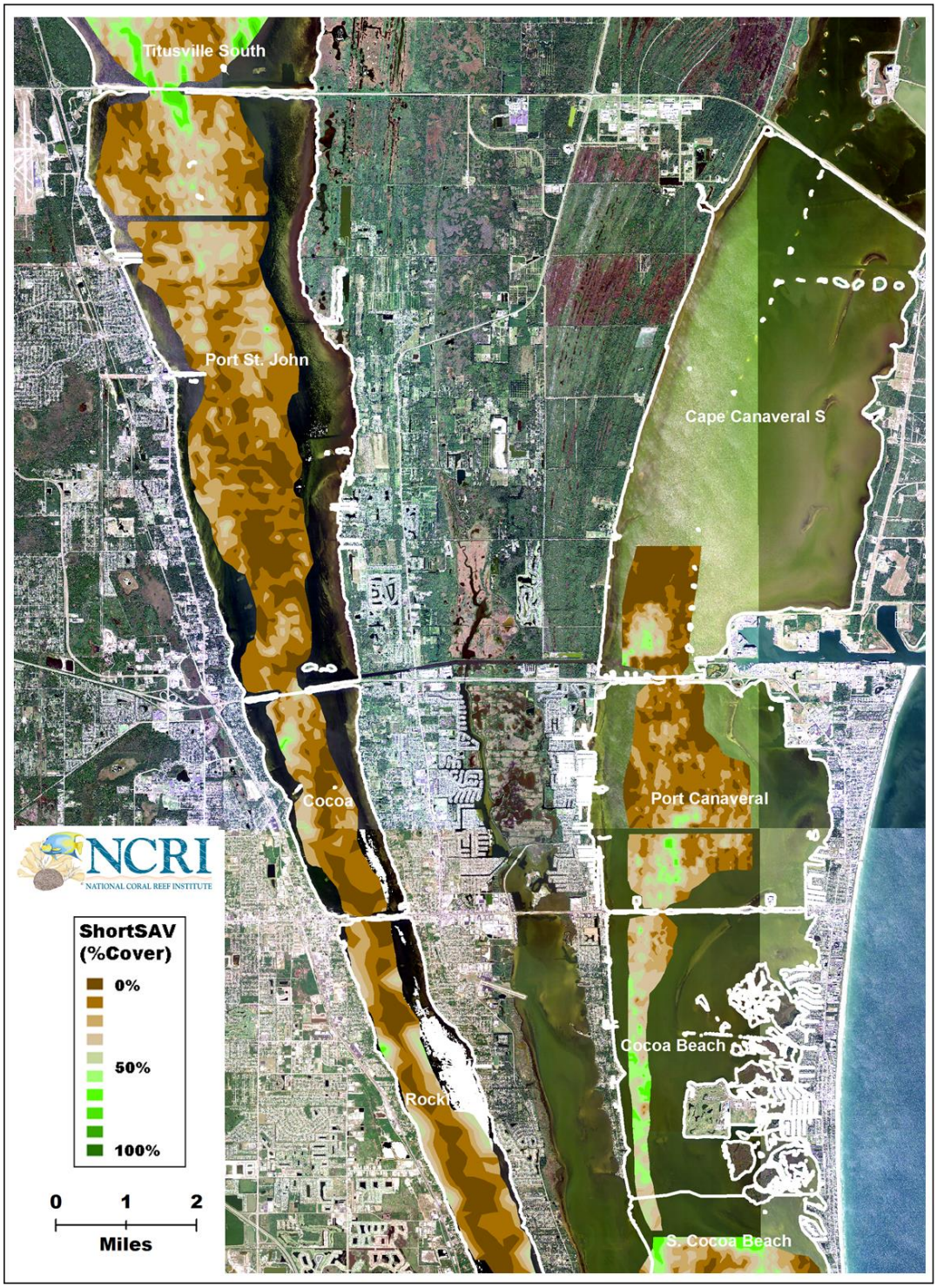

Appendix 2.A5. (Port St John to Rockledge) Kriged contour plot of acoustically-predicted short SAV cover (~10cm<). The boundaries of SJRWMD segments are displayed for reference.

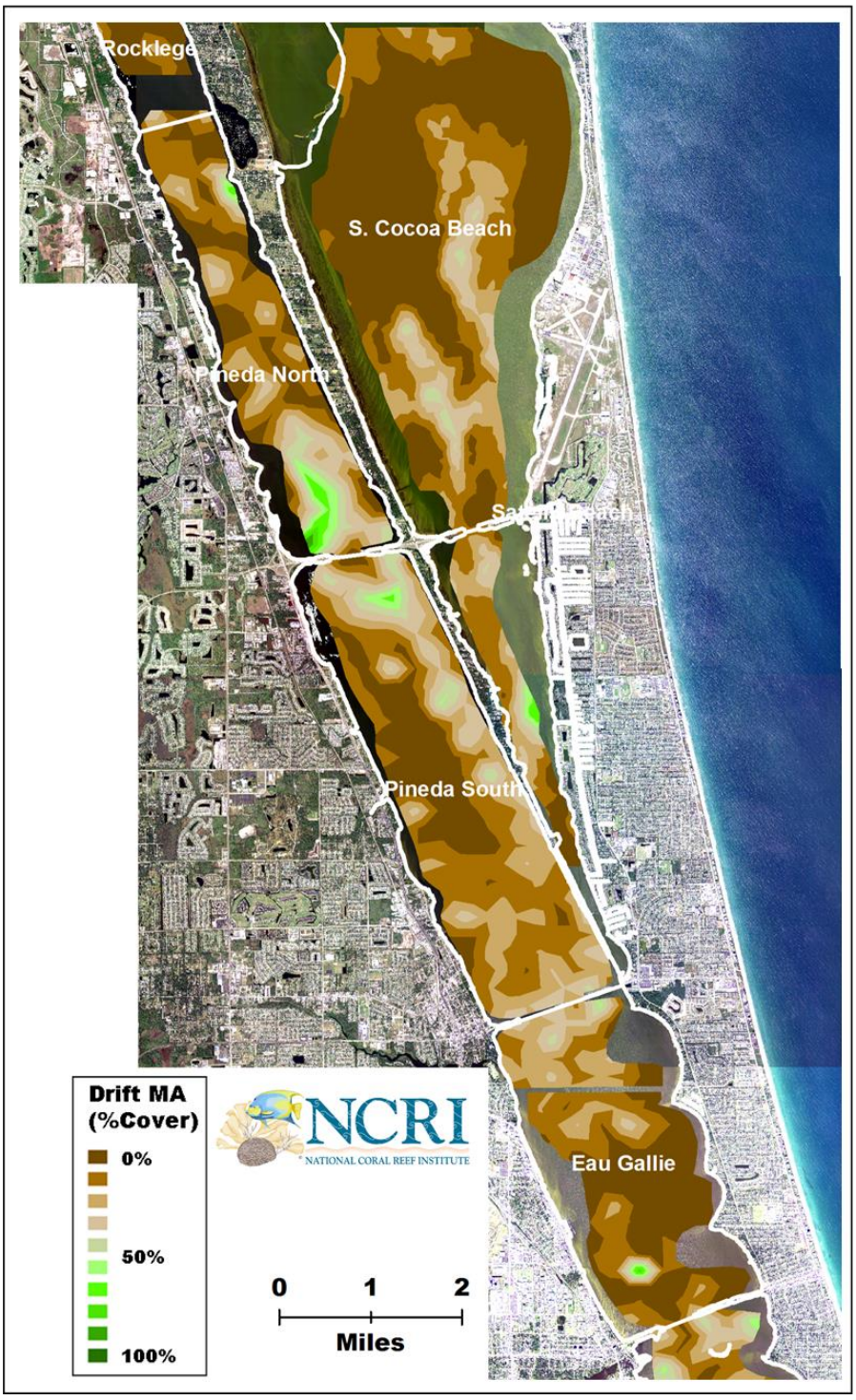

Appendix 2A6. (Pineda North to Eau Gallie) Kriged contour plot of acoustically-predicted drift macroalgae cover. The boundaries of SJRWMD segments are displayed for reference.

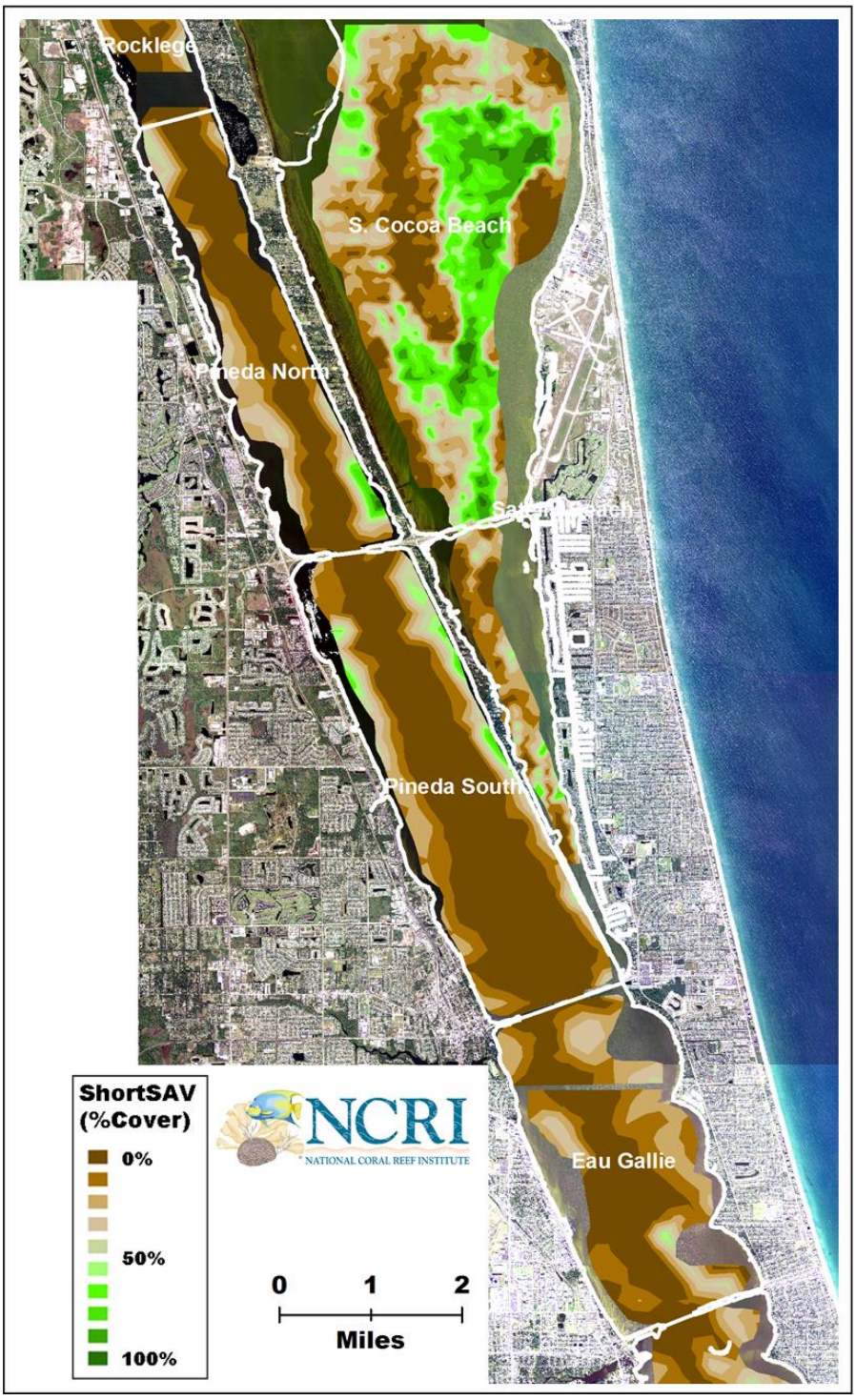

Appendix 2.A7. (Pineda North to Eau Gallie) Kriged contour plot of acoustically-predicted short SAV cover (~10cm<). The boundaries of SJRWMD segments are displayed for reference.

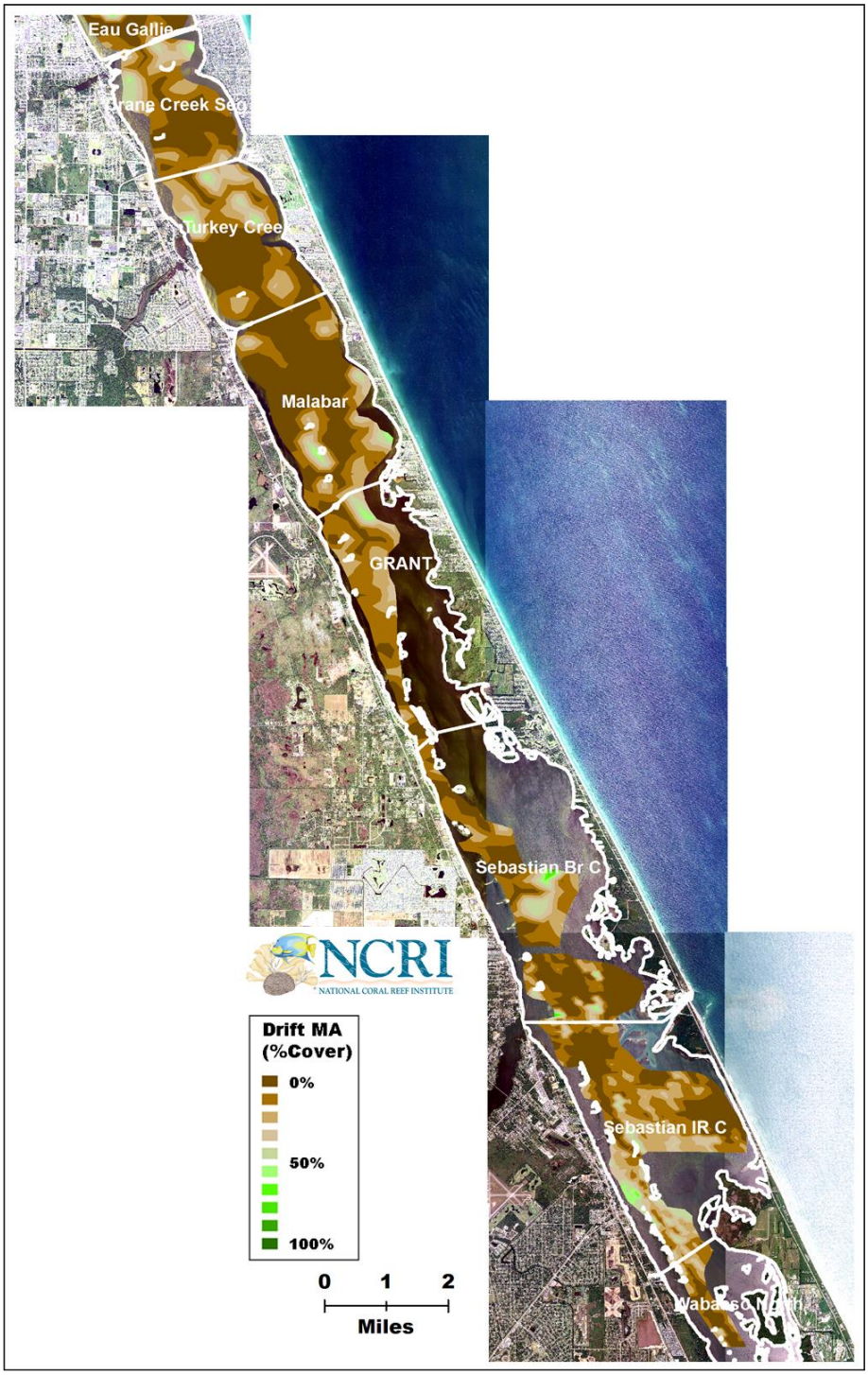

Appendix 2.A8. (Crane Creek to Wabasso) Kriged contour plot of acoustically-predicted drift macroalgae cover. The boundaries of SJRWMD segments are displayed for reference.

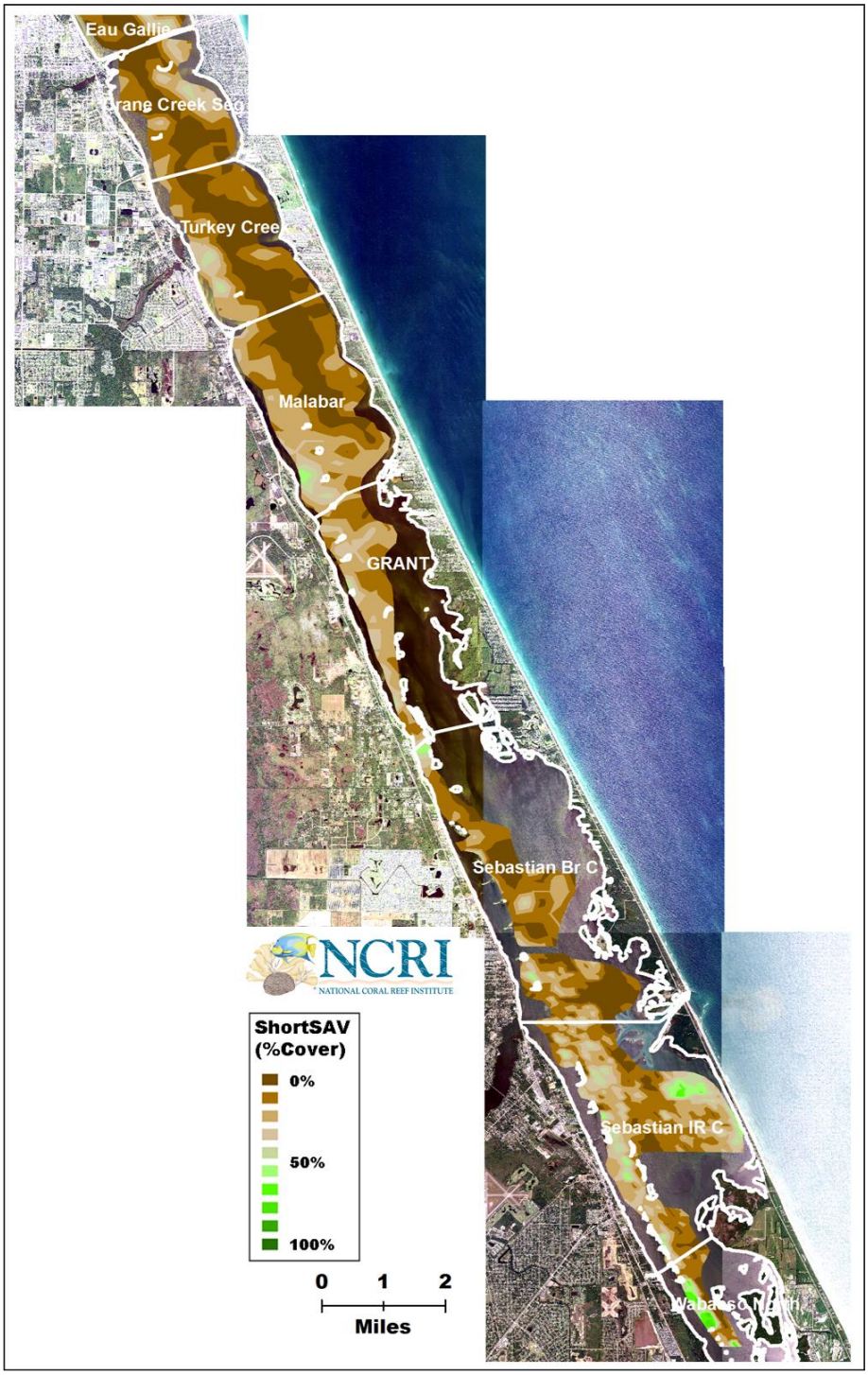

Appendix 2.A9. (Crane Creek to Wabasso) Kriged contour plot of acoustically-predicted short SAV cover (~10cm<). The boundaries of SJRWMD segments are displayed for reference.

CHAPTER 3 APPENDIX

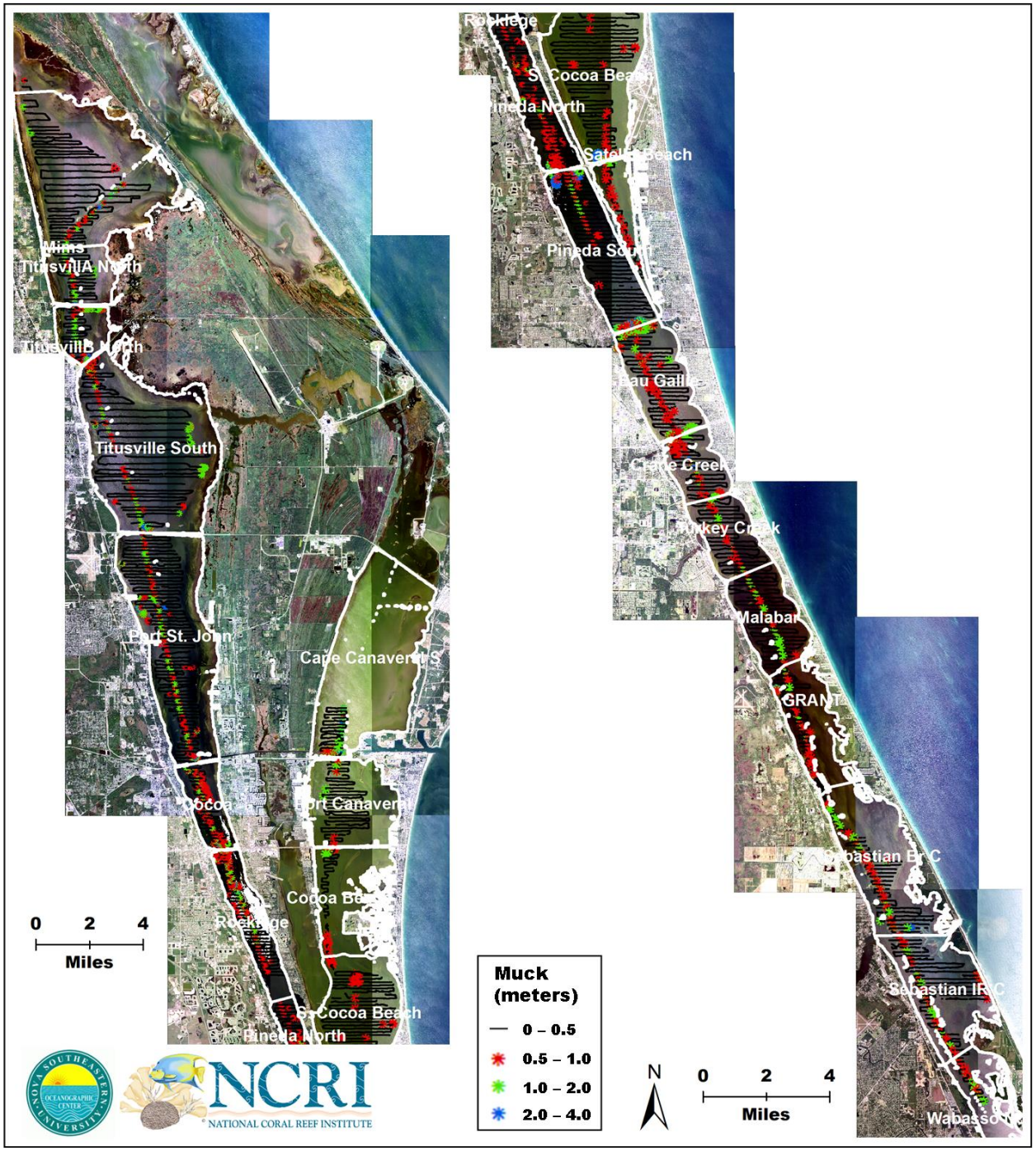

Appendix 3.A1. Extent of the 2008 hydroacoustic muck survey, displayed as the trackplot of muck layer thickness predictions derived from the 38 kHz hydroacoustic signal. The Indian River was surveyed from its origin in the Titusville area southward to Wabasso. The Banana River was surveyed from the Federal Manatee Zone near Cape Canaveral southward to its convergence with Indian River in the Melbourne area.

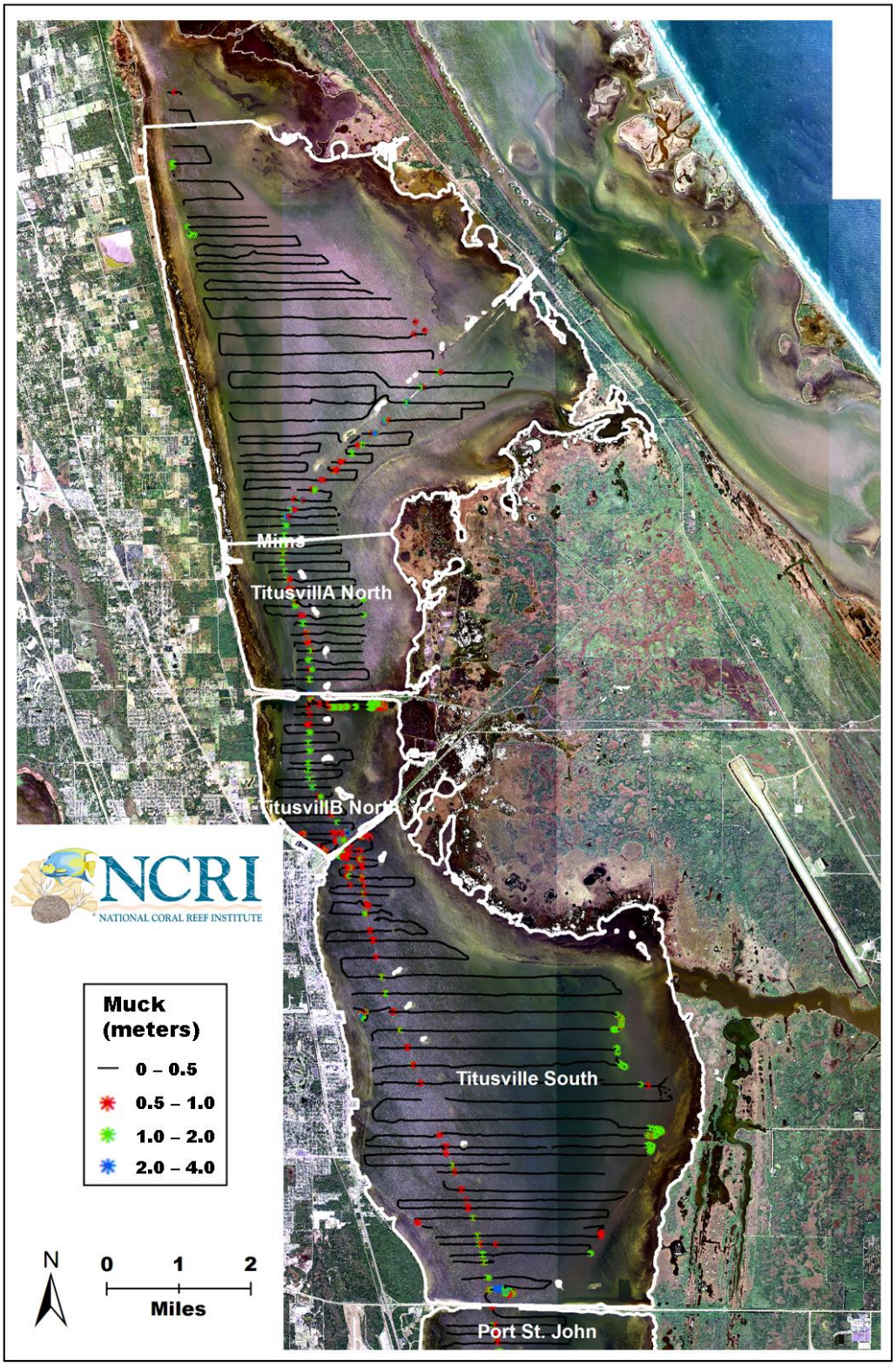

Appendix 3.A2. (Mims to Titusville) Trackplot of acoustically-predicted muck thickness, derived from the 38 kHz hydroacoustic signal.

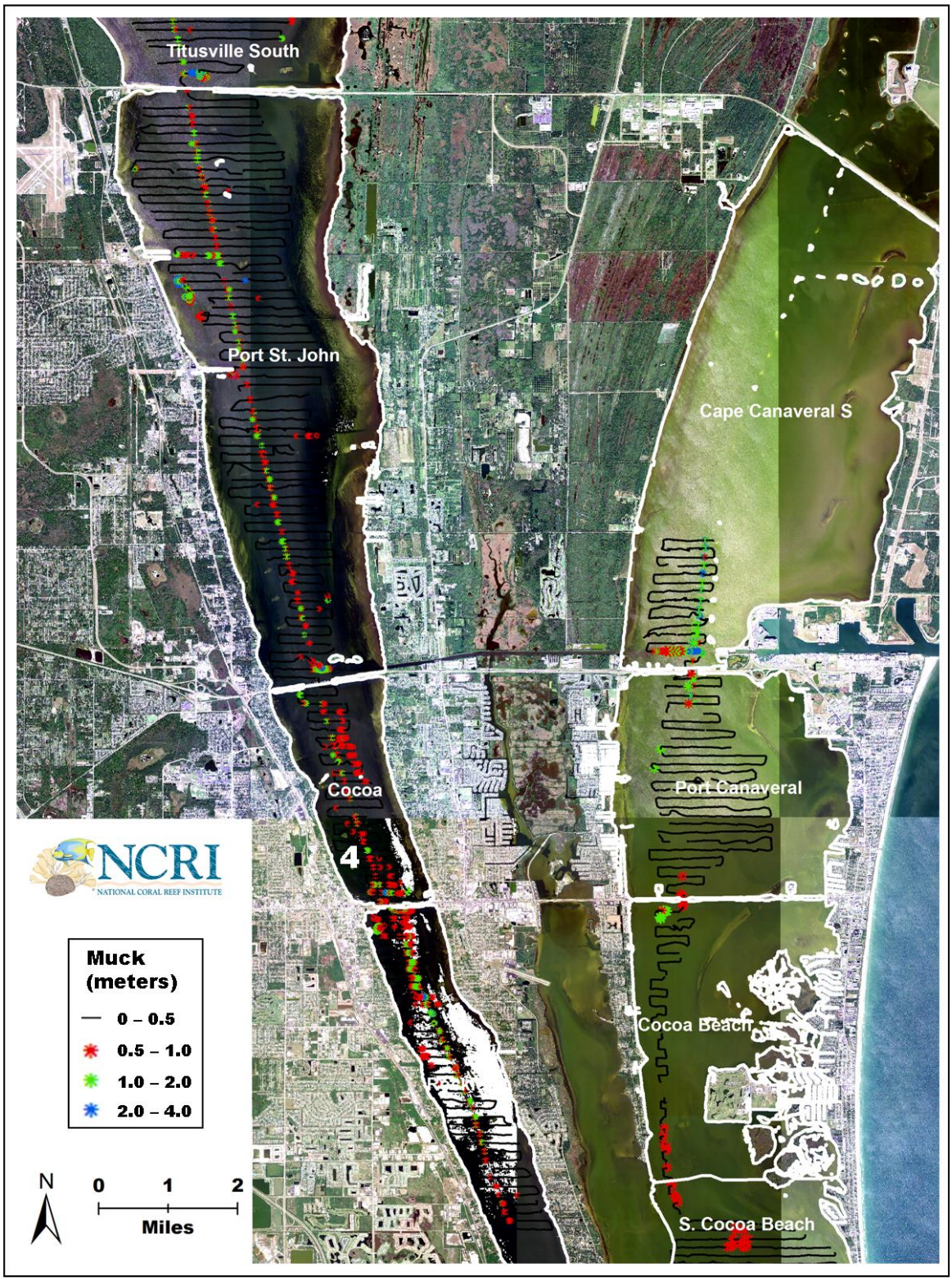

Appendix 3.A3. (Port St John to Cocoa Beach) Trackplot of acoustically-predicted muck thickness, derived from the 38 kHz hydroacoustic signal.

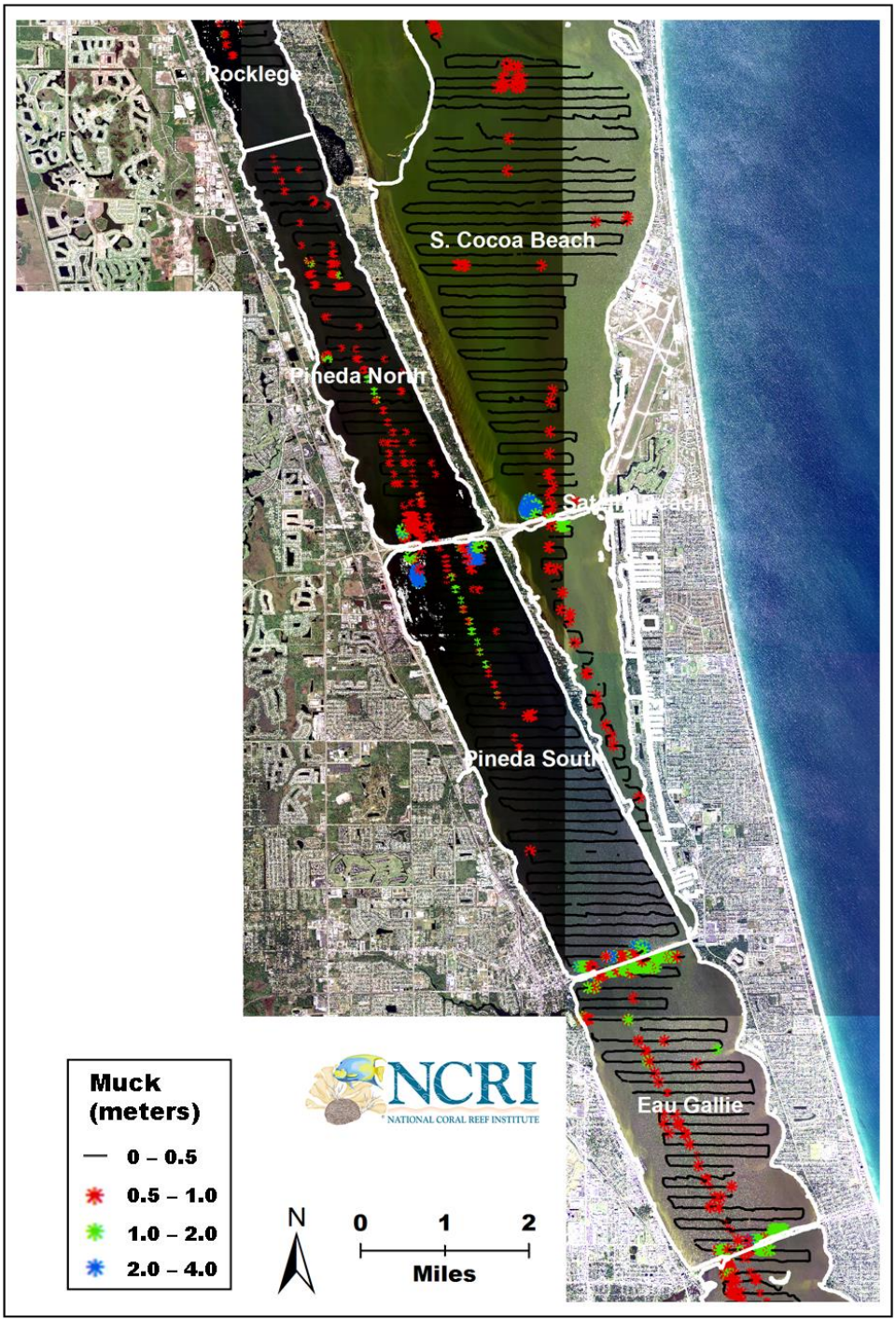

Appendix 3.A4. (Rockledge to EauGallie) Trackplot of acoustically-predicted muck thickness, derived from the 38 kHz hydroacoustic signal.

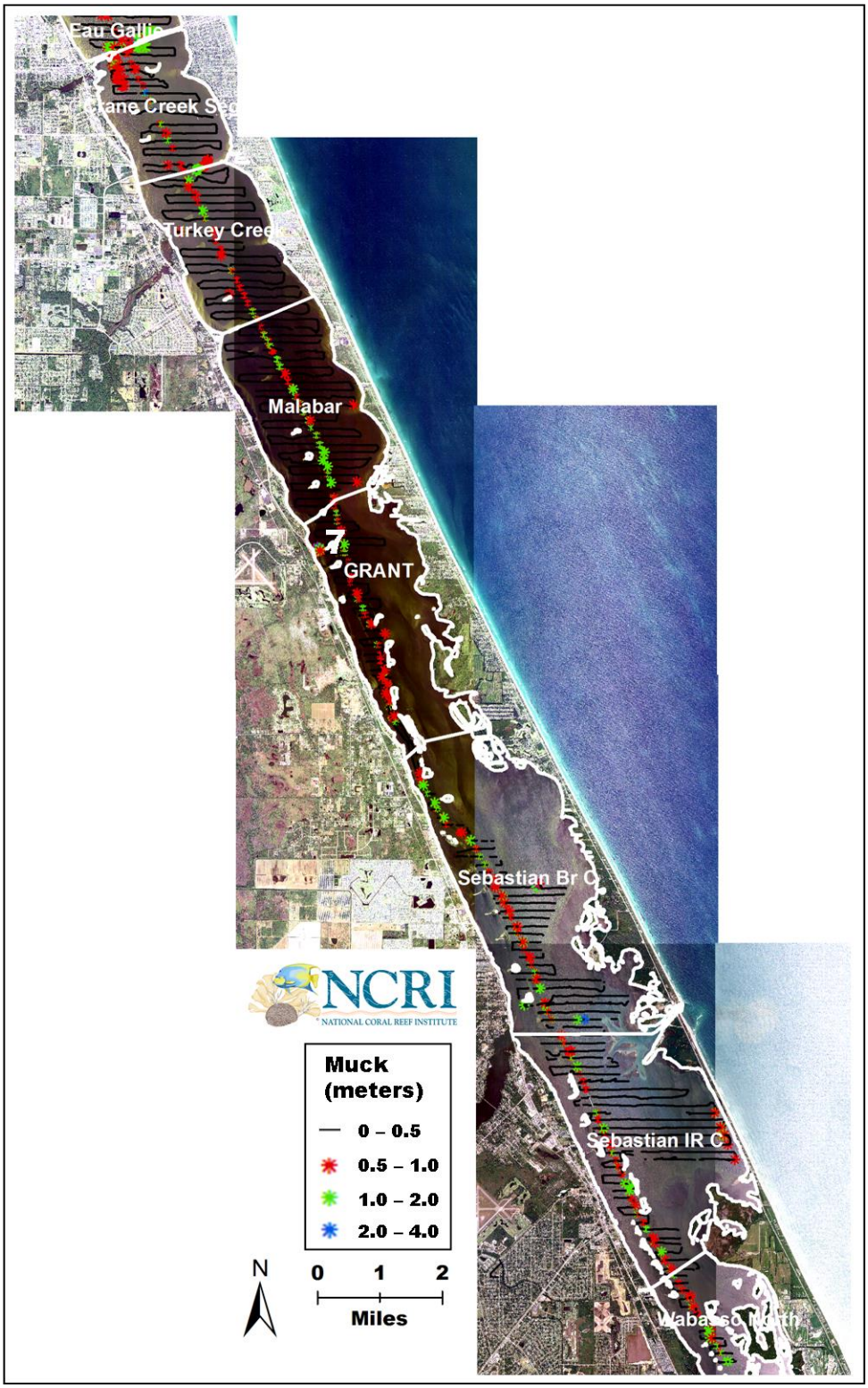

Appendix 3.A5. (Crane Creek to Wabasso) Trackplot of acoustically-predicted muck thickness, derived from the 38 kHz hydroacoustic signal.

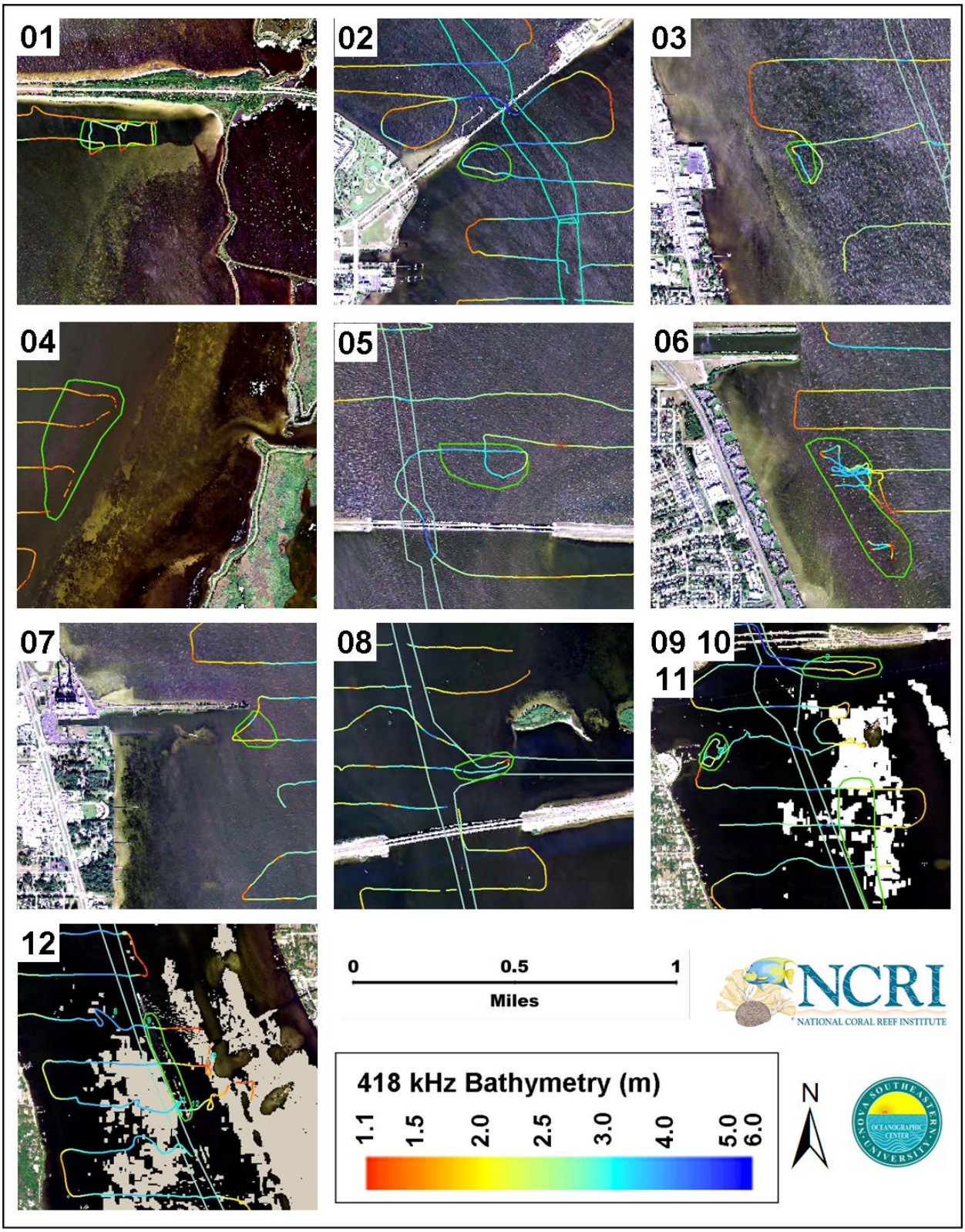

Appendix 3.B1. Demarcations of muck deposits (1-12 of 23) identified in the Indian and Banana Rivers (green polygons), displayed over 2004 DOQQ's (map scale = 1:10,000). Also displayed are the trackplots of the 420 kHz bottom picks and the ICW shapefile (cyan polygons).

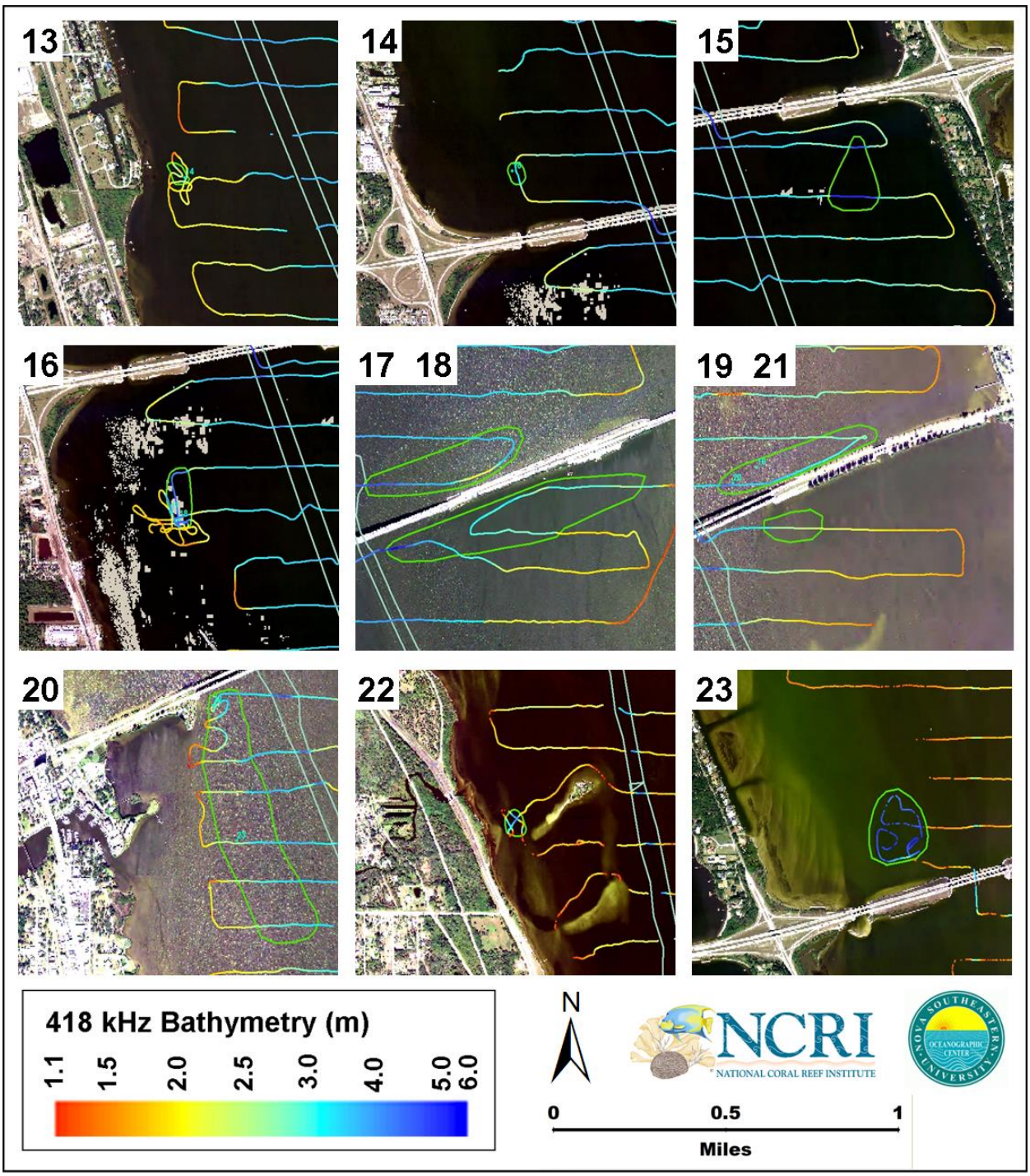

Appendix 3.B1. Demarcations of muck deposits (13-23 of 23) identified in the Indian and Banana Rivers (green polygons), displayed over 2004 DOQQ's (map scale = 1:10,000). Also displayed are the trackplots of the 420 kHz bottom picks and the ICW shapefile (cyan polygons).

CHAPTER 5 APPENDIX

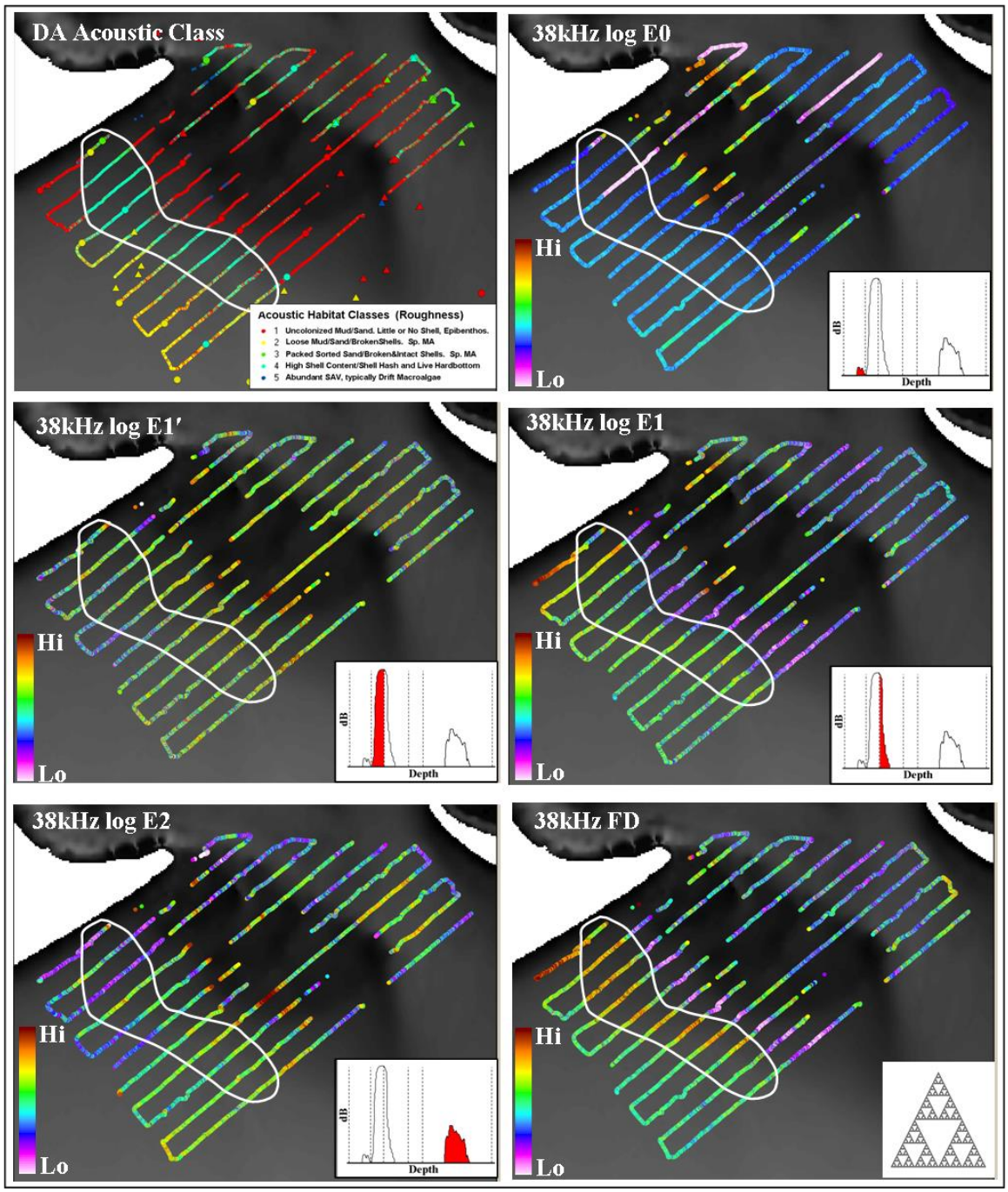

Appendix 5.A1. (Lighthouse Point) Classified acoustic trackplot (upper-left) and trackplots of 38 kHz acoustic energy and fractal dimension. The boundary of the acoustically-predicted region of consolidated shell hash is indicated for reference.

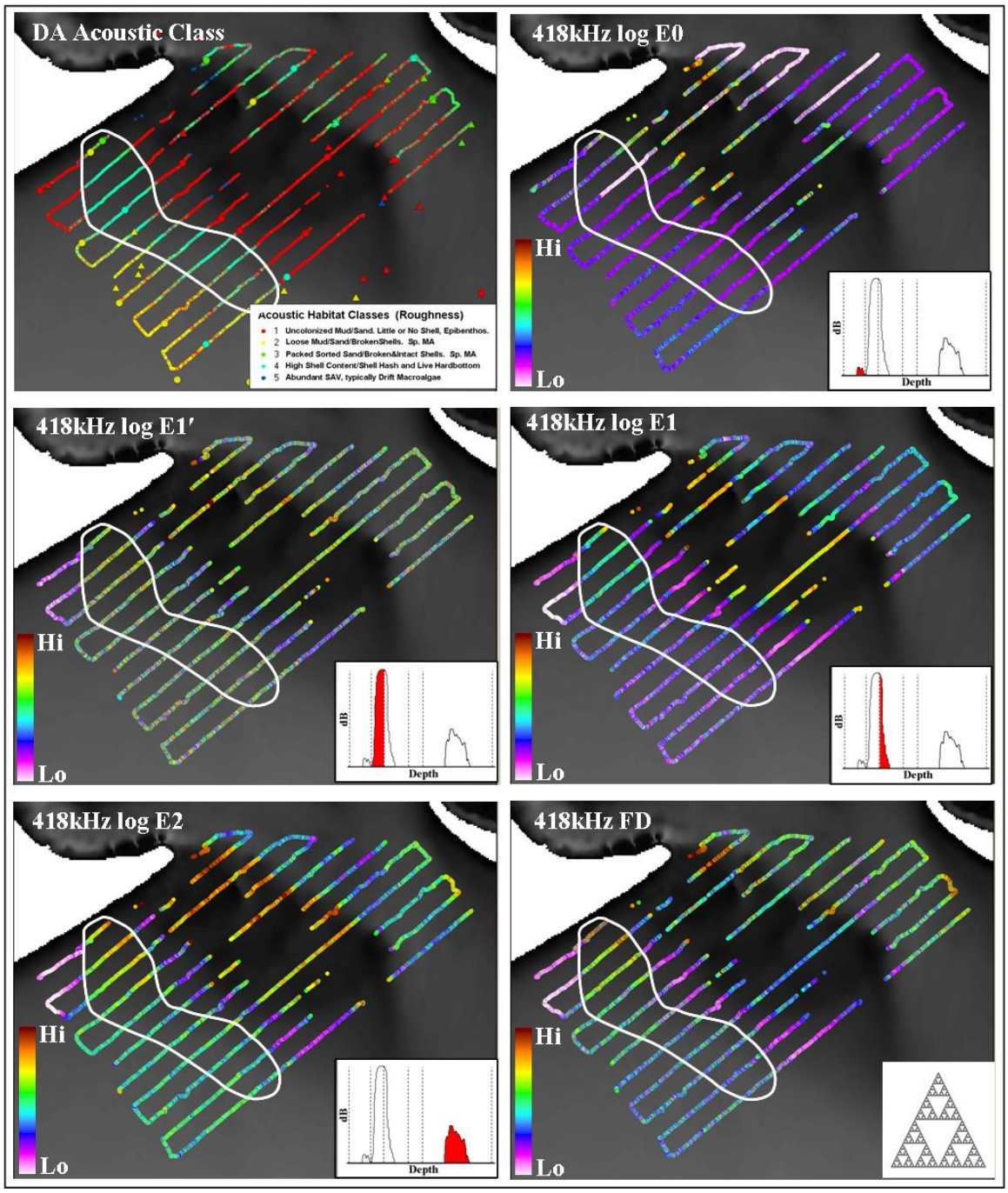

Appendix 5.A2. (Lighthouse Point) Classified acoustic trackplot (upper-left) and trackplots of 418 kHz acoustic energy and fractal dimension. The boundary of the acoustically-predicted region of consolidated shell hash is indicated for reference.

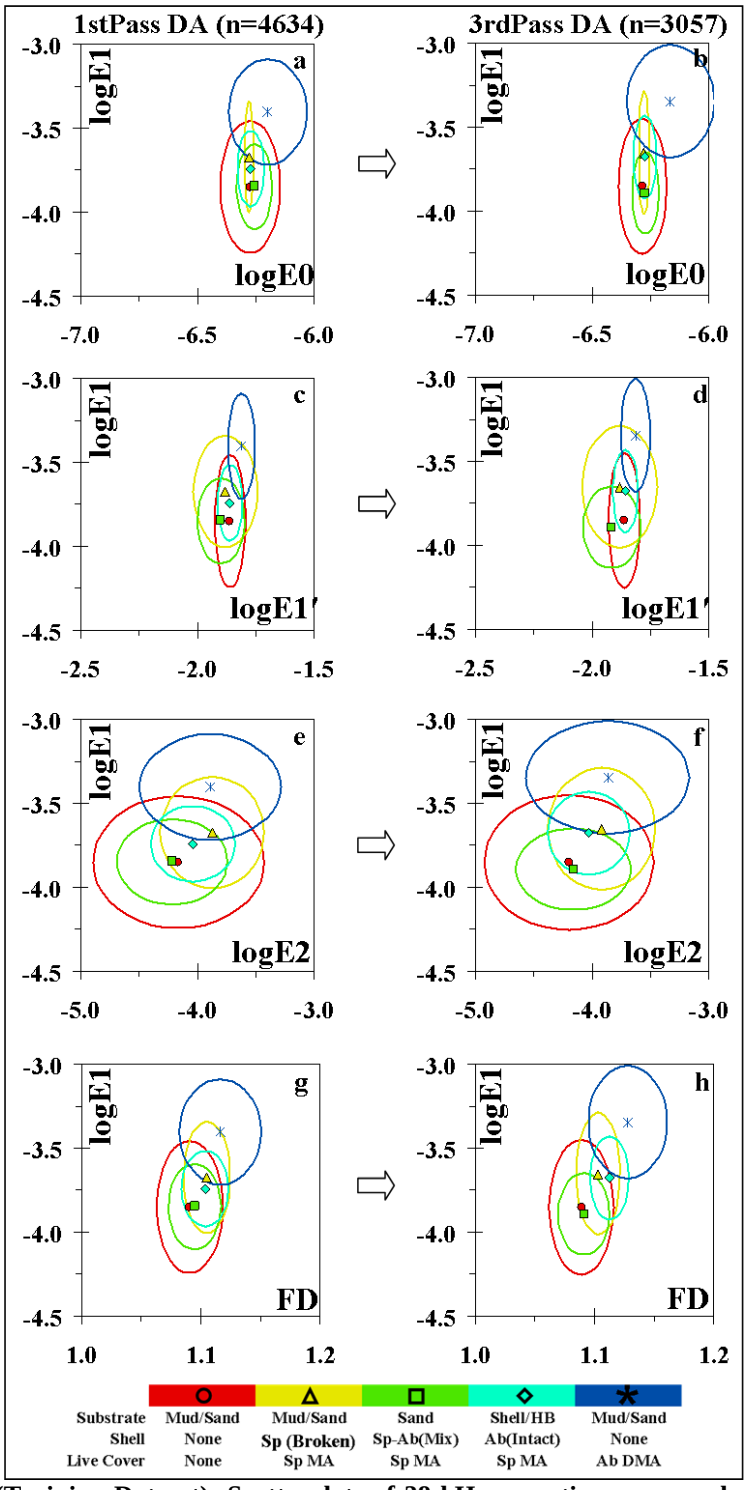

Appendix 5.B1. (Training Dataset) Scatterplots of 38 kHz acoustic energy and shape parameters. Centerpoints denote cluster averages, ellipses are dispersion (1 standard deviation) about x and y. (left) Data submitted to 1st descriptive DA and (right) 3rd-Pass descriptive DA.

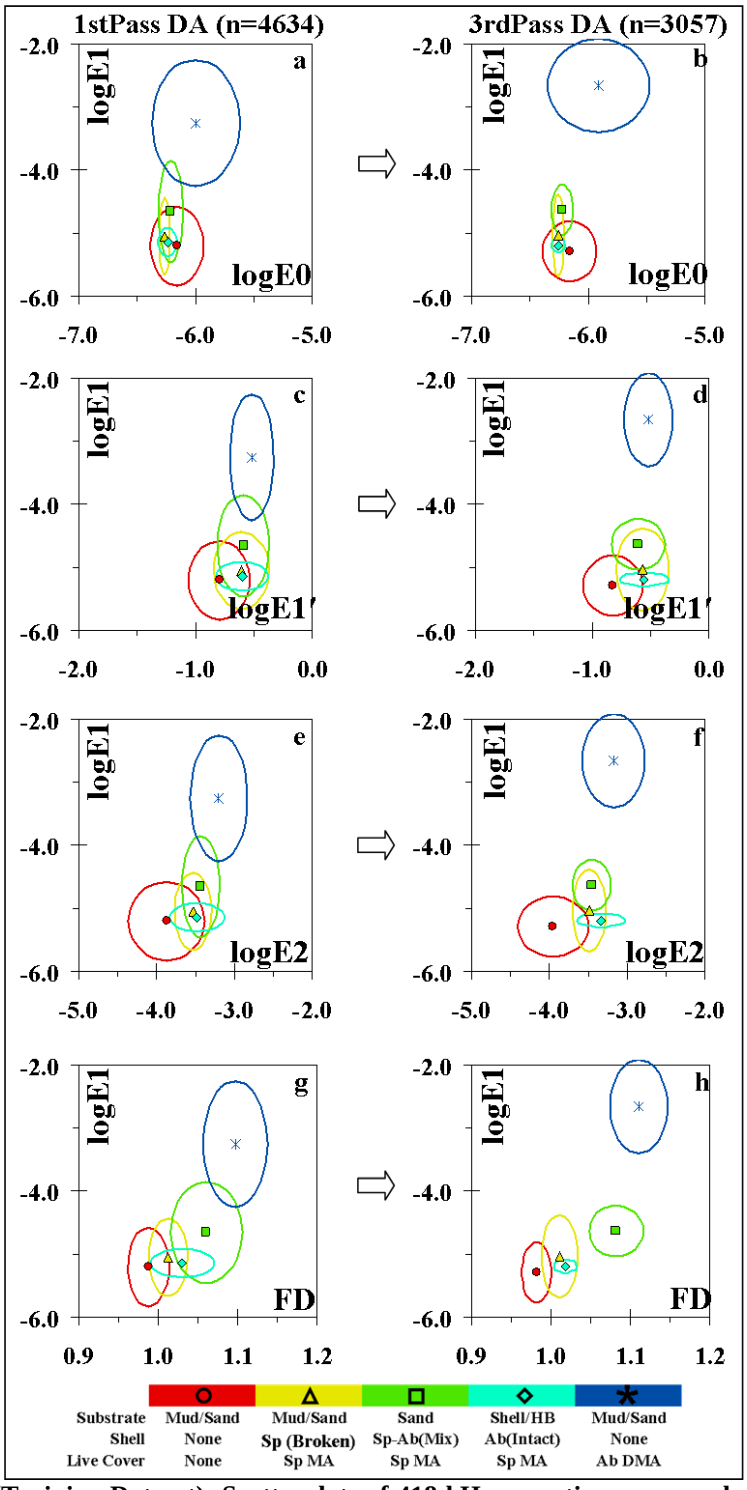

Appendix 5.B2. (Training Dataset) Scatterplots of 418 kHz acoustic energy and shape parameters. Centerpoints denote cluster averages, ellipses are dispersion (1 standard deviation) about x and y. (left) Data submitted to 1st descriptive DA and (right) 3rd-Pass descriptive DA.

CHAPTER 6 APPENDIX

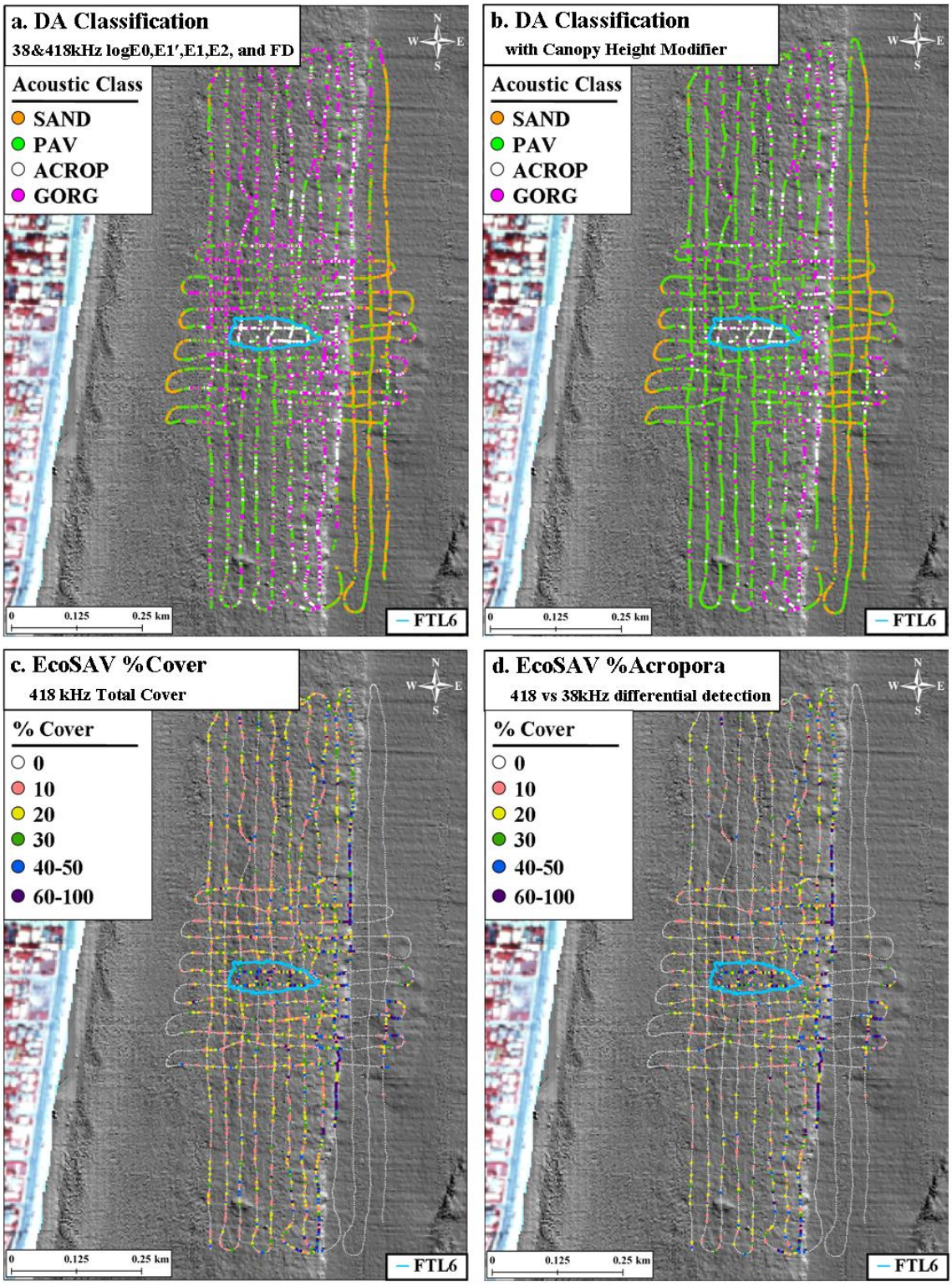

Appendix 6.A1 Classified acoustic trackplots of FTL6 site by (a) multi-pass discriminant analysis, (b) multi-pass discriminant analysis with EcoSAV canopy-height modifier, (c) 418 kHz EcoSAV Total Cover, and (d) 38vs418 kHz EcoSAV *Acropora* cover.

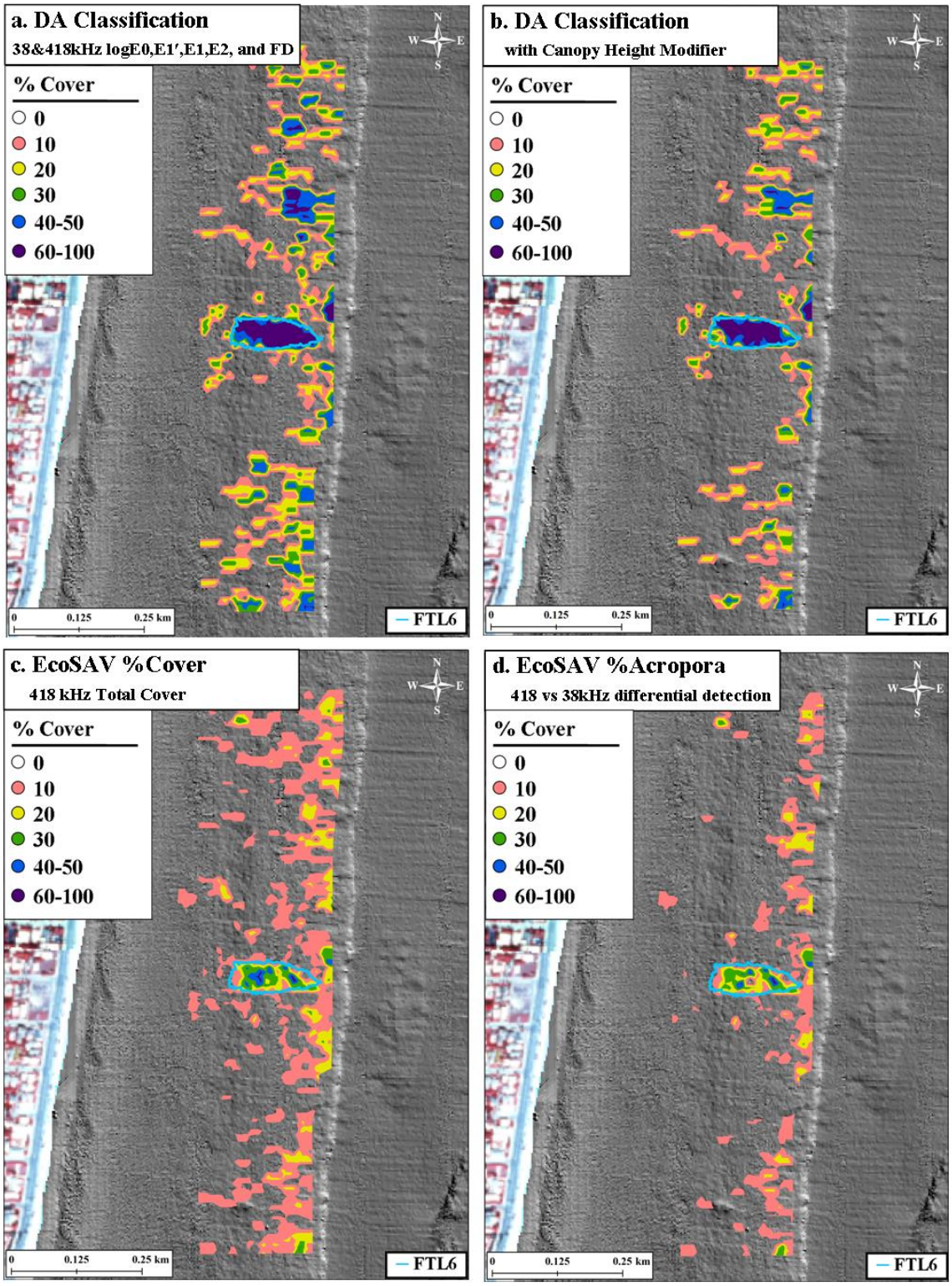

Appendix 6.A2 (FTL6) Continuous surfaces of predicted cover, created by Kriging of classified acoustic trackplots by (a) multi-pass discriminant analysis, (b) multi-pass discriminant analysis with EcoSAV canopy-height modifier, (c) 418 kHz EcoSAV Total Cover, and (d) 38vs418 kHz EcoSAV *Acropora* cover.

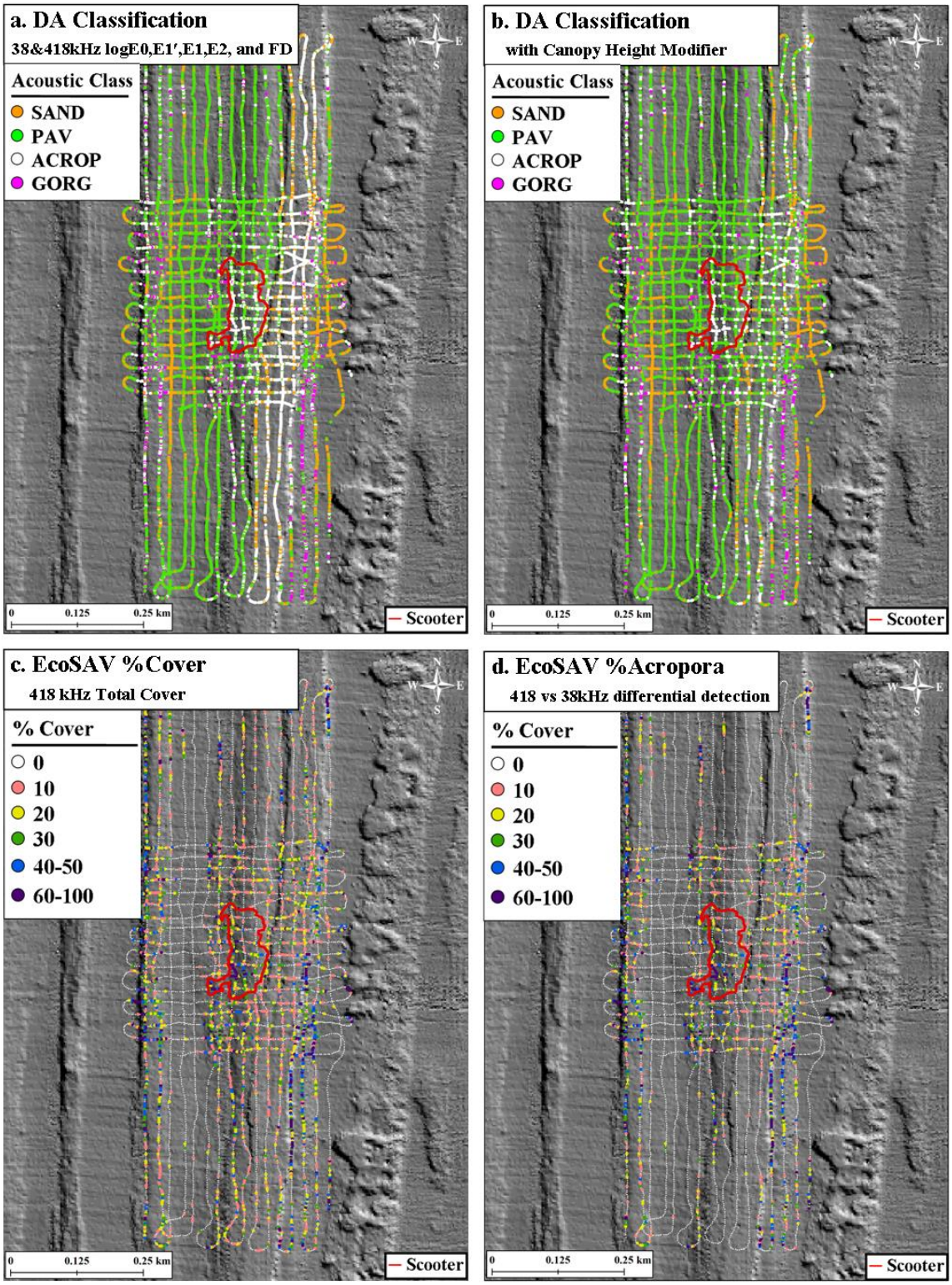

Appendix 6.B1 Classified acoustic trackplots of Scooter site by (a) multi-pass discriminant analysis, (b) multi-pass discriminant analysis with EcoSAV canopy-height modifier, (c) 418 kHz EcoSAV Total Cover, and (d) 38vs418 kHz EcoSAV *Acropora* cover.

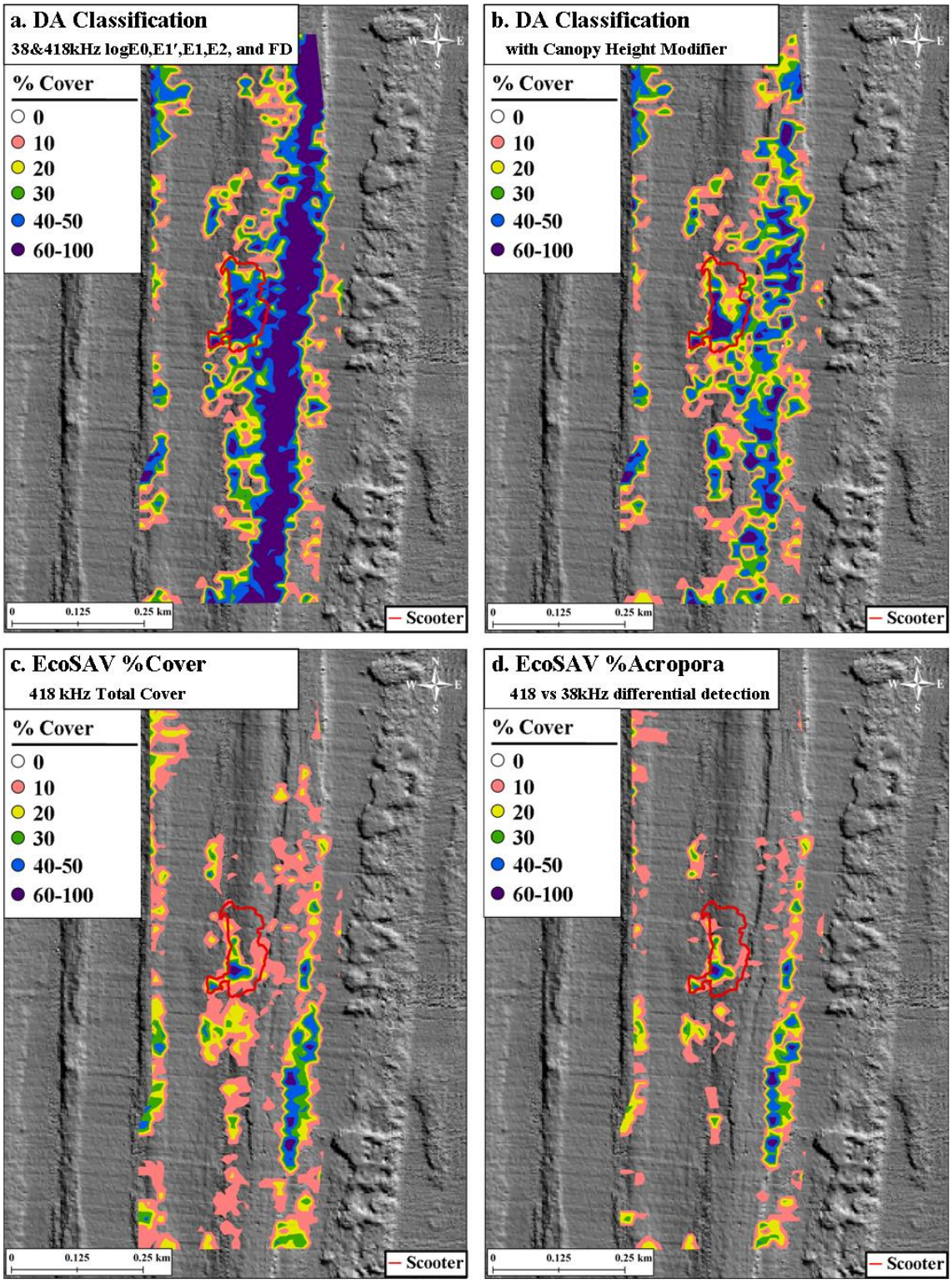

Appendix 6.B2 (Scooter) Continuous surfaces of predicted cover, created by Kriging of classified acoustic trackplots by (a) multi-pass discriminant analysis, (b) multi-pass discriminant analysis with EcoSAV canopy-height modifier, (c) 418 kHz EcoSAV Total Cover, and (d) 38vs418 kHz EcoSAV *Acropora* cover.

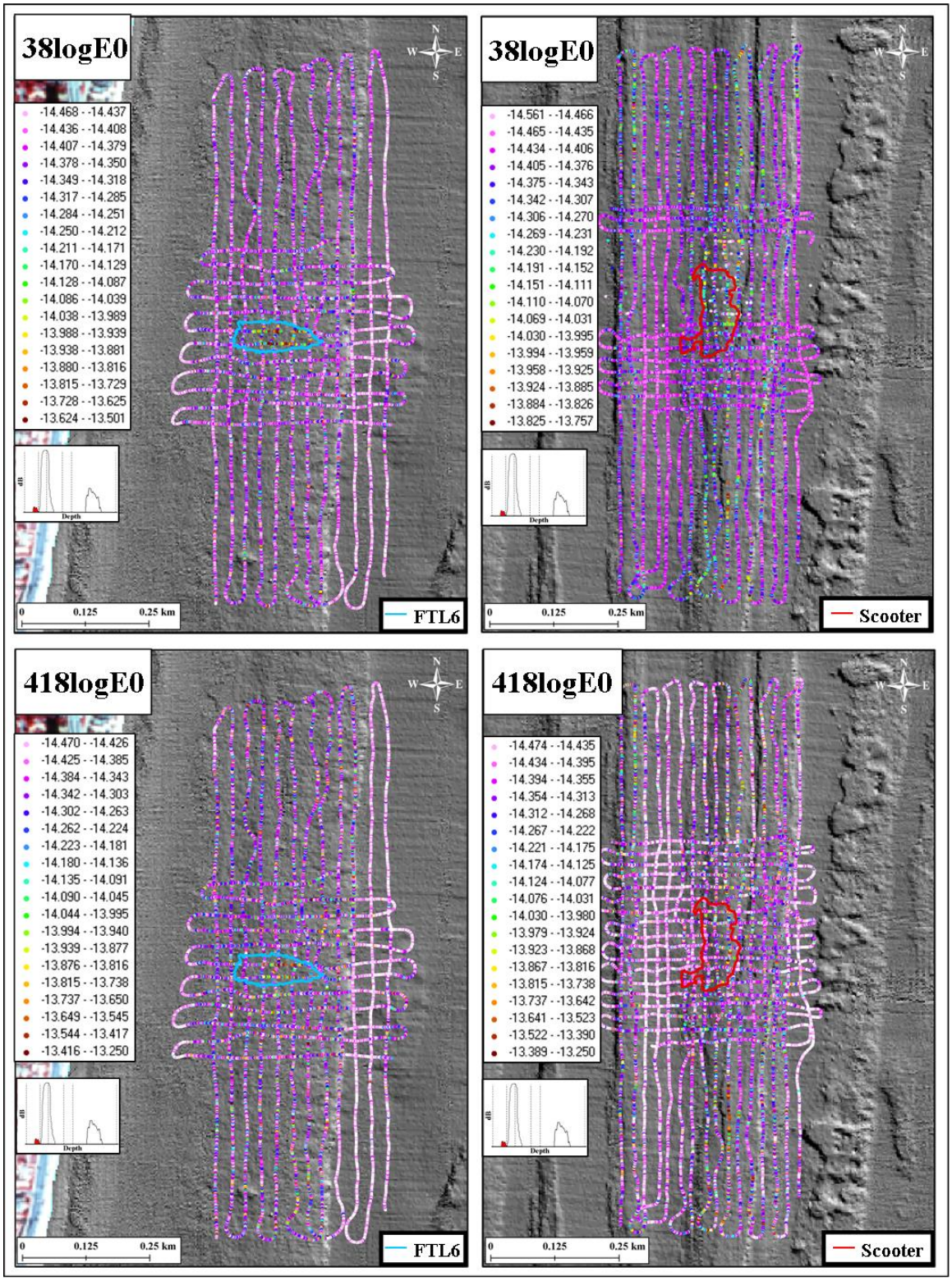

Appendix 6.C1 Acoustic trackplots of the 38 and 418 kHz logE0 acoustic energy parameter.

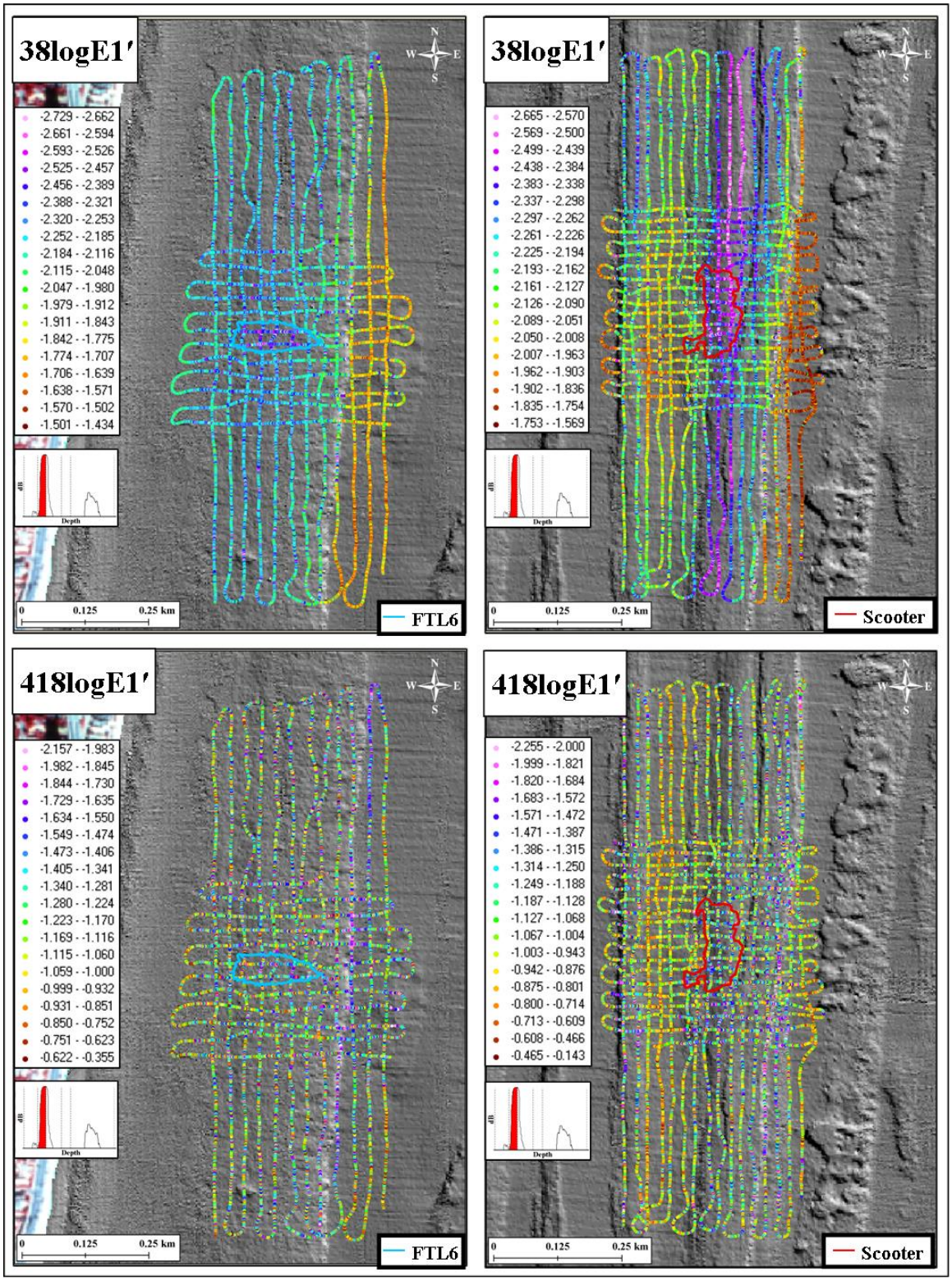

Appendix 6.C2 Acoustic trackplots of the 38 and 418 kHz logE1′ acoustic energy parameter.

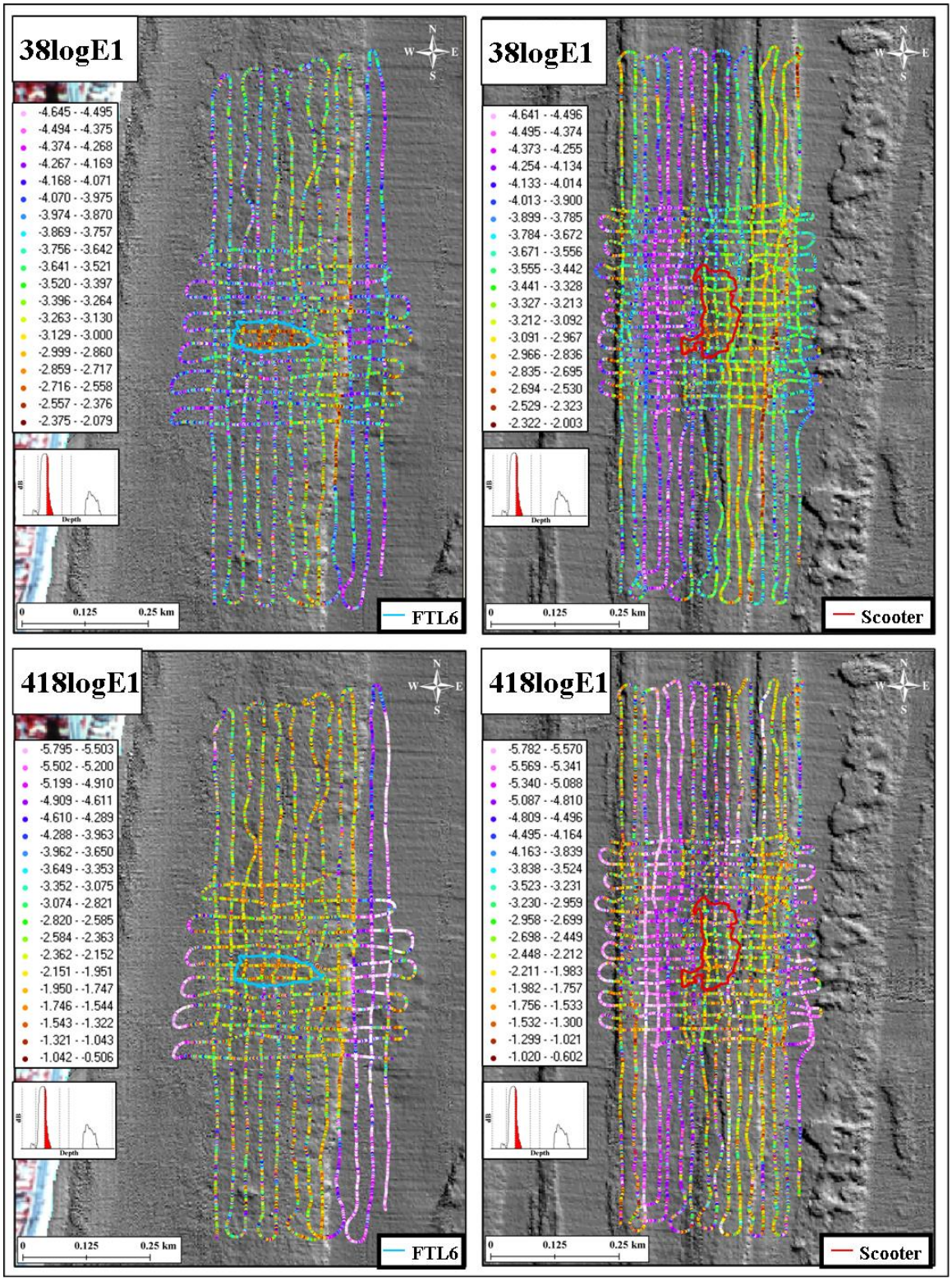

Appendix 6.C3 Acoustic trackplots of the 38 and 418 kHz logE1 acoustic energy parameter.

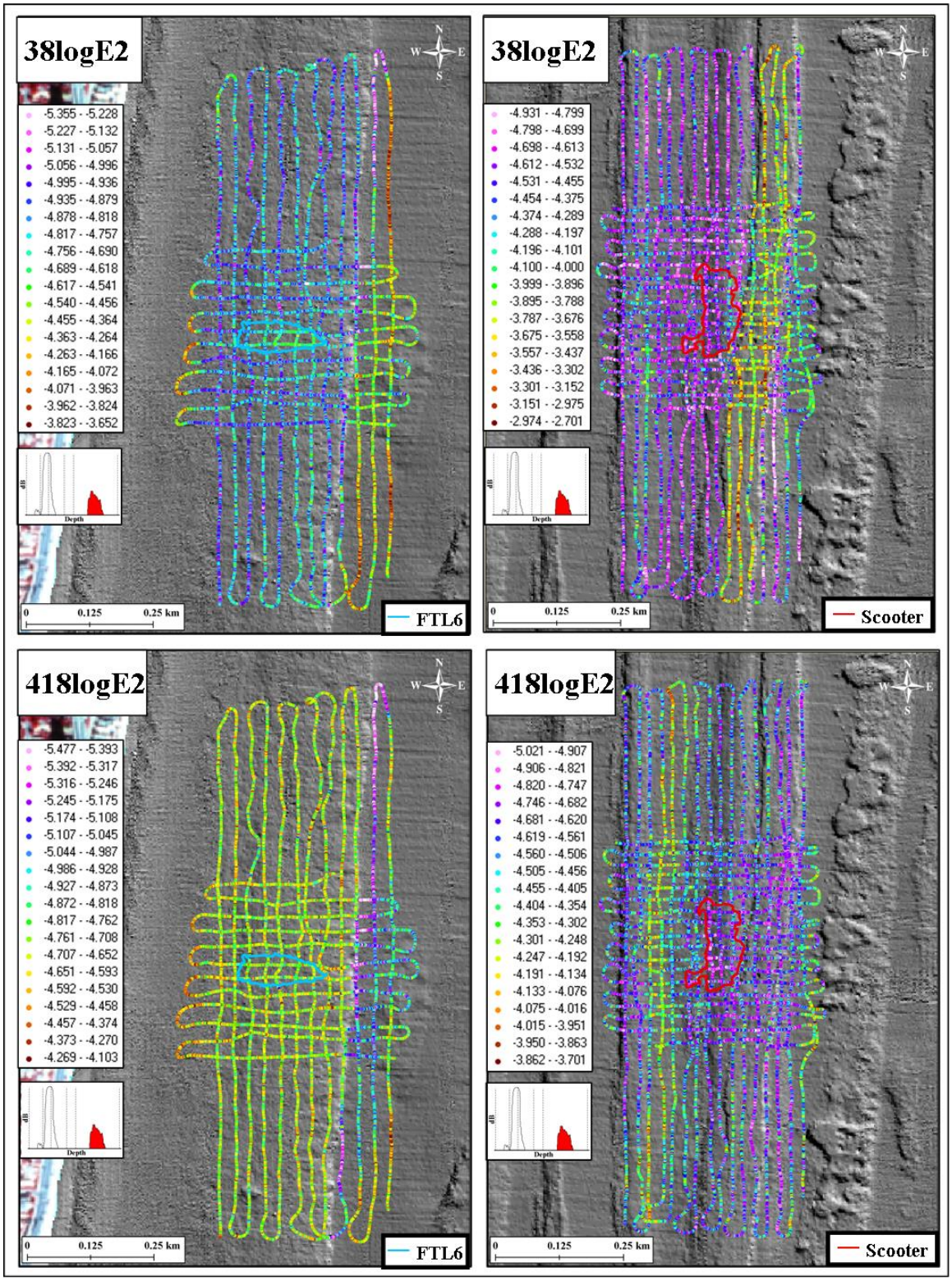

Appendix 6.C4 Acoustic trackplots of the 38 and 418 kHz logE2 acoustic energy parameter.

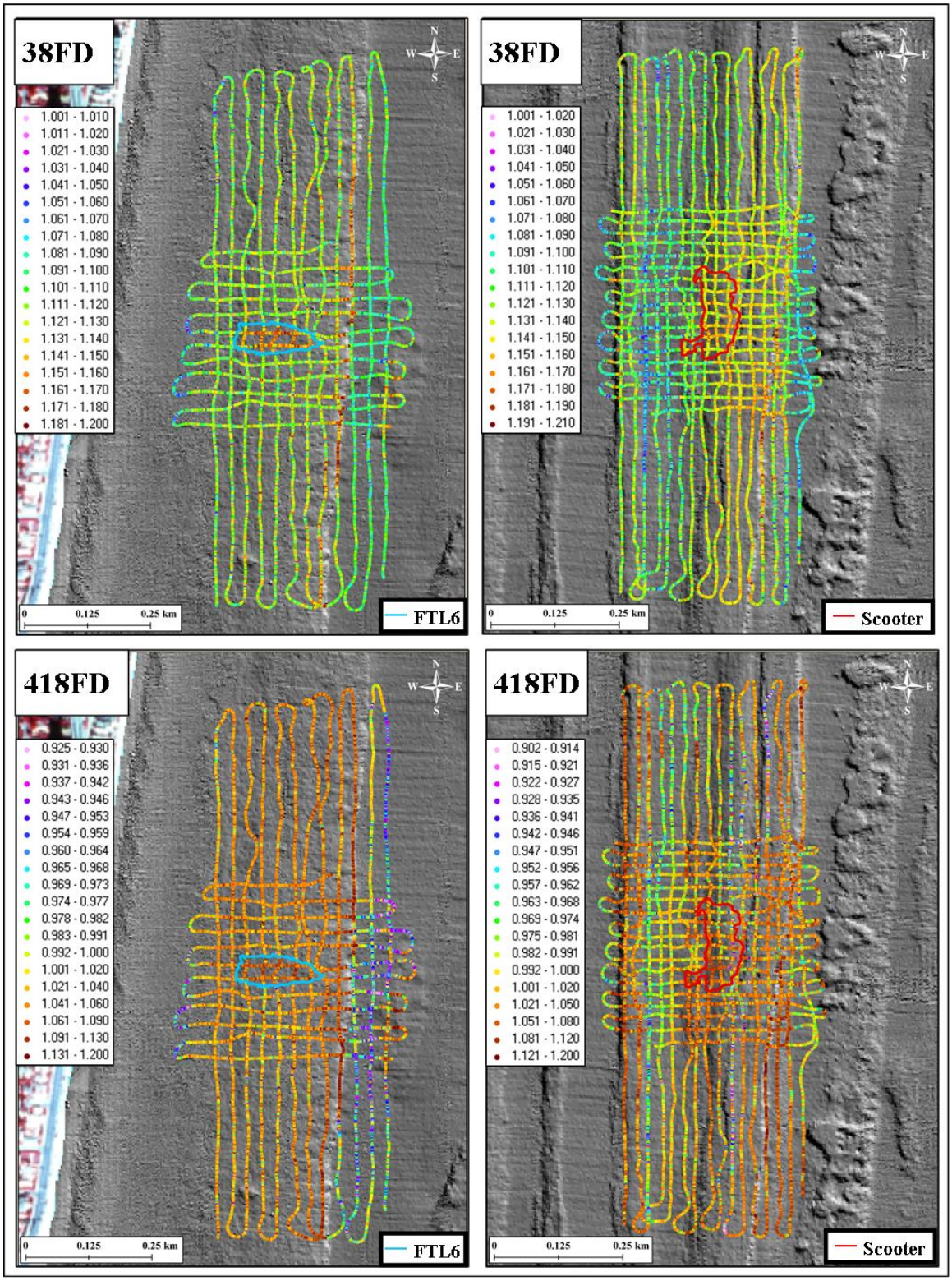

Appendix 6.C5 Acoustic trackplots of the 38 and 418 kHz Fractal Dimension echo envelope shape parameter.

LITERATURE CITED

Afifi, A., Clark, V.A., & May, S. (2004). *Computer-Aided Multivariate Analysis*, 4th ed. (p. 62). Boca Raton: Chapman & Hall/CRC Press.

Anderson, M.J. (2008) Animal-sediment relationships re-visited: Characterising species' distributions along an environmental gradient using canonical analysis and quantile regression splines. *Journal of Experimental Marine Biology and Ecology*, 366, 16-27.

Applied Physics Laboratory, 1989. APL-UW High Frequency Ocean Environmental Acoustic Models. Seattle, Washington. University of Washington. *APL* Technical Report APL-UW TR-8907.

Battista, T.A., Costa, B.M., and Anderson, S.M. 2007a. Shallow-Water Benthic Habitats of the Main Eight Hawaiian Islands (DVD). NOAA Technical Memorandum NOS NCCOS 61, Biogeography Branch. Silver Spring, MD.

Battista, T.A., Costa, B.M., & Anderson, S.M. 2007b. Shallow-Water Benthic Habitats of the Republic of Palau (DVD). NOAA Technical Memorandum NOS NCCOS 59, Biogeography Team. Silver Spring, MD.

Bax, N., Kloser, R., Williams, A., Gowlett-Holmes, K., & Ryan, T. (1999). Seafloor habitat definition for spatial management in fisheries: a case study on the continental shelf of southeast Australia. *Oceanologica Acta*, 22(6), 705-719.

Brekhovskikh, L. and Lysanov, Y., 1982. *Fundamentals of Ocean Acoustics*. Ed. L.Felsen. Springer Series in Electrophysics Volume 8. Springer-Verlag, Berlin, 304p.

Brown, C.J., Cooper, K.M., Meadows, W.J., Limpenny, D.S., & Rees, H.L. (2002). Small-scale mapping of sea-bed assemblages in the eastern English Channel using sidescan sonar and remote sampling techniques. Estuarine, Coastal and Shelf Science, 54, 263-278.

Burczynski, J. (1999). Bottom classification. Seattle, WA: BioSonics Inc.
[See http://www.biosonicsinc.com/doc_library/docs/bottom_classification.pdf].

Burns, D.R., Queen, C.B., Sisk, H., Mullarkey, W., & Chivers, R.C. (1989). Rapid and convenient acoustic sea-bed discrimination for fisheries applications. Proceedings of the Institute of Acoustics 11, Part 3, 169-178.

Calinksi, T., & Harabasz, J. (1974). A dendrite method for cluster analysis. *Communications in statistics*, 3(1), 1-27.

Chivers, R.C., Emerson, N., & Burns, D. (1990). New acoustic processing for underway surveying. *The Hydrographic Journal*, 56, 8-17.

Collier, J.S., & Brown, C.J. (2005) Correlation of sidescan backscatter with grain size distribution of surficial seabed sediments. *Marine Geology*, 214, 431–449.

Collins, W., Gregory, R., & Anderson, J. (1996). A digital approach to seabed classification. *Sea Technology*, 37, 83–87.

Davis, M.W., Zimmermann, C.Z., & Montgomery, J. (1983). Sediment-associated macroalgae act as biological filters in estuaries. *Estuaries*, 6 312.

den Hartog, C. (1994). Suffocation of a littoral *Zostera* bed by *Enteromorpha radiata*. Aquatic Botany, 47, 21-28.

Dommisse, M., Urban, D., Finney, B., & Hills, S. (2005). Potential depth biasing using the Biosonics VBT Seabed Classification Software. *Marine Technology Society Journal*, 39(2), 90-93.

Ellingsen, K.E., Gray, J.S., & Bjørnbom, E. (2002). Acoustic classification of seabed habitats using the QTC VIEW system. *ICES Journal of Marine Science*, 59, 825–835.

Foster, G., Walker, B.K., & Riegl, B.M. (2009) Interpretation of single-beam acoustic backscatter using lidar-derived topographic complexity and benthic habitat classifications in a coral reef environment. *Journal of Coastal Research*, SI 53, 16-26.

Foster-Smith, R.L. & Sotheran, I.S. (2003). Mapping marine benthic biotopes using acoustic ground discrimination systems. *International Journal of Remote Sensing*, 24(13), 2761-2784.

Freitas, R., Rodrigues, A.M., and Quintino, V. (2003a). Benthic biotopes remote sensing using acoustics. *ICES Journal of Marine Science*, 60, 599-608.

Freitas, R., Silva, S., Quintino, V., Rodrigues, A.M., Rhynas, K., and Collins, W. T. (2003b). Acoustic seabed classification of marine habitats: studies in the western coastal-shelf area of Portugal. *ICES Journal of Marine Science*, 60, 599-608.

Freitas, R., Sampaio, L., Oliveira, J., Rodrigues, A.M., & Quintino, V. (2006) Validation of soft bottom benthic habitats identified by single-beam acoustics. *Marine Pollution Bulletin*, 53, 72–79.

Gleason, A.C.R.; Reid, R.P.; Eklund, A.M., and Koch, V., 2006. Acoustic Signatures of the Seafloor: Tools for Predicting Grouper Habitat. *In* Emerging technologies for reef fisheries research and management, J.C. Taylor (ed.), NOAA Professional Paper NMFS 5, 38-47.

Gleason, A.C.R. (2009) "Single-beam acoustic seabed classification in coral reef environments with application to the assessment of grouper and snapper habitat in the upper Florida Keys, USA". PHD Thesis, University of Miami, USA.

Goodwin, H. & Goodwin, L. (1976). *The Indian River – an American Lagoon*. Compass Publications, Arlington, VA, 66pp.

Gray, J.S. (1974). Animal–sediment relationships. *Oceanography and Marine Biology: An Annual Review*, 12, 223–261.

Greenstreet, S.P.R., Tuck, I.D., Grewar, G.N., Armstrong, E., Reid, D.G., & Wright, P.J. (1997). An assessment of the acoustic survey technique, RoxAnn, as a means of mapping seabed habitat. *ICES Journal of Marine Science*, 54(5), 939-959.

Guan, W.; Chamberlain, R.H.; Sabol, B.M., and Doering, P.H., 1999. Mapping Submerged Aquatic Vegetation with GIS in the Caloosahatchee Estuary: Evaluation of Different Interpolation Methods. *Marine Geodesy*, 22(2), 69-91.

Halley, V. and Bruce, E., 2007. Thematic accuracy assessment of acoustic seabed data for shallow benthic habitat mapping. *International Journal of Environmental Studies*, 64(1), 93–107.

Hamilton, L.J. (1998). Calibration and interpretation of acoustic backscatter measurements of suspended sediment concentration profiles in Sydney Harbour. *Acoustics Australia*, 26(3), 87-93.

Hamilton, L.J., Mulhearn, P.J., & Poeckert, R. (1999). Comparison of RoxAnn and QTC-View acoustic bottom classification system performance for the Cairns area, Great Barrier Reef, Australia. *Continental Shelf Research*, 19(12), 1577-1597.

Hamilton, L. J., 2001. Acoustic Seabed Classification Systems. Department of Defence, Defence Science and Technology Organisation. 150 pp.

Hastings, H.M., & Sugihara, G. (1994). *Fractals. A user's guide for the natural sciences*. Oxford: Oxford University Press.

Heald, G.J., & Pace, N.G. (1996). Implications of a bi-static treatment for the second echo from a normal incidence sonar. In *Proceedings of the Third European Conference on Underwater Acoustics*, 649-654.

Hearn, S.J.; Williamson, H.J.; Ockenden, M.C., and Waters, C.B., 1993. Fine resolution acoustic mapping related to sediment erosion shear strength. *Proceedings of the Institute of Acoustics 15*, Part 2, 41-48.

Huberty, C.J. (1994). *Applied Discriminant Analysis*. New York: Wiley.

Humm, H.J. (1973). Benthic algae of the eastern Gulf of Mexico. In: Jones, J.I. et al. (eds.), A Summary of Knowledge of the Eastern Gulf of Mexcio, 1973. State University System of Florida Institute of Oceanography, St. Petersburg, FL. IIIB: 1-15.

Hutin, E., & Simard, Y. (2005). Acoustic detection of a scallop bed from a single-beam echosounder in the St. Lawrence. *ICES Journal of Marine Science*, 62, 966-983.

Jagodzinski, Z., 1960. Multiple echoes in echosounders and the probability of detection of small targets. *International Hydrographic Review*, 37(1), 63-68.

Jenness, J., 2006. Surface Tools (surf_tools.avx) extension for ArcView 3.x, v. 1.6a. Jenness Enterprises. URL: http://www.jennessent.com/arcview/surface_tools.htm.

Kachigan, S.K. (1986). *An Interdisciplinary Introduction to Univariate and Multivariate Models*. New York: Radius Press.

Kendall, M.S.; Kruer, C.R.; Buja, K.R.; Christensen, J.D., Finkbeiner, M., and Monaco, M.E., 2001. Methods Used to Map the Benthic Habitats of Puerto Rico and the U.S. Virgin Islands. Silver Spring, MD. *NOAA/NOS Biogeography Program Technical Report*, 45 p.

Kloser, R.J., Bax, N.J., Ryan, T., Williams, A., & Barker, B.A. (2001). Remote sensing of seabed types in the Australian South East Fishery; development and application of normal incident acoustic techniques and associated 'ground truthing'. *Marine and Freshwater Research*, 52(4), 475-489.

Knudby, A. & LeDrew, E. (2007). Measuring Structural Complexity on Coral Reefs. Proceedings of the American Academy of Underwater Sciences 26th Symposium.Dauphin Island, AL: AAUS; 2007.

Kramer, C.Y., 1956. Extensions of multiple range tests to group means with unequal number of replications. *Biometerics*, 12(3), 307-310.

Krzanowski, W. J. (1977). The performance of Fisher's linear discriminant function under non-optimal conditions. *Technometrics*, 19, 191-200.

Lachenbruch, P. A., Sneeringer, C., & Revo, L.T. (1973). Robustness of the linear and quadratic discriminant functions to certain types of non-normality. *Communications in Statistics*, 1, 39-56.

Lapointe, B. E., Bedford, B. J. 2006. Drift rhodophyte blooms emerge in Lee County, FL: Evidence of escalating coastal eutrophication. *Harmful Algae* 6(3): 421-437.

Legendre, P., Ellingsen, K.E., Bjornbom, E., & Casgrain, P. (2002) Acoustic seabed classification: improved statistical method. *Canadian Journal of Fisheries and Aquatic Sciences*, 59, 1085-1089.

Limpert, E., Stahel, W.A., & Abbt, M. (2001) Log-normal distributions across the sciences: keys and clues. *BioScience*, 51(5), 341-352.

Livingston, R.J., (). Historical trends of human impacts on seagrass meadows in Florida. *Florida Marine Bulletin*, 42, 139-151.

Lubniewski, Z., & Stepnowski, A. (1997). Sea bottom typing using fractal dimensions. International symposium on hydroacoustics and ultrasonics. Gdansk-Jurata, Poland. 6pp.

Lurton, X. and Pouliquen E., 1992. Automated sea-bed classifcation system for echo-sounders. *IEEE Oceans '92 Conference Proceedings*, 317-321.

Ma, Z., & Redmond, R.L. (1995). Tau coefficients for accuracy assessment of classification of remote sensing data. *Photogrammetric Engineering and Remote Sensing*, 61, 435-439.

Magorrian, B.H., Service, M., & Clarke, W. (1995). An acoustic bottom classification survey of Strangford Lough, Northern Ireland. *Journal of the Marine Biological Association of the United Kingdom*, 75(4), 987-992.

Mandelbrot, B. B. (1982). *The Fractal Geometry of Nature*. Freeman: San Francisco.

Marcos, M.S.A., David, L., Penaflor, E., Ticzon, V. & Soriano, M. (2008). Automated benthic counting of living and non-living components in Ngedarrak Reef, Palau via subsurface underwater video. *Environmental Monitoring Assessment*, 145, 177-184.

McCune, B., & Grace, J.B. (2002). *Analysis of Ecological Communities*. MJM Software Design: Oregon.

McKinney, C.M. and Anderson, C.D., 1964. Measurements of backscattering of sound from the ocean bottom. *Journal of the Acoustical Society of America*, 36(1), 158-163.

Milligan, G.W., & Cooper, M.C. (1985). An examination of procedures for determining the number of clusters in a data set. *Psychometrika*, 50, 159-179.

Monaco, M.E., Christensen, J.D., & Rohmann, S.O. (2001). Mapping and Monitoring of U.S. Coral Reef Ecosystems. *Earth System Monitor*, 2(1), 1-16.

Moyer, R.P.; Riegl, B.; Banks, K., and Dodge, R.E., 2005. Assessing the accuracy of acoustic seabed classification for mapping coral reef environments in South Florida (Broward County, USA). *Revista de Biologia Tropical*, 53 Suppl 1, 175-184.
Orlowski, A. (1984). Application of multiple echo energy measurements for evaluation of sea bottom type. *Oceanlogia*, 19, 61-78.

Penrose, J.D.; Siwabessy, P.J.W.; Gavrilov, A.; Parnum, I.; Hamilton, L.J.; Bickers, A.; Brooke, B.; Ryan, D.A., and Kennedy, P., 2005. Acoustic Techniques for Seabed Classification. Cooperative Research Centre for Coastal Zone Estuary and Waterway Management, *Technical Report 32*.

Quester Tangent, 2002. QTC IMPACT Acoustic Seabed Classification, User Guide Version 3.00. Integrated Mapping, Processing and Classification Toolkit. Sidney, B.C., Canada. Quester Tangent.

Riegl, B.M., Moyer, R.P., Morris, L.J., Virnstein, R.W., Purkis, S.J., 2005. Distribution and seasonal biomass of drift macroalgae in the Indian River Lagoon (Florida, USA) estimated with acoustic seafloor classification (QTCView, Echo*plus*). *Journal of Experimental Marine Biology and Ecology*, 326, 89-104.

Riegl, B.M. and Purkis, S.J., 2005. Detection of shallow subtidal corals from IKONOS satellite and QTC View (50, 200 kHz) single-beam sonar data (Arabian Gulf; Dubai, UAE). *Remote Sensing of Environment*, 95, 96-114.

Riegl, B.M., Halfar, J., Purkis, S.J., & Godinez-Orta, L. (2007). Sedimentary facies of the Eastern Pacific's northernmost reef-like setting (Cabo Pulmo, Mexico). *Marine Geology*, 236, 61-77.

Rukavina, N.A., 1997. Substrate mapping in the Great Lakes nearshore zone with a RoxAnn acoustic sea-bed classification system. *Canadian Coastal Conference 1997*, 12pp.

Sabol, B. and Melton, R.E., 1996. Development of an Automated System for Detection and Mapping of Submersed Aquatic Vegetation with Hydroacoustic and Global Positioning System Technologies; Report 1: The Submersed Aquatic Vegetation Early Warning System (SAVEWS)—System Description and User's Guide (Version 1.0). Knoxville, Tennessee: Tennessee Valley Authority. Joint Agency Guntersville Project Aquatic Plant Management, *TVA/WR-95-00*.

Schlagintweit, G.E.O., 1993. Real-time acoustic bottom classification: a field evaluation of RoxAnn. *Proceedings of Oceans '93*, 214-219.

Seiderer, L.J., & Newell, R.C. (1999). Analysis of the relationship between sediment composition and benthic community structure in coasal deposits: Implications for marine aggregate dredging. *ICES Journal of Marine Science*, 56, 757-765.

Snelgrove, P.V.R., & Butman, C.A. (1994). "Animal-sediment relationships revisited: cause versus effect." *Oceanography and Marine Biology: an Annual Review*, 32, 111-177.

Sokal, R.R., & Rohlf, F.J. (1981). *Biometry*, 2nd ed. W.H.Freeman: San Francisco, CA.

SPSS for Windows, Rel. 11.0.0.2001. Chicago: SPSS Inc.

Story, M., & Congalton, R. (1986) Accuracy assessment: A user's perspective. *Photogrammetric Engineering and Remote Sensing*, 52, 397-399.

Tabachnick, B.G., & Fidell, L. S. (2007). *Using Multivariate Statistics*, 5th ed. Boston: Allyn and Bacon.

Tegowski, J., & Lubniewski, Z. (2000). The use of fractal properties of echo signals for acoustical classification of bottom sediments. *Acta Acustica*, l86, 276-282.

Vergara, M.W.B., & Licuanan, W.Y. (2007). Survey of coral communities using digital photography. 9th National Symposium in Marine Science. Iloilo City, Philippines.

von Szalay, P.G. and McConnaughey, R.A., 2002. The effect of slope and vessel speed on the performance of a single-beam acoustic seabed classification system. *Fisheries Research (Amsterdam)*, 56(1), 99-112.

Virnstein, R.W., & Carbonara, P.A., (1985). Seasonal abundance and distribution of drift algae and seagrasses in the mid-Indian River Lagoon, Florida. *Aquatic Botany*, 23, 67-82.

Voulgaris, G. and Collins, M.B., 1990. USP RoxAnn Ground Discrimination System: A Preliminary Evaluation. ARE Portland UTH *Tech Memo 36/90. RE005314*. University of Southampton, Department of Oceanography, Marine Consultancy Services, *Technical Report No: SUDO/TEC/90/5C*.

Wahl, P. W., & Kronmal, R. A. (1977). Discriminant functions when covariances are unequal and sample sizes are moderate. *Biometrics*, 33, 479-484.

Walker, B.K.; Riegl, B.M., and Dodge, R.E., 2008. Mapping coral reef habitats in Southeast Florida using a combined technique approach. *Journal of Coastal Research*. SI 53, 16-26.

Wang, P., Davis, R. A., & Kraus, N. C. (1998) Cross-shore distribution of sediment texture under breaking waves along low-wave-energy coasts. Journal of Sedimentary Research, 68(3), 497-506.

White, W.H.; Harborne, A.R.; Sotheran, I.S.; Walton, R., and Foster-Smith, R.L., 2003. Using an Acoustic Ground Discrimination System to map coral reef benthic classes**.** *International Journal of Remote Sensing*, 24(13), 2641-2660.

Wilding, T.A., Sayer, M.D.J., & Provost, P.G. (2003). Factors affecting the performance of the acoustic ground discrimination system RoxAnn. *ICES Journal of Marine Science*, 60, 1373-1380.

Williams, B. K. (1982). A simple demonstration of the relationship between classification and canonical variates analysis. *American Statistician*, 36, 363-365.

Williams, B. K. (1983). Some Observations of the Use of Discriminant Analysis in Ecology. *Ecology*, 64(5), 1283-1291.